EVALUATION OF THE SPECTRAL ANALYSIS OF SURFACE WAVES (SASW) TEST METHOD FOR FLORIDA DEPARTMENT OF TRANSPORTATION (FDOT) APPLICATIONS

By

DAVID JOSEPH HORHOTA

A DISSERTATION PRESENTED TO THE GRADUATE SCHOOL
OF THE UNIVERSITY OF FLORIDA IN PARTIAL FULFILLMENT
OF THE REQUIREMENTS FOR THE DEGREE OF
DOCTOR OF PHILOSOPHY

UNIVERSITY OF FLORIDA

1996

This dissertation is dedicated to my Lord and my God, for the many blessings He has given me in my life. Of these blessings, this is also dedicated to my parents and to Sharilynn, for their influence in my life.

ACKNOWLEDGEMENTS

There have been so many people involved in this work and without whose help, it would have been impossible to have completed it. To all the knowledge, talent, and abilities of these people, I hope that I do them justice with the results of this research.

I have to first acknowledge the role of God in my work. He comes first and foremost in my life, and made this opportunity come available to me. He saw me through the stagnant times, and gave me strength to finish the race.

I need to recognize my parents and brothers, who stressed the importance of knowledge and education at an early age and sacrificed for me to get a sound early educational beginning, as well as being solid role models. Without this foundation (pun intended), any advanced education would not have been possible.

Frank C. Townsend served as chairman of my committee. He is the person who made me want to come back to the University of Florida for graduate school. Besides the technical support, guidance, and bad jokes, he gave me the confidence I needed to enter into the Ph.D. program, and once there, said that there would low times when you never think you're going to finish. He was right, but helped me through them. If I ever teach, those poor students will have this man to blame for their misfortune.

Dave Bloomquist always showed enthusiasm and interest in my work even though he had a million other things to do. He truly is a role model for my technical career, with a child-like enthusiasm for engineering and research which if I keep in mind will never make my engineering life boring.

Paul Y. Thompson was always interested in my research and career, and his time never went unnoticed or unappreciated. I enjoyed his Graduate Seminar classes, and hope that I still hold the record for number of times a student has taken it.

Daniel Spangler provided a much-needed view from a non-engineering perspective. He made my interest in geology grow far beyond just 'looking at rocks'. I truly enjoyed his class, and hope to be able to take more classes from him after I graduate.

Walter Zimpfer taught me so much at the DOT and at the university. His time and devotion to the engineering profession are a model that I strive toward. I pray he has found eternal peace and happiness.

Jamshid Armaghani replaced Walter Zimpfer on my committee upon his retirement. I want to thank him for the commitment of his time and his interest in my career to willingly accept being on my committee. His time and input were deeply appreciated.

Many debts of gratitude go out to the people at the State Materials Office who helped in so many ways. Special thanks must go to Larry L. Smith and Dr. K. H. Ho, who made it possible to advance my graduate studies while remaining a full-time employee as well as making it possible to perform this research (as well as my master's research). It would be a long list if I included everyone's name here, but I will anyway since without their assistance, none of this would be possible:

Pam Moore
John Shoucair
Ken Hahn
Lee Cogdill
Ronnie Lewis
Rufus Green
Dave Bass
Willie Henderson
Tim Blanton
Gary Mitchell
Tommie Harvey
George Dillow
Robert Robertson
John Thompson
Jerry Moxley
Harold Godwin
Neal Brockington
Ron Aparicio
David Benefield
Todd Britton
Glenn Salvo

I must also acknowledge all others outside the State Materials Office who contributed to this research. Special thanks to Dr. Glenn Rix, Bubba Knight, Dr. Paul Cosentino, Dr. Virgil Ping, Dr. David Weintraub, Ling Ge, Philip Erbland, and Amy Knittel.

Finally, I must thank all my friends who supported me when I needed it (in good times as well as the bad ones) and kept aggravating me by asking when was I finally going to graduate. Special thanks to Sharilynn, who had the patience to see me through to the end.

TABLE OF CONTENTS

Page

ACKNOWLEDGEMENTS iii

LIST OF TABLES x

LIST OF FIGURES xiv

ABSTRACT xxvii

CHAPTERS

1 INTRODUCTION 1

- 1.1 Introduction 1
- 1.2 Problem Statement 3
  - 1.2.1 Geotechnical Applications 4
  - 1.2.2 Pavement Applications 7
- 1.3 Scope of Research 11
  - 1.3.1 Geotechnical Applications 11
  - 1.3.2 Pavement Applications 13

2 REVIEW OF LITERATURE 17

- 2.1 Background Information 17
- 2.2 Basic Seismic Wave Theory 19
  - 2.2.1 Effect of Water (Saturated Conditions) 25
- 2.3 Material Properties 26
  - 2.3.1 Shear Modulus 27
    - 2.3.1.1 Cohesionless soils 30
    - 2.3.1.2 Cohesive soils 36
  - 2.3.2 Young's Modulus 40
    - 2.3.2.1 Laboratory results 42
    - 2.3.2.2 Field results 45
  - 2.3.3 Constrained Modulus 51
  - 2.3.4 Nonlinear Effects on Moduli 52
  - 2.3.5 Poisson's Ratio 57

3 EQUIPMENT AND FIELD PROCEDURES 59

- 3.1 Equipment 59
  - 3.1.1 Signal Analyzer 59
    - 3.1.1.1 Spectral analysis 61

        3.1.1.2 Dispersion calculations 63
    3.1.2 Receivers 66
        3.1.2.1 Geophones 66
        3.1.2.2 Accelerometers 67
    3.1.3 Source 68
3.2 Software 71
    3.2.1 Transfer Program 71
    3.2.2 Inversion Program 74
3.3 Field Procedures 78
    3.3.1 Common Receivers' Midpoint Geometry (CRMP) 80
    3.3.2 Common Source Geometry (CS) 82
        3.3.2.1 Automated SASW method 82
    3.3.3 Common Near Receiver Geometry (CNR) . . 84
    3.3.4 Pavement Surface Layer Analysis 85
    3.3.5 Effects of Reflected Waves 87

4 TESTING PROGRAM 90

4.1 Introduction 90
4.2 General Testing Procedures 90
    4.2.1 Field Testing 91
        4.2.1.1 Signal analyzer settings . . . 97
        4.2.1.2 Data collection 103
    4.2.2 Construction of the Field Composite Dispersion Curve 108
    4.2.3 Inversion of the Dispersion Curve . . 110
4.3 Testing Program 112
    4.3.1 Geotechnical Applications 112
        4.3.1.1 Dynamic compaction site . . . 112
        4.3.1.2 Polk County Parkway 113
        4.3.1.3 Kanapaha site 113
        4.3.1.4 Live Oak site 114
    4.3.2 Pavement Applications 114
        4.3.2.1 Test pit studies 114
        4.3.2.2 Field trench sites 116
        4.3.2.3 Florida Institute of Technology test sites 116
        4.3.2.4 US-98 (Panama City) test site 117

5 GEOTECHNICAL APPLICATIONS 118

5.1 Introduction 118
5.2 Dynamic Compaction Site 118
    5.2.1 Background Information 119
    5.2.2 Site Information 121
    5.2.3 SASW Testing 123
5.3 Polk County Parkway Site 129
    5.3.1 Background Information 130
    5.3.2 SASW Testing 132
5.4 Kanapaha Site 142
    5.4.1 Background Information 143

5.4.2 SASW Testing 144
5.4.2.1 Location of top of limerock . 147
5.4.2.2 Comparison of field moduli results 157
5.4.2.3 Detection of anomalies in limerock 162
5.4.2.4 Comparison of sources 165
5.4.2.5 Comparison of SASW and DCP results 171
5.4.2.6 Reproducibility of the SASW test 177
5.5 Live Oak Site 180
5.5.1 Background Information 180
5.5.2 SASW Testing 184

6 PAVEMENT APPLICATIONS 195

6.1 Introduction 195
6.2 Test Pit Studies 195
6.2.1 Background Information 197
6.2.2 SASW Testing 202
6.2.2.1 Subgrade materials 205
6.2.2.2 Base materials 250
6.3 Field Trench Sites 271
6.3.1 Background Information 271
6.3.2 SASW Testing 274
6.3.2.1 Layer thickness measurements 276
6.3.2.2 Layer stiffness measurements 284
6.4 Florida Institute of Technology Test Sites 329
6.4.1 Background Information 330
6.4.2 SASW Testing 334
6.5 US-98 (Panama City) Test Site 337
6.5.1 SASW Testing 339
6.5.2 SASW Results 342

7 SUMMARY, CONCLUSIONS, AND RECOMMENDATIONS . . . 349

7.1 Summary 349
7.2 Conclusions 351
7.2.1 Geotechnical Applications 351
7.2.2 Pavement Applications 356
7.3 Recommendations 361

APPENDICES

A GEOTECHNICAL APPLICATIONS' DATA 367

A.1 Introduction 367
A.2 Dynamic Compaction Site 367
A.3 Polk County Parkway 376
A.4 Kanapaha Site 382
A.5 Live Oak Site 398

B PAVEMENT APPLICATIONS' DATA 407

B.1 Introduction 407
B.2 Test Pit Studies 407
B.3 Field Trench Sites 427

REFERENCE LIST 435

BIOGRAPHICAL SKETCH 443

LIST OF TABLES

Table | Page

2.1 Distribution of Total Energy Based on Wave Type . 23

2.2 Values of Exponent K versus Plasticity Index . . . 37

2.3 Typical Values of Young's Modulus 42

2.4 Typical Values of Poisson's Ratio and Total Unit Weight 57

5.1 SASW, DMT, and SPT Locations for the Polk Co. Parkway 133

5.2 SASW, DMT, and SPT Depth Results for the Polk Co. Parkway 137

5.3 SASW, DMT, and SPT Stiffness Results for the Polk Co. Parkway 139

5.4 SASW and DMT Young's and Constrained Moduli Results for the Polk Co. Parkway 142

5.5 SASW and DCP Locations for the Kanapaha Site . . 145

5.6 CPT Locations for the Kanapaha Site 146

5.7 SASW Results for the Kanapaha Site 152

5.8 CPT Depths to Limerock for the Kanapaha Site . . 153

5.9 Comparison of SASW and DCP Results for the Kanapaha Site 173

5.10 CPT Locations for the Live Oak Site 183

5.11 SASW and Soil Boring Locations for the Live Oak Site 185

5.12 SASW Results for the Live Oak Site 189

6.1 List of Materials Tested in the Test Pit 205

6.2 Laboratory Test Results of the Test Pit Subgrade Soils 206

6.3 In-situ Densities and Moisture Contents for the SR-200 (Ocala) Subgrade 208

6.4 SASW Results for the SR-200 (Ocala) Subgrade . . 212

6.5 Static Plate Load Test Results for the SR-200 (Ocala) Subgrade 214

6.6 Dynamic Plate Load Test Results for the SR-200 (Ocala) Subgrade 217

6.7 Resilient Modulus Test Results for the SR-200 (Ocala) Subgrade 221

6.8 In-situ Densities and Moisture Contents for the I-75 (Alachua) Subgrade 228

6.9 SASW Results for the I-75 (Alachua) Subgrade . . 231

6.10 In-situ Densities and Moisture Contents for the SR-30A (Panama City) Subgrade 232

6.11 SASW Results for the SR-30A (Panama City) Subgrade 234

6.12 In-situ Densities and Moisture Contents for the SR-50 (Brooksville) Subgrade 235

6.13 SASW Results for the SR-50 (Brooksville) Subgrade 238

6.14 Inversion Results for the SR-50 (Brooksville) Subgrade 239

6.15 In-situ Densities and Moisture Contents for the SR-369 (Crawfordville) Subgrade 240

6.16 SASW Results for the SR-369 (Crawfordville) Subgrade 243

6.17 Inversion Results for the SR-369 (Crawfordville) Subgrade 244

6.18 SASW Results for the Flexbase Study 256

6.19 In-situ Densities and Moisture Contents for the Dolomite Study 258

6.20 SASW Results for the Dolomite Study 260

6.21 In-situ Densities and Moisture Contents for the RAP Study 266

6.22 SASW Results for the RAP Study 270

6.23 Thickness of the Trench Site Layers 277

6.24 Summary of Thickness Comparisons for the Field Trench Sites 282

6.25 Material Properties for the Trench Site Soils . 287

6.26 Stiffness Results of the Base Layer Tests from the Trench Sites 295

6.27 Linear Regression Results for the Base Moduli Comparisons from the Trench Sites 298

6.28 Resilient Modulus Test Results for the US-441 (Osceola County) Base 302

6.29 Stiffness Results of the Subgrade/Embankment Layer Tests from the Trench Sites 311

6.30 Linear Regression Results for the Subgrade/Embankment Moduli Comparisons from the Trench Sites . 316

6.31 Summary of Moduli-Strain Relationships 326

6.32 SASW Results for the FIT Campus Ministries Site 336

A.1 Additional SASW Results for the Kanapaha Site . 383

B.1 Static Plate Load Test Results for the I-75 (Alachua) Subgrade 409

B.2 Dynamic Plate Load Test Results for the I-75 (Alachua) Subgrade 410

B.3 Resilient Modulus Test Results for the I-75 (Alachua) Subgrade 411

B.4 Static Plate Load Test Results for the SR-30A (Panama City) Subgrade 413

B.5 Dynamic Plate Load Test Results for the SR-30A (Panama City) Subgrade 414

B.6 Resilient Modulus Test Results for the SR-30A (Panama City) Subgrade 415

B.7 Static Plate Load Test Results for the SR-50 (Brooksville) Subgrade 417

B.8 Dynamic Plate Load Test Results for the SR-50 (Brooksville) Subgrade 418

B.9 Resilient Modulus Test Results for the SR-50 (Brooksville) Subgrade 419

B.10 Static Plate Load Test Results for the SR-369 (Crawfordville) Subgrade 421

B.11 Dynamic Plate Load Test Results for the SR-369 (Crawfordville) Subgrade 422

B.12 Resilient Modulus Test Results for the SR-369 (Crawfordville) Subgrade 423

B.13 Static Plate Load Test Results for the Dolomite Study 425

B.14 Dynamic Plate Load Test Results for the Dolomite Study 426

LIST OF FIGURES

Figure Page

2.1 Variation in Particle Motion versus Depth for R-Waves (Richart et al., 1970) 19

2.2 Relationship between Seismic Wave Velocities and Poisson's Ratio (Richart et al., 1970) 21

2.3 Principle of Dispersion for a Layered System (Rix and Stokoe, 1989) 24

2.4 Shear Wave Deformation (Bay and Stokoe, 1992) . . 28

2.5 CPT Procedure for Estimating the Maximum Shear Modulus (Olsen, 1988) 35

2.6 Unconstrained Compression Wave Deformation (Bay and Stokoe, 1992) 40

2.7 Drained Young's Modulus at 0.1% Strain from the CPT for Silica Sand (Riaund and Miran, 1992a) 46

2.8 Relationship between Elastic Young's Modulus and the DCP Penetration Index (Burnham and Johnson, 1993) 48

2.9 Constrained Compression Wave Deformation (Bay and Stokoe, 1992) 52

2.10 Nonlinear Soil Behavior based on Initial Tangent and Secant Moduli (Rix and Stokoe, 1989) 53

2.11 Variation of Normalized Shear Modulus and Plasticity Index for Cohesive Soils (Vucetic, 1991) . . . 55

2.12 Variation of Normalized Young's Modulus and Plasticity Index for Compacted Subgrade Soils (Kim and Stokoe, 1992) 55

2.13 Variation of Normalized Young's Modulus and Effective Octahedral Normal Stress for Sand Samples (Nazarian et al., 1987) 55

2.14 Effect of Frequency and Temperature on Small-Strain Shear Modulus of Asphalt Concrete (Roesset et al., 1990) 56

3.1 SASW Field Test Configuration 79

3.2 Common Receivers' Midpoint Geometry (CRMP) Configuration (Nazarian and Stokoe, 1984) 81

3.3 Common Source Geometry (CS) Configuration (Heisey, 1982b) 83

3.4 Common Near Receiver Geometry (CNR) Configuration (Drnevich et al., 1990) 85

3.5 Determination of Surface Layer Thickness from a Dispersion Curve (Roesset et al., 1990) 86

3.6 Comparison of Measured Dispersion Curve with the True Curve with No Reflections (Sheu et al., 1988) 88

4.1 L-4C 1.0 Hz Geophones 94

4.2 L-28B 4.5 Hz Geophones 95

4.3 728T Accelerometers and the P702 Power Supply/ Amplifiers 96

4.4 HP-35665A Signal Analyzer 98

4.5 Measurement Settings from the HP-35665A Signal Analyzer 99

4.6 Input Settings from the HP-35665A Signal Analyzer 99

4.7 Sources used at Pavement Sites 105

4.8 Sources used at Soil Sites 106

4.9 Plots of Channel 1 & 2 Time Histories from the HP-35665A Signal Analyzer 107

4.10 Plots of Cross Spectrum and Coherence from the HP-35665A Signal Analyzer 107

4.11 Gibson Half-Space Shear Modulus Profile 111

5.1 Plan View of the Dynamic Compaction Site 121

5.2 Dispersion Curves from the Dynamic Compaction Site (Sta 472+00, 50' Lt) 124

5.3 S-Wave Velocity Profiles from the Dynamic Compaction Site (Sta 472+00, 50′ Lt) 124

5.4 Comparison of S-Wave Velocity Profiles from the Dynamic Compaction Site (Sta 472+00, 50′ Lt) . 127

5.5 S-Wave Velocity Profile using the Dynamic Compaction Weight (Sta 473+50, 100′ Rt) 128

5.6 Comparison of S-Wave Velocity Profiles using the Dynamic Compaction Weight (Sta 473+50, 100′ Rt) 129

5.7 Dispersion Curve from the Polk Co. Parkway (Sta 779+80, 165′ Rt) 135

5.8 Comparison of Dispersion Curves from the Polk Co. Parkway (Sta 729+00, 5′ Lt) 136

5.9 DMT Shear Modulus Profile from the Polk Co. Parkway (Sta 780+00, 159′ Rt) 141

5.10 Comparison of DMT and SASW Shear Modulus Profiles from the Polk Co. Parkway (Sta 780+00, 165′ Rt) 141

5.11 Plan View of the Kanapaha Site 144

5.12 Dispersion Curves for the N.E. Quadrant of the Kanapaha Site 148

5.13 Dispersion Curves for the N.W. Quadrant of the Kanapaha Site 148

5.14 Dispersion Curves for the S.E. Quadrant of the Kanapaha Site 149

5.15 Dispersion Curves for the S.W. Quadrant of the Kanapaha Site 149

5.16 Boring Log at Site 5 (25′N 40′W) from the Kanapaha Site (Townsend et al., 1991) 156

5.17 Comparison of CPT Shear Modulus Profiles from the Kanapaha Site (40′N 58′W) 159

5.18 Comparison of Shear Modulus Profiles from the Kanapaha Site (40′N 58′W) 159

5.19 Comparison of Young′s Modulus Profiles from the Kanapaha Site (40′N 58′W) 161

5.20 DCP Test Results from the Kanapaha Site (35′N 56′W) 163

5.21 Dispersion Curve from the Kanapaha Site (35'N 56'W) 163

5.22 S-Wave Velocity Profile from the Kanapaha Site (35'N 56'W) 165

5.23 Signal Analyzer Plots using the Sledgehammer (3' Spacing) 168

5.24 Signal Analyzer Plots using the DCP (3' Spacing) 168

5.25 Signal Analyzer Plots using the Sledgehammer (9' Spacing) 169

5.26 Signal Analyzer Plots using the DCP (9' Spacing) 169

5.27 Signal Analyzer Plots using the Sledgehammer (20' Spacing) 170

5.28 Signal Analyzer Plots using the Concrete Block (20' Spacing) 170

5.29 Comparison of DCP and SASW Young's Modulus Profiles from the Kanapaha Site (25'N 100'W) 175

5.30 Relationship between SASW E_{max} and DCP CBR . . . 177

5.31 Dispersion Curves for various Time Periods from the Kanapaha Site (35'N 56'W) 178

5.32 Soil Boring Results from the Live Oak Site . . . 181

5.33 Plan View of the Live Oak Site 182

5.34 Dispersion Curves from the Live Oak Site 185

5.35 Comparison of CPT Shear Modulus Profiles from the Live Oak Site (120'S 200'W) 191

5.36 Comparison of Shear Modulus Profiles from the Live Oak Site (80'S 40'W) 193

5.37 Comparison of Shear Modulus Profiles from the Live Oak Site (160'S 40'W) 193

6.1 Sectional View of the Test Pit 196

6.2 Schematic Diagram of the Test Pit Loading System (Cox, 1971) 197

6.3 Idealized Load Cycle (Cox, 1971) 200

6.4 Idealized Dynamic Plate Load Test Deflection Plot (Cox, 1971) 201

6.5 Dispersion Curves for the SR-200 (Ocala) Subgrade in the Test Pit 209

6.6 Dispersion Curves for the SR-200 (Ocala) Subgrade at Optimum Condition in the Test Pit 210

6.7 Static Plate Load Test Results for the SR-200 (Ocala) Subgrade 215

6.8 Dynamic Plate Load Test Results for the SR-200 (Ocala) Subgrade 219

6.9 Resilient Modulus Test Results for the SR-200 (Ocala) Subgrade 223

6.10 Variation of Young's Modulus and Strain for the SR-200 (Ocala) Subgrade 225

6.11 Variation of Normalized Modulus and Strain for the SR-200 (Ocala) Subgrade 227

6.12 Dispersion Curves for the I-75 (Alachua) Subgrade in the Test Pit 229

6.13 Dispersion Curves for the SR-30A (Panama City) Subgrade in the Test Pit 233

6.14 Dispersion Curves for the SR-50 (Brooksville) Subgrade in the Test Pit 236

6.15 Dispersion Curves for the SR-369 (Crawfordville) Subgrade in the Test Pit 241

6.16 Variation of Normalized Modulus and Strain for the Subgrade Soils 246

6.17 Normalized Modulus-Strain Relationships for the Test Pit Subgrade Soils 250

6.18 Signal Analyzer Plots for the Flexbase at Drained Condition 253

6.19 Dispersion Curve for the Flexbase at Drained Condition (1/2-Foot Spacing) in the Test Pit 253

6.20 Dispersion Curves for the Flexbase at Drained Condition in the Test Pit 255

6.21 Dispersion Curves for the Dolomite in the Test Pit 259

6.22 Variation of Young's Modulus and Strain for the Dolomite 263

6.23 Dispersion Curves for the RAP in the Test Pit . 266

6.24 Dispersion Curve for the RAP at Optimum Condition (1/2-Foot Spacing) in the Test Pit 268

6.25 Diagram of a Typical Field Plate-Bearing Test (AASHTO, 1993) 272

6.26 Dispersion Curves for US-1 (Tamiami Trail, Dade Co.) Site #1, Subgrade Layer 279

6.27 Comparison of Layer Thickness Measurements for the Trench Sites 281

6.28 Comparison of LBR Ratio and Percent Difference of the SASW Thickness Measurements 284

6.29 Field Plate Load Test Results for the US-441 (Osceola Co.) Base Layer 293

6.30 Load Cycle Curve for the US-441 (Osceola Co.) Base Layer 293

6.31 Comparison of Corrected Plate and SASW Base Layer Moduli for the Trench Sites 299

6.32 Resilient Modulus Test Results for the US-441 (Osceola Co.) Base 303

6.33 Variation of Normalized Modulus and Strain for the Base Layer Trench Sites 305

6.34 Variation of Normalized Modulus and Strain for the Base Layer Resilient Modulus 308

6.35 Normalized Modulus-Strain Relationships for the Base Layer Trench Sites 308

6.36 Comparison of E_i and SASW Subgrade/Embankment Moduli for the Trench Sites 315

6.37 Variation of Normalized Modulus and Strain for the Subgrade Layer Resilient Modulus 319

6.38 Normalized Modulus-Strain Relationships for the Subgrade Layer Trench Sites 319

6.39 Variation of Normalized Modulus and Strain for the Embankment Layer Resilient Modulus 321

6.40 Normalized Modulus-Strain Relationships for the Embankment Layer Trench Sites 321

6.41 Comparison of Corrected E_i and SASW Moduli for the Trench Sites 324

6.42 Comparison of LBR and SASW Moduli for the Trench Sites 324

6.43 Comparison of Normalized Modulus-Strain Relationships for a 10 psi Deviator Stress 327

6.44 Plan View of the FIT Campus Ministries Site (Erbland, 1993) 331

6.45 Proposed Resilient Modulus PPMT Test (Erbland, 1993) 333

6.46 Dispersion Curves for the FIT Campus Ministries Site 334

6.47 Variation of Moduli and Measured Strain with the PPMT (Erbland, 1993) 337

6.48 Plan View of the US-98 (Panama City) Site . . . 342

6.49 Dispersion Curves for the US-98 (Panama City) Pavement Test Sites 343

6.50 Comparison of the S-Wave Velocity Profiles from the US-98 (Panama City) Shoulder Test Sites 346

A.1 Dispersion Curves from the Dynamic Compaction Site (Sta 472+00, 50′ Rt) 368

A.2 S-Wave Velocity Profiles from the Dynamic Compaction Site (Sta 472+00, 50′ Rt) 368

A.3 Dispersion Curves from the Dynamic Compaction Site (Sta 472+00, C.L.) 369

A.4 S-Wave Velocity Profiles from the Dynamic Compaction Site (Sta 472+00, C.L.) 369

A.5 Dispersion Curves from the Dynamic Compaction Site (Sta 472+50, 100′ Rt) 370

A.6 S-Wave Velocity Profiles from the Dynamic Compaction Site (Sta 472+50, 100′ Rt) 370

A.7 Dispersion Curves from the Dynamic Compaction Site (Sta 473+00, 100′ Rt) 371

A.8 S-Wave Velocity Profiles from the Dynamic Compaction Site (Sta 473+00, 100′ Rt) 371

A.9 Dispersion Curves from the Dynamic Compaction Site (Sta 473+50, C.L.) 372

A.10 S-Wave Velocity Profiles from the Dynamic Compaction Site (Sta 473+50, C.L.) 372

A.11 Comparison of S-Wave Velocity Profiles from the Dynamic Compaction Site (Sta 472+00, 50′ Rt) . . 373

A.12 Comparison of S-Wave Velocity Profiles from the Dynamic Compaction Site (Sta 472+00, C.L.) . . . 373

A.13 Comparison of S-Wave Velocity Profiles from the Dynamic Compaction Site (Sta 472+50, 100′ Rt) . 374

A.14 Comparison of S-Wave Velocity Profiles from the Dynamic Compaction Site (Sta 473+00, 100′ Rt) . 374

A.15 Comparison of S-Wave Velocity Profiles from the Dynamic Compaction Site (Sta 473+50, C.L.) . . . 375

A.16 Dispersion Curve from the Polk Co. Parkway (Sta 742+00, 75′ Rt) 377

A.17 Dispersion Curve from the Polk Co. Parkway (Sta 773+70, 137′ Rt) 377

A.18 Dispersion Curve from the Polk Co. Parkway (Sta 773+70, 209′ Rt) 378

A.19 Dispersion Curve from the Polk Co. Parkway (Sta 780+55, 165′ Rt) 378

A.20 DMT Shear Modulus Profile from the Polk Co. Parkway (Sta 729+00, 25′ Lt) 379

A.21 Comparison of Shear Modulus Profiles from the Polk Co. Parkway (Sta 729+00, 5′ Lt) 379

A.22 DMT Shear Modulus Profile from the Polk Co. Parkway (Sta 742+00, 80′ Rt) 380

A.23 Comparison of Shear Modulus Profiles from the Polk Co. Parkway (Sta 742+00, 75′ Rt) 380

A.24 DMT Shear Modulus Profile from the Polk Co. Parkway (Sta 771+90, 155′ Rt) 381

A.25 Comparison of Shear Modulus Profiles from the Polk Co. Parkway (Sta 770+70, 137/209′ Rt) 381

A.26 CPT Tip Resistance Profile from the Kanapaha Site (40′N 58′W) 386

A.27 CPT Tip Resistance Profile from the Kanapaha Site (40′N 74′W) 386

A.28 CPT Tip Resistance Profile from the Kanapaha Site (40′N 90′W) 387

A.29 CPT Tip Resistance Profile from the Kanapaha Site (38′N 105′W) 387

A.30 CPT Tip Resistance Profile from the Kanapaha Site (25′N 54′W) 388

A.31 CPT Tip Resistance Profile from the Kanapaha Site (25′N 63′W) 388

A.32 CPT Tip Resistance Profile from the Kanapaha Site (25′N 80′W) 389

A.33 CPT Tip Resistance Profile from the Kanapaha Site (25′N 100′W) 389

A.34 CPT Tip Resistance Profile from the Kanapaha Site (14′N 50′W) 390

A.35 CPT Tip Resistance Profile from the Kanapaha Site (14′N 70′W) 390

A.36 CPT Tip Resistance Profile from the Kanapaha Site (14′N 90′W) 391

A.37 CPT Tip Resistance Profile from the Kanapaha Site (39′N 46′W) 391

A.38 Comparison of Shear Modulus Profiles from the Kanapaha Site (40′N 74′W) 392

A.39 Comparison of Shear Modulus Profiles from the Kanapaha Site (40'N 90'W) 392

A.40 Comparison of Shear Modulus Profiles from the Kanapaha Site (38'N 105'W) 393

A.41 Comparison of Shear Modulus Profiles from the Kanapaha Site (25'N 54'W) 393

A.42 Comparison of Shear Modulus Profiles from the Kanapaha Site (25'N 63'W) 394

A.43 Comparison of Shear Modulus Profiles from the Kanapaha Site (25'N 80'W) 394

A.44 Comparison of Shear Modulus Profiles from the Kanapaha Site (25'N 100'W) 395

A.45 Comparison of Shear Modulus Profiles from the Kanapaha Site (14'N 50'W) 395

A.46 Comparison of Shear Modulus Profiles from the Kanapaha Site (14'N 70'W) 396

A.47 Comparison of Shear Modulus Profiles from the Kanapaha Site (14'N 90'W) 396

A.48 Comparison of Shear Modulus Profiles from the Kanapaha Site (39'N 46'W) 397

A.49 CPT Tip Resistance Profile from the Live Oak Site (80'S 40'W) 399

A.50 CPT Tip Resistance Profile from the Live Oak Site (120'S 40'W) 399

A.51 CPT Tip Resistance Profile from the Live Oak Site (120'S 80'W) 400

A.52 CPT Tip Resistance Profile from the Live Oak Site (130'S 120'W) 400

A.53 CPT Tip Resistance Profile from the Live Oak Site (120'S 200'W) 401

A.54 CPT Tip Resistance Profile from the Live Oak Site (160'S 40'W) 401

A.55 CPT Tip Resistance Profile from the Live Oak Site (160'S 80'W) 402

A.56 CPT Tip Resistance Profile from the Live Oak Site (160'S 120'W) 402

A.57 CPT Tip Resistance Profile from the Live Oak Site (160'S 160'W) 403

A.58 Comparison of Shear Modulus Profiles from the Live Oak Site (120'S 40'W) 403

A.59 Comparison of Shear Modulus Profiles from the Live Oak Site (120'S 80'W) 404

A.60 Comparison of Shear Modulus Profiles from the Live Oak Site (130'S 120'W) 404

A.61 Comparison of Shear Modulus Profiles from the Live Oak Site (120'S 160'W) 405

A.62 Comparison of Shear Modulus Profiles from the Live Oak Site (160'S 80'W) 405

A.63 Comparison of Shear Modulus Profiles from the Live Oak Site (160'S 120'W) 406

A.64 Comparison of Shear Modulus Profiles from the Live Oak Site (160'S 160'W) 406

B.1 Static Plate Load Test Results for the I-75 (Alachua) Subgrade 409

B.2 Dynamic Plate Load Test Results for the I-75 (Alachua) Subgrade 410

B.3 Resilient Modulus Test Results for the I-75 (Alachua) Subgrade 411

B.4 Variation of Normalized Modulus and Strain for the I-75 (Alachua) Subgrade 412

B.5 Static Plate Load Test Results for the SR-30A (Panama City) Subgrade 413

B.6 Dynamic Plate Load Test Results for the SR-30A (Panama City) Subgrade 414

B.7 Resilient Modulus Test Results for the SR-30A (Panama City) Subgrade 415

B.8 Variation of Normalized Modulus and Strain for the SR-30A (Panama City) Subgrade 416

B.9 Static Plate Load Test Results for the SR-50 (Brooksville) Subgrade 417

B.10 Dynamic Plate Load Test Results for the SR-50 (Brooksville) Subgrade 418

B.11 Resilient Modulus Test Results for the SR-50 (Brooksville) Subgrade 419

B.12 Variation of Normalized Modulus and Strain for the SR-50 (Brooksville) Subgrade 420

B.13 Static Plate Load Test Results for the SR-369 (Crawfordville) Subgrade 421

B.14 Dynamic Plate Load Test Results for the SR-369 (Crawfordville) Subgrade 422

B.15 Resilient Modulus Tests Results for the SR-369 (Crawfordville) Subgrade 423

B.16 Variation of Normalized Modulus and Strain for the SR-369 (Crawfordville) Subgrade 424

B.17 Profiles of the Clay Co. Trench Sites 428

B.18 Profiles of the Seminole Co. Trench Sites . . . 428

B.19 Profiles of the Osceola Co. Trench Sites 429

B.20 Profiles of the Dade Co. Trench Sites 429

B.21 Profiles of the Polk Co. Trench Sites 430

B.22 Profiles of the Martin Co. Trench Sites 430

B.23 Comparison of Uncorrected Plate and SASW Base Layer Moduli for the Trench Sites 431

B.24 Comparison of LBR and SASW Moduli for the Base Layer Trench Sites 431

B.25 Comparison of E_p and SASW Subgrade/Embankment Moduli for the Trench Sites 432

B.26 Comparison of E_r and SASW Subgrade/Embankment Moduli for the Trench Sites 432

B.27 Comparison of LBR and SASW Moduli for the Subgrade/ Embankment Layer Trench Sites 433

B.28 Comparison of Uncorrected Plate and SASW Moduli for the Trench Sites 434

B.29 Comparison of Corrected E_p and SASW Moduli for the Trench Sites 434

Abstract of Dissertation Presented to the Graduate School
of the University of Florida in Partial Fulfillment of the
Requirements for the Degree of Doctor of Philosophy

EVALUATION OF THE SPECTRAL ANALYSIS OF SURFACE WAVES (SASW) TEST METHOD FOR FLORIDA DEPARTMENT OF TRANSPORTATION (FDOT) APPLICATIONS

By

David Joseph Horhota

December 1996

Chairperson: Frank C. Townsend
Cochairperson: David Bloomquist
Major Department: Civil Engineering

The Spectral Analysis of Surface Waves (SASW) test method is a relatively new in-situ test which can produce the stiffness profile at a test site from the ground surface. This field test can be performed on either pavement or soil surfaces. Because of these capabilities, this test method has a broad range of engineering applications and the potential of providing the engineer with a useful tool. This research was initiated to obtain the equipment to perform the SASW test and to evaluate this test method in a wide assortment of applications that the Florida Department of Transportation (FDOT) can utilize.

A testing program consisting of both geotechnical and pavement sites was developed to fully utilize the capabilities of the SASW test equipment. In addition to using the test

method for use in various applications suitable for FDOT purposes, the SASW results were used to compare with other field and laboratory test results commonly used by the FDOT. These tests included the cone penetrometer test (CPT), dilatometer test (DMT), ground penetrating radar (GPR), pressuremeter, plate load tests (dynamic and static), resilient modulus test, dynaflect, and falling weight deflectometer.

The overall results from this research showed that the SASW test method is a versatile, accurate, and reliable test with many useful applications suitable for the FDOT, and its use should be continued to improve procedures and explore new applications. The two areas that need to be addressed in further studies are improving the source to generate very high and very low frequency surface waves and improving the inversion software in order to generate a stiffness profile for pavement sites. The results from the geotechnical applications showed that the SASW test can be used for quality control of ground modification projects, that it can be used to delineate soft surface layers as well as the top of a stiff layer near the ground surface, that its results are capable of detecting anomalies near the ground surface, and that its results are comparable to other test methods' results particularly the CPT. The results from the pavement applications showed that the SASW test can be compared to other test methods in order to develop a relationship between modulus and strain, that its thickness measurements were accurate to within approximately one inch, and that its results can be used to evaluate the stiffness profile from a deficient section of an existing roadway.

CHAPTER 1
INTRODUCTION

1.1 Introduction

The Spectral Analysis of Surface Waves (SASW) method is an in-situ seismic test which provides a means to determine the shear wave velocity profile at a site. Based on this shear wave velocity profile, several material properties and site characteristics can be obtained either directly or indirectly. For example, the initial shear modulus and maximum Young's modulus can be directly determined, the in-situ density and the amount of natural cementation can be inferred, the in-situ stress state can be estimated, and the relative degree of sampling disturbance can be evaluated. This information has direct application to profiling pavements, foundation integrity testing, site assessment, and ground modification monitoring.

The SASW method provides many improvements over traditional seismic testing methods. Since this method involves the generation and measurement of Rayleigh waves propagating along the surface, all testing is performed on the ground surface and produces a continuous profile of the soil stiffness at the test site. Other seismic tests (such as downhole and crosshole seismic testing) require the installation of boreholes at a test site, but no boreholes are required for the SASW method which allows testing in hard-to-sample soils. This test is a nondestructive method since only low energy waves need to be generated in most cases. Finally, traditional surface seismic tests (such as refraction surveys) cannot detect lower velocity layers which are below higher velocity layers, but the SASW method can account for this by use of an inversion algorithm.

Compared to traditional methods of in-situ seismic testing, the SASW method is a very flexible test with a wide range of applications. This test method can be utilized on rigid and flexible pavement sites, and also on soil sites. Several applications that this equipment has been used for in previous case histories are as follows:

(1) determining profiles for soil/pavement systems without prior knowledge of the site (Nazarian et al., 1988),

(2) determining the stiffness of the pavement, base, and subgrade which can provide quality control before, during, and after placement of the pavement (Rix and Stokoe, 1989),

(3) determining the variation of the elastic modulus (modulus gradient) within an individual pavement layer (Nazarian et al. 1988),

(4) estimating small-strain moduli values of both the soil and pavement structure, which can be combined with

laboratory and/or empirical results to determine moduli in the non-linear range (Rix and Stokoe, 1989),

(5) evaluating in-situ densities by comparing the measured shear wave velocities to empirically determined values for sands and gravels at loose, medium dense, and dense conditions (Stokoe et al. 1988, 1989),

(6) providing a means to verify the integrity of in-place concrete beams (Bowen et al., 1992),

(7) evaluating the integrity of drilled shafts (Harrell and Stokoe, 1984 and Rix et al., 1993),

(8) determining the elastic Young's modulus for concrete cylinders which can also be applied to rock cores (Bay and Stokoe, 1992),

(9) verifying the effectiveness of ground modification techniques such as grouting (Stokoe et al., 1989), dynamic compaction (Stokoe et al., 1988), and vibroflotation,

(10) evaluating liquefaction of soils due to seismic events (Stokoe et al., 1988),

(11) providing a nondestructive method of determining the maximum aggregate size used in both concrete and asphaltic concrete (AC) pavements (Sheu et al., 1986).

1.2 Problem Statement

Due to the versatility of the SASW test method, it can be utilized for both geotechnical (soils) and pavement applications. Therefore, the approach taken for this research was to divide the testing into geotechnical and pavement applications.

1.2.1 Geotechnical Applications

A site's subsurface condition needs to be known in order to perform any reasonably 'engineered' foundation analysis prior to any roadway construction. This is usually accomplished by subsurface borings or soundings of some type. This proves to be impractical in hard-to-sample soils (Stokoe et al. 1988, 1989) or in difficult conditions due to the size and weight of the drilling rig (for instance, at potential landslide sites), and penetration testing might be impossible at sites containing contaminated soils (such as landfill sites). The SASW test allows for direct stiffness measurement of a given site at the ground surface without the need for boreholes.

Since penetration tests are typically several inches in diameter, it can only be used to evaluate the stiffness properties of the soil within a small zone of the boring or sounding. A roadway construction project can be many miles long, and borings or soundings are typically performed every 100 feet. The results from the borings or soundings must be used to determine soil properties along the entire length of the project in order to perform an engineering analysis. This does not present any problems if conditions are uniform, but this is seldom the case, especially in Florida. Since the SASW test utilizes seismic waves traveling between two receivers to measure the soil's stiffness at a test site, a larger volume of soil is sampled by the SASW test as compared to a penetration test. Therefore, the stiffness results from the SASW test represent a larger, global stiffness of the soil mass. This capability of the SASW test has many implications for standard geotechnical applications. For ground modification sites which need some kind of field test method for construction control and acceptance, the SASW test provides a means to evaluate the degree of improvement and the depth of improvement which represent a large volume of soil that is not greatly affected by boulders or debris at the test site. Another potential need exists to map out zones of soft surficial soils (clay or organic soils) or to delineate the depths to the top of limerock. Due to the variability in these areas, many times borings will not map out these zones accurately resulting in problems during construction which could have been avoided if more accurate soil conditions were provided during design. In addition, many regions of Florida have a karst topography creating very variable subsurface conditions, such as variable depths to the limerock surface, sinkholes, cavities, and considerable amounts of boulders. Due to these variable conditions, a field test is needed that can measure a larger volume of the test site's soils to evaluate more of the global stiffness. Once the global conditions are available, more concentrated testing can be performed, using penetration testing, at any potential problem areas. This approach will ensure the most economic use of the geotechnical investigation budget, while providing the most comprehensive data to the designer.

The SASW test provides a direct measurement of a soil's stiffness (shear wave velocity versus depth) at the test site. This has the disadvantage of resulting in parameters not commonly used in geotechnical design analyses, but with elastic theory, this stiffness profile can be used to obtain the Young's modulus or shear modulus which can be utilized for engineering analyses. Many in-situ tests involve empirical correlations to indirectly obtain commonly used engineering parameters for design purposes which leads to an uncertainty factor, and makes the engineer raise the factor of safety used in design and thereby increases the total cost of the construction project. The analysis of the raw data obtained from the SASW test has the advantage of not being based on empirically-based correlations, but rather on theoretically-based relationships. Therefore, efforts need to be made to compare the results from the various test methods to evaluate if these current empirically-derived values are adequate, or if they are too conservative and need to be revised.

In summary, the problems to be addressed by this research for the geotechnical applications are to assess the viability of the SASW test for the following items:

(1) comparison of soil modulus values used for foundation design versus stiffness values obtained by global measurements,

(2) evaluation of ground modification treatments,

(3) determination of the location of soft areas, top of limerock, and other areas of concern, and

(4) evaluation of empirical in-situ correlations used to estimate foundation deign parameters.

1.2.2 Pavement Applications

For standard pavement design procedures, one stiffness value (the soil support value, SSV) is used to represent the underlying support of the foundation soils. While this approach simplifies the pavement design process, it produces a degree of conservatism that is not warranted at this present time. Since computers allow the designer to use a stiffness profile to more accurately model the conditions that exist in the field, a new approach is needed to truly reflect the varying roadway stiffness profile and applied traffic loadings.

In current practice, many types of tests are used to express the final results in terms of the SSV, but little effort has been made to relate these various test methods together. For material acceptance prior to its use on any roadway project, test pit studies (involving both static and dynamic plate load tests) need to be performed to establish standard values for that material. For new construction, materials used for the project need to be tested using the Limerock Bearing Ratio (LBR) test method to establish design values. New design procedures involve changing the standard test method to the resilient modulus test rather than using a SSV, but no criteria has been established on how to utilize the resilient modulus test results for pavement design, and it is still in the research stage. On existing roadways in need of rehabilitation, nondestructive testing (NDT) is performed to establish a stiffness of the existing roadway profile. For research purposes, field plate load tests at existing roadways have been used to relate the results from the nondestructive tests to a representative SSV. Therefore, a systematic approach is needed to relate these various stiffness measurements to incorporate them into a more rational method which has the capability to be used for the design of pavements.

Nondestructive testing (NDT) methods are commonly used to determine the stress-strain relationships for a pavement system since they are fast and do not disturb the existing roadway. The two types of NDT methods that exist to determine the pavement system's moduli in-situ are tests that use deflection basin measurements and tests that use surface wave propagation measurements (which are based on velocity measurements rather than deflection measurements). The deflection basin tests can be divided into the following groups:

(1) static loading (i.e. the Benkelmann Beam and plate bearing test),
(2) steady state dynamic loading (i.e. Dynaflect),
(3) impact loading (i.e. falling weight deflectometer).

The moduli for the pavement system is back-calculated from these deflection basin test methods by using multilayer elastic analysis. Based on Nazarian et al. (1983), these deflection basin test methods and the back-calculation analysis have the following problems:

(1) only the overall stiffness is determined,
(2) determination of individual layer stiffness is difficult and results in nonunique solutions,
(3) the number and thicknesses of the layers should be known in advance (either assumed or from coring),
(4) for the steady state and impact loading methods, a dynamic loading is actually used in the field, but it is analyzed as a static loading in the elastic analysis, resulting in a difference between the actual and assumed stress distributions.

The surface wave propagation test method (i.e. SASW test) measures the velocities of elastic Rayleigh wave (R-wave) traveling through the pavement layers. Of all the nondestructive test methods, it is the most direct method to evaluate the in-situ elastic moduli and layer thicknesses. Since the wave velocity is directly related to the stiffness of the medium it is traveling through, elastic moduli can be directly determined. With the inversion process, moduli for individual layers can be determined, and from this moduli profile, layer thicknesses can be determined without any prior knowledge of the site. Based on experience by Drnevich et al. (1990) and Nazarian and Stokoe (1989), the model used for the SASW inversion analysis is more flexible than that of the model used to analyze deflection basin data, since more layers can be used during the analysis and the existence of a stiff subgrade (bedrock) at shallow depths does not create a problem with the solution.

In summary, the problems to be addressed by this research for the pavement applications are to assess the viability of the SASW test for the following items:

(1) determination of a relationship between the SASW test results and laboratory resilient moduli in order to obtain pavement design parameters directly in the field,

(2) determination of a relationship between the SASW test results and plate bearing moduli (both test pit and field) in order to relate this new method to existing methods for establishing pavement design parameters,

(3) evaluation of the accuracy of the SASW test method at estimating the surface layer thickness in the field,

(4) determination of a relationship between the SASW test results and the pavement pressuremeter (PPMT) to obtain moduli of the roadway substructure directly in the field, and

(5) determination of a roadway's substructure stiffness profile in order to evaluate the condition of the roadway and decide if it is safe to be left open to existing traffic.

1.3 Scope of Research

Currently, the Florida Department of Transportation (FDOT) does not possess the equipment for any type of seismic testing and the only means of performing any geophysical testing is by either ground penetrating radar or electrical resistivity, which are both very limited test methods. Therefore, as part of this research the SASW equipment was acquired and training on its use was conducted. However, the main objective was to evaluate the SASW test method and extending its use to geotechnical and pavement applications that are important to the FDOT. As a result, SASW testing was performed at several trial sites for direct application to FDOT needs for both soil and pavement sites.

1.3.1 Geotechnical Applications

A series of SASW tests were used to evaluate the effectiveness of a ground modification technique, and its results were used to determine degree of stiffness improvement and depth of improvement. This case study evaluated the SASW test with other methods to ensure proper compaction at the site either more accurately reflecting a larger volume of soil (compared to the in-situ penetration tests) or within a shorter period of time.

The stiffness profiles from SASW tests for various soil conditions were compared to stiffness profiles produced from empirically-derived relationships from different in-situ tests, such as the cone penetrometer and dilatometer tests. The SASW test is a direct means to develop an elastic stiffness profile at a test site, while these empirical relationships typically are obtained from correlations using a database consisting of both laboratory and field testing. This can lead to errors especially if testing is performed on soils which were not used in the initial database.

The SASW test was used to locate areas of soft surficial soils (either clay or organic deposits) on a roadway project. This study evaluated the potential of the SASW test to isolate problem areas where large deposits of soft surficial soils were present. These results could then be used to plan a soil testing program of penetration tests in these locations.

The SASW test was used to map out the top of limerock over a given test site. Due to the variability of the top of limerock throughout the state of Florida, many times penetration testing performed at intervals of 100 feet will not be sufficient to determine this depth accurately between test sites. This information is crucial in deep foundation design to establish pile or drilled shaft depths. The SASW results reflect more of a global stiffness which could be used to determine the top of limerock more accurately than individual penetration tests every 100 feet.

The SASW test was used for the detection of sinkholes and voids near the ground surface. Since the SASW test is a seismic test performed at the ground surface, a much larger volume of soil will be sampled for an individual test site compared to a penetration test. Therefore, the SASW test has the capability to detect large cavities near the ground surface over a much larger test area than an individual penetration test. Testing was performed in conjunction with ground penetrating radar (GPR) which is the standard means for the FDOT to map out potential sinkholes at a potentially high-risk site.

A portion of the field testing was performed to evaluate the reproducibility of the data obtained from the SASW test. Therefore, tests were performed at the same site under similar conditions with some time interval between tests, and the results compared to determine their similarity to account for the reliability of the test method.

1.3.2 Pavement Applications

A series of SASW tests on various base and subgrade materials was performed in the FDOT test pit facility. This study evaluated the effects of the materials' stiffness with moisture. The SASW results were related to the plate load tests results and the laboratory resilient modulus results.

To compare the various test results, a series of plots for similar materials were developed which show the relationship between modulus, strain, and applied stress.

A series of SASW tests were performed in the field in conjunction with field plate load tests performed at locations throughout the state. Relationships were developed to relate the SASW results with the field plate and laboratory LBR results since these are the existing means to evaluate the material's stiffness for roadway applications. As with the test pit results, a series of modulus versus strain curves were developed from the resilient modulus test results.

The SASW results were used in conjunction with pavement pressuremeter (PPMT) results in order to develop a modulus versus strain curve directly in the field. This has the advantage of testing the material under the same conditions that exist in the field (primarily the density and moisture content).

The primary focus of the pavement applications was to develop the modulus versus strain relationships for a variety of materials throughout the state on roadway construction. This was the most rational means to relate the various stiffness results from the numerous test methods commonly in use by the FDOT. In order for the SASW test to be a practical test for FDOT usage, these curves had to be developed as a first step in order for the SASW results to be related to other test results and to any design conditions (expressed in terms of a modulus for a desired strain). This correlation is needed because the stiffness from the SASW test is an elastic stiffness, and the values obtained from other tests and used for design purposes are in the nonlinear range and will be lower. Since these curves relate the modulus, axial strain, and applied stress for a variety of materials, they can be used to classify and relate various materials based on stiffness. In addition, these curves can be meaningful in providing data that could be used to obtain a stiffness profile for the various roadway layers which more accurately models the stiffness of the existing profile and the soil's response to an applied loading. This approach can be the first step in providing a more comprehensive stiffness profile for the pavement design process, instead of using a single value.

The SASW test was used to determine the layer thickness of the pavement, base, and subgrade layers at various field sites throughout the state, and these results were compared to the actual layer thickness to evaluate the accuracy of the SASW test method at detecting the layer interface.

The SASW test was used in a case study to evaluate the subsurface conditions at a roadway site with a potential void 10 feet under the pavement. This method was the only means available to develop a stiffness profile under the pavement surface as deep as was needed. The traffic was too heavy to allow coring through the pavement for penetration testing and the sampling depths for the falling weight deflectometer (FWD) and dynaflect tests were too shallow. Therefore, this study was used to determine if the SASW test could provide the necessary information for a determination of whether the roadway was safe to be left open to traffic.

CHAPTER 2
REVIEW OF THE LITERATURE

2.1 Background Information

The SASW method is not the first field seismic test to utilize surface waves (Rayleigh waves) to infer material properties at a site. Many publications by Jones (1958, 1962, and 1963) have shown the use of a method called the steady-state Rayleigh-wave method. This test consisted of an electromagnetic vibrator driven by a variable frequency oscillator and power amplifier, and a seismic geophone. The vibrator was set at a single frequency and the geophone was moved progressively away from the vibrator so that positions were measured when the vibrations were in phase with those at the source. The distance between successive positions were equal to one wavelength (λ_R) of the vibrations. Since the frequency (f) of the vibrations was known, the surface wave velocity (V_R) was determined by

$$V_R = f \cdot \lambda_R. \tag{2.1}$$

Adjusting the frequencies on the vibrator and repeating this procedure, a dispersion plot (surface wave velocity versus wavelength or frequency) was developed for the test site. This was time consuming and a simplified means to analyze the data had to be used, since more accurate methods to model the field data (inversion process) required more powerful computers. A typical means to interpret the field data (Heukelom and Foster, 1960) was to assume the following:

$$V_S = 1.1 \cdot V_R \tag{2.2}$$

$$Z = \frac{\lambda}{2} \tag{2.3}$$

where: V_S = shear wave velocity

V_R = surface wave velocity

Z = depth below ground surface

λ = wavelength.

Other researchers (Szendrei and Freeme, 1970 and Heisey et al., 1982a) used an effective sampling depth equal to the wavelength divided by three, since the centroid of the wave energy distribution is located at approximately $\lambda/3$ (see Figure 2.1). This empirical inversion process is based on the assumption of a homogeneous, half-space. The closer the test site is to a uniform profile, the better this analysis works. Since this is seldom the condition that exists at real sites (especially pavement sites), this process rarely produces meaningful results.

2.2 Basic Seismic Wave Theory

Seismic waves can be classified into two categories: body waves and surface waves. Body waves consist of either P-waves (primary, compression, or dilatational waves) or S-waves (secondary, shear, or distortional waves). Surface waves consist of such waves as Rayleigh waves (R-waves) and Love waves.

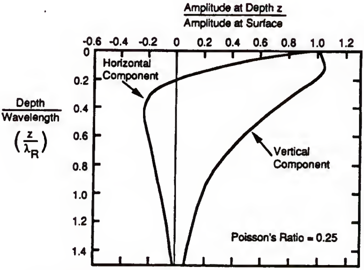

Figure 2.1 Variation in Particle Motion versus Depth for R-Waves (Richart et al., 1970)

The following characteristics of each wave is based on its propagation through an ideal medium, which is considered to be a homogeneous, isotropic, elastic half-space. A homogeneous material possesses a uniform structure or composition throughout the medium. An isotropic material has identical properties in all directions. An elastic material is one that returns to its initial form after deformation (removal of a load).

The particle motion for P-waves is a push-pull type of movement which is parallel to the direction of the wave front. For S-waves, the particle motion is a shearing movement, with a transverse displacement normal to the direction of the wave front. Particle displacement for R-waves have both a vertical and horizontal component, and the path of motion is a retrograde ellipse. As seen in Figure 2.1, the amplitude of the R-wave quickly decays with depth, and at a depth of one wavelength, the amplitude of particle motion is only 30% of the original amplitude at the surface, and at 1.5 times the wavelength, the amplitude is only 10% of the original.

The velocities of these waves are dependent upon the Poisson's ratio, ν, of the medium they propagate through. These velocities are propagation velocities of the wave fronts, and not particle velocities of the medium itself due to the wave energy. Comparing the various wave velocities, the P-wave is the fastest and will arrive at the receiver first. The R-wave is the slowest of the three wave types, but has a velocity which is close to that of the S-wave. The ratio of P- and R-wave velocities to S-wave velocity versus Poisson's ratio is illustrated in Figure 2.2.

The ratio of Rayleigh wave velocity to shear wave velocity (V_R/V_S) changes slightly with respect to the Poisson's ratio for an isotropic and homogeneous material, from 0.874 at

ν=0 to 0.955 at ν=0.5 (an incompressible material). This variation can be expressed by the following linear relationship (Roesset et al., 1990):

$$V_S = C \cdot V_R \tag{2.4}$$

$$C = 1.135 - 0.182 \cdot \nu \quad (for\ \nu \geq 0.1) \tag{2.5}$$

For most instances, the ratio of Rayleigh wave velocity to shear wave velocity can be assumed to be 0.90, which should result in an error of no larger than 5 percent (Nazarian et al., 1983).

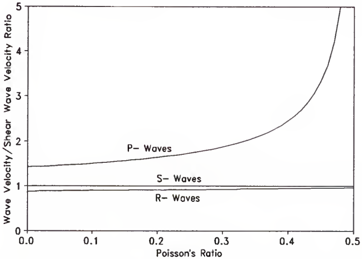

Figure 2.2 Relationship between Seismic Wave Velocities and Poisson's Ratio (Richart et al., 1970)

The ratio of compression wave velocity to shear wave velocity (V_P/V_S) can be related to the Poisson's ratio by the following theoretical elastic relationship:

$$\nu = \frac{0.5\left(\frac{V_P}{V_S}\right)^2 - 1}{\left(\frac{V_P}{V_S}\right)^2 - 1} \qquad (2.6)$$

The relationship between the S-wave velocity and the P-wave velocity can be approximated by the following equation but with a much higher degree of error:

$$V_S \approx 0.45 \cdot V_P \qquad (2.7)$$

Research by Woods (Richart et al., 1970) has shown that body waves (P- and S-waves) generated by a circular footing propagate outward along a hemispherical wave front, whereas R-waves propagate outward along a cylindrical wave front. The geometric damping is the decrease in energy or displacement amplitude due to the greater volume of half-space encountered by the wave. The damping of the body waves as they propagate outward from the source has been shown to be proportional to the ratio of 1/r (where r is the distance from the source) except along the surface of the half-space, where the damping is proportional to $1/r^2$. The geometric damping for R-waves generated by a similar source is proportional to a ratio of $1/r^{0.5}$.

Research by Miller and Pursey (Richart et al., 1970) has shown that a vertical oscillating, uniform distributed, circular energy source on the surface of a homogeneous, isotropic, elastic half-space produces a distribution of total input energy among the three elastic waves as shown in Table 2.1.

Table 2.1 Distribution of Total Energy Based on Wave Type

Wave Type	% of Total Energy
Rayleigh (R-Waves)	67
Shear (S-Waves)	26
Compression (P-Waves)	7

The following characteristics of R-waves make them an ideal choice for use in an in-situ seismic test:

(1) approximately 2/3 of the total input energy is transmitted away from the source as R-waves, and

(2) R-waves decay much slower than either P- or S-waves.

For a homogeneous, isotropic, elastic half-space (material properties are independent of depth), the R-wave velocity is independent of the frequency of the wave, and therefore all frequencies yield the same velocity. For an elastic half-space whose properties change with depth or a layered medium, the R-wave velocity varies with frequency, and this property is known as dispersion (refer to Figure 2.3 and note that the particle motion is the same pattern as shown in Figure 2.1).

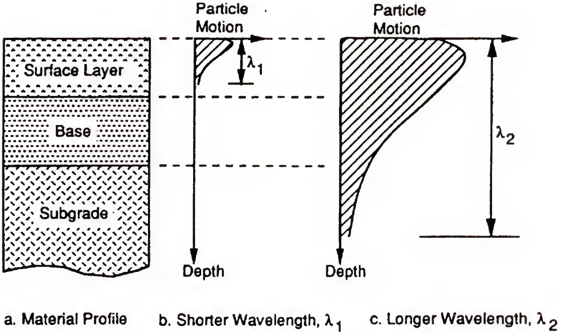

Figure 2.3 Principle of Dispersion for a Layered System (Rix and Stokoe, 1989)

Dispersion is the critical physical property behind the SASW test since it results in longer wavelengths sampling deeper materials (i.e. more soil layers) than shorter wavelengths (which sample only the top layers). For a given wavelength (see Figure 2.1), the average properties are sampled within approximately one wavelength of the ground surface; and therefore, the depth of measurement (or sampling depth) is approximately equal to $\lambda/2$ (assuming that the average properties are equally weighted over the full λ).

Since the centroid of the wave energy distribution is located at a depth of approximately $\lambda/3$, the average sampling depth is sometimes approximated as $\lambda/3$.

2.2.1 Effect of Water (Saturated Conditions)

Research by Biot (Richart et al., 1970) has shown that for an ideal-saturated solid, two types of dilatational waves exist: a compression wave transmitted through the fluid and another compression wave transmitted through the elastic structure. For this saturated medium, only compression waves are transmitted through the pore fluid. Therefore, the effect of the water table for granular soils acts like a interface to P-waves. Since pore water cannot transmit shear, the presence of the water table does not affect S-waves, and R-waves are only slightly affected. Because of this characteristic, there is a great advantage in using these waves (S- or R-waves) for in-situ steady-state seismic techniques.

The major difference between granular and cohesive soils under saturated conditions is the time required for consolidation to occur between load intervals. Therefore, reliable shear wave velocities for cohesive soils in the laboratory can be obtained at higher confining pressures if given enough time to allow a major part of the primary consolidation to occur. For some cohesive soils, the effects of secondary compression (in which the shear wave velocity continues to increase with time without increasing the load) can be significant.

Even though fully saturated conditions do not affect the transmission of S- or R-waves through the material, the presence of water does affect the soil's properties (especially its stiffness). For cohesionless soils, a saturated medium affects the shear wave velocity by adding to the mass of the particles in motion. If the particle mass increases, the shear wave velocity will decrease and thereby decrease the shear modulus (and the stiffness) of the material based on the relationship between shear modulus and shear wave velocity (Eqn. 2.10). To account for this added weight during the analysis, one needs to use the soil's total unit weight and the effective stress. This reduction of the soil's stiffness is supported by field work using the SASW test by Nazarian et al. (1987) on sites which were wet due to rain from previous tests at the same sites. The moist soil at the surface caused a significant drop in the elastic properties for the top several feet of soil.

2.3 Material Properties

The SASW test generates a R-wave profile directly from the field data (dispersion curve). Since R-wave velocities have little engineering significance in applications to design, this R-wave velocity profile is related to S-wave velocities through the inversion process. It is from this final step that the elastic properties of the medium can be determined, with practical parameters for engineering design.

Material properties can be determined either from field testing at the site or collecting samples from the site and performing laboratory tests on them. Based on Nazarian and Stokoe (1985), the problems with laboratory tests are sample disturbance, difference in the state of stress, nonrepresentative samples, and age effects. Although laboratory testing is essential to study the parameters affecting the properties of the materials at a site.

2.3.1 Shear Modulus

The shear modulus is a constant which relates the shear distortion caused by a shearing stress (refer to Figure 2.4) by the following relationship:

$$\gamma_{zx} = \frac{\tau_{zx}}{G} \tag{2.8}$$

where:
γ_{zx} = shear strain
τ_{zx} = shear stress
G = shear modulus.

Based on elastic theory, the shear modulus is related to the other elastic constants, Young's modulus (E) and Poisson's ratio (ν), by:

$$G = \frac{E}{2(1+\nu)} \tag{2.9}$$

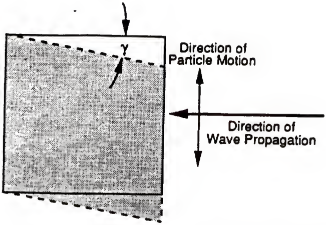

Figure 2.4 Shear Wave Deformation (Bay and Stokoe, 1992)

The shear modulus is directly related to the shear wave velocity in an isotropic and homogeneous material by the following elastic theory equations:

$$G = \rho (V_S)^2 = \frac{\rho (1-2\nu)(V_P)^2}{2(1-\nu)} \tag{2.10}$$

where:
G = shear modulus
ρ = mass density = γ_t/g
γ_t = total unit weight of material
g = gravitational acceleration constant
= 9.80 m/s^2 = 32.2 ft/s^2
V_S = shear wave velocity
ν = Poisson's ratio
V_P = compression wave velocity.

Based on research from Anderson and Stokoe (1978), the small-strain shear modulus determined from resonant column testing under a sustained pressure increases with time of confinement. This age effect consists of two modes: an initial phase from primary consolidation and a long-term time effect. Cohesionless soils only exhibit the long-term effect, which is a straight line on a semi-logarithmic plot of modulus versus time, while cohesive soils exhibit both phases. Studies from Anderson and Woods (1975) show that comparisons between field and laboratory shear moduli are good (within 10%) when this age factor is taken into account.

Direct measurement of shear wave velocity (and therefore, shear modulus) in the field can be accomplished by shear wave seismic tests such as crosshole or downhole shear wave testing (refer to ASTM D 4428/D 4428M; Stokoe and Woods, 1972; or Nazarian and Stokoe, 1984), or by use of the seismic cone penetrometer. The disadvantage of these test methods is that penetration of the soil or boreholes are necessary. The crosshole seismic test consists of installing a series of boreholes (usually 2 or 3) along a common line at a known distance apart. In one of the boreholes, a source is inserted to create a seismic wave. Receivers placed in the remaining borehole(s) measure the arrival of the seismic wave. Compression and shear wave velocities can be determined from the travel time of the seismic wave between a known distance apart (from source to receiver).

2.3.1.1 Cohesionless soils

Laboratory results. The shear modulus for cohesionless soils is affected by three major factors (Seed et al., 1986): the confining pressure, strain amplitude, and void ratio (or relative density). The effect of void ratio and confining pressure on both the shear wave velocity and shear modulus can be estimated by empirical relationships developed by Hardin and Richart (Richart et al., 1970). For round-grained sands (e < 0.80):

$$V_S = (170 - 78.2e)(\sigma_o')^{0.25} \tag{2.11}$$

$$G_{\max} = \frac{2630(2.17-e)^2}{1+e}(\sigma_o')^{0.5} \tag{2.12}$$

and for angular-grained materials:

$$V_S = (159 - 53.5e)(\sigma_o')^{0.25} \tag{2.13}$$

$$G_{\max} = \frac{1230(2.97-e)^2}{1+e}(\sigma_o')^{0.5} \tag{2.14}$$

where:
V_S = shear wave velocity (ft/sec)
$G_{\max}$ = small-strain shear modulus (lb/in^2)
e = void ratio
σ'_o = effective confining pressure (lb/in^2).

Based on experiments from Seed and Idriss (Seed et al., 1986), the following equation was developed:

$$G_{\max} = 1000K_2(\sigma'_m)^{0.5} \tag{2.15}$$

where: $G_{\max}$ = small-strain shear modulus (lb/ft^2)

K_2 = soil modulus coefficient

σ'_m = effective mean principal stress (lb/ft^2).

The soil modulus coefficient, K_2, is primarily a function of soil's grain size, the relative density, and the shear strain developed; and therefore, this one parameter takes into account the influence of void ratio and strain amplitude. This coefficient achieves a maximum value at strains on the order of 10^{-4}% for sand. Based on laboratory testing, values of $(K_2)_{\max}$ range from 30 for loose sands to 75 for dense sands. For gravels, values of $(K_2)_{\max}$ range from 80 to 180. The following equation can be used to determine appropriate values of $(K_2)_{\max}$:

$$(K_2)_{\max} \simeq 20(N_1)_{60}^{1/3} \tag{2.16}$$

where: $(N_1)_{60}$ = corrected SPT N-value at 60% efficiency.

Stokoe et al. (1988) have shown that Eqn. 2.15 can be used to infer in-situ densities from a measured shear wave velocity profile. Seed's equation for $G_{\max}$ can be written in the following form (with the units for V_S in ft/sec):

$$V_S = [(1000)(g/\gamma)(K_2)]^{0.5}(\sigma_m')^{0.25} \qquad (2.17)$$

where σ'_m (with the units in psf) is the mean effective stress and typically calculated as:

$$\sigma_m' = \frac{\sigma_v'(1+2K_o)}{3} \qquad (2.18)$$

where K_o is the effective coefficient of earth pressure at rest and σ'_v is the vertical effective stress at the depth of interest. Using Eqn. 2.18 involves the following assumptions: (1) level ground, (2) principal stresses oriented in the vertical and horizontal directions, (3) intermediate and minor principal stresses are equal, (4) age of deposit can be neglected, and (5) little or no cementation exists. Based on research from Stokoe et al. (1985), using σ'_m in relationships involving V_S or G_{max} is not correct since testing under true triaxial conditions has shown that V_S depends on the principal stresses in the directions of wave propagation and particle motion, and is relatively independent of the third principal stress. However, it was shown that the maximum variation by using σ'_m was only 12%, and it was reasonable to use as an approximation if further information was not available.

The variation of V_S with density and depth can then be plotted by assuming various values of K_2 for various qualitative density states (i.e. K_2 values of 30, 50, and 70 are representative values for a loose, medium dense, and very dense sand, respectively) and by calculating σ'_m for each depth.

Field results. For cohesionless soils, G_{max} and the cone penetrometer end bearing resistance (q_c) are dependent on the same variables: density and effective vertical and horizontal stresses. Even though both parameters occur at two widely different strain levels, q_c can be used to estimate G_{max} because both are a function of similar properties. The cone penetrometer sleeve friction resistance (f_s) is also a high strain strength index, but it is highly influenced by fabric sensitivity and over-consolidation effects, as is G_{max}.

Based on Riaund and Miran (1992a), the cone penetrometer test (CPT) can be used to estimate in-situ values of G_{max} by the following relationship developed by Jamiolkowski:

$$\frac{G_{max}}{q_c} \approx 30.1\,(\frac{\sigma'_m}{p_a})^{-0.08}\exp(-1.84D_r) \qquad (2.19)$$

where:

p_a = atmospheric pressure = 98.1 kPa

D_r = relative density (as a fraction of one)

q_c = cone resistance (kPa).

Riaund and Miran also present the following relationship developed by Imai and Tonouchi which can be used to estimate G_{max}:

$$G_{\max} = 125N^{0.611} \quad with \quad N = \frac{q_c}{4.5} \tag{2.20}$$

where: N = SPT N-value (blows per foot)

$G_{\max}$ and q_c are in bars.

Olsen (1988) developed a relationship for the CPT to predict the values of normalized maximum shear modulus, $(G_{\max})_1$ and K_2 as shown in Figure 2.5. This figure can be used for both cohesionless and cohesive soils, and it is recommended to use the range of $(G_{\max})_1$ or K_2 since the CPT measurements are only influenced and not controlled by the shear modulus. For normally consolidated conditions, the value of n presented in Figure 2.5 ranges from approximately 0.56 for coarse sands to slightly under 1 for clays and 0.79 to 0.9 for soil mixtures and silts.

Small-strain shear modulus can also be estimated by use of the dilatometer test (DMT) method using the following empirical relationship developed from research performed by Hryciw (1990):

$$G_{\max} = \frac{530}{\left(\frac{\sigma'_v}{P_a}\right)^{0.25}} \; \frac{\left(\frac{\gamma_D}{\gamma_w}\right) - 1}{2.7 - \left(\frac{\gamma_D}{\gamma_w}\right)} \; K_o^{0.25} \; (\sigma'_v \, P_a)^{0.25} \tag{2.21}$$

where: γ_D = DMT-determined total unit weight

γ_w = unit weight of water

σ'_v = effective vertical stress

P_a = atmospheric pressure

K_o = coefficient of lateral stress at rest.

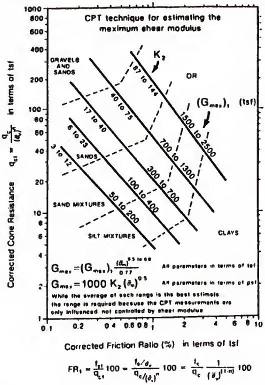

Figure 2.5 CPT Procedure for Estimating the Maximum Shear Modulus (Olsen, 1988)

Equation 2.21 seems valid for sands, silts, and clays. The average error in using this equation was 23% when compared to G_{max} values from in-situ crosshole and seismic cone tests.

There have been many empirical relationships developed to correlate the standard penetration test (SPT) blow count (N-value) with V_S or G_{max}. For a comparison study, refer to Sykora and Koester (1988). These are not included here since this study found a substantial range of potential errors associated with each relationship which may range from +50% to -40% of the calculated value.

2.3.1.2 Cohesive soils

Laboratory results. For cohesive soils, studies (Hardin and Black, 1968, 1969; Hardin and Drnevich, 1972a, 1972b) show that the small-strain shear modulus, G_{max}, is affected by void ratio (e_o), mean effective stress (σ_o'), overconsolidation ratio (OCR), and plasticity index (PI). Hardin and Black (1968, 1969) performed resonant column tests to develop the following empirical relationship for normally consolidated clays at the end of primary consolidation:

$$G_{max} = 625 F_e (P_a \sigma_o')^{0.5} OCR^k \tag{2.22}$$

where: G_{max} = small-strain shear modulus (lb/in^2)

F_e = void ratio function

P_a = atmospheric pressure (lb/in^2)

σ'_o = mean effective stress (lb/in^2)

OCR = overconsolidation ratio

K = empirical exponent related to plasticity.

The value of K, which depends on the plasticity index of the soil, can be obtained from the the values presented in Table 2.2 (Hardin and Drnevich, 1972b).

Table 2.2 Values of Exponent K versus Plasticity Index

PI	K
0	0
20	0.18
40	0.30
60	0.41
80	0.48
≥100	0.50

Hardin and Black (1968, 1969) first introduced the void ratio function (F_e) as (where e_o is the void ratio):

$$F_e = 0.51\frac{(2.973-e_o)^2}{(1+e_o)} \tag{2.23}$$

and substituting Eqn. 2.23 into Eqn. 2.22 and including the atmospheric pressure, the following relationships can be used as an estimate of shear modulus (G_{max}) and shear wave velocity (V_S):

$$G_{max} = \frac{1230\,(2.973-e_o)^2}{(1+e_o)}\,(OCR)^k\,(\sigma_o')^{0.5} \tag{2.24}$$

$$V_S = (159-53.3e_o)\,(OCR)^{k/2}\,(\sigma_o')^{0.25} \tag{2.25}$$

Other relationships that have been developed for F_e by Hardin and Jamiolkowski, Leroueil, and Lo Presti (Mayne and Rix, 1993), which studied larger databases to include a wider range of void ratios, are as follows:

$$F_e = \frac{1}{0.3+0.7(e_o)^2} = \frac{1}{(e_o)^{1.3}} \tag{2.26}$$

The effective octahedral normal stress (σ'_o) to be used in the preceding equations is as follows:

$$\sigma'_o = \frac{(\sigma'_1+\sigma'_2+\sigma'_3)}{3} \tag{2.27}$$

where σ'_1, σ'_2, and σ'_3 are the effective principal stresses, but can be estimated in the field by use of Eqn. 2.18.

Field results. Mayne and Rix (1993) have built a database of in-situ shear wave velocity (V_S) measurements and profiles of cone tip resistance (q_c) for 31 clay sites. The shear wave velocities at these sites were measured by either conventional crosshole (CHT) or downhole tests (DHT), Spectral Analysis of Surface Waves (SASW) tests, or seismic cone penetration tests (SCPT). The equation of the best-fit regression line for all 31 clay sites' data is as follows:

$$G_{max} = 2.78q_c^{1.335} \tag{2.28}$$

where G_{max} and q_c are both in kPa.

Relating this field data with other soil parameters at the test sites, Mayne and Rix determined that G_{max} is dependent on the in-situ void ratio (e_o), overburden stress (σ'_{vo}), and stress history (OCR). The parameter of q_c in clays is not greatly affected by e_o, but can be substituted for the interrelated parameters (σ'_{vo} and OCR) despite the incompatible strain levels between G_{max} and q_c. Based on multiple regression analyses, a better relationship for G_{max} utilizing q_c (and thus σ'_{vo} and OCR) and e_o is as follows:

$$G_{max} = \frac{406\,(q_c)^{0.695}}{e_o^{1.130}} \tag{2.29}$$

where G_{max} and q_c are both in kPa. This equation can be expressed in the following dimensionless form:

$$G_{max} = \frac{99.5\,(p_a)^{0.305}\,(q_c)^{0.695}}{e_o^{1.130}} \tag{2.30}$$

where: p_a = atmospheric reference pressure (same units as G_{max} and q_c).

This equation is quite limited since a profile of e_o at a test site is not usually known. Therefore, the use of the cone penetrometer test to obtain a shear modulus profile of a site consisting of clays is, at best, only an approximate method.

2.3.2 Young's Modulus

The Young's modulus is a constant which relates the axial compression and lateral expansion caused by a uniaxial stress (refer to Figure 2.6) by the following relationship:

$$\epsilon_a = \frac{\sigma_a}{E} \tag{2.31}$$

where:
ϵ_a = axial compression
σ_a = uniaxial stress
E = Young's modulus of elasticity
$\nu\epsilon_a$ = lateral expansion
ν = Poisson's Ratio.

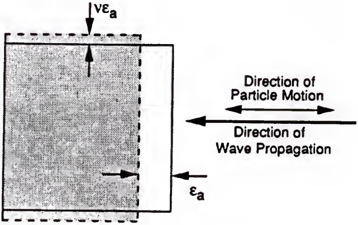

Figure 2.6 Unconstrained Compression Wave Deformation (Bay and Stokoe, 1992)

Since the wave propagation through the soil is a direct means of determining the stiffness of that soil, the Young's modulus for an isotropic and homogeneous material can be readily obtained from the following equations based on elastic theory:

$$E = 2G(1+\nu) = 2\rho(V_S)^2(1+\nu) = \rho(V_P)^2\left[\frac{(1+\nu)(1-2\nu)}{(1-\nu)}\right] \qquad (2.32)$$

where:

E = Young's Modulus

ρ = mass density

V_S = shear wave velocity

ν = Poisson's ratio

V_P = compression wave velocity.

Typical Young's moduli for some standard materials used in roadway construction obtained by SASW testing (Nazarian et al., 1988; and Nazarian and Stokoe, 1986a) are included in Table 2.3. The authors note that these values seem reasonable based on their experience, except for the wide range in the crushed limestone (which was probably caused by exposure to moisture and effects of time) and the high values for the sandy clay material.

Yoder and Witczak (1975) report typical Young's modulus values of 15 to 110 ksi for granular bases and subbases and 50 to 2,000 ksi for treated bases and subbases. For asphaltic cement, typical values range from 200 to 1,100 ksi (which is dependent upon age and temperature), and a range of shear wave velocities of 1,700 to 4,200 fps. For Portland cement concrete, typical moduli are 3,000 to 6,000 ksi (which is dependent upon curing time, type of aggregate, and water/cement ratio), and a range of compression wave velocities of 10,000 to 14,000 fps.

Table 2.3 Typical Values of Young's Modulus

Material Tested	Range of SASW Young's Moduli (ksi)
Asphaltic Concrete	338 - 605
Crushed Limestone	32 - 509
Crushed Limestone + 4% Cement	2500 - 3390
Crushed Limestone + 2% Lime	1200 - 1340
Sandy Gravel	25 - 33
Sandy Clay	50 - 51
Plastic Clay	17 - 34

2.3.2.1 Laboratory results

Resonant column and torsional shear tests. These laboratory tests can measure Young's moduli below the elastic threshold strain (0.001%) and to intermediate strains (0.1%). This range of Young's moduli is necessary to develop the complete stress-strain behavior of a soil in order for the nonlinear behavior to be taken into account when using the SASW modulus results.

For a torsional fixed-free type of resonant column test, a sample is rigidly fixed against rotation at the base, and the top end is connected to a drive system that is used to create a torsional motion on the sample. The sample is vibrated to the first mode of torsional motion, which is defined as the frequency at which the maximum top cap motion occurs during a sweep of frequencies (the material in a given cross-section at every elevation vibrates in-phase with the top of the sample). The resonant frequency and amplitude of vibration are measured, and the V_s, G, and shearing strain amplitude (γ) are determined. For a more detailed explanation of the test procedures, refer to ASTM D 4015 or Richart et al., 1970.

The torsional shear test uses the same equipment, but a cyclic torsional force with a given frequency is applied to the top of the sample (with a fixed bottom). The angle of twist and applied torque are measured, from which a stress-strain hysteresis loop is determined and the shear modulus and shearing strain amplitude are calculated. The resonant column test can generate higher strains at the same applied torque than the torsional shear test, so that more of the moduli versus strain curve can be developed.

Resilient modulus tests. This test has been adopted by AASHTO in 1986 for use in pavement design (refer to AASHTO T-292 or SHRP P-46). It is a cyclic triaxial test which tries to simulate the physical conditions and stress states of underlying soils under pavements subjected to traffic loadings. It cannot measure moduli at strains smaller than about 0.01%, so the complete stress-strain behavior of subgrade soils cannot be obtained (since the threshold strain cannot be determined) unless the soil is very stiff.

The sample is prepared to field conditions and is subjected to stress conditioning (200 to 1,000 cycles depending on the method used). The test is performed by applying numerous load/unload cycles (at a frequency of 1/3 to 1 cycle per second, typically with a 0.1 second loading cycle and 0.9 second rest period), and the load and resilient deformation (the strain that will be recovered once the load is removed) are recorded. The resilient modulus, M_r, is determined by dividing the deviator stress by the resilient axial strain.

To compare cyclic triaxial test results with resonant column results, Eqn. 2.32 can be used along with the following equation to relate axial strain (ϵ_a) to cyclic shearing strain (γ_c), where ν is the Poisson's ratio:

$$\epsilon_a = \frac{\gamma_c}{(1+\nu)} \tag{2.33}$$

This relationship is for uniaxial loading which relates normal strain and shear strain to Poisson's ratio, and it is common to assume a similar strain dependency between Young's modulus and axial strain as has been found for shear modulus and shearing strain.

Based on research by Kim and Stokoe (1992), results from resonant column, torsional shear, and resilient modulus tests overlap when the results are adjusted to a similar loading frequency and normalized based on confining pressure. This is an important point since the effects of strain amplitude and loading frequency need to be addressed to compare various field nondestructive tests (NDT) with the laboratory resilient modulus in order for it to be a practical design parameter.

2.3.2.2 Field results

Cone penetrometer tests (CPT). This test consists of a instrumented cylindrical rod with conical point being pushed into the ground under a constant rate of advancement. The parameters measured and recorded are the tip resistance, q_c, and the sleeve frictional resistance, f_s.

Several studies have been performed to evaluate the relationship between q_c and the Young's modulus, taking into account the appropriate strain level. Beraldi (Riaund and Miran, 1992a) performed studies on sands and recommended Figure 2.7 as an estimate of Young's modulus for a normal strain equal to 0.1%.

Dilatometer tests (DMT). This test consists of a steel blade being pushed into the ground. There is an expandable metal membrane on one side of the blade which can be expanded by pressurized gas. At a given test depth, a test is performed by measuring the pressures required to begin membrane movement and to expand the membrane into the soil 1.1 millimeter.

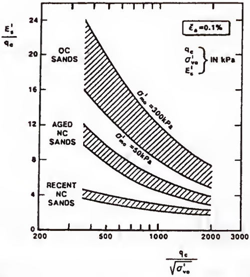

Figure 2.7 Drained Young's Modulus at 0.1% Strain from the CPT for Silica Sand (Riaund and Miran, 1992a)

Based on several sources, Robertson, Campanella, Baldi, and Bellotti (Riaund and Miran, 1992b), the initial tangent Young's modulus can be estimated from DMT results using the following equation:

$$E_i = F \cdot E_D \tag{2.34}$$

where: E_i = initial tangent Young's modulus

F = correction factor

E_D = dilatometer modulus.

The suggested values of F range from 2 for sands to 10 for cohesive soils.

Pressuremeter tests (PMT). The pressuremeter consists of a cylindrical probe typically inserted at a desired depth in a pre-drilled borehole. It can also be inserted by driving, pushing, or self-boring methods. This probe contains a flexible rubber membrane which is inflated with pressurized water so that it expands into the surrounding soils cylindrically. Typically, the measured volume change or hoop strain, $\Delta R/R$ (where $\Delta R/R$ is the change in radius divided by the initial radius), is plotted against applied pressure. The pavement pressuremeter (PPMT) is a smaller version of this test to be used in the relatively thin pavement system layers and is strain controlled to allow more detailed results and more accurate load/unload data for determination of resilient moduli (refer to Briaud, 1989).

The pressuremeter is a useful in-situ test because it can generate various moduli over a range of strains directly in the field. The strains involved are higher than the elastic threshold, but combining its results with the SASW test, a complete E/E_{max} versus strain curve for the soil conditions as they exist in the field can be generated.

Dynamic cone penetrometer tests (DCP). This test consists of a steel rod with a steel cone attached to one end which is driven into the ground using a sliding mass. Either the number of blows required to advance the cone into the ground at certain increments (usually 1 to 6 inches) or the depth of penetration after a certain set of hammer blows are recorded. The Penetration Index is defined as the average penetration depth resulting from one blow of the hammer, expressed in distance (inches or millimeters) per blow. This test provides a quick, simple, and inexpensive method to estimate the soil strength index of the in-place soils which is useful for roadway applications.

Preliminary research by Chua (Burnham and Johnson, 1993) has proposed a tentative empirical relationship between small-strain Young's modulus (MPa) and the DCP Penetration Index (mm/blow), which is presented in Figure 2.8.

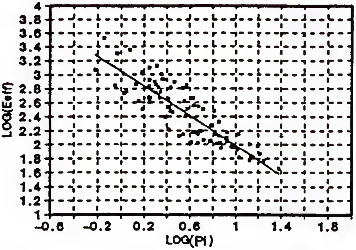

Figure 2.8 Relationship between Elastic Young's Modulus and the DCP Penetration Index (Burnham and Johnson, 1993)

The following is the equation for the best-fit line through the data as displayed in Figure 2.8:

$$Log\ E_{max} = 3.1 - 1.1(Log\ PI) \tag{2.35}$$

where: E_{max} = small-strain Young's modulus (MPa)

PI = DCP Penetration Index (mm/blow).

Static plate load tests. The plate load test involves a circular steel plate having a diameter ranging from 6 to 30 inches (typically 12 inches) which is placed at the surface of the material to be tested. A load, either static or dynamic, is applied to this plate. The load and deflections of the plate are measured.

The modulus for this test is determined from the following equation (assuming a one-layer system, or E_c is determined which is a composite modulus of a multi-layered system):

$$E_p = \frac{1.18pa}{\delta} \tag{2.36}$$

where: E_p = plate load modulus

p = applied pressure

a = radius of plate

δ = deflection of plate at pressure, p

1.18 = factor for rigid plate (use 1.5 for flexible plate).

The factor of 1.18 in Equation 2.36 is based on a Poisson's ratio of 0.50. It has been noted that granular soils used in roadway construction have Poisson's ratios typically ranging from 0.35 to 0.40, which might introduce some error in the use of Equation 2.36 with these types of materials.

Falling weight deflectometer (FWD). This test device provides a nondestructive test used to evaluate pavements. It consists of a trailer unit with a 150-kilogram weight mounted on a vertical shaft which can be hydraulically lifted to various predetermined heights (ranging from 0 to 400 mm). The weight is dropped onto a rubber pad to distribute the load uniformly, and the resulting force impulse is measured by load cells and 5 to 7 geophones. A deflection basin is determined, and a back-calculation analysis is performed to determine the stiffness profile at the test site which will result in a similar deflection basin for a static loading condition.

Based on comparison studies performed by Nazarian et al. (1988), FWD and SASW moduli compare well when pavement layers are thick and stiff so that both tests are performed in the linear elastic range and the pavement structure is simple; otherwise, the heavy loads used in the FWD test may be in the inelastic range and the moduli would be lower than the SASW moduli. Also, the FWD moduli will decrease with an increasing load level. Drnevich et al. (1990) report that FWD and SASW results give similar moduli if the assumptions associated with the models used for each test method are satisfied.

Dynaflect. This method is another nondestructive test to evaluate pavements, similar to the FWD. It also is a trailer unit, but its loading consists of two counter-rotating eccentric masses. This provides a cyclic loading of 1,000-pound (at a frequency of 8 Hz) in addition to the 1,000-pound base load of the loading wheels. This force is transmitted to the pavement by two 4-inch wide wheels. The deflection basin caused by this loading is measured by five geophones mounted on the trailer at one foot intervals. The FDOT has performed its own research to relate the Dynaflect deflections to field plate load test moduli in order to correlate the results to soil support values and structural layer coefficients.

Based on studies by Nazarian et al. (1983), moduli obtained from the Dynaflect varied from 13% to 45% with the SASW moduli. This difference can be attributed to the difference in strain amplitudes utilized by the two test methods.

2.3.3 Constrained Modulus

The ratio of axial stress (σ_a) to axial strain (ϵ_a) for confined compression (ϵ_r=0) is called the constrained modulus (M), as indicated in Figure 2.9.

The constrained modulus can be determined by the following elastic theory relationships for an isotropic and homogeneous material:

$$M = \rho\,(V_p)^2 = \frac{E(1-\nu)}{(1+\nu)(1-2\nu)} \tag{2.37}$$

where: M = Constrained Modulus

ρ = mass density

V_P = compression wave velocity

ν = Poisson's ratio.

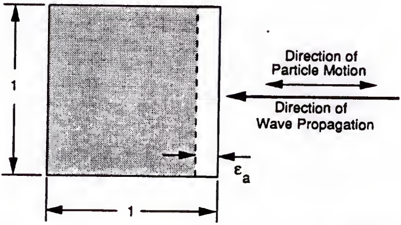

Figure 2.9 Constrained Compression Wave Deformation (Bay and Stokoe, 1992)

2.3.4 Nonlinear Effects on Moduli

For practical purposes, soil is an inelastic material. It has a very small elastic range, which is the range of strains that the soil particles recover their original shape and position after removal of an applied stress. The measured modulus of the soil is dependent upon the strain level at which measurements are recorded, as seen in Figure 2.10.

Because the SASW test is a seismic test, the distortion of the soil particles caused by the surface waves traveling through the soil medium is such a low strain (<0.001% strain) that the behavior of the soil is in the elastic range. Therefore, any material property obtained from this test is an elastic modulus, which represents the maximum limit for that material.

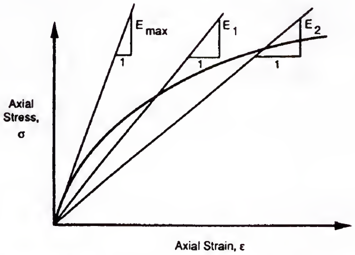

Figure 2.10 Nonlinear Soil Behavior based on Initial Tangent and Secant Moduli (Rix and Stokoe, 1989)

Other means of laboratory testing (resonant column or torsional shear) or field testing (pressuremeter) are needed to develop material curves relating modulus with axial strain. Several of these typical curves relating either the normalized shear modulus (G/G_{max}) or Young's modulus (E/E_{max}) with strain for various soil conditions (PI = Plasticity Index and σ'_o = effective octahedral normal stress) for both sands and clays are included in Figures 2.11 to 2.13. These curves were developed from resonant column test results and can be used as a first approximation to account for higher strain levels, but additional testing may be needed for more accurate results. As can been seen by these figures, the plasticity of the soil has a major affect on the nonlinear behavior of soils, shifting the normalized modulus towards increasing strain and an increasing elastic threshold as the PI increases (Bay and Stokoe, 1992 and Vucetic, 1991). Kokusho et al. (1982) have reported the value of overconsolidation ratio (OCR) has little effect on the position of the normalized modulus versus strain curve. For sands, the normalized modulus is affected by the confining pressure, but the difference is fairly small (Seed et al., 1986) and average results can be used to account for nonlinear behavior.

With these curves, the in-situ modulus at any given strain can be determined from the following equation (Rix and Stokoe, 1989):

$$E_{\epsilon,field} = E_{seismic} \cdot \left(\frac{E_\epsilon}{E_{max}}\right)_{lab} \tag{2.38}$$

where: $E_{seismic}$ = small-strain SASW modulus

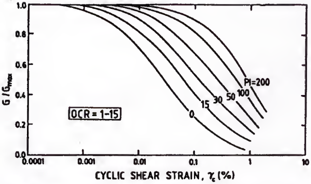

Figure 2.11 Variation of Normalized Shear Modulus and Plasticity Index for Cohesive Soils (Vucetic, 1991)

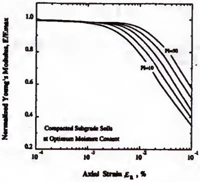

Figure 2.12 Variation of Normalized Young's Modulus and Plasticity Index for Compacted Subgrade Soils (Kim and Stokoe, 1992)

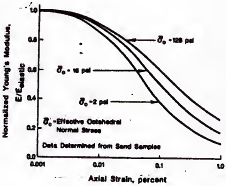

Figure 2.13 Variation of Normalized Young's Modulus and Effective Octahedral Normal Stress for Sand Samples (Nazarian et al., 1987)

$(E_\epsilon/E_{max})_{lab}$ = normalized modulus from cyclic lab test at a strain amplitude of ϵ

$E_{\epsilon,field}$ = field modulus at strain amplitude of ϵ.

The effect of the high frequencies used during SASW testing (especially for testing pavement surface layers), as well as the small strains, have a drastic effect on the comparisons of SASW moduli with other test results for asphaltic concrete (AC) materials. Based on studies by Roesset et al. (1990), the SASW results will be stiffer by a factor as high as four compared to falling weight deflectometer (FWD) results (refer to Figure 2.14) due to this frequency effect.

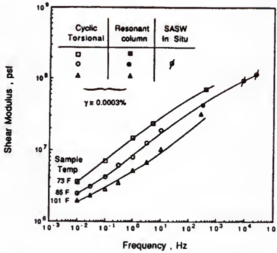

Figure 2.14 Effect of Frequency and Temperature on Small-Strain Shear Modulus of Asphalt Concrete (Roesset et al., 1990)

2.3.5 Poisson's Ratio

The Poisson's ratio, ν, is defined from elastic theory by the following relationship (refer to Figure 2.6):

$$\nu = \frac{-\epsilon_{lateral}}{\epsilon_{axial}} \tag{2.39}$$

The theoretical limits for the Poison's ratio for all isotropic materials are between 0 and 0.5, with practical limits being between 0.15 (concrete) and 0.5 for incompressible materials (saturated subgrades). Based on the Nazarian et al. (1988), typical values of Poisson's ratio and total unit weight based on the material's shear wave velocity are shown in Table 2.4. These values can be used for SASW analyses for different materials.

Table 2.4 Typical Values of Poisson's Ratio and Total Unit Weight

Shear Wave Velocity (ft/sec)	Poisson's Ratio	Total Unit Weight (lb/ft^3)
<1000	0.33	110
>1000 and <2500	0.25	125
>2500 (except for AC)	0.15	135

Typical values used for SASW analyses with an asphaltic-concrete surface layer were a Poisson's ratio of 0.25 and a total unit weight of 125 lb/ft^3. For common highway materials, Yoder and Witczak (1975) have reported typical values of Poisson's ratio of 0.20 to 0.45 for granular and treated bases and subbases, 0.25 to 0.40 for asphaltic cement (with a total unit weight of 125 to 145 lb/ft^3), and 0.10 to 0.25 for Portland cement concrete (with a total unit weight of 140 to 150 lb/ft^3).

The previous values of Poisson's ratio (Nazarain et al., 1988) were obtained from crosshole seismic tests (by measuring both shear and compression wave velocities), and reflect small-strain parameters which are representative for use during SASW analyses. Chen and Krizek (Nazarian and Stokoe, 1986a) report a variation of Poisson's ratio with strain, with values as low as 0.1 for small-strain measurements on sand.

CHAPTER 3
EQUIPMENT AND FIELD PROCEDURES

3.1 Equipment

The field equipment needed for SASW testing consists of two vertical receivers (either velocity transducers or accelerometers), a dynamic signal analyzer, a portable microcomputer, and a random wave generator. The following sections outline this equipment in more detail.

3.1.1 Signal Analyzer

The waveform analyzer is used to capture, store, and process the receivers' outputs. The signal analyzer is basically a dual-channel oscilloscope with a built-in microprocessor that rapidly filters and converts an analog signal to a digitized signal, and allows operations to be performed in either the time or frequency domain. With equipment that can perform frequency domain measurements, similar procedures used for the steady state R-wave method outlined in the previous chapter can be utilized as a practical and efficient field test.

Based on studies performed by Gucunski and Woods (1991), the disadvantages of using a full-function, dual-channel fast-Fourier-transform (FFT) digital signal analyzer is the cost (since the analyzer is being used to only a fraction of its capabilities) and the time lost in transferring the field data from the analyzer to the computer. Both of these factors need to be addressed for the SASW test to be a production-oriented test method. Gucunski and Woods have suggested other systems which are more cost effective. The first is a commercial software/hardware package for the computer which can perform data acquisition, waveform processing, and specific computer functions. The second option is a digital, transient waveform reader which can gather, digitize, and temporarily store the data until it is transferred to a computer to perform the FFT, dispersion, and inversion calculations. The third package is a FFT analyzer with a built-in DOS computer.

Current improvements in equipment are making it more cost effective to purchase a multi-channel signal analyzer. Research by Gucunski and Woods have shown that higher Rayleigh wave modes can influence the wave propagation pattern. Because of the interference of two or more Rayleigh wave modes of different phase velocities, the measured wavelength depends on the receiver locations. With a multi-channel analyzer, the receivers can be spaced in a grid pattern which can lead to automation (time savings) with a higher precision in the determination of the soil profile. The disadvantage of using a multi-channel analyzer is that more sophisticated data reduction procedures (including software) are needed.

3.1.1.1 Spectral analysis

The digital signal analyzer performs a FFT analysis to transform the time domain waveforms from both receivers into the frequency domain. It then performs various spectral analyses (or statistical operations on one or two signals in the frequency domain) on each frequency component. The advantages of performing a spectral analysis on the field data are as follows (based on Heisey et al., 1982a):

(1) data can be extracted that is not apparent in the time domain (for instance, the amplitude and phase of each frequency component),

(2) relationships between two signals can be identified,

(3) ease of numerical operations, and

(4) most measurements do not require a synchronized trigger.

The two primary spectral analyses functions performed during SASW testing are the cross power spectrum and the coherence function (for more information concerning FFT and spectral analyses functions, refer to Heisey et al., 1982a and 1982b; Nazarian and Stokoe, 1986a). Plots of typical Channel 1 and 2 time histories, as well as the cross spectrum and coherence as they appear on the signal analyzer are presented in Chapter 4 as Figures 4.9 and 4.10.

The first step in the analysis is that for each spacing, the time histories recorded by both receivers are broken down by frequency into a linear spectra, $S_x(f)$, of the two signals. The linear spectrum is the Fourier transform of the signal and provides both magnitude and absolute phase information for all frequencies within the measured bandwidth. The cross spectrum, $G_{yx}(f)$, is the Fourier transform of the cross correlation function between two different signals, X(t) and Y(t), and is defined as:

$$G_{yx}(f) = S_y(f) \cdot S_x^*(f) \tag{3.1}$$

where: $S_y(f)$ = linear spectrum of output

$S_x^*(f)$ = complex conjugate of linear spectrum of input.

The signal from the first channel is classified as the 'input', and the second channel as the 'output'.

The phase of $G_{yx}(f)$ is the relative phase between two signals for each frequency in the measured bandwidth and is used to determine the phase relationships between two signals (detected by a pair of receivers) which are caused by time delays, propagation delays, or varying the wave paths between receivers. Since it is a relative phase, measurements can be made without the use of an synchronized trigger.

The coherence function, $\gamma^2(f)$, is a real-valued function which is the ratio of response (output) power caused by the measured input to the total measured response power, and is an indication of the quality of the input signal at each frequency in the measured bandwidth. The coherence function requires two or more averages to be determined because for only one set of input and output, the coherence function will always equal one. A low value is an indication that there is background noise in the measurement, resulting in a poor quality signal, or it may suggest that more averaging is required to improve the signal to noise ratio. The signal analyzer needs to be able to average two or more signals (and allow the operator to accept/reject an individual blow from being averaged) in order to cancel out the background (random) noise while the impulse (source) remains constant and repeatable. A high value of coherence (0.90 to 1.0) indicates little background noise and a strong signal, since a value of one means that all the output at a particular frequency is due to the measured input. It is within this range of high coherence that the phase of the cross spectrum is used for the data reduction process in order to assemble the field dispersion curve.

3.1.1.2 Dispersion calculations

The cross power spectrum represents the relative phase lag or shift between the two receivers for each frequency in the measured bandwidth, and this phase lag occurs due to the signal having to travel further to get the second receiver. The cross power spectrum is displayed on the signal analyzer in a wrapped format and needs to be converted into an un-wrapped format (see Figure 4.10) before any calculations can be performed. Since space is limited on the screen of the signal analyzer, the phase of the cross spectrum is viewed between the limits of +180° and -180°. The plot displays jumps between these two limits, which represent the same points, and the actual phase for each frequency is determined by keeping count of the number of 360° cycles preceding each frequency and adding that to the fraction of the remaining cycle.

A time lag equal to one period of the signal represents a phase lag of 360°. Therefore, the time for the signal to travel between the two receivers is as follows:

$$t(f) = \left(\frac{\phi(f)}{360}\right)T = \frac{\left(\frac{\phi(f)}{360}\right)}{f} \tag{3.2}$$

where:
$\phi(f)$ = phase of the cross power spectrum
$t(f)$ = time
T = period = $1/f$
f = frequency = $1/T$.

Knowing the signal's travel time between the two receivers and the spacing between them, the phase velocity can be determined from the following equation:

$$V_{ph}(f) = \frac{x}{t(f)} = \frac{xf}{\left(\frac{\phi(f)}{360}\right)} \tag{3.3}$$

where:
$V_{ph}(f)$ = phase velocity
x = spacing between receivers.

With this information, the wavelength at a particular frequency for the signal can be determined by:

$$\lambda_{ph}(f) = \frac{V_{ph}(f)}{f} = \frac{x}{(\frac{\phi(f)}{360})} \tag{3.4}$$

where: $\lambda_{ph}(f)$ = wavelength.

Using these equations, a field dispersion curve (phase velocity versus wavelength or frequency) can be developed for the entire range of frequencies analyzed. The dispersion curve is usually plotted with respect to wavelength because it relates directly to sampling depth. By definition the phase velocity is the velocity at which a seismic disturbance of a single frequency propagates through the medium. Values of phase velocity are also called apparent Rayleigh wave (R-wave) velocities. They are not actual R-wave velocities for individual layers because they represent composite velocities for the entire profile, which are the result of overlying layers affecting the velocities of underlying layers. The inversion process is needed to determine actual R-wave velocities from these apparent R-wave velocities. If surface layers with similar velocities are encountered, comparison of dispersion curves can be performed as an indicator of the relative percent difference in the stiffness of different sites. This is especially useful for situations involving a 'good' versus 'bad' site as a quick indicator (since no inversion is required) that something is wrong at the 'bad' site. In the case of a layered medium in which there is no significant contrast in velocities, which is more applicable to soil sites, the apparent and actual R-wave velocities are approximately equal, and the empirical inversion process (as outlined in Section 2.1) can be used to estimate velocities.

3.1.2 Receivers

Two types of receivers are used during field testing, depending upon the application. These receivers consist of either geophones or accelerometers. For pavement sites, Nazarian and Stokoe (1985) have used accelerometers for short spacings (1/2 to 8 feet) and geophones for longer spacings (greater than 8 feet). Typically, geophones are used exclusively for soil sites, and either accelerometers alone or a combination are used for pavement sites depending on the desired depth of surveying. Based on Heisey et al. (1982a), geophones have a good response up to at least 3 kHz, and for higher frequencies, accelerometers should be used.

3.1.2.1 Geophones

Based on experience by Stokoe et al. (1989), geophones (velocity transducers) should be used primarily for soil sites so that lower frequency waves (less than 500 Hz) can be captured. Nazarian and Stokoe (1985) have indicated that the capture of lower frequencies (i.e. greater sampling depths) is limited by the natural frequency of the receiver (the undamped natural frequency of the coil-magnet system of the geophone) as well as the lowest frequency being generated by the source.

Lower frequency waves (corresponding to longer wavelengths) are needed for soil surveys since the waves have to penetrate deeper soil deposits to adequately test the site. As a general rule, the average effective sampling depth of soils surveyed is from one-half to one-third of the wavelength of the source wave (Heisey et al., 1982a and 1982b). Vertical geophones are used in order to measure the vertical component of the R-wave motion. Studies by Heisey et al. (1982b) have shown that horizontal geophones should not be used since they are more sensitive to P-wave motions.

Good coupling between receiver and material being tested is essential for accurate seismic measurements. Krohn (1984) has suggested that for very loose soils, geophones should be buried slightly for better coupling. For firmer soils, the use of spikes attached to geophones is adequate.

3.1.2.2 Accelerometers

Research by Stokoe et al. (1989) have shown that accelerometers should be used on pavement sites since higher frequency waves (greater than 20 kHz) need to be captured to adequately sample the shallow layers of the pavement profile. Piezoelectric accelerometers have a high natural frequency (30 to 100 kHz) which allow them to perform more accurately at higher frequencies, and they are much smaller than geophones which make them more appropriate for closer spacings (since errors in spacings are directly proportional to errors in the velocity measurements). Research by Sheu et al. (1986)

revealed that accelerometers should be used in pairs (same type and model) because pairing different types of accelerometers has been shown to cause erroneous results. This research also has shown that the natural frequency of the accelerometer has no effect on the measurements, rather it is the resonant frequency of the coupled accelerometer/pavement surface system which has a significant impact on the measurements.

Typically, the accelerometers are attached to the pavement surface by using a mounting wax (beeswax), with just enough wax to ensure adequate bonding. Sheu et al. (1986) have shown that without adequate coupling (i.e. receivers placed freely on the ground surface without any coupling mechanism), the accelerometers tend to collect low quality data. Magnetic bases can be used to attach the accelerometers to steel disks that have been epoxyed to the pavement surface or to nails which have been driven into the asphalt surface. This option is necessary because the wax can melt on very hot days, and a proper bond between pavement and accelerometer is not achieved. Proper coupling becomes even more critical when monitoring higher frequencies (especially for concrete pavements), otherwise the high frequency data is lost and the near-surface layers will not be accurately measured.

3.1.3 Source

Since the SASW method requires the dispersive characteristic of seismic waves to reflect the site's layer changes, the source needs to generate surface waves over a wide frequency range with a minimal amount of P- and S-wave energy. SASW testing performed for studies by Stokoe et al. (1989) have used waves ranging from 10 Hz to more than 50 kHz. The significant criteria for the source is the range of frequencies which can be excited and not the stress level induced by the impact. Research by Heisey et al. (1982b) has shown that the magnitude of energy generated by the source is not as critical as the coupling, or energy transfer, of the source to the soil. Therefore, it is desirable to use a large flat mass directly in contact with the soil, without the use of an intermediate plate, in order to provide better coupling between the hammer and soil to generate low frequency waves.

For soil sites, the source to be used is dependent on the transducer spacing. A sledge hammer can be used for lower spacings (up to a spacing of about 16 feet). For intermediate spacings (16 to 32 feet), a drop hammer device has proven successful. Spacings larger than 32 feet require a bulldozer moving back and forth within a 15 to 20 foot strip parallel to the receivers (Stokoe et al., 1989). Research has also shown that a deep dynamic compaction drop hammer works well, but with this type of source, the SASW test would not be classified as a nondestructive method. Case studies by Stokoe et al. (1988) indicate that surveys using deep dynamic drop hammers have generated wavelengths measured as long as 500 feet.

For pavement sites, several types of hammers are needed. Based on the opinions of Nazarian and Stokoe (1985), the source to be used for flexible pavements should generate frequencies up to 6 kHz, and the upper boundary for rigid pavements is on the order of 10 to 20 kHz. The duration of the source is proportional to its weight (Hiltunen and Woods, 1990). Lighter hammers produce a short-duration impulse which spreads out energy over a wide range of frequencies which are needed to sample the uppermost layer (asphalt layer). A larger hammer (i.e. sledgehammer) produces a long-duration impulse in which the energy is concentrated at the lower frequencies which is needed to sample the lower layers of the system (base and subgrade layers). In fact, Hiltunen and Woods (1990) have suggested that no single source can duplicate 'optimum' results, and that the best results are obtained when the data is combined using both a light-weight source (4-oz. ball-peen hammer) and a heavier source (sledgehammer).

Based on studies by Nazarian and Stokoe (1983), a sledgehammer was used as a source on concrete pavements, which generated frequencies up to 3,900 Hz (corresponding to sampling depths of approximately 3 inches). Therefore, a source is needed to develop higher frequencies in order to sample the top of the pavement, thereby improving the resolution of the dispersion curve and accuracy of the results. A V-meter, which is commonly used to measure compressive wave velocities of ultrasonic pulses traveling through solid materials, has been used as an effective source (Sheu et al., 1986) for generating frequencies up to 100 kHz for near-surface profiling (within the top 2 inches of AC pavement layers). The disadvantage of the V-meter is that it's output energy is fixed so the distance between receivers and source is limited to about 1.5 feet, making its application restricted to only shallow sampling depths. Research using pulsating crystals has proven successful to generate high frequency waves (greater than 20 kHz) to sample the upper portion of the pavement surface layer. Similarly, piezoelectric shakers have produced waves with frequencies ranging from 1 to 50 kHz (Roesset et al., 1990).

3.2 Software

The two computer programs needed to analyze the SASW field data are a Transfer and an Inversion program. Without this software, the empirical methods previously described need to be used to analyze the data, limiting the accuracy of the SASW results.

3.2.1 Transfer Program

The Transfer program assembles a single composite field dispersion curve from the forward and reverse profiles at each of the individual spacings, using the data within the acceptable ranges of coherence (0.9 to 1.0). This program employs a filtering criteria which is used on the raw data to eliminate the near-field effects (contamination of R-waves by shear and compression waves). Since body waves have different dispersive characteristics than surface waves, their effects need to be eliminated or the resulting dispersion curve would be altered. The typical procedure is to select the spacings between receivers, perform the SASW test, reduce the data to determine wavelengths and velocities, and eliminate the data that does not satisfy this filtering criteria. There have been many numerical studies to evaluate which criteria should be followed to ensure the existence of only plane R-waves (Sheu et al., 1988 and Roesset et al., 1990). Heisey et al. (1982b) have reported that this filtering criteria should be set according to the following relationship:

$$\frac{X}{2} < \lambda_R < 3X \qquad (3.5)$$

where: X = distance between receivers

λ_R = measured wavelength.

It was determined by Sheu et al. (1986) that the lower limit (X/2 <) should be removed since it was related to the accuracy of the measuring equipment, and found not to be justified with the new equipment in use. Sanchez-Salinero et al. (1987) determined that the useful range of measured wavelengths was less than the distance between receivers (X) for a desirable SASW testing configuration of:

$$\frac{d_2}{d_1} \geq 2 \qquad (3.6)$$

where: d_2 = distance between source and far receiver

d_1 = distance between source and near receiver.

Based on field data from further research (Sheu et al., 1986 and 1988), this criteria proved to be too conservative and suggested that the upper limit of the old Heisey criteria (< 3X) provided good results, as well as providing additional low frequency data which is important to the analysis.

The research by Hiltunen and Woods (1990) has shown that wavelengths longer than 2X should be eliminated and if this criteria is followed, the distance between the source and near receiver (D) should not affect the final results. This is an important criteria to follow if the SASW test is to be developed into a automated trailer unit using the common source geometry configuration (which is outlined in Section 3.3.2).

The composite dispersion curve is made up of hundreds of individual points from different spacings which will overlap over a wide range of wavelengths or frequencies. This redundant data provides confidence to the user concerning the accuracy of the overall dispersion curve. Since computer storage and run-time are limited, the number of points is reduced to 30 to 60 by statistical means. The average value and corresponding standard deviation are calculated for each point as a measure of the scatter of the data. This average dispersion curve, which has the points evenly distributed between the minimum and maximum measured wavelengths, is then used in the inversion process.

3.2.2 Inversion Program

The Inversion program develops a theoretical dispersion curve based on an assumed stiffness profile, which is compared to the actual field dispersion curve until a match is obtained. The idealized model used for the SASW inversion process assumes each layer in the soil or pavement profile to be continuous with a constant thickness in all horizontal directions, as well as being homogeneous, elastic, and isotropic. It is important to consider this model during field testing since sites consisting of broken-up concrete pavement as a base or those with badly cracked pavements will yield bad results because this model is being violated, as indicated by Drnevich et al. (1990).

The assumed input parameters for each layer of this theoretical profile are the mass density (ρ), Poisson's ratio (ν), shear wave velocity (V_S), and layer thickness (t). Since the mass density and Poisson's ratio have less than a 10% effect on the final shear wave velocity profile (Nazarian and Stokoe, 1986b and Stokoe et al., 1988), these values are usually assumed initially from existing typical values and remain constant throughout the trial and error process.

Nazarain and Stokoe (1986a and 1986b) studied the influence of the input parameters on the shape of the dispersion curve. It was determined that the absolute values of the mass densities of different layers do not affect the shape of the dispersion curve, but rather it is the contrast in mass densities which cause some changes in the curve. This study also concluded that if the thickness of the layers were changed by a constant factor, the shape of the dispersion curve was not altered, but the curve was scaled proportionally to this factor.

It is best to know as much information about the site as possible to determine any layer breaks (i.e. boreholes or cone penetrometer soundings), since work by Rix and Leipski (1991) has shown that the inversion process will average the velocities of the true soil profile when a single layer in the inversion analysis spans the boundary between two or more layers in the true profile. Therefore, if little is known about the site, thinner layers need to be used in the inversion analysis to reflect the true soil profile. Also, thinner layers should be used near the ground surface with larger layers being used as the depth increases, especially for pavement sites since near-surface materials are generally of most interest.

Rix and Leipski (1991) performed numerical analyses to determine how various effects influence the accuracy and resolution of the inversion results. This research evaluated the influences of the distribution of dispersion data with wavelength, of the maximum wavelength measured, and of the number of dispersion points used in the analysis. Their results indicated that the best solution was to use a dispersion curve with points that are evenly distributed between the minimum and maximum measured wavelengths, with a maximum measured wavelength equal to one to two times the desired depth of sampling to yield reasonably accurate and well-resolved back-calculated velocities. Increasing the number of points used for the dispersion curve (from 20, 40, to 60) increased the resolution of each layer, but the differences were slight. Since the number of points increases the computer run-time, this advantage is not worth increasing the number of points.

Based on a sensitivity study performed by Rix and Stokoe (1989) on a pavement site, the surface layer modulus (for a concrete slab) was determined to within 10% of its in-situ value (determined by crosshole seismic testing). The moduli of the other near-surface layers were determined to within 10 to 30% of the in-situ values. This study also determined that the lateral variability of a site (primarily for soil sites) played an important role in determining the resolution of the SASW results, especially for the near-surface layers. Other studies (Nazarian and Stokoe, 1989) have also indicated that the difference between SASW and crosshole seismic moduli is typically within 25%, and the shear wave velocities are within 10% to 20%, but are usually less. Hiltunen and Woods (1988) have concluded that 30% of this discrepancy can be accounted for by ignoring the wave path curvature in crosshole tests, yielding velocities which are too high. Sheu et al. (1986) have reported that the SASW method is very reproducible, and testing at the same site produced less than 5% scatter among three or more tests.

The inversion process is the critical process in the SASW analysis, and the area where most of the current research is being performed to improve the existing methods. Meier and Rix (1993) performed a feasibility study to determine if an artificial neural network can be used for the inversion process. A neural network consists of many interconnected processing units similar to the organization of the neurons in the brain, and it can be 'trained' through repeated exposure to a set of data (consisting of input-output pairs) to recognize common features and generalize an ideal mapping from imperfect examples. Based on their findings, this approach offers a much quicker solution than existing inversion programs and it can take advantage of realistic, 3-D solutions, whereas current methods are limited to 2-D solutions.

For a layered system, higher order modes of Rayleigh wave vibrations may occur, depending upon soil stratification, frequency of excitation, and material properties at the site. Therefore, it is possible to have different velocities for any given frequency. Research by Tokimatsu (1992) has shown that higher modes or multiple modes of Rayleigh waves can be created for stiff over soft profiles (i.e. pavement sites). This can lead to ambiguity in the uniqueness of the soil profile produced by the inversion process, since these algorithms assume that the observed dispersion characteristics are that of the fundamental Rayleigh mode. This research has developed formulas to take into effect these multiple modes on the R-wave dispersion curve which can be incorporated into any of the current inversion analyses. For sites with shear wave velocities increasing with depth (i.e. typical soil sites), this research determined that the fundamental mode dominates and no correction was necessary.

3.3 Field Procedures

Conceptually, the steady-state Rayleigh wave method and the SASW test are similar except for the source, which is a transient source for the SASW test that excites a wide range of frequencies, and the means to analyze the field data. For a single impact record, many different frequencies (and therefore, wavelengths and velocities) can be measured and construction of the dispersion curve can be developed in less time. With the advances in signal analyzer technology, which can analyze component frequency data rapidly, the SASW test has become a practical engineering tool.

Based on experience from Nazarian et al. (1987), the usual time to perform a standard SASW test can be divided into two portions: the field work, which takes approximately 30 minutes to perform, and in-office data reduction, which can take as long as two hours. The typical configuration used for a standard SASW test is shown in Figure 3.1. The only pieces of equipment not shown in this figure are a portable microcomputer, which is not necessary since the signal analyzer allows storage of the field results on a 3.5-inch disk and the data reduction can be performed entirely in the office, and a portable generator which supplies power to the signal analyzer. With a portable microcomputer in the field, the operator can create the field dispersion curve for the test to ensure the quality of the data and determine instantly if retesting is needed.

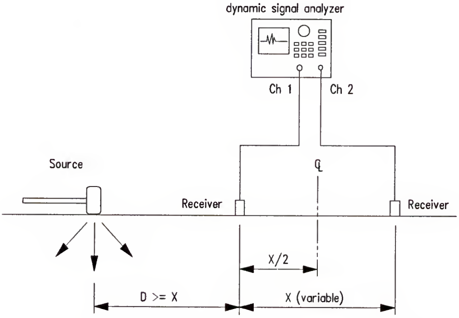

Figure 3.1 SASW Field Test Configuration

A single spacing per test can theoretically be used to assess the stiffness profile at a site, but practical considerations such as attenuation (wave energy diminishing with distance traveled), resolution (not being able to measure longer wavelengths at closer spacings), and near-field effects (contamination of R-waves by body waves) make it necessary to vary the spacings.

Studies by Heisey, et al. (1982a) indicate that the following factors affect the appropriate spacing of the receivers: velocity of the material, depth of the investigation, range of frequencies tested, attenuation properties of the substructure, and sensitivity of the instrumentation (both of the receivers and recording device).

3.3.1 Common Receivers' Midpoint Geometry (CRMP)

Several types of source/receiver arrangements have been used by researchers. The most common arrangement, presented by Nazarian and Stokoe (1984), is the common receivers' midpoint geometry (CRMP) shown in Figure 3.2. The centerline for the two transducers remains fixed and the spacing between them is increased. A forward and reverse profile is performed at each spacing to eliminate any phase shift due to the receivers and signal analyzer, and to average out any variation at the site due to sloping layers. It is important to note that the area between the receivers is important, and the properties of the materials between the source and near receiver have little effect on the results (Nazarian et al., 1983). This is an important consideration for excessively hard impacts, since the possibility of a localized non-linear zone can occur in this area, but the material between the receivers is still in the linear elastic range. For a soil site, typical distances betweens transducers are 4, 8, 16, 32, 64, and 128 feet to evaluate soils to an approximate depth of 60 feet (Stokoe et al., 1988). Figure 3.2 presents typical spacings which can be used for pavement applications to evaluate shallower depths.

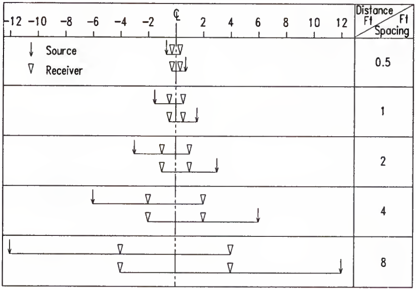

Figure 3.2 Common Receivers' Midpoint Geometry (CRMP) Configuration (Nazarian and Stokoe, 1984)

Research by Rix and Leipski (1991) has shown that the CRMP configuration results in dispersion curves with a large number of short wavelength data. Therefore, they suggest that the field spacings be altered to collect less short wavelength data and concentrate on medium to longer wavelength data (i.e. 1, 4, 16, 32, 64, and 128 feet spacings), or to record the field data using a log frequency scale instead of the commonly used linear scale, which would provide more longer wavelength data.

3.3.2 Common Source Geometry (CS)

In the common source geometry (CS) arrangement, shown in Figure 3.3, the source remains fixed and the receivers are moved the appropriate distances to ensure the proper spacings. Based on work by Hiltunen and Woods (1989), the results obtained from these two types of configurations, CRMP and CS, are similar for pavement sites since the material is placed under controlled conditions and the lateral extent of the array is less for pavement sites (± 8 feet) than soil sites (50 to 100 feet).

3.3.2.1 Automated SASW method

The CS arrangement is the preferred geometry for a multiple receiver array with a fixed source location needed to adapt the SASW test to a fully automated test which could be performed on a trailer unit. Preliminary research by Hiltunen and Woods (1990) have evaluated factors needed to be addressed in order for this automated process to be initiated which include source-receiver configuration, location of source, and types of sources. With the CS configuration, multiple receivers would be lowered onto the pavement surface, a single wave would be generated, and a multi-channel signal analyzer would process the signals from each of the receivers simultaneously. This would be necessary if this testing method were to be used as a production-oriented field test for long surveys involving pavements.

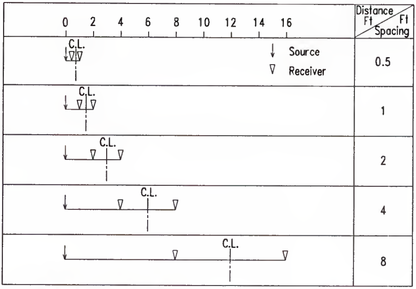

C.L. = Centerline of Receivers' Geometry

Figure 3.3 Common Source Geometry (CS) Configuration (Heisey, 1982b)

Nazarian et al. (1994) have developed such a system, including the software. The field testing involves a 16-channel system which uses a data acquisition board with signal analysis software, making the system more cost effective. The total test time, including reduction of field data, takes approximately 30 minutes. The software involves two programs which uses the field data from each of the receivers and assembles the composite dispersion curve (Nazarian and Desai, 1993), and uses this curve to produce a stiffness profile at the site (shear wave velocities and layer thicknesses are generated). This software has been shown to be effective for both soil sites (Yuan and Nazarian, 1993a) as well as for pavement sites (Yuan and Nazarian, 1993b). A 10 to 15% variation in the final shear wave velocity profile is anticipated using the automated software, but the advantages of this automated method are that less time and a less trained operator are required for its use.

3.3.3 Common Near Receiver Geometry (CNR)

A third arrangement used by Drnevich et al. (1990) is the common near receiver (CNR) geometry presented in Figure 3.4, in which the receiver closest to the source remains fixed, and the source and the second receiver are moved to ensure the proper spacings. The CNR has the advantage of saving some field testing time since only one receiver needs to be moved, and moving the receivers is a time-consuming process during field testing.

Both the CS and CNR arrangements do not have a common centerline (as seen in Figures 3.3 and 3.4), so that reversing the profile is not possible as it is in the CRMP arrangement. Therefore, these arrangements will not reflect any nonhomogeneity at the site, and should be used only for pavement sites which have uniform and horizontal layers. For soil sites, the CRMP arrangement is recommended since reversing the profile is possible which should average out the effect of sloping layers at a site, and research by Nazarian and Stokoe (1983) have shown that the CRMP configuration gives less scatter than the CS arrangement.

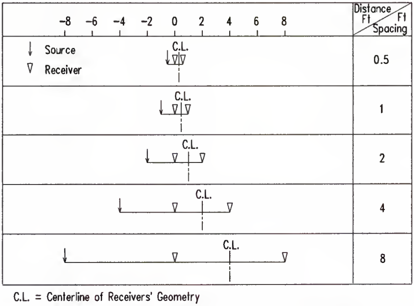

Figure 3.4 Common Near Receiver Geometry (CNR) Configuration (Drnevich et al., 1990)

3.3.4 Pavement Surface Layer Analysis

A simplified testing procedure and data reduction analysis has been proposed by Roesset et al. (1990) in order to determine the stiffness and thickness of the pavement surface layer. A piezoelectric shaker is used as a source to generate wavelengths less than or equal to the thickness of the surface layer, and the receiver spacings vary from 3 to 12 inches depending on the particular site. For accurate measurements in the upper 2 inches of the surface layer of pavement (either AC or concrete), surface waves with frequencies in the range of 30 to 70 kHz should be generated. Since the R-wave velocity is constant for a half-space (independent of wavelength), the top layer appears as a uniform half-space for waves with short wavelengths (high frequencies) up until the critical wavelength (L_c) is measured, as shown in Figure 3.5.

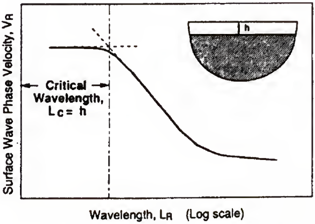

Figure 3.5 Determination of Surface Layer Thickness from a Dispersion Curve (Roesset et al., 1990)

The results can be obtained immediately from the dispersion curve since the critical wavelength is equal to the thickness of the surface layer. The horizontal axis (wavelength) is a logarithmic scale since the high frequencies in the near-surface ranges, corresponding to shallow depths, are magnified. The Young's modulus is obtained from V_R by assuming a Poisson's ratio and mass density, and by using Equations 2.4 and 2.32. This method is an excellent means for testing the stiffness variations of asphaltic concrete (AC) with surface temperature or concrete during curing (Sheu et al., 1986 and Roesset et al., 1990).

3.3.5 Effects of Reflected Waves

Sheu et al. (1986, 1988) have studied the effects of reflected waves from boundaries, such as edges or joints of a pavement system, and horizontal interfaces between pavement layers. Three cases were analyzed: (1) reflected surface waves from boundaries perpendicular to array, (2) reflected surface waves from boundaries parallel to array, and (3) reflected body waves from a vertical pavement interface.

The reflected surface waves appear on the dispersion curve as fluctuations or ripples along what the true curve should be and cause more disturbances in the low frequency range (longer wavelengths) than at higher frequencies, as seen in Figure 3.6. Therefore, shallow depths are less sensitive to these disturbances. If the effect of the reflected waves were removed, the dispersion curve would basically be a smooth curve.

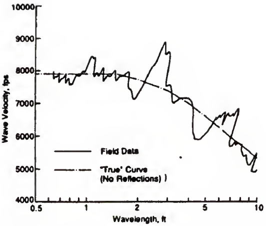

Figure 3.6 Comparison of Measured Dispersion Curve with the True Curve with No Reflections (Sheu et al., 1988)

To minimize the effect of these surface wave reflections, the source should be placed between the boundary and receivers for arrays perpendicular to the reflection boundary so that the reflected waves propagate in the same direction as the direct waves. If this is not possible, the array should be placed as far away from the reflection boundary as possible so as to minimize the amplitudes of the reflected waves. For arrays parallel to the boundary, the array should be placed close to the boundary (≤ 0.2D, where D is the distance between the source and near receiver) so that the reflected waves are in-phase with the direct waves, or far enough from the boundary (≥ 3D) that the reflected waves' amplitudes have decreased. This study concluded that reflected SV-waves (shear waves whose direction of propagation and particle motion are contained in a vertical plane) have the most effect of any body wave (both direct and reflected), but that their effect is not as important as the reflected surface waves. Therefore, it is not necessary to consider their effect in most situations.

CHAPTER 4
TESTING PROGRAM

4.1 Introduction

The previous chapter covered the work done by researchers to develop standardized procedures used currently for SASW testing. This chapter will focus on how this research incorporated these procedures (as outlined in the General Testing Procedures section) into a testing program to develop practical applications to be utilized by the FDOT (as outlined in the Testing Program section).

4.2 General Testing Procedures

A complete SASW investigation consists of the following three phases:

(1) field testing,
(2) construction of field composite dispersion curve, and
(3) inversion of dispersion curve.

Each of these phases will be covered in the following sections to present the procedures used during the course of this research. The field work for this research covered the span of over two years. The equipment and software were acquired at the beginning of this research, and a trial and error process was used to evaluate slight modifications to the procedures and to enhance the learning process. The equipment was chosen primarily because of consultation with Dr. Glenn Rix. A short training session was provided by Dr. Rix, which included a series of SASW tests at a couple of field sites. Dr. Rix currently teaches at Georgia Institute of Technology, and received his Ph.D. under Dr. Kenneth Stokoe at the University of Texas at Austin performing SASW research. Along with this training, he provided the software required to analyze the field data.

4.2.1 Field Testing

The field testing consisted of (1) site layout, (2) mapping out the position of the receivers and source, (3) placing the receivers at the first spacing, (4) connecting the wires, (5) selecting the appropriate signal analyzer settings, (6) producing the impact and receiving data, (7) saving the data, (8) reversing the profile at this spacing, and (9) continuing this procedure for the subsequent spacings until the maximum spacing was tested.

The site layout consisted of obtaining all the information about the site that was available, especially previous borings or soundings. The next step was determining the exact locations of the SASW test sites, and the spacings to be used during testing. The maximum spacing was based on the maximum sampling depth desired, as well as the practical limit of the source which was available at the time. The sampling depth for the SASW test was taken to be approximately equal to the maximum spacing used in the configuration. The spacings were typically doubled until the maximum spacing was achieved.

The majority of the testing was performed using the common receivers' midpoint configuration, with forward and reverse profiles at each spacing. The only exception to this was the test pit studies. Since space was limited, the common near receiver configuration was used which prevented reversing the profile. Since the material in the test pit was placed under controlled conditions, the lateral nonhomogeneity of the site was limited.

When the centerline of the survey and the receiver spacings were chosen, the receivers were placed on the ground surface at the shortest spacing. Reversing the profile was accomplished by switching the connections for Channels 1 and 2 at the signal analyzer. After testing was completed for this spacing, the receivers were manually moved the next spacing. For all the testing, only one receiver type was used for an individual test; either geophones for soil sites or accelerometers for pavement sites. The type of receivers used during this research were based on the recommendations of previous research which evaluated many types of receivers. These particular receivers were chosen based on their reliability and ease of use.

The two geophones used during testing were Mark Products model L-4C 1.0 Hz vertical geophones. A photograph of the 1.0

Hz geophones is included as Figure 4.1. These geophones are cylindrical and were placed directly on the ground surface after the top few inches of soil and vegetation had been cleared. A pair of Mark Product model L-28B 4.5 Hz geophones were also purchased. A photograph of the 4.5 Hz geophone is included as Figure 4.2. These geophones had limited use since they could only be used at shorter spacings (1 to 8 feet). They were used when the ground surface was relatively soft, particularly at the field trench sites for the subgrade and embankment layers. The L-28B geophones are mounted on a spike which was pushed into the ground. Since the L-4C geophones proved successful in collecting data at these shorter spacings, it was easier to use these geophones exclusively during a single test for most cases.

The accelerometers used during this research were Wilcoxin Research model 728T with the model P702 power supply/ amplifier, which used battery power. A photograph of the accelerometers and their power supply/amplifiers is included as Figure 4.3. These accelerometers are small so that attaching them to the pavement surface was accomplished by using a mounting wax (beeswax), with just enough wax to ensure adequate bonding. On hot days, the wax would melt preventing a proper bond so nails were driven into the pavement surface and magnetic bases, which threaded onto the accelerometer base, were used to attach them to the nail head. The magnetic bases were also used on occasion for limerock and aggregate

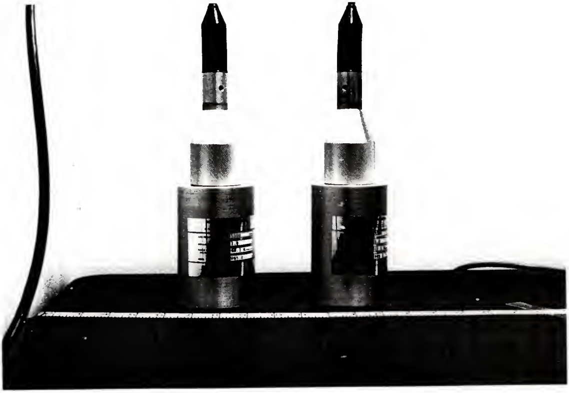

Figure 4.1 L-4C 1.0 Hz Geophones

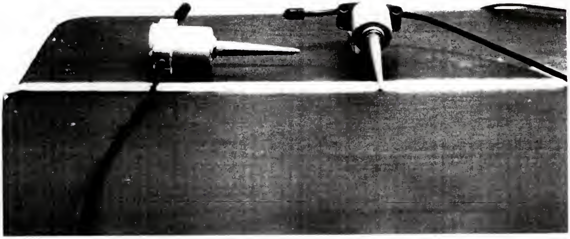

Figure 4.2 L-28B 4.5 Hz Geophones

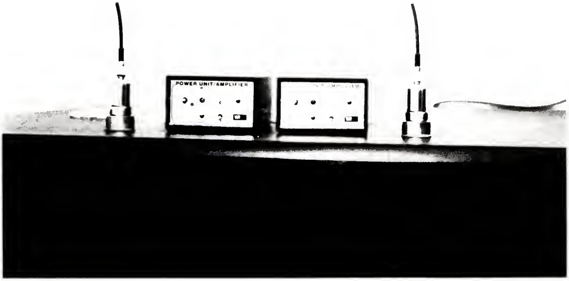

Figure 4.3 728T Accelerometers and the P702 Power Supply/Amplifiers

base sites. The accelerometers in Figure 4.3 are shown mounted on the magnetic bases.

4.2.1.1 Signal analyzer settings

The signal analyzer used for this research was a Hewlett-Packard model 35665A. A photograph of the signal analyzer is included as Figure 4.4. This model is a two-channel analyzer which can receive the output from the receivers (time domain data). It can then perform a fast-Fourier-transform (FFT) analysis on this data (converting it into frequency domain data) by means of a built-in microprocessor. It stores this data (either the time or frequency domain data) by means of an internal disk drive.

The settings on the signal analyzer were saved so that they were automatically recalled as the system was turned on. Figures 4.5 and 4.6 show the default settings used for the signal analyzer to receive and process the input signals from the two receivers. The only settings that needed changing at a test site were the input voltage range for both channels, the frequency bandwidth to be monitored, and the pretrigger delay time.

The input voltage range was set manually to maintain a specific input range. The range to monitor the input signal from the receivers was selected as low as possible (increased sensitivity) to gain the best resolution as possible (approximately one-half to full scale) without receiving an overload signal. The voltage inputs were set differently for the two

Figure 4.4 HP-35665A Signal Analyzer

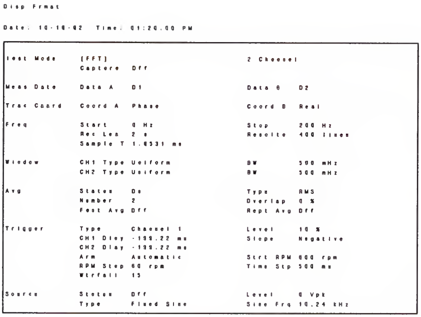

```
Disp Frmat

Date: 10-10-02   Time: 01:20.00 PM

Test Mode      [FFT]                          2 Channel
               Capture  Off

Meas Data      Data A   D1                    Data B    D2

Trac Coord     Coord A  Phase                 Coord B   Real

Freq           Start    0 Hz                  Stop      200 Hz
               Rec Len  2 s                   Resoltn   400 lines
               Sample T 1.9531 ms

Window         CH1 Type Uniform               BW        500 mHz
               CH2 Type Uniform               BW        500 mHz

Avg            State    On                    Type      RMS
               Number   2                     Overlap   0 %
               Fast Avg Off                   Rept Avg  Off

Trigger        Type     Channel 1             Level     10 %
               CH1 Dlay -199.22 ms            Slope     Negative
               CH2 Dlay -199.22 ms
               Arm      Automatic             Strt RPM  600 rpm
               RPM Step 60 rpm                Time Stp  500 ms
               Wtrfall  15

Source         State    Off                   Level     0 Vpk
               Type     Fixed Sine            Sine Frq  10.24 kHz
```

Figure 4.5 Measurement Settings from the HP-35665A Signal Analyzer

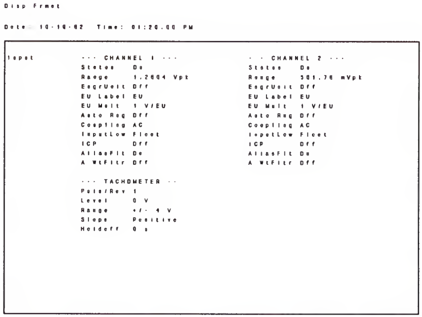

```
Disp Frmat

Date: 10-10-02   Time: 01:20.00 PM

Input          --- CHANNEL 1 ---              --- CHANNEL 2 ---
               State    On                    State    On
               Range    1.2604 Vpk            Range    501.76 mVpk
               EngrUnit Off                   EngrUnit Off
               EU Label EU                    EU Label EU
               EU Mult  1 V/EU                EU Mult  1 V/EU
               Auto Rng Off                   Auto Rng Off
               Coupling AC                    Coupling AC
               InputLow Float                 InputLow Float
               ICP      Off                   ICP      Off
               AliasFlt On                    AliasFlt On
               A WtFltr Off                   A WtFltr Off

               --- TACHOMETER ---
               Puls/Rev 1
               Level    0 V
               Range    +/- 4 V
               Slope    Positive
               Holdoff  0 s
```

Figure 4.6 Input Settings from the HP-35665A Signal Analyzer

receivers since the signal was weaker when it reached the second (further) receiver. Therefore, the range for the second receiver was set more sensitive (about one-half the range of the near receiver) than the first receiver. As the receivers' spacings doubled (increasing the distance between the source and the near receiver), the input ranges for both channels were typically halved to increase the sensitivity of the measurements.

The frequency bandwidth was set to optimize the capture of good quality data. Nazarian and Stokoe (1985) recommend an optimum bandwidth such that 3/4 of the frequency range consists of good quality data (coherence greater than 0.90). This ensures that the resolution in the frequency domain is good, which improves the resolution of the resultant dispersion curve. Typically, the frequency span was halved as the receiver spacing was doubled, since the maximum measured frequency decreased (and the measured wavelength increased). The analyzer digitizes each record based on the resolution defined by the user. A resolution of 400 was used, so each trace was defined by 1024 points. The record (or time) length, T, and frequency bandwidth, F, are related by the number of points digitized, N, by:

$$N = F \cdot T \tag{4.1}$$

so that if either F or T is set, the other parameter is automatically adjusted by the analyzer.

The pretrigger setting allows a small portion of the record before the actual arrival of the signal to be monitored. Nazarian and Stokoe (1985) recommend a pretrigger time on the order of 10 percent of the time length sampled, T. This pretrigger time must be the same for both channels to prevent any internal time or phase difference between the two sets of data.

The actual trigger was set internally by using the signal from the first receiver in the pair (Channel 1 input) so that the analyzer started recording the measurement when the input signal created by the impact reached the Channel 1 receiver and met the specified trigger conditions. A trigger level was specified as a percentage of the current input range. When the input signal crossed this level, the analyzer was triggered. This trigger level needed to be increased occasionally, especially at long spacings, to prevent background noise from triggering the system. The trigger was also set to monitor a negative (or falling) signal which is appropriate for an impact source in order to capture the entire waveform.

The signal analyzer has the capability to allow the user to preview each time record and manually select or reject it from being included in the FFT averaging analysis. This prevented poor impacts from being included in the averaging. A root-mean-square (rms) averaging method was used to provide a standard average (equally weighted) for the specified number of time records. This averaging provides the most direct means to cancel out background (random) noise, which tends to be variable, while the impulse (source) remains constant and repeatable. The number of time signals used for averaging was set at two records. In most cases, this was sufficient to provide consistent data and speed up the test time. In order to ensure consistent impacts, the user looked at the display and noticed how the cross spectrum results changed from the first to second impacts. If the event was judged to be representative of a reproducible impact of the source, the data was accepted into the averaging sequence. Based on Heisey et al. (1982b), there is little difference in the quality of the data between 5 and 25 averages. Although, the test time is increased by a factor of 5 when 25 averages are used.

A window is a time-domain weighting function applied to the input signal, which filters out signals that are not periodic. A certain portion of the input time record is accentuated depending upon the type of window used in the analysis. A uniform window was chosen because it is most appropriate for transient signals, since it weighs all parts of the time record equally. Sheu et al. (1986) have used a exponential window to eliminate the effect of reflected waves arriving after the direct wave in order to improve the quality of the dispersion curve.

These settings required several adjustments in the field, depending on the specific site conditions, to optimize the data obtained from testing. This required initially adjusting the settings that the user thought were appropriate, performing the test, and changing them based on the results until the largest amount of useable data was collected.

4.2.1.2 Data collection

Once the settings for the signal analyzer were input, the analyzer waited for some event to trigger it to begin monitoring. A variety of sources were used to make the impact (striking the ground or pavement surface) in order to create a transient seismic wave that possessed a broad range of frequencies. For pavement sites, a wrench (3 to 4 oz.) was used for the short spacings (0.5 to 2 feet), and a ball-peen hammer (1 lb.) or a short sledgehammer (3.5 lbs.) was used for longer spacings (2 to 8 feet). A photograph of the sources used for testing at pavement sites is included as Figure 4.7. For soil sites, the short sledgehammer (3.5 lbs.) was used for the short spacings (1 to 8 feet). The sledgehammer (9.5 lbs.) was used for the intermediate spacings (8 to 20 feet). For longer spacings (20 to 40 feet), a 155-pound standard penetration test (SPT) portable hammer or a concrete cinder block was used to impact the ground surface. At one site, a 20-ton weight used for deep dynamic compaction, dropped from a crane, provided the source signal for a test spacing of 85 feet, but could have been used as a source for much longer spacings. The dynamic cone penetrometer (DCP) was used for a source for the series of tests at the Kanapaha site. This concept proved successful at other sites, using a rod embedded in the ground and impacting it with a hammer, for short spacings (2 to 8 feet) where the surface soils were loose, dry sands. Using a hammer at these sites produced poor quality data because the loose surface dampened the impact too much. The concrete cinder block also proved successful at these sites, as well as at sites which had saturated surface soils or even standing water. The block has a large impact surface area which allowed more energy to be transmitted directly to the ground than any type of hammer. Regardless of the source, the impact needs to be a single impulse. Any bounces of the source (double hits) will affect the signal if the second hit occurs during the data collection time window. The typical sources used for testing at soil sites is included as Figure 4.8.

The time histories of the impact were recorded for both channels. Typical plots as they appeared on the signal analyzer are presented in Figure 4.9. From these time histories of both channels, FFT functions (phase of the cross power spectrum and coherence) are performed and displayed on the screen after each successive impact. Typical plots of the phase of the cross spectrum and coherence as they appeared on the display of the signal analyzer are presented in Figure 4.10, which was measured at a two foot spacing for a pavement site. From this figure, the usable range of cross spectrum is from approximately 80 Hz to 2,000 Hz, where the coherence is above 0.90. Beyond these frequency limits, the coherence (as

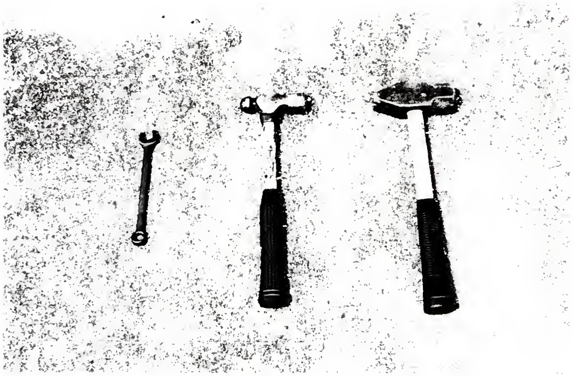

Figure 4.7 Sources used at Pavement Sites

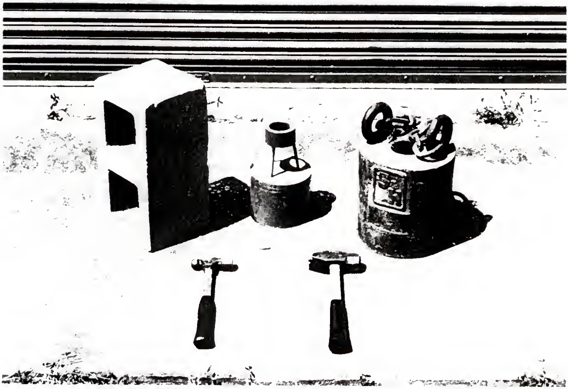

Figure 4.8 Sources used at Soil Sites

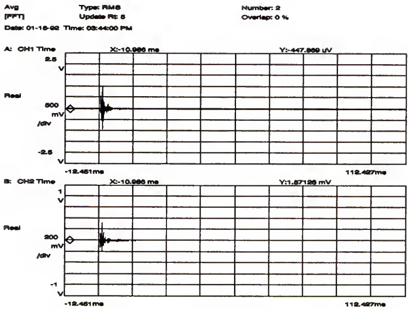

Figure 4.9 Plots of Channel 1 & 2 Time Histories from the HP-35665A Signal Analyzer

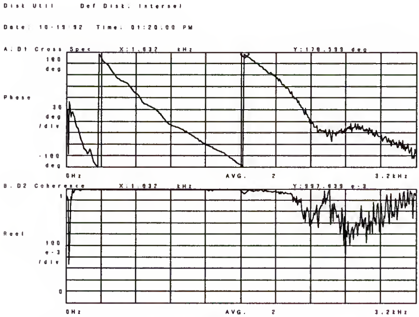

Figure 4.10 Plots of Cross Spectrum and Coherence from the HP-35665A Signal Analyzer

well as the cross spectrum) is erratic and this data was discarded from the analysis.

The data displayed in Figure 4.10 was saved into two separate data files (cross power spectrum and coherence) using the internal 3.5-inch disk drive on the HP signal analyzer. This data was saved for each spacing, and for both the forward and reverse profiles. These files were collected in the field, and this raw data was used as input for construction of the dispersion curve.

4.2.2 Construction of the Field Composite Dispersion Curve

This process was accomplished in the office, but with the use of a portable computer, this process could be performed in the field to evaluate the quality of the data and refine the testing procedures if necessary.

The first step in this process was to convert the field data files into ASCII format to be compatible with the analysis software. Using a utility program supplied with the signal analyzer (SDFTOASC), each cross power spectrum file was converted into an ASCII file containing frequency data and the real and imaginary components of the cross spectrum for the entire range of frequencies monitored.

The computer program, DISP, was used to read in the raw field data (only the phase of the cross power spectrum was used as input data) and assemble the field composite dispersion curve. This program prompts the user for the distances between the receivers (X) and between the source and near receiver (D), as well as the ratio of the distance between the source and near receiver and the wavelength (D/λ). This ratio was selected as 0.33 during the analysis, which corresponds to the Heisey filtering criteria (Eqn. 3.5) to eliminate any raw data which might be contaminated with body waves. The user manually eliminated the ranges of data which had low coherence. The cross power spectrum and coherence plots were viewed on the signal analyzer at the same time, and a marker was used to identify the specific points of frequency on each trace. The program unwrapped the cross power spectrum trace by keeping track of the jumps (shifting the phase data by the appropriate multiples of 360°). After performing the dispersion calculations on this data (Eqns. 3.2 through 3.4), the individual dispersion curve (either wavelength or frequency versus phase velocity) was viewed on the screen. The remaining cross power spectrum data files were read into the program, and this process was repeated in order to combine the individual dispersion curves into a composite field dispersion curve. The user specified the number of points to average the composite dispersion curve between the minimum and maximum measured wavelengths. This averaged dispersion curve was used as input for the inversion program.

4.2.3 Inversion of the Dispersion Curve

The program, INVERT, was used to perform the inversion analysis on the averaged composite dispersion curve. The program developed by Dr. Glenn Rix is based on the Least Squares Inversion Algorithm (Kausel and Roesset, 1981) which utilizes a stiffness matrix to determine a characteristic equation at each frequency contained in the field dispersion curve. Since the number of data points in the dispersion curve is much larger than the layers used to model the soil profile, optimization techniques are used to determine the unknowns in the series of equations. The INVERT program utilizes the Newton-Raphson procedure (Tarantola, 1987), which involves an iterative solution since the problem is nonlinear. Other methods have been used by other researchers for the inversion process to develop a theoretical dispersion curve to compare with the field dispersion curve, such as the transfer matrix method developed by Haskell and Thomson (Nazarian and Stokoe, 1984, 1986a, and 1986b) and the finite difference method (Hossain and Drnevich, 1989).

The procedures used for the inversion analysis were similar to those outlined in Nazarian and Stokoe (1985). The initial shear wave velocity profile was determined from empirical relationships (Eqns. 2.1 and 2.2). For soil sites, the initial values were estimated by using closed-form methods to develop the dispersion curve for a Gibson half-space (Vardoulakis and Vrettos, 1988) using the following equation:

$$G = G_o(1 + mz) \tag{4.2}$$

where: G = shear modulus at depth, z

G_o = initial shear modulus (at z=0)

m = slope of shear modulus profile.

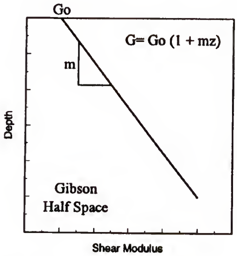

Figure 4.11 Gibson Half-Space Shear Modulus Profile

This method assumes a linear shear modulus profile with depth, as shown in Figure 4.11. From this shear modulus profile, values of shear wave velocity can be estimated from the following equation:

$$V_S = V_{S_o}(1 + mz)^{1/2} \tag{4.3}$$

where: V_S = shear wave velocity at depth, z

V_{So} = initial shear wave velocity (at z=0).

It was standard practice to start with a profile with fewer and thicker layers, and as the match between the theoretical and field dispersion curves got closer, the profile was refined by dividing the initial profile into sublayers so that a closer match could be obtained. Nazarian and Stokoe (1985) recommend defining a shear wave velocity profile to a depth of 1/2 to 1/3 of the maximum wavelength and below this depth, the medium should be defined as a half-space.

4.3 Testing Program

The following is an outline of all SASW tests, divided into pavement and geotechnical applications, performed for this research. The results from each of these studies will be presented in Chapter 5 for the geotechnical applications and in Chapter 6 for the pavement applications.

4.3.1 Geotechnical Applications

4.3.1.1 Dynamic compaction site

SASW testing was performed before and after the compaction, and compared to determine the effect of the site improvement (stiffness increase) due to the dynamic compaction. SASW testing at one site utilized the 20-ton dynamic compaction drop weight as the source, which was used to evaluate the feasibility of using such a large source to survey deep soil deposits.

4.3.1.2 Polk County Parkway

A series of SASW tests were performed at sites which had phosphatic slime/clay at or near the surface. Dilatometer (DMT) testing was performed adjacent to the SASW test sites to compare moduli results. No CPT soundings were possible because the ground surface was too soft and wet to allow access of the cone truck. These sites provided an indication of testing in poor site conditions (limited access and water at the ground surface). The results from this study were an example of how a quick method for data reduction could be used to produce thickness and stiffness results if the surface layer consists of a homogeneous, isotropic material.

4.3.1.3 Kanapaha site

SASW testing was performed to determine the top of the limerock. This site was chosen because the top of limerock was fairly shallow and very irregular. One of the sites had a void (approximately 2 feet in diameter which was 18 inches below the ground surface) at the centerline of the SASW test location. The location of the void was detected by the dynamic cone penetrometer. This site was used to determine the effect of a cavity on the SASW data reduction. SASW tests were performed at one of these sites over the span of two years to determine the reproducibility of the results of this test method. Additional testing at this site included cone penetrometer tests (CPT), used to compare moduli and to determine the top of limerock, and dynamic cone penetrometer tests (DCP), used to compare near-surface variations at the test sites.

4.3.1.4 Live Oak site

This site was the location of a sinkhole survey for a planned retention pond. SASW testing was performed as a comparison with anomalies detected with a ground penetrating radar (GPR) survey. Existing soil borings, performed during preliminary design of the retention pond, were used as a comparison of the existing soil layers at the site. In addition, CPT soundings were performed at the sites where the GPR showed possibly anomalies to determine if voids existed at these locations.

4.3.2 Pavement Applications

4.3.2.1 Test pit studies

The FDOT's test pit facility allows testing of roadway base, subgrade, and embankment materials which are placed under similar conditions as used in the field. Typically, it models a two-layer cross-section (base/subgrade or subgrade/ embankment) of the roadway. Plate load tests are performed at both static or dynamic loading conditions. These studies provided a comparison of the SASW and plate load test modulus results for different moisture conditions (optimum, soaked, and drained-dried) for the following materials:

(a) FSU's subgrade research. This research project provided a comparison of plate load test results with laboratory triaxial resilient moduli. The following soils were tested to reflect various subgrade materials used throughout the state:

i) SR-200, Ocala (limerock stabilized sand subgrade),
ii) I-75, Alachua (limerock stabilized sand subgrade),
iii) SR-30A, Panama City (clay stabilized subgrade),
iv) SR-50, Brooksville (sand subgrade), and
v) SR-369, Crawfordville (sand subgrade).

(b) Flexbase. This material is a lime-stabilized bottom ash designed mixture. Two different design batches were tested. SASW testing was performed at soaked and drained condition. This material provided a good indicator of a strong interface signal between the flexbase and sand subgrade (stiff over soft materials).

(c) Dolomite. This material was tested for approval as a granular base for roadway construction. The SASW program consisted of testing at optimum, soaked, and drained conditions.

(d) RAP (recycled asphalt). This material is the product of milling the asphalt pavement of an existing roadway. Its intended use was as a base material for roadways. The SASW program consisted of testing at optimum, soaked, and drained conditions.

4.3.2.2 Field trench sites

Several sites throughout the state were chosen so that field plate moduli from each layer of the pavement profile (base, subgrade, and embankment) could be correlated with laboratory triaxial resilient moduli (from samples taken back and recompacted at field density and moisture). At each site, falling weight deflectometer (FWD) tests were performed at the pavement surface. SASW tests were performed at the pavement surface and adjacent to the field plate load test sites at each layer of the two sites at the following locations:

(a) US-17, Green Cove Springs,
(b) SR-414, Maitland Boulevard,
(c) US-441, Yeehaw Junction,
(d) US-41, Tamiami Trail,
(e) US-1, Jupiter, and
(f) US-17/92, Haines City.

4.3.2.3 Florida Institute of Technology test sites

SASW tests were performed at two separate sites on the Florida Institute of Technology (FIT) campus for comparison with results obtained with research efforts to modify the pavement pressuremeter to enable low-strain level resilient moduli determination. The first site was an existing site consisting of sandy soils (with no improvements or compaction). The second site was at a small (20 by 15 feet) test section consisting of a cemented coquina base material (compacted to approximately 97% of optimum density). The field data was used to develop a variation of the modulus versus strain-level for the materials directly in the field. The SASW results provided the upper portion of the curve (the maximum modulus). No results from the second site are included in this report since the pressuremeter results were not made available in time.

4.3.2.4 US-98 (Panama City) test site

SASW testing was performed at this site because of subsidence of US-98 due to a possible leak, and washing out of embankment material, of a cross-drain pipe. Maintenance engineers wished to know if the roadway was safe to be left open to traffic and repairs delayed to a later date when there would be less traffic. This site provided a use of dispersion curves, comparing a 'good' versus 'bad' site, to analyze the field data.

CHAPTER 5
GEOTECHNICAL APPLICATIONS

5.1 Introduction

This chapter contains the applications listed in Chapter 4 concerning the portion of the testing program directed toward geotechnical engineering uses. This primarily concerns the testing at soil sites. Each individual project will be covered by a separate section, including background information, the SASW testing (as well as additional in-situ testing), and the results obtained from these field tests.

5.2 Dynamic Compaction Site

The dynamic compaction site was located along Section 5 of the Veterans Expressway (State Project No. 97102-3304) in Tampa. The site consisted of a landfill containing construction debris (primarily wood, concrete blocks, scrap metal, etc.) between stations 471+00 and 473+80. Test pits at the site revealed the depths of the debris to be between 13 and 18 feet. This was deeper than first anticipated, and dynamic compaction was chosen to densify the site.

5.2.1 Background Information

Dynamic compaction is a ground modification technique which densifies subsurface soils at a site by repeatedly dropping a heavy weight onto the ground surface from a free fall. The weight is lifted and dropped by a conventional crane using a single cable. The typical weights used for dynamic compaction range from 6 to 30 tons, with drop heights usually ranging from 30 to 75 feet. The weight is dropped in a grid pattern along the site to ensure adequate densification of the subsurface soils.

Quality control for the site is performed by in-situ tests such as the SPT or CPT before and after compaction to evaluate the strength (stiffness) gain at a given site. The problem with this approach occurs when large blocks of rubble are present at a site which prevents these tests from penetrating the obstacles. Another potential problem is a site which contains hazardous materials, and any type of penetration tests that passes through these materials is to be avoided. Another method, which was used at this site, is to construct a conical test load (CTL). This is a mound of soil which is placed at the site (typically 15 to 20 feet in height), and a settlement plate is placed on the ground surface below the center of the mound of soil. Settlement data is recorded over a span of time to indicate the relative degree of densification of the in-place soils. The disadvantage of the CTL method is that it is time consuming, typically taking two weeks to be monitored, which can be an unacceptable delay for high priority projects.

The design of a deep dynamic compaction (DDC) project is performed using the following equation:

$$D = n\sqrt{WH} \tag{5.1}$$

where: D = depth of improvement (m)

n = empirical coefficient

W = weight of DDC mass (tonnes)

H = drop height (m).

The coefficient, n, is a correction factor used to account for other factors which can affect the depth of improvement, such as type of deposit being densified, applied energy, contact pressure, cable drag, and presence of energy absorbing layers. Based on Lukas (1986), the recommended values of n range from 0.50 to 0.70 for pervious granular deposits and from 0.37 to 0.60 for semi-pervious deposits. From case studies involving building rubble, a value of n was back-calculated to be between 0.56 and 0.62.

The magnitude of improvement is dependent upon the soil deposit being densified, the amount of energy being applied at the ground surface, and initial relative density of the deposit. For deposits containing building rubble, Lukas (1986) suggests that the range of anticipated improvement is 200 to 300 percent as measured by in-situ tests. This strength increase assumes an applied energy ranging from 100 to 300 tonnes-m/m^2. The magnitude of improvement is usually not uniform throughout the predicted depth of improvement, and the maximum improvement is usually within a zone between 1/3 to 1/2 the predicted depth of improvement, below which the improvement decreases with depth.

5.2.2 Site Information

The plan view of the dynamic compaction site is shown in Figure 5.1, revealing the test site along the centerline of construction of the Veterans Expressway.

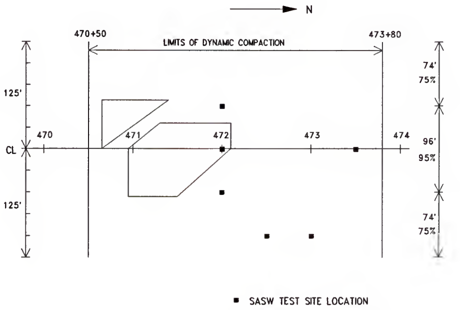

Figure 5.1 Plan View of the Dynamic Compaction Site

Based on the depth of deposits to be densified and the availability of a 20-ton drop weight, the design called for a drop height of 60 to 65 feet, using a value of n of 0.40. An initial ironing pass of the dynamic compaction was performed over the entire area. A 3-foot sand blanket was placed to level the ground surface over the area to be treated, and to stabilize areas of loosened surface soils. The spacing of the drops was 8-foot on center (o.c.) and each site received two drops from a height of 15 feet. This ironing pass was used to create a more homogeneous deposit of subsurface soils prior to the actual dynamic compaction passes, in order to collapse any existing voids at the site and to break up any hardened surface deposits.

The spacings of the primary compaction passes were based on the coverage needed for the design recommendations. For the area that was included in the roadway embankment construction, 95% coverage was used for design (13-foot o.c. spacing). Areas outside the toe of the embankment slope received 75% coverage (15-foot o.c. spacing) of the dynamic compaction weight. The design called for two passes with an average of 8 drops at each location until refusal. Refusal is defined as the maximum weight penetration of 6 inches per drop.

The two areas outlined in Figure 5.1 (near Stations 471+00 and 472+00) show the locations where a 3-foot layer of crushed stone was used in place of the 3-foot sand blanket. This was due to an underlying layer of clay and organic soils which was encountered during the initial dynamic compaction passes. This allowed the stone to displace and intermix with the clay and organic soils, thereby stabilizing these areas.

The final settlements obtained from the CTL were 0.02 inches over the period of two weeks. These results indicated that the dynamic compaction was successful in densifying the site to allow construction of the embankment without additional compaction of the existing soils, except for standard compaction of the surface soils.

5.2.3 SASW Testing

A total of six locations were tested before and after the compaction to compare the effect of the site improvement (stiffness increase) due to the dynamic compaction. The locations of the SASW sites are shown in Figure 5.1. The spacings used at each of the test sites were 3, 9, and 20 feet.

The results from all six of the locations show an increase of stiffness after the dynamic compaction. Figure 5.2 presents typical dispersion curves comparing the before-compaction (initial) and after-compaction (final) test results. Figure 5.3 shows the shear wave velocity profiles obtained from the data in Figure 5.2 after performing an inversion analysis. The dispersion curves and shear wave profile plots for the other test locations are included in Appendix A as Figures A.1 through A.10.

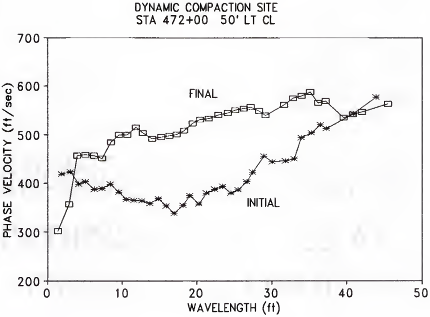

Figure 5.2 Dispersion Curves from the Dynamic Compaction Site (Sta 472+00, 50′ Lt)

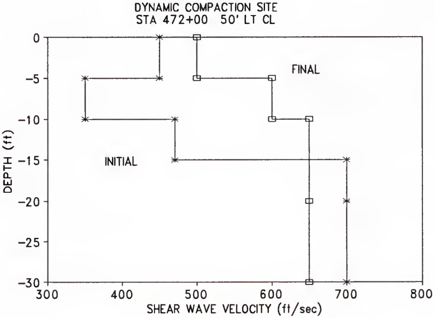

Figure 5.3 S-Wave Velocity Profiles from the Dynamic Compaction Site (Sta 472+00, 50′ Lt)

The SASW dispersion curves can be used to reveal the depth of improvement of the subsurface soils from the dynamic compaction. The after-compaction curves show an increased zone of velocities to a certain wavelength (corresponding to increasing depths), at which point the two curves (before- and after-compaction) match each other closely. There were a couple of sites in which this trend did not occur, but this was probably due to the limited maximum spacing used during the testing (20 feet). Since the maximum wavelength is approximately equal to the maximum spacing, the 20-foot spacing was just long enough to sample the depth of soils to be compacted, and a longer maximum spacing was needed to adequately define the depth of improvement at some areas. Using Eqn. 5.1 and the parameters used for this project, the depth of improvement (D) should be approximately 24 feet, based on the design n-value of 0.4. This value seemed high compared to the shear wave profiles resulting from the SASW tests, which typically showed a depth of improvement in the range of 15 to 20 feet. This could be the result of using a maximum spacing of 20 feet, which limited the resolution of the longer wavelength data needed to accurately define this depth of improvement.

The stiffness increase indicated by the SASW results was in the range of 135 to 205 percent improvement from the original velocities. This improvement is consistent with the anticipated range of improvement typically obtained for building rubble sites, although it is at the lower end of the anticipated range of improvement. The total energy per site was determined to be 254 tonnes-m/m^2, which is within the suggested range of applied energy needed to treat rubble landfill sites (Lukas, 1986). The SASW dispersion curves also reveal that the after-treatment surface layer velocities are typically less than the initial values. This is due to the loosening and disturbing effects from the surface craters. This is normal for dynamic compaction operations, and compaction of these surface soils is achieved using conventional equipment (i.e. compaction roller).

Shear wave velocity profiles were developed from Seed's empirical relationships (Eqns. 2.17 and 2.18). The value of K_2 was altered to account for the density (void ratio) of the material. Based on recommendations by Stokoe et al. (1988), values of K_2 of 30, 50, and 70 were taken as representative of loose, medium dense, and very dense sands, respectively. These derived profiles are compared with the measured shear wave velocities in order to infer the density of the in-place soils and evaluate the degree of compaction which was achieved. This approach gives only a qualitative sense of the in-place densities, and actual densities are not obtained from this analysis. An example of the typical results from this analysis is presented in Figure 5.4, and the remaining sites are included in Appendix A as Figures A.11 through A.15. These results show that prior to compaction, the site was very loose from the depths of 5 to 15 feet. This is due to the collection and dumping of the construction debris at the site, as well as the numerous test pits excavated in this area and filled without any means of compaction. After the dynamic compaction, the shear wave velocities were representative of a medium dense to very dense soil, indicating that the compaction was successful in improving the stiffness of the underlying soils.

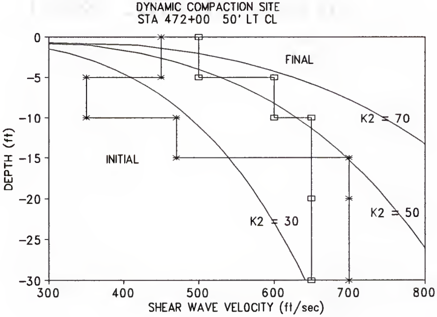

Figure 5.4 Comparison of S-Wave Velocity Profiles from the Dynamic Compaction Site (Sta 472+00, 50' Lt)

The 20-ton weight used for the dynamic compaction was used as a source for the SASW test at 100 feet right of the centerline of Station 473+50. The geophone spacing for this test was 85 feet, and the weight was dropped approximately 15 to 20 feet. A full drop of the weight for the 85-foot spacing was not possible, since the signal from the impact overloaded the signal analyzer. This means that a much longer spacing was possible, which would allow the sampling of very deep deposits. The data from the 85-foot spacing was combined with the after-compaction results from the SASW test at this same site to form a composite dispersion curve. After performing an inversion analysis on this dispersion curve, the resulting shear wave velocity profile is shown in Figure 5.5.

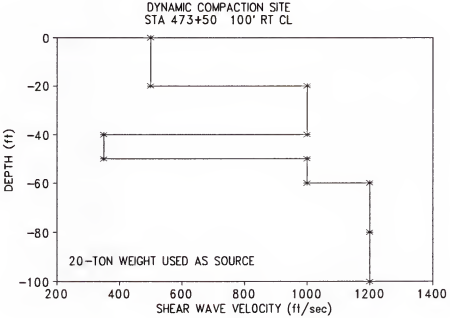

Figure 5.5 S-Wave Velocity Profile using the Dynamic Compaction Weight (Sta 473+50, 100' Rt)

A series of shear wave velocity profiles were developed from Seed's empirical relationships to infer the site's density at Station 473+50, 100 feet right of the centerline (refer to Figure 5.6). Based on these results, the subsurface soils are medium dense to very dense, except for a layer of very loose soils at a depth of 40 to 50 feet. Borings were not obtained to confirm the existence of this low density layer. The intended purpose of this test was to evaluate the practicality of using a large weight as a source to sample very deep soil deposits.

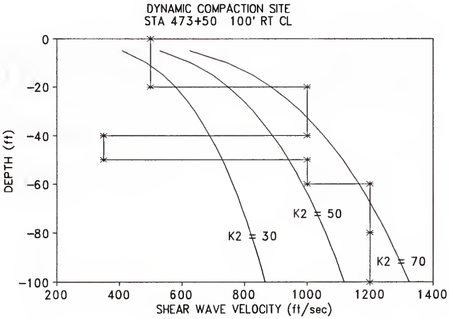

Figure 5.6 Comparison of S-Wave Velocity Profiles using the Dynamic Compaction Weight (Sta 473+50, 100′ Rt)

5.3 Polk County Parkway Site

The testing at this site was performed along the proposed alignment of Section 5 of the Polk County Parkway (State Project No. 97160-1310) in Lakeland. This site has several areas which were disturbed by phosphate mining and/or reclamation operations. The most critical areas consist of old clay settling ponds, where waste clay slimes were contained over unmined soils. Historical data indicates that by 1952, this area contained mine cuts which were being filled with waste clay slimes. By 1958, addition of slimes to the mine cuts was completed. These clay slimes were allowed to consolidate in these ponds either under their own self-weight or covered by a layer of sand tailings.

5.3.1 Background Information

The presence of the phosphatic slime along the proposed alignment of the Polk County Parkway created many problems during the design phase. Due to variability of the locations and depths of the pockets of slime at the project site, there was concern that differential settlement of the roadway might occur. Total amounts of settlement in areas were estimated to be as high as 5 to 6 feet. To lessen the effect of this differential settlement, a surcharge loading was proposed along the critical areas. This surcharge is an additional amount of fill material to the roadway embankment (and in the case of this project, 10 to 15 feet), which is allowed to remain in place for a period of time to over-consolidate the underlying soft soils. When this additional fill material (or applied loading) is removed, the underlying soils would have experienced a higher loading than under the design loading of the roadway. Therefore, more settlement will occur and reduce the amount of secondary settlement, reducing the differential settlement along the extent of the alignment. Typically, wick drains are used to accelerate the time to consolidate the underlying soft soils, since they shorten the length of the drainage path that the water within the soil has to travel. Initially, wick drains were not going to be used on this project because previous research indicated that the phosphatic slime has a tendency to clog the openings in the geotextile fabric surrounding the plastic inner core of the wick drain. However, in the interest of reducing the period of time that the surcharge needed to be in-place, wick drains were decided to be used even if they remained effective for a shorter period of time than the surcharge was in-place.

With the increased heights of embankments due to the large amount of surcharge, an area of concern during design was the stability of the slopes (some as high as 30 to 35 feet) over the soft slimes. A second area of concern was determining the rate of consolidation of the phosphatic slimes. In order to estimate the soil parameters of the slime (strength, consolidation, and permeability), in-situ tests were the best means to gather reliable results since obtaining undisturbed samples in the slime would have been extremely difficult. These in-situ tests provided an estimate of the strength and the drainage characteristics of the soils.

5.3.2 SASW Testing

A series of nine SASW tests (six of which had phosphatic slime/clay at or near the ground surface) were performed along various locations of the proposed Polk County Parkway alignment, Section 5. In addition, five dilatometer (DMT) soundings were performed by FDOT State Materials Office and District I personnel. Four of these DMT locations were close to the SASW test sites, and were used as a comparison of moduli results between the two test methods. The fifth DMT site was located in an area which had approximately one foot of surface water, making any SASW testing in this area impossible. The DMT soundings were achieved by using the equipment from an all-terrain, 'mud bug' boring rig. The sites containing the phosphatic slime proved to be too inaccessible to the cone truck to perform any cone penetrometer (CPT) soundings. Numerous SPT borings were performed along the alignment of the project during the preliminary geotechnical investigation, which were used to identify the zones of phosphatic slime and soil layering.

This study provided an opportunity to test a site under difficult conditions. Most of the sites had a water table at the ground surface, and some of the testing was performed at sites which had an inch or two of surface water. The equipment was transported to the site and hand-carried to a particular location, proving the SASW test could be used at a remote and difficult-access site. The sites with surface water provided an opportunity to evaluate various sources under saturated conditions. The source which produced the best quality raw data was the cinder block which was rammed into the ground surface. This source provided a large surface area and a controlled impact that created a consistent transient wave even with water at the surface.

The SASW tests were performed as close to the DMT soundings as possible. Due to soil disturbances at the ground surface resulting from the DMT soundings, some distance (typically 10 to 20 feet) was required to find an accommodating location for the SASW test. Table 5.1 shows the locations of the SASW and DMT tests, as well as the closest SPT boring performed during the preliminary geotechnical investigation. The locations in Table 5.1 are referenced from stations and offset distances based on the centerline of construction.

Table 5.1 SASW, DMT, and SPT Locations for the Polk Co. Parkway

Site Number	SASW Location	DMT Location	SPT Location
4	729+00 5′ Lt	729+00 25′ Lt	729+00 15′ Lt
2	742+00 75′ Rt	742+00 80′ Rt	742+00 131′ Rt
4	773+70 137′ Rt	771+90 155′ Rt	774+00 155′ Rt
4	773+70 209′ Rt		
5	779+80 165′ Rt	780+00 159′ Rt	778+00 158′ Rt
6	780+55 165′ Rt		780+00 159′ Rt

The SASW test can be used as a quick means to determine the total thickness of the slime deposit at the test site. Since the slime can be considered a uniform, homogeneous surface layer, the critical wavelength can be directly related to the depth of the top layer (as outlined in Section 3.3.4, and refer to Figure 3.5). This is the same approach for determining the surface pavement thickness and stiffness from a SASW dispersion curve. This method of analysis has the advantage of being a quick means to reduce field data (determining the depth of the slime deposit at the test site within 15 to 20 minutes), compared to spending additional time to perform an inversion analysis (saving at least an hour or two of the operator's time). A typical dispersion curve from one of the SASW test sites (site 5) is presented in Figure 5.7. The remaining dispersion curves from the other SASW test sites are included in Appendix A as Figures A.16 through A.19.

Referring to Figure 5.7, several trends need to be addressed concerning the SASW results. The portion of the curve from wavelengths 0 to 6 feet contain slightly higher velocity material than the portion of the curve from wavelengths 6 to 25 feet. This initial portion of the curve either represents the slime crust near the ground surface, which is the phosphatic clay that has a lower moisture content than the deeper deposits, or a surface layer of sand tailings. This surface layer has higher shear strength values than the underlying clay, which is represented by the higher velocities from the dispersion curve.

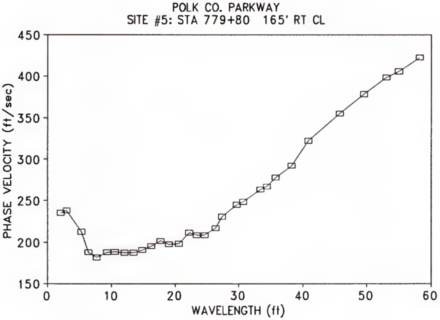

Figure 5.7 Dispersion Curve from the Polk Co. Parkway (Sta 779+80, 165′ Rt)

The portion of the dispersion curve in Figure 5.7 from wavelengths 6 to 25 feet represents the high moisture content phosphatic slime deposit. This part of the curve is very consistent, indicating a very homogeneous material. This was a very low velocity material (180 to 200 feet/sec), representing a low stiffness (with a Young's modulus of approximately 2,250 psi). Based on visual appearance, the phosphatic slime had the consistency of toothpaste. At wavelengths greater than 25 feet, a dramatic increase of velocity occurs, which is the result of the stiffer natural soils at this location. The

SPT borings indicated these soils consist of a sandy silt with traces of phosphates (with N-values of approximately 30). This stiff material provided a sharp contrast to the soft slime, resulting in a noticeable interface between the two layers.

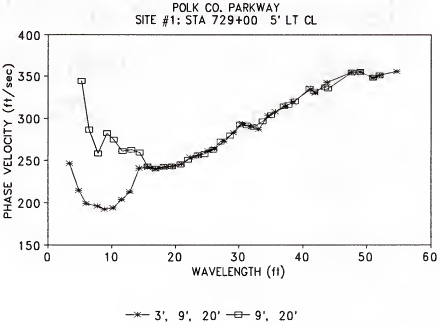

Figure 5.8 Comparison of Dispersion Curves from the Polk Co. Parkway (Sta 729+00, 5' Lt)

During the data reduction (development of the composite field dispersion curve), the importance of the shorter spacings for a highly variable site was noted. Figure 5.8 shows two dispersion curves for site 1. The first curve is the result of using all three test spacings (3, 9, and 20 feet), and the second curve uses only the data from the 9- and 20-foot spacings. Since the SASW test is a seismic test which measures the material properties of the soils between the two receivers, the properties of dissimilar materials are averaged. Smaller pockets of an isolated layer of material can be missed since its material properties are blended into the surrounding materials. This is the case with the results presented in Figure 5.8. The second curve (9- and 20-foot spacings) averaged the velocities of the phosphatic slime with the surrounding sand tailings, causing higher velocities than the corresponding curve using the smaller 3-foot spacing. The smaller spacing was able to sample the properties of the slime, while the longer spacings (9 and 20 feet) sampled the properties of the slime as well as the surrounding sand tailings yielding slightly higher velocities.

Table 5.2 SASW, DMT, and SPT Depth Results for the Polk Co. Parkway

Site Number	SASW Dispersion (ft)	SASW Inversion (ft)	DMT (ft)	SPT (ft)
4	10.5-14.5	10-15	14.5	16.5
2	26.0	24	14.5	17.5
3	23.0	12.5	18.5-23.5	23.5
4	18.0-22.5	17		
5	20.5-24.5	12	12.5-20.5	22.5
6	23.0-26.5	17		21.5

Using the method outlined in Section 3.3.4, the thickness of the phosphatic slime deposit was determined using the dispersion curves from each of the SASW test sites. For each dispersion curve, an inversion analysis was performed to determine the shear wave velocity profile for the test location. Table 5.2 shows the depths of the slime deposit from both methods, as well as the depths of slime from the DMT soundings and SPT borings. The Site Number in Table 5.2 refers to the SASW site location listed in Table 5.1.

As seen in Table 5.1, there were some differences in the locations of the various tests which could have resulted in some error in relating the total depth of deposits between the different test methods. The differences in the depths between the two SASW methods of analyses (the inversion analysis yielded smaller depths than the dispersion analysis) can be attributed to the maximum spacing used during the field testing being only 20 feet. The maximum wavelength measured was close to the depths that needed to be measured (approximately 20 to 25 feet). To accurately define the dispersion curve, longer wavelengths are needed to gather enough information for greater depths of soil deposits to be resolved during the inversion analysis. Typically, the maximum spacing should be twice that of the deepest soil deposit to be surveyed. This was not possible at this site because of the difficulty in transporting a large mass to the remote sites. Except for the depths resulting from the SASW inversion analyses, the depths from the other test methods (SPT, DMT, and the SASW dispersion analysis) were quite similar.

Based on the DMT results, the maximum shear moduli (DMT G_{max}) were determined for the various test depths using Eqn. 2.21. The results from this analysis (the average of the G_{max} values for the entire phosphatic slime layer) are presented in Table 5.3. Table 5.3 also includes the maximum shear moduli from the SASW test (SASW G_{max}) using the shear wave velocities generated from the inversion analyses, and the average of the SPT N-values within the slime layer from the preliminary borings. The Site Number in Table 5.3 refers to the SASW site location listed in Table 5.1.

Table 5.3 SASW, DMT, and SPT Stiffness Results for the Polk Co. Parkway

Site Number	SASW G_{max} (psi)	DMT G_{max} (psi)	SPT N-Value (Avg. Blows/ft)
1	1,035	2,045	1.5
2	1,007	2,022	1.5
3	919	2,232	2.1
3	718		
5	675	2,260	1.4
6	602		3.1

A typical DMT shear modulus profile is presented in Figure 5.9. A comparison of the shear modulus profiles from the SASW and DMT results for this same location (sites 5 and 6) is shown in Figure 5.10. The shear modulus profiles for the remaining test sites are included in Appendix A as Figures A.20 through A.25.

Referring to either shear modulus profile (SASW or DMT), the limits of the phosphatic slime are very apparent since the low stiffness of the soft clay contrasts significantly with the underlying soils. The stiffness profiles also reveal that the slime is quite consistent, with a narrow range of modulus values. The results from Eqn. 2.21 (DMT G_{max}) did not agree well with the SASW results. Referring to Table 5.3, the DMT shear moduli were much higher than the SASW moduli. Since the DMT equation is empirically-based, the differences can be due to the limited database from which it was derived. It was based on studies from nine test sites which included a variety of soil types (gravel, sand, silt, and clay). Due to the unique nature of the phosphatic slime/clay, it is uncertain that its properties can be defined by empirical relationships derived from a database of conventional soil types.

The initial Young's modulus was calculated from Eqn. 2.34 using the DMT results. The constrained modulus was determined by Eqn. 2.37 using the elastic properties (V_S, G_{max}, and E_{max}) obtained from the SASW test, and compared with the drained constrained modulus (M) which is one of the output parameters from the DMT software. The DMT constrained modulus was obtained from correlations developed by Marchetti. Neither of these comparisons yielded any better results than the shear

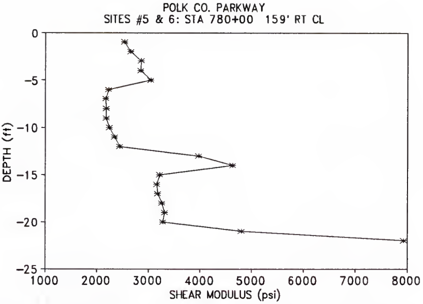

Figure 5.9 DMT Shear Modulus Profile from the Polk Co. Parkway (Sta 780+00, 159′ Rt)

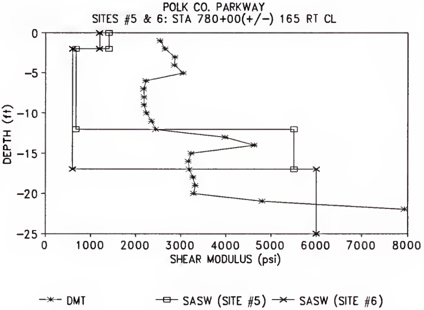

Figure 5.10 Comparison of DMT and SASW Shear Modulus Profiles from the Polk Co. Parkway (Sta 780+00, 165′ Rt)

modulus, but the results in these cases were much lower than the SASW results. The initial tangent Young's moduli were in the range of 15 to 60 percent of the SASW Young's moduli. The DMT constrained moduli were on the order of 1.5 to 6.5 percent of the SASW constrained moduli. These results are summarized in Table 5.4. Since the SASW moduli are elastic parameters, they represent a maximum value. These others relationships were developed at higher strain levels, and therefore; the resulting moduli would represent moduli in the inelastic range and would result in a lower value than the SASW results.

Table 5.4 SASW and DMT Young's and Constrained Moduli Results for the Polk Co. Parkway

Site Number	Young's Modulus (psi)		Constrained Modulus (psi)	
	SASW	DMT	SASW	DMT
1	2,690	1,062	3,621	161
2	2,625	387	3,534	56
3	2,391		3,219	
4	1,867	635	2,513	97
5	1,755		2,363	
6	1,565	1,016	2,107	135

5.4 Kanapaha Site

This site was located in the Kanapaha region of Gainesville, approximately one mile west of Tower Road (SW 75th Street) and Archer Road (SR-24), on FDOT owned land. The site was chosen because many soundings and borings were performed at the site in conjunction with previous research by the University of Florida, which indicated that the top of the limerock was quite variable and relatively near the surface. Due to the variable nature of the top of limerock throughout Florida, there is concern when designing foundations on this material. This site was chosen to determine if the SASW test method could be useful to map out a larger area of the subsurface conditions than other in-situ tests, and to determine the competency of the limerock over a certain area.

5.4.1 Background Information

Based on previous field testing (Townsend et al., 1991), nonhomogeneous subsurface conditions were present at this site, which is the norm for this area of the state (i.e. surficial sands, clay cap, and limerock). The CPT soundings performed by University of Florida (UF) personnel revealed that the typical profile at this site consisted of surface sands that varied from depths of 5 to 20 feet, a clay layer at depths of 5 to 29 feet (with a thickness of 4 to 12 feet), a soft limerock layer at depths of 13 to 43 feet (with a thickness of 1 to 29 feet), and a competent limerock layer at depths of 24 to 43 feet.

5.4.2 SASW Testing

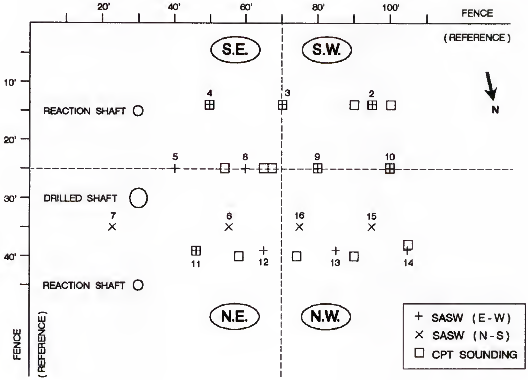

Figure 5.11 Plan View of the Kanapaha Site

A series of 15 SASW tests were performed over an area of approximately 30 feet by 70 feet. All of the SASW tests utilized individual spacings of 3, 9, and 20 feet. Surveys were performed in a north-south orientation as well as an east-west alignment in order to evaluate the nonhomogeneity of the top of limerock of the test area. Thirteen cone penetrometer soundings were performed by FDOT personnel to determine the soil profile at the SASW test sites. In addition, eight cone penetrometer soundings and two SPT borings were performed in conjunction with the previous research study at this site. Dynamic cone penetrometer (DCP) tests were performed at the centerline of each of the SASW test locations and were performed to a typical depth of four feet.

Table 5.5 SASW and DCP Locations for the Kanapaha Site

SASW / DCP Site No.	Testing Orientation	Test Site Location, ft North	West
2	E-W	14	95
3	E-W	14	70
4	E-W	14	50
5	E-W	25	70
6	N-S	35	56
7	N-S	35	23
5	E-W	25	65
5	E-W	25	70
10	E-W	25	100
1[illegible]	E-W	39	65
1[illegible]	E-W	39	65
13	E-W	39	85
14	E-W	39	105
15	N-S	35	95
16	N-S	35	75

Figure 5.11 shows the locations of the various tests which were performed for this current research. It does not include the locations of the borings and soundings which were performed for the previous drilled shaft research project.

The drilled shaft and reaction shafts shown in Figure 5.11 are from this previous project. Table 5.5 shows the site numbers and locations for the SASW and DCP tests, and Table 5.6 reveals the same information for the cone penetrometer (CPT) soundings. The site numbers for the SASW test locations (as well as for the DCP tests), which are shown in Table 5.5, are displayed in Figure 5.11 alongside the representative symbol.

Table 5.6 CPT Locations for the Kanapaha Site

CPT Sounding No.	Test Site Location, ft North	West
1	40	58
2	40	70
3	40	95
4	40	105
5	25	50
6	25	67
7	25	50
8	25	50
9	25	100
10	40	50
11	40	70
12	40	95
13	14	100
14	14	90
15	39	46

The test locations displayed in Tables 5.5 and 5.6 are referenced from the fencelines (in feet) shown in Figure 5.11. The SASW test at site 1 (not included in Table 5.5) was outside the limits of the general test area, and was performed prior to the decision to use the area shown in Figure 5.11. The results from this test were not used in this analysis. A row of north-south SASW tests was not performed between the southernmost two rows of tests because of a lack of space to drop the source weight for the 20-foot spacing.

5.4.2.1 Location of top of limerock

The analysis of the SASW tests was divided into four quadrants over the entire area tested. The boundaries for each quadrant are identified on Figure 5.11. Sites 5, 6, 7, 8, 11, and 12 were grouped into the northeast quadrant; sites 9, 10, 13, 14, 15, and 16 were in the northwest quadrant; sites 3, 4, 5, and 8 made up the southeast quadrant; and sites 2, 3, 9, and 10 comprised the southwest quadrant. The dispersion curves for the SASW tests for each of these quadrants are presented in Figures 5.12 to 5.15. The same X- and Y-axis scales are used for all four plots so that a comparison of the individual dispersion curves is possible. Gridlines are also used on the plots to aid in this process.

In order for the SASW test method to be used as quick means to determine the top of the limerock and to get a general map of the subsurface conditions, the results need to be obtained as quickly as possible. Therefore, a comparison

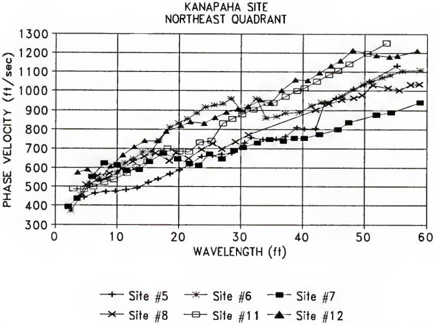

Figure 5.12 Dispersion Curves for the N.E. Quadrant of the Kanapaha Site

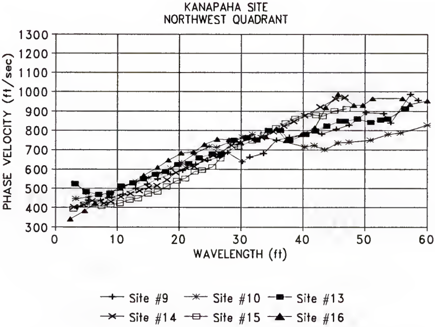

Figure 5.13 Dispersion Curves for the N.W. Quadrant of the Kanapaha Site

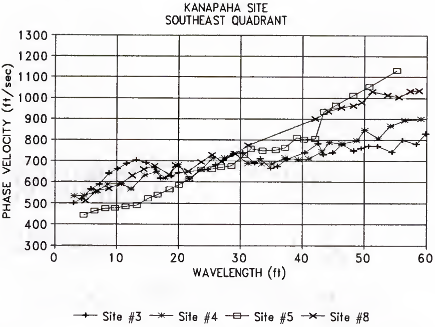

Figure 5.14 Dispersion Curves for the S.E. Quadrant of the Kanapaha Site

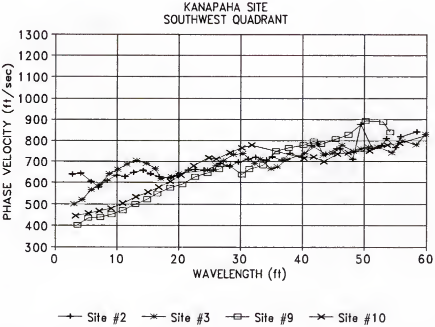

Figure 5.15 Dispersion Curves for the S.W. Quadrant of the Kanapaha Site

of dispersion curves would provide a quick means to provide the stiffness profile of a test site. If a competent limerock is within the depth of the SASW survey, a dramatic stiffness increase should appear on the dispersion curve. Comparison of dispersion curves has the advantage of speed, but the disadvantage of only providing a relative indicator of stiffness and depth. If quantitative values are needed, an inversion analysis can be performed, but SASW data reduction in karst topography would be difficult (since the resulting dispersion curve is highly irregular) and would require more time than a standard inversion analysis.

Based on the comparison of dispersion curves, most of the sites in the northeast quadrant (sites 5, 6, 8, 11, and 12) have higher surface wave velocities than the remaining dispersion curves. The only exception is site 7 which was located on the fringe of the test area. The higher measured velocities in the northeast quadrant would indicate that limerock (or some stiff material) is present within the depth of the SASW survey. Since the maximum spacing was 20 feet, the approximate survey depth of the SASW tests was 20 feet as well. The dispersion curves also reveal that the limerock at sites 5 and 8 is deeper than at sites 6, 11, and 12 because the higher velocities occurred at longer wavelengths (approximately 42 feet) compared to the other sites (about 20 to 30 feet), and longer wavelengths correspond to deeper soil deposits.

Inversion analyses were performed for each of the SASW tests. These results are presented in Table 5.7 for the SASW sites which appeared to have limerock within the limits of the survey depth (based on the analysis of the dispersion curves). The remaining inversion results are included in Appendix A as Table A.1. The H-S in Table 5.7 represents the half-space used for the analysis. The shear moduli and Young's moduli were determined by using assumed values of Poisson's ratio of 0.25 and mass density of 3.0 lb/ft^3 (where the bulk density is defined as the total unit weight divided by the gravitational constant, γ_t/g).

From the results of the CPT soundings, the depth to the limerock was estimated using the tip resistance (q_c) profile. The depth at which the CPT tip resistance rose sharply and maintained this higher tip resistance was taken as the depth to competent limerock. On many occasions the sounding was stopped at this point due to the system quitting for an excessive inclination of the cone tip. This is a safety measure to ensure the rods are not out of vertical alignment to a degree that if a stiff layer is encountered, buckling of the rods could cause one of the joints to break. If this occurred at a reasonable depth, this was assumed to be the depth to competent limerock and not due to encountering a boulder. Table 5.8 contains the estimated depths to the limerock for each of the CPT locations. It also contains the peak tip resistance at the point that the q_c profile rose

Table 5.7 SASW Results for the Kanapaha Site

Layer Thickness (ft)	Total Depth (ft)	Shear Wave Velocity (ft/sec)	Shear Modulus (psi)	Young's Modulus (psi)
Site No.5				
5.0	5.0	500	5,210	13,020
5.0	10.0	650	8,800	22,010
5.0	15.0	950	18,800	47,010
H-S	H-S	1000	20,830	52,080
Site No.6				
2.0	2.0	450	4,220	10,550
3.0	5.0	600	7,500	18,750
10.0	15.0	1100	25,210	63,020
H-S	H-S	900	16,875	42,200
Site No.8				
5.0	5.0	600	7,500	18,750
5.0	10.0	800	13,330	33,330
7.0	17.0	850	15,050	37,630
H-S	H-S	850	15,050	37,630
Site No.11				
5.0	5.0	550	6,300	15,760
6.0	11.0	850	15,050	37,630
5.0	16.0	950	18,800	47,010
H-S	H-S	950	18,800	47,010

Table 5.7 (Continued)

Site No.12				
Layer Thickness (ft)	Total Depth (ft)	Shear Wave Velocity (ft/sec)	Shear Modulus (psi)	Young's Modulus (psi)
3.5	3.5	580	7,010	17,520
3.0	6.5	880	16,130	40,330
10.0	16.5	1000	20,830	52,080
H-S	H-S	1000	20,830	52,080

Table 5.8 CPT Depths to Limerock for the Kanapaha Site

CPT Sounding Number	Estimated Depth to Limerock (ft)	Tip Resistance of Limerock (tsf)
1	21	224
2	30	172
3	20	230
4	30	221
5	25-36 (Cavities)	233-224
6	5	276 (Quit for Inclination)
7	30	196
8	30	196
9	19	435 (Probable Boulder)
10	30	196
11	36	391
12	-	Quit at 3.6 ft (Hit Boulder)
13	-	Quit at 2.0 ft (Hit Boulder)
14	32	235
15	20	222

sharply, indicating a competent limerock interface. The raw CPT field data (cone tip resistance versus depth plots) are included in Appendix A as Figures A.26 to A.37.

Based on Table 5.8, the CPT soundings revealed shallower depths of limerock in the northeast quadrant (sites 1, 5, 6, and 15), which support the SASW results. The only exceptions were sites 3 and 9, and the cone tip probably hit a boulder at site 9. The CPT depths to limerock in the northeast quadrant ranged from 20 to 25 feet, which was within the sampling range of the SASW test (maximum spacing of 20 feet). The remaining sites showed limerock at depths of 30 feet and greater, which was beyond the sampling depth of the SASW tests performed for this study.

The results from the SASW inversion analyses (Table 5.7) indicate a stiff layer in the range of depths from 15 to 17 feet, which does not correspond well with the depths to limerock obtained from the CPT soundings. This might be due to the limited maximum spacing used during the SASW field tests. The 20-foot spacing was used because of the limited space (due to the location of the fences) and the lack of an available source that could produce source waves which could be detected by longer spacings. The 20-foot spacings allowed measurement of wavelengths which were just long enough to sample the limerock. This is reflected in the dispersion curves, but not in the inversion analyses. The dispersion curves are useful for this purpose since changes in the stiffness profile are reflected for the entire depth of the SASW survey. For the inversion analysis, the greater depths of the SASW survey affect the final profile less than the shallower depths. Typically, the maximum depth of the theoretical profile (above the half-space) should be on the order of one-half to one-third of the maximum wavelength measured. During this analysis, a range of velocities of approximately 500 ft/sec for layers at depths greater than 15 feet produced very small changes in the shape of the resulting dispersion curve. This lack of sensitivity to resolve deeper layers indicates that a SASW survey needs to be performed at spacings long enough to produce wavelengths that can sample soils much deeper than solely the depths of interest. This will ensure that the soil parameters within the depths of interest are accurately defined in the theoretical profile established from the inversion analysis. This must be considered prior to field testing because a source needs to be obtained to create surface waves which can be detected at these longer spacings.

Figure 5.16 is the SPT boring log from the previous University of Florida study performed at this site. It corresponds to SASW test site 5 (25'N 40'W), so has been included in this report. It shows that competent limerock is present at depths from 23 to 25 feet (based on N-values greater than 20 blows/ft). This is consistent with the results from the CPT soundings in this area. This log also

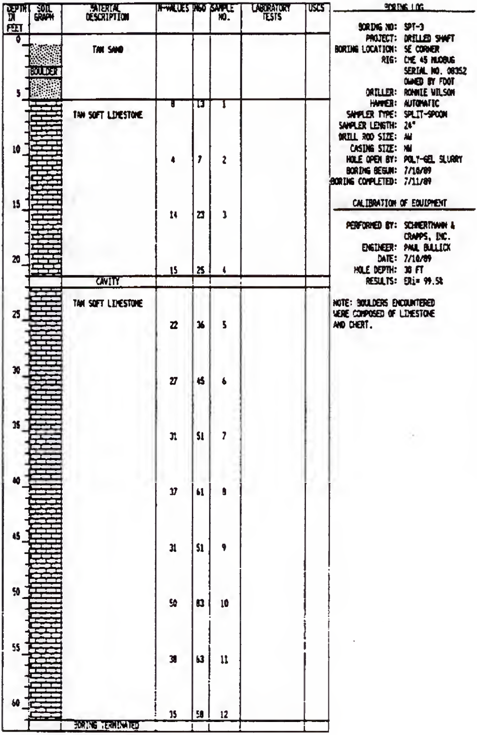

DEPTH IN FEET	SOIL GRAPH	MATERIAL DESCRIPTION	N-VALUES	N60	SAMPLE NO.	LABORATORY TESTS	USCS
		TAN SAND					
		TAN SOFT LIMESTONE	8	13	1		
			4	7	2		
			14	23	3		
			15	25	4		
		CAVITY					
		TAN SOFT LIMESTONE	22	36	5		
			27	45	6		
			31	51	7		
			37	61	8		
			31	51	9		
			50	83	10		
			38	63	11		
			35	58	12		
		BORING TERMINATED					

BORING LOG

BORING NO: SPT-3
PROJECT: DRILLED SHAFT
BORING LOCATION: SE CORNER
RIG: CME 45 MUDBUG
SERIAL NO. 08352
OWNED BY FDOT
DRILLER: RONNIE WILSON
HAMMER: AUTOMATIC
SAMPLER TYPE: SPLIT-SPOON
SAMPLER LENGTH: 24"
DRILL ROD SIZE: AW
CASING SIZE: NW
HOLE OPEN BY: POLY-GEL SLURRY
BORING BEGUN: 7/10/89
BORING COMPLETED: 7/11/89

CALIBRATION OF EQUIPMENT

PERFORMED BY: SCHMERTMANN & CRAPPS, INC.
ENGINEER: PAUL BULLICK
DATE: 7/10/89
HOLE DEPTH: 30 FT
RESULTS: ERi= 99.5%

NOTE: BOULDERS ENCOUNTERED WERE COMPOSED OF LIMESTONE AND CHERT.

Figure 5.16 Boring Log at Site 5 (25'N 40'W) from the Kanapaha Site (Townsend et al., 1991)

reveals how soft the weathered limerock is at this site (from depths of 5 to 21 feet), with N-values ranging from 4 to 15 blows/ft. These values are representative of a loose sand, and show how difficult it can be to determine an absolute depth to the limerock using the CPT since no sample is recovered. The variable nature of limerock could make any depth resulting from a seismic test, which measures the stiffness of soils for the volume of soil between the receivers, not as accurate as a point resistance loading. The seismic test 'averages' this volume of soil sampled so any variations (pinnacles in the limerock or transitions caused by weathered and intact limerock) will not appear as drastic as with a point loading. The CPT (i.e. point loading) samples a small volume of soil (diameter of cone tip is 35.7 mm), so it can detect small variations which might be encountered during a sounding. This might not always be advantageous since small variations, such as a boulder, might cause misleading results and end the test before the true top of limerock is encountered. Another disadvantage of penetration tests is the soil disturbance created by the cone or split-barrel sampler (SPT) being pushed or driven into the ground. This action can break up any natural cementation of the underlying soils and result in lower stiffness values than actually exist.

5.4.2.2 Comparison of field moduli results

Several methods were used to estimate the stiffness profiles at the SASW test locations. Figure 5.17 presents a comparison of several methods using CPT data to estimate the maximum shear modulus: relationships derived from Jamiolkowski (Eqn. 2.19), Imai and Tonouchi (Eqn. 2.20), and Olsen (Fig. 2.5). The Jamiolkowski equation and the Imai and Tonouchi equation primarily are affected by the CPT's tip resistance (q_c), and both equations yielded similar results. These two equations produced stiffness profiles which had the same shape as the CPT q_c profile, and the primary difference was the constant which was multiplied to the value of q_c. The Olsen method produced results which were favorable to the other two methods, but was cumbersome to use for a large amount of data (since a figure is required). The Imai and Tonouchi equation was used to estimate a shear modulus profile for the remaining CPT soundings because of the similarity of results between the various relationships and the ease of using this equation which allowed its use in a spreadsheet.

Equation 2.20 is a relationship to estimate the maximum shear modulus so it can be compared with the elastic modulus values obtained from the SASW test. Figure 5.18 presents a typical comparison of the SASW and CPT (using the Imai and Tonouchi relationship) methods to estimate shear modulus. The remaining plots comparing the results from the two test methods for similar locations are included in Appendix A as Figures A.38 through A.48.

A comparison of the two stiffness profiles for several sites reveals that both yield similar results up to depths of

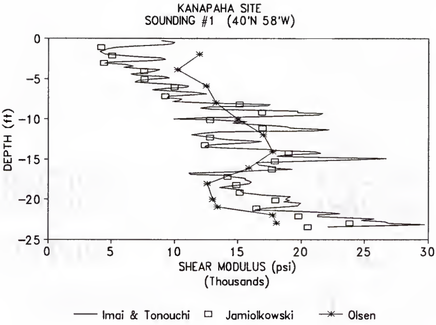

Figure 5.17 Comparison of CPT Shear Modulus Profiles from the Kanapaha Site (40'N 58'W)

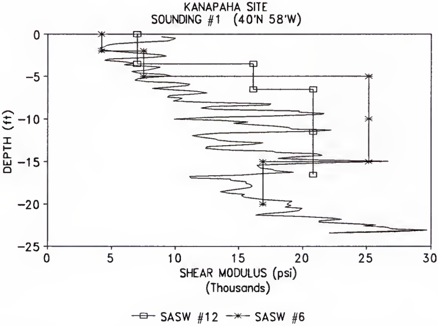

Figure 5.18 Comparison of Shear Modulus Profiles from the Kanapaha Site (40'N 58'W)

approximately 10 feet. Based on the results from the sites where the centerline of the SASW survey was performed at the exact location of the CPT sounding, the shear moduli from the two tests were generally within 20 percent agreement for depths up to 10 feet, with maximum differences being as high as approximately 50 percent (due to peaks in the CPT sounding). The comparison at greater depths is typically less favorable, with the SASW results usually being higher. During the inversion analyses, the velocities of the deeper layers had a smaller influence on the resulting theoretically-derived dispersion curve (resulting in a wider range of velocities that would produce a similar dispersion curve). This is the result of the field dispersion curve not being extended to long enough wavelengths to define these greater depths. Also, a possible reason why the SASW moduli are typically higher than the CPT's results is that the SASW's moduli truly reflect an elastic modulus of the soil, while the CPT moduli are based on empirical relationships and might not take into account the soil disturbance due to the penetration of the cone tip for all soil types. This effect could be severe for cemented soils since the disturbance could break down the soil and cause lower stiffness values than an undisturbed test method.

Figure 5.19 presents a comparison of various methods to estimate the Young's modulus from a typical test location. The Imai and Tonouchi shear moduli (from Figure 5.17) were used with the elastic theory equation (Eqn. 2.32), assuming a Poisson's ratio of 0.25, to develop a Young's modulus profile.

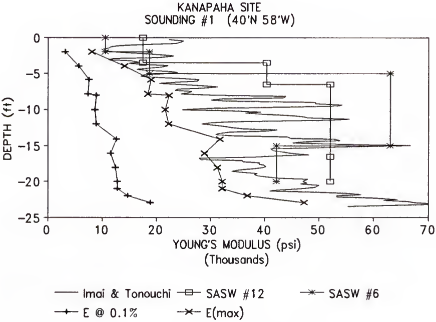

Figure 5.19 Comparison of Young's Modulus Profiles from the Kanapaha Site (40'N 58'W)

Since the estimated shear modulus is a maximum value, it can be used to estimate an elastic Young's modulus. This was compared with the two SASW test results near this CPT sounding. The method from Beraldi (Figure 2.7) was used to estimate the Young's modulus at 0.1% strain at several test depths. Since this strain level is higher than the elastic threshold (approximately 0.001%), a correction factor was needed in order to be able to compare these moduli with the other results. This was achieved by using Figure 2.13, which results in a normalized Young's modulus ratio ranging from

0.40 to 0.50. The data points labeled E(max) are the Beraldi results with a correction factor of 0.40 applied to them.

The drastic differences in the Young's moduli based on strain level are apparent by referring to Figure 5.19. The original Beraldi results (E @ 0.1%) are much lower than the elastic moduli results. Even with a correction of 40%, these results are still lower, especially in the range of depths from 5 to 15 feet.

5.4.2.3 Detection of anomalies in limerock

Based on the dynamic cone penetrometer (DCP) test performed at the centerline of the SASW test at site 6, a small void (approximately 16 inches in depth) was discovered about 1.5 feet below the ground surface. This provided an excellent opportunity to determine the capability of the SASW test for void detection. The results of the DCP test at this location are shown in Figure 5.20.

Since it was known that a small void existed close to the ground surface, a dispersion curve was created at this location using only the 3- and 9-foot spacings in order to obtain a better defined curve at lower wavelengths (corresponding to shallower depths). Figure 5.21 shows this resulting dispersion curve. It can be seen that a small dip exists in this dispersion curve from wavelengths of approximately 6 to 9 feet. Dividing these wavelengths by three (refer to Section 2.1), the approximate depths corresponding to this dip (2 to 3 feet) are consistent with the depths of

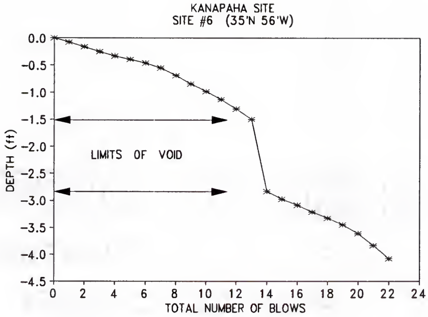

Figure 5.20 DCP Test Results from the Kanapaha Site (35'N 56'W)

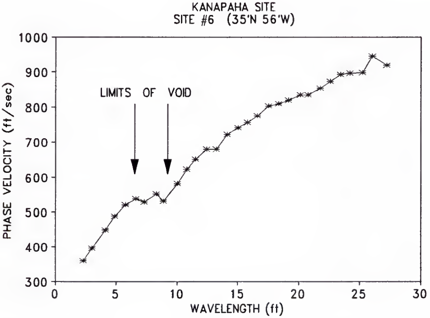

Figure 5.21 Dispersion Curve from the Kanapaha Site (35'N 56'W)

the void. It should be noted that this small dip in the dispersion curve for site 6 could not be distinguished in the dispersion curve using the 20-foot spacing, since the expanded scale made this anomaly too small to be identified. Therefore, the void detection capability of the SASW test is dependent upon the size of the void, the depth of the void, and the maximum wavelength measured during the field test.

An inversion analysis was performed on the dispersion curve shown in Figure 5.21. The resulting soil profile is presented in Figure 5.22. Based on these results, it can be seen that a lower velocity layer exists from depths of 2 to 4 feet. This was consistent with the depths recorded by the DCP test. Since the SASW method samples a volume of soil, there is an averaging of nonhomogeneous layers. Therefore, the void is a zero velocity material, but is averaged with the surrounding soils which do have a velocity. Due to this, it cannot be determined whether an anomaly is a open cavity or it is filled with a lower velocity material than the surrounding soils.

It must be noted that this analysis was performed knowing the void existed and its location. Without any prior knowledge of the soil profile at this site (i.e. from borings or soundings), it would have been impossible to know for certain the presence of a void. Since a lower velocity layer appears in the final results, it is not known if this layer represents a void, a clay-filled void, or just a less stiff layer between two stiffer layers. Although, seeing this occurrence should be an indication that additional field testing at this site might be warranted.

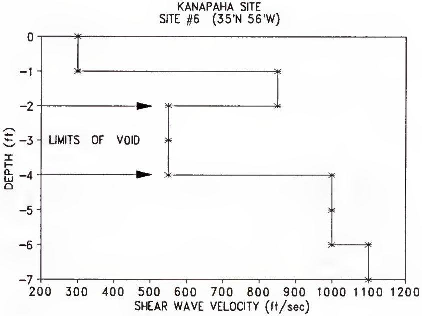

Figure 5.22 S-Wave Velocity Profile from the Kanapaha Site (35’N 56’W)

5.4.2.4 Comparison of sources

Several types of sources were used to evaluate them in obtaining the highest quality raw data. The field data (cross power spectrum) was judged based on the corresponding coherence trace to decide which source gave a wider range of useable data. The sources were also judged based on the resultant dispersion curves by comparing the individual dispersion curves to determine which yielded more consistent data. For shorter spacings (3 and 9 feet), the sledgehammer, drop hammer, and dynamic cone penetrometer (dropping the mass while the rod was in the ground) were evaluated as sources. For the longer spacing (20 feet), the sledgehammer, 140-lb drop hammer, and dropping a flat concrete block were evaluated.

Figures 5.23 and 5.24 are the cross power spectrum and coherence plots of typical field results from the signal analyzer using the sledgehammer and DCP for a 3-foot spacing. There was not much difference in the results between the sledgehammer and the DCP at this spacing. Based on Figures 5.23 and 5.24, both sources produced consistent data up to a frequency of approximately 220 Hz (based on coherence values greater than 0.90), and the resultant dispersion curves were similar.

Figures 5.25 and 5.26 are the signal analyzer plots for a 9-foot spacing from the same test site. These figures indicate that the DCP produced useable data over a wider range of frequencies than the sledgehammer (nearly the entire bandwidth, 200 Hz, versus approximately 130 Hz). The resulting dispersion curve for this DCP data is more consistent at the higher frequency (lower wavelength) range than the corresponding curve from the sledgehammer data. This difference is typically insignificant since this data is combined with the data from the remaining spacings, and the entire number of data points are averaged to produce the composite dispersion curve.

Figures 5.25 and 5.26 show that the DCP typically produced higher quality data in the higher frequency range than the sledgehammer. This is consistent with previous research, which has shown that lighter weight sources with a quick impulse will produce higher frequency source waves as compared to heavier ones with a longer impulse (i.e. the sledgehammer). As a general rule, the DCP (or hitting a rod embedded into the ground with a hammer) provided a better source for sites with dry, loose surficial soils. This is because the DCP allowed more of the input energy to be transmitted into the ground because of the embedment of the rod. The energy from the sledgehammer blow was dampened by the loose surface soils, and the source wave was weaker as it traveled to the receivers.

For the longer spacings, the larger contact area (the sledgehammer, drop weight, or concrete block) usually worked better than the DCP. The larger contact area allowed more energy from the blow to be transmitted directly into the ground. Since the drop weight and concrete block were heavier and had a larger contact area than the sledgehammer, they were able to trigger the signal analyzer at a lower threshold energy. When data was recorded from the sledgehammer, the results were very similar to the drop weight or concrete block. Figures 5.27 and 5.28 show typical results for the sledgehammer and concrete block for the same site at a 20-foot spacing. The large drop weight (140-lb SPT hammer) produced

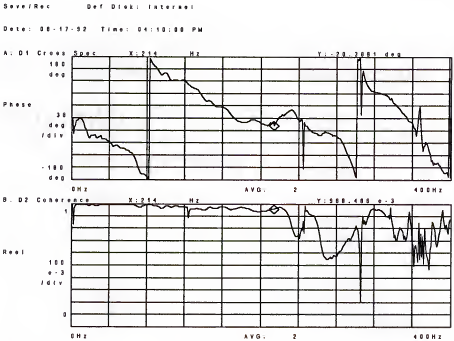

Figure 5.23 Signal Analyzer Plots using the Sledgehammer (3′ Spacing)

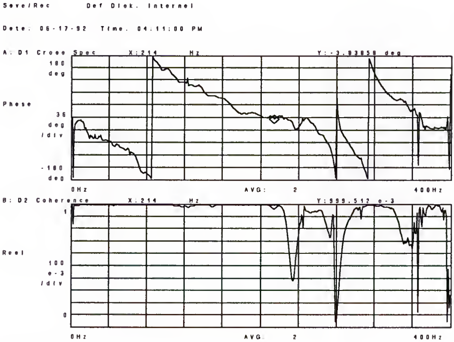

Figure 5.24 Signal Analyzer Plots using the DCP (3′ Spacing)

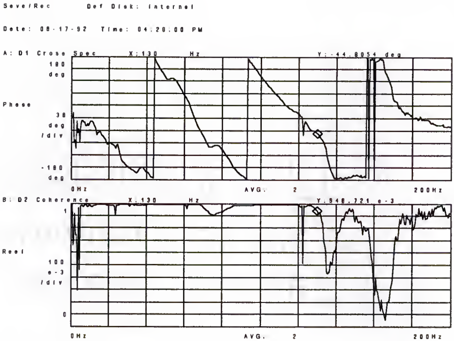

Figure 5.25 Signal Analyzer Plots using the Sledgehammer (9′ Spacing)

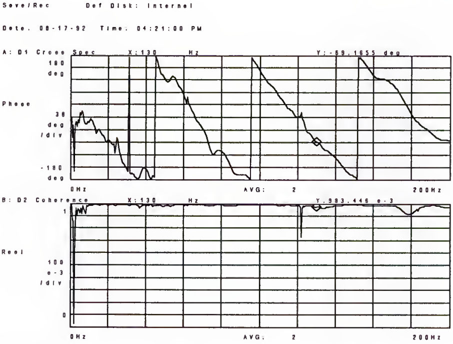

Figure 5.26 Signal Analyzer Plots using the DCP (9′ Spacing)

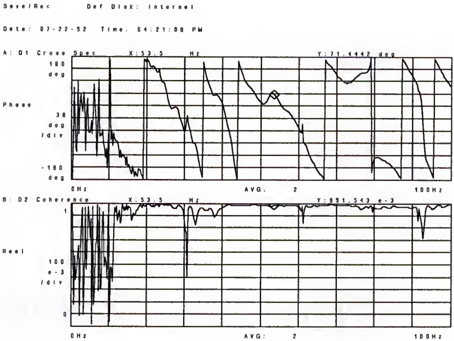

Figure 5.27 Signal Analyzer Plots using the Sledgehammer (20′ Spacing)

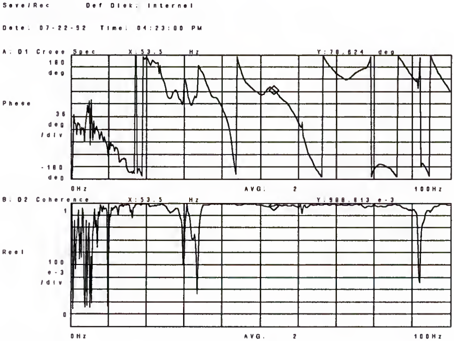

Figure 5.28 Signal Analyzer Plots using the Concrete Block (20′ Spacing)

good results at long spacings, but proved to be hard to use. It was difficult for two people to drop the mass at the same time with the proper alignment to get a solid impact, and there was concern over the safety of the people repeatedly dropping this large mass.

Comparing the different sources has shown that each one will produce the same final results. The difference is the range of useable data obtained in order to produce a well-defined dispersion curve. This is especially true for the longest spacing, since it is desirable to obtain the highest quality low frequency data to extend the dispersion curve out to the longest possible wavelength to analyze the deepest possible soil deposits. Although, it is important to remember that the success of an individual source is very site dependent, and not just dependent upon the spacing used during the test. The attenuation properties of the site's soils will determine how the source wave will travel through the medium to be detected by the two receivers. Therefore, the general rule used during the field testing for this research was to bring all the sources that were available to the site, and use an individual source based on the receivers' spacing, site conditions, number of personnel available, and past success of that source under similar conditions.

5.4.2.5 Comparison of SASW and DCP results

A dynamic cone penetrometer (DCP) test was performed at the centerline of each SASW survey. These tests were performed by David Weintraub in conjunction with his research project, which was to develop an automated DCP prototype and to evaluate unsurfaced airfield seismic surveying using SASW technology (Weintraub, 1993). The DCP tests were performed to a depth of four feet, and a continuous record of total penetration for each drop of the hammer was recorded. Based on the following empirical relationship developed from research performed at the Waterways Experiment Station (Webster et al., 1992), California Bearing Ratio (CBR) values were obtained:

$$Log\ CBR = 2.46 - 1.12(Log\ DCP) \tag{5.2}$$

where: CBR = California Bearing Ratio (%)

DCP = DCP penetration index (mm/blow).

Table 5.9 shows the averaged CBR values from the DCP tests for the entire test depth. If the test was ended prior to reaching full-depth (sites 11, 12, and 16) because of hitting rock or a boulder, two CBR values are recorded; the first is the CBR above the rock and the second is the value obtained upon hitting the rock. The DCP E_{max} values in this table were obtained from the relationship developed by Chua (Figure 2.8) using Eqn. 2.35. Table 5.9 also includes the averaged CPT tip resistance (q_c) for the initial four feet of penetration, if a sounding was performed at the DCP site or in the near vicinity (otherwise no data is given). Results from the SASW inversion analyses (V_S and E_{max}) for the theoretical profile to depths of approximately 5 feet are also presented. If two results are given for an individual site, the theoretical profile contained two layers within the initial five feet.

Table 5.9 Comparison of SASW and DCP Results for the Kanapaha Site

SASW Site No.	DCP Avg. CBR (%)	DCP Avg. E_{max} (psi)	CPT Avg. q_c (tsf)	SASW V_S (ft/sec)	SASW E_{max} (psi)
2	30.2	15,356	34.2	680	24,170
3	9.9	7,410	27.9	550	18,750
4	9.5	7,900	29.3	550	18,610
5	15.6	10,410	-	450	12,780
6	4.2 (Void)	3,624	-	450 600	7,500 18,750
7	11.2	8,210	-	467 758	11,390 29,930
8	8.9	6,450	30.3	600	18,750
9	11.9	8,330	38.7	450	10,690
10	12.9	9,210	58.1	500	12,920
11	15.4 105$^+$	10,600 53,890	37.7	550 850	15,700 37,700
12	84$^+$	25,410 39,460	41.3	580 880	17,500 40,350
13	12.5	12,310	47.9	547	15,560
13	11.0	9,100	56.2	450	10,560
15	11.5	9,520	-	450	15,560
16	11.6 96$^+$	8,530 63,520	-	400 750	8,330 29,240

Based on the analysis of the SASW dispersion curves, the top of limerock was encountered within the range of the SASW survey depth (approximately 20 feet) for sites 5, 6, 8, 11, and 12; indicating limerock is near the ground surface in the northeast quadrant of the test area. These results also revealed that the limerock was closest to the ground surface for sites 6, 11, and 12. This is consistent with the DCP test results. The DCP tests which ended prior to the full-depth of testing because of hitting a boulder were sites 11, 12, and 16; located in the northeast quadrant. In addition, the DCP test at site 6 encountered a void, which was also located in the northeast quadrant.

The SASW and CPT tests revealed that the top of limerock was deeper than four feet (the test depth of the DCP). Both test methods showed that more competent limerock was present at shallower depths in the northeast quadrant compared to the other areas. It would be anticipated that the zone of weathered limerock would be present at very shallow depths in the northeast quadrant. Referring to Figure 5.16, the SPT boring revealed weathered limerock at 5 feet, and a boulder at 2 feet. This layer of weathered limerock contains numerous boulders, which the DCP tests at sites 11, 12, and 16 probably hit during testing.

The SASW Young's moduli were consistently higher than the DCP values. This can be seen in Figure 5.29 which presents a comparison of the DCP and SASW Young's moduli for a typical test site. The DCP modulus profile reveals high points which are probably the result of the tip hitting a small rock, causing lower penetrations. These high points were not used in determining the average DCP moduli which are presented in Table 5.9.

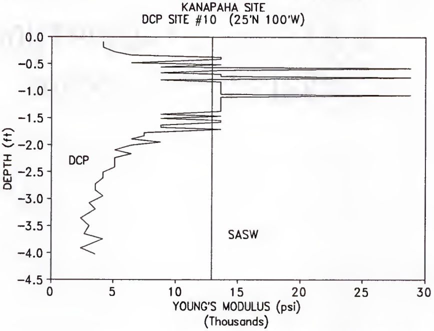

Figure 5.29 Comparison of DCP and SASW Young's Modulus Profiles from the Kanapaha Site (25'N 100'W)

It is uncertain for which soil types the Chua relationship was formulated. A weathered limerock would not fall into the category of a classical soil type, and poses the problem of breaking down as the cone tip is driven into the ground. Therefore, it is uncertain whether the Chua relationship applies to this type of soil. Based on this analysis, it seems to under-predict the material's stiffness. This analysis indicates the difficulty of predicting elastic properties of soils using field tests performed at high strain levels. Although, it must also be noted that the SASW inversion analyses were performed using all three test spacings (3, 9, and 20 feet), and this limited the sensitivity of the inversion analyses to define the velocities of the soils within the top four feet of the ground surface. This would limit the accuracy of comparing the two moduli values.

There seems to be little relationship between the CPT q_c values and the DCP CBR values. A better relationship occurs between the SASW E_{max} results and the DCP CBR values, which is presented in Figure 5.30. A regression analysis of the data produced an equation, with a r^2 value of 0.81, as follows:

$$E_{max} = -9{,}657 + 22{,}306\,(Log\ CBR) \tag{5.3}$$

where: E_{max} = small-strain Young's modulus (psi)

CBR = California Bearing Ratio (%).

The intent of this regression analysis was not so much to correlate these two parameters, as to indicate a typical range of stiffness values for the transition between a granular soil (possibly a weathered limerock) and a competent limerock. This is an important criteria that is needed to use the SASW test to delineate the top of limerock. Based on the results presented in Figure 5.30, a range of E_{max} values between 30,000 to 40,000 psi appears reasonable for a transition between lower CBR material (sand or clay) and higher CBR material (limerock). This range of Young's moduli corresponds to shear wave velocities between 750 to 850 ft/sec.

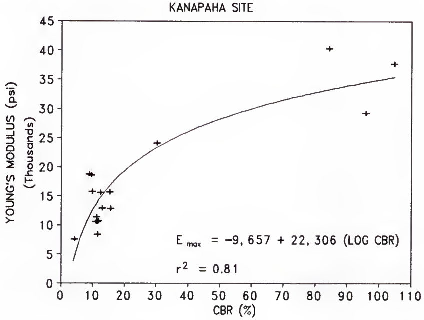

Figure 5.30 Relationship between SASW E_{max} and DCP CBR

5.4.2.6 Reproducibility of the SASW test

A series of three SASW tests was performed at the same site over the span of approximately nine months to determine the reproducibility of the SASW test results. The Kanapaha site was chosen for this purpose because of the ease of accessibility and it was located near the FDOT State Materials Office. The test location used for this analysis was site 6 (35 feet north and 56 feet west from the respective fence-lines). The field tests consisted of the same procedures used for the other SASW sites (spacings of 3, 9, and 20 feet). The same centerline and orientation of testing (North-South) was used for each of the three tests. The resulting dispersion curves from the three tests are displayed in Figure 5.31.

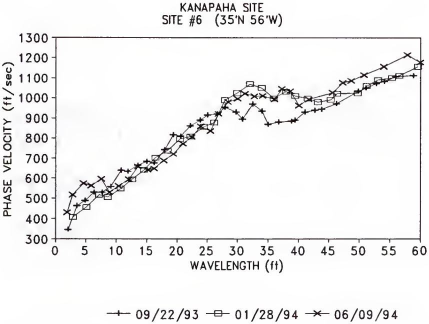

Figure 5.31 Dispersion Curves for various Time Periods from the Kanapaha Site (35'N 56'W)

The three dispersion curves are similar, except for the portion from wavelengths of about 30 to 40 feet. Since the final check for an inversion analysis is a comparison of the field and theoretically-derived dispersion curves, the differences in the three dispersion curves up to wavelengths of 30 feet would not affect the inversion results. Any small variations in the dispersion curves up to 30 feet are insignificant compared to difference in the inversion results which are the result of the user's judgement in determining the closeness of the field and theoretical dispersion curves. However, the differences in the dispersion curves from wavelengths of 30 to 40 feet are significant (difference in phase velocities of approximately 100 to 150 ft/sec) and would affect the inversion results by the relative difference between the curves (approximately 10 to 15 percent for the values of V_S). The difference represents a maximum value, and for most engineering analyses it is acceptable. This error is much smaller than some of the more commonly used in-situ tests, in particular the SPT N-values which can have errors as high as 100 percent or more (refer to ASTM D 1586).

Since the maximum spacing used during the field testing was 20 feet, the maximum wavelengths measured were restricted by this spacing. Therefore, the resolution of the resulting dispersion curves at higher wavelengths (about 30 to 60 feet) was limited. The data collected at these higher range of wavelengths was widely spaced and there was no overlap of data between two spacings to give redundant data confirming the user's confidence in the field data. Therefore, the soil profile of the deeper soil deposits resulting from this data is less well-defined. If a more accurate soil profile of the deeper soils is needed, longer spacings need to be performed during the SASW test.

5.5 Live Oak Site

This site was located in the city of Live Oak (Suwannee County) on property between Suwannee and Church Avenues, and one block south of US-90. The testing was performed on an area of land (320 feet by 240 feet) which was to be used to construct a retention pond (State Project No. 37010-1519). The SASW testing was performed at the request of the District II Geotechnical Engineer after a ground penetrating radar (GPR) survey was completed by FDOT personnel. The GPR survey was requested because of the sinkhole potential at this location.

5.5.1 Background Information

Five borings were performed during the preliminary site investigation to delineate soil types and layering. Based on these borings, the soil layering at this site was quite variable. The top of limerock was located at depths of approximately 17 to 18 feet based on the two boring locations on the west end of the site. Limerock was not encountered in the remaining three boring locations, at the central and east portions of the site (and these borings were terminated at 25 feet). At the central and west portions of the site, the surficial soils consisted of a 4- to 5-foot thick surface sand layer, with a clay to clayey sand layer varying in thickness from 12 to greater than 20 feet. At the east end of the site, the soils were primarily sand, occasionally intermixed with thin clay layers. Figure 5.32 presents the soil strata and identifications from these preliminary boring logs. The locations of the soil borings are indicated on Figure 5.33.

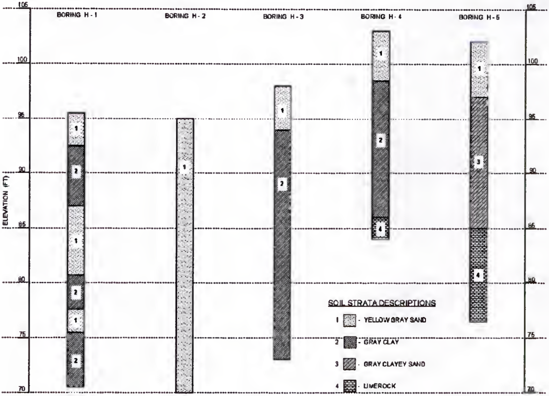

Figure 5.32 Soil Boring Results from the Live Oak Site

Based on the interpretation of the GPR return signals, several locations gave a strong indication of possible anomalies. The GPR survey followed a grid pattern, with north-south passes 20 feet apart and east-west passes 50 feet apart. The radar emitter/detector was dragged across the site, and the return signal was displayed on a monitor. The operator viewed the return signals, interpreted them, and indicated the areas where a strong signal occurred. These areas were marked on the ground surface for further evaluation. The approximate locations of these areas are indicated on Figure 5.33.

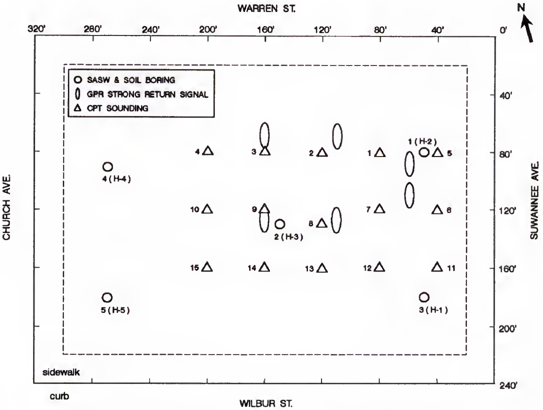

Figure 5.33 Plan View of the Live Oak Site

Because of the results of the GPR survey, it was decided that CPT soundings should be performed at this site to evaluate the subsurface conditions. Fifteen CPT soundings were performed in a grid pattern over the area which the GPR showed the strongest return signals (on 40-foot spacings in an area covering 160 feet by 80 feet at the central and east portions of the test area). Table 5.10 shows the locations of the CPT soundings. These locations are referenced from the curb on either Warren Street from the south or Suwannee Avenue from the west. The locations of the CPT soundings are included on the plan view of the site in Figure 5.33. The CPT sounding numbers, referenced in Table 5.10, are included in Figure 5.33 alongside the representative symbols. Results from several of the CPT soundings (tip resistance, q_c, versus depth plots) are included in Appendix A as Figures A.49 through A.57.

Table 5.10 CPT Locations for the Live Oak Site

CPT Sounding No.	Test Site Location, ft South	West
1	80	80
7	80	120
4	80	160
4	80	200
5	80	80
6	120	80
7	120	80
7	130	120
9	120	160
10	120	200
10	160	40
12	160	40
13	160	120
14	160	160
15	160	200

5.5.2 SASW Testing

A series of five SASW tests were performed at the same locations as the soil borings. The spacings used for each of the SASW tests were 3, 9, 20, and 40 feet. These tests were performed prior to the CPT soundings and without any specific knowledge of the GPR results, except for the fact that strong return signals were obtained which might indicate possible anomalies (but not the location of these signals). The only prior site information that was available was the preliminary soil boring logs. Therefore, the SASW test sites were chosen based on these boring locations. Table 5.11 contains the locations for the SASW tests and the corresponding soil borings performed for the preliminary investigation, referenced from the curb on either Warren Street or Suwannee Avenue. These locations refer to the centerline of the SASW surveys, which are also shown on the plan view in Figure 5.33. The SASW site numbers in Table 5.11 are shown alongside the representative symbol in Figure 5.33, as well as the soil boring numbers in parenthesis.

The dispersion curves for the five SASW tests are shown in Figure 5.34. It can be seen that all the dispersion curves are quite similar at the lower wavelengths (less than approximately 8 feet), indicating the surficial soils are consistent across the test site. This seemed to be consistent with a visual inspection of the surface soil conditions at the test area at the time of the SASW tests.

Table 5.11 SASW and Soil Boring Locations for the Live Oak Site

SASW / Boring Site No.	Testing Orientation	Test Site Location, ft	
		South	West
1 / H-2	N-S	80	50
2 / H-3	E-W	135	145
3 / H-1	N-S	180	50
4 / H-4	N-S	80	275
5 / H-5	N-S	180	275

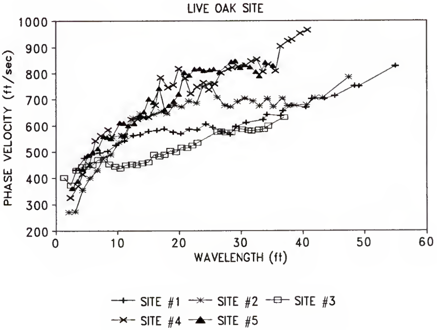

Figure 5.34 Dispersion Curves from the Live Oak Site

The dispersion curves for sites 1 and 3 in Figure 5.34 revealed lower velocities than the remaining curves. Both of these sites were on the east end of the test area. Site 3 produced much lower velocities in the range of wavelengths from 8 to 28 feet, which could be the result of lower densities of the underlying soils, probably the interbedded clay layers indicated on the boring log (H-1). These two curves (sites 1 and 3) converge at about 28 feet indicating similar underlying soils. The curve from site 2 (from the central portion of the test area) is similar to sites 4 and 5 to a wavelength of about 25 feet. At this point, the velocities decrease and the curve converges with those from sites 1 and 3. The low velocities obtained at site 3 from wavelengths of 8 to 28 feet were of concern since the cause of these low velocities was unknown. Even though the top of limerock was deep at this site, it was possible to have piping of the overlying sands into a deeper void in the limerock. This would result in lower velocities to have appeared on the dispersion curve. The only means to fully satisfy any concerns about the subsurface conditions was to perform some kind of penetration tests to determine soil resistances.

The curves from sites 4 and 5 (located on the west end of the test area) resulted in a stiffer soil profile than the other test sites. This indicates that a stiffer material (probably limerock) was present within the SASW survey depth at the west end of the test area, and not at sites 1, 2, and

3 (the central and east portions of the test area). The deeper soil deposits at sites 1, 2, and 3 were similar since the three dispersion curves eventually converge at the longer wavelengths. These results are consistent with the soil boring logs. Limerock was encountered in borings 4 and 5 (at the west end) at a depth of approximately 17 feet. This layer of limerock was not encountered in the remaining borings (at the central and east portions). Therefore, the top of the limerock appears to dip down from the west to east end of the site. It was deeper at the central and east portions of the test area (greater than 25 feet, the termination depth of the soil borings). Based on the CPT soundings, the depths to a competent limerock layer at the central and east portions were in the range of 35 to 50 feet. Since the maximum SASW spacing was 40 feet, these depths to the limerock were greater than the SASW survey depths.

The depths to limerock were based upon the CPT tip resistance profiles at the point in which the q_c value increased suddenly. The CPT interpretations of soil type indicated that many of the test sites contained a clay layer above the limerock. This clay provided low q_c values, so the point at which limerock was encountered was very noticeable. Refer to Figures A.49 through A.57 in Appendix A for q_c versus depth plots which show several profiles revealing the sudden increase in tip resistance values as the stiffer limerock layer was encountered.

The results from the SASW inversion analyses are presented in Table 5.12. The modulus values in this table were calculated by assuming a Poisson's ratio of 0.25 and a mass density of 3.0 lb/ft^3. The H-S in Table 5.12 represents the half-space used for the site's inversion analysis.

The inversion results from sites 4 and 5 made it difficult to determine an absolute top of limerock, since both profiles revealed a consistently increasing stiffness with depth. There was no sudden increase of stiffness which could be defined as a transition from soil to rock, but this is a typical condition for a profile involving a Florida limerock. It can be a soft rock, especially if it is weathered, with a stiffness close to a dense granular soil. Since only sites 4 and 5 had shear wave velocities which were 1,000 ft/sec and greater within the profile, it was assumed that this velocity was representative of the limerock in this area. If this is assumed, the depth to limerock was 10 to 20 feet. This is within the range of depths shown on the soil boring logs. Since these borings did not include SPT tests and the material descriptions were vague (the logs did not indicate any relative hardness of the limerock samples), the depths to competent limerock could not be determined accurately. No CPT soundings were performed at the east end of the test area to aid in the determination of the top of limerock because this area did not contain any strong return signals from the GPR survey.

Table 5.12 SASW Results for the Live Oak Site

Layer Thickness (ft)	Total Depth (ft)	Shear Wave Velocity (ft/sec)	Shear Modulus (psi)	Young's Modulus (psi)
Site No. 1				
2.0	2.0	680	4,220	10,550
2.0	6.0	680	8,270	20,670
2.0	6.0	700	10,210	25,520
4.0	10.0	680	9,630	24,080
10.0	20.0	530	5,850	14,630
10.0	30.0	680	15,050	37,630
H-S	H-S	600	16,875	42,190
Site No. 2				
2.0	2.0	320	2,130	5,330
2.0	6.0	680	15,410	38,520
2.0	6.0	680	16,130	40,330
4.0	10.0	600	13,330	33,330
10.0	20.0	600	13,330	33,330
10.0	30.0	900	13,330	33,330
H-S	H-S	900	13,330	33,330
Site No. 3				
2.0	2.0	460	4,410	11,020
2.0	4.0	550	6,300	15,760
2.0	6.0	440	9,630	10,550
4.0	10.0	560	6,530	16,330
10.0	20.0	460	10,210	25,520
10.0	30.0	600	16,875	42,190
H-S	H-S	900	16,875	42,190

Table 5.12 (Continued)

Site No. 4				
Layer Thickness (ft)	Total Depth (ft)	Shear Wave Velocity (ft/sec)	Shear Modulus (psi)	Young's Modulus (psi)
2.0	2.0	410	3,850	8,760
2.0	6.0	850	10,210	25,520
2.0	6.0	850	15,050	37,630
4.0	10.0	1000	20,830	52,080
10.0	20.0	1000	20,830	52,080
10.0	30.0	1000	25,210	63,020
H-S	H-S	1100	25,210	63,020
Site No. 5				
2.0	2.0	630	3,850	9,630
2.0	6.0	630	8,270	20,670
2.0	6.0	825	14,180	35,450
4.0	10.0	950	15,050	47,010
10.0	20.0	1000	20,830	52,080
10.0	30.0	1000	20,830	52,080
H-S	H-S	1000	20,830	52,080

Two methods were used to estimate a shear modulus profile in order to compare with the SASW results. The Imai and Tonouchi relationship (Eqn. 2.20) was used for each of the CPT soundings. The Mayne and Rix relationship (Eqn 2.28) was used on the sites which had a thick layer of clay (based on the CPT interpreted soil types), but was not used for layers identified as granular soils since the resulting shear moduli were unrealistically high. The Mayne and Rix equation was used since it was specifically derived for clays using seismic test results in the database. This relationship yielded shear moduli that were typically higher (approximately 2,000 to 5,000 psi higher) than the Imai and Tonouchi relationship for the clay layers. A typical comparison is shown in Figure 5.35, which presents values of G_{max} using Eqn. 2.28 for only the depths of soils identified as clays.

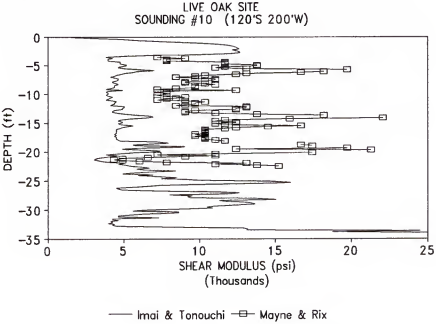

Figure 5.35 Comparison of CPT Shear Modulus Profiles from the Live Oak Site (120'S 200'W)

The higher moduli from the Mayne and Rix relationship is due to the fact that it yields a true maximum modulus since it was developed from seismic test results. Seismic testing will produce less disturbance than a penetration test (i.e. CPT), resulting in a more accurate determination of the soils' elastic stiffness. A penetration test will break down the structure of the soil, resulting in a lower stiffness.

A comparison of the SASW test results and the two CPT methods to estimate G_{max} reveals some variation among the different methods. Figures 5.36 and 5.37 present plots showing the comparison of the three shear modulus profiles. These plots were used because they show the sites where the SASW test and CPT sounding locations were the closest. For both plots, the two tests were not performed in the same location so some variation in the stiffness profiles can be expected. The soils presented in Figure 5.36 represent more granular soils, and the comparison between the Imai and Tonouchi relationship and the Mayne and Rix equation was not very close. Although, the SASW shear modulus profile compared well with the Imai and Tonouchi values. Figure 5.37 presents a location where a thicker clay layer was present, and the Mayne and Rix relationship seem to yield more reliable results. The resulting moduli were on the order of 2,000 to 4,000 psi higher than the Imai and Tonouchi results, which was typical for most of the other test locations. The SASW modulus profile did not compare well with the Imai and Tonouchi results, but did agree more closely with the Mayne and Rix values in the clay layer (depths ranging from 9 to 22 feet). Additional comparisons for the remaining CPT sounding

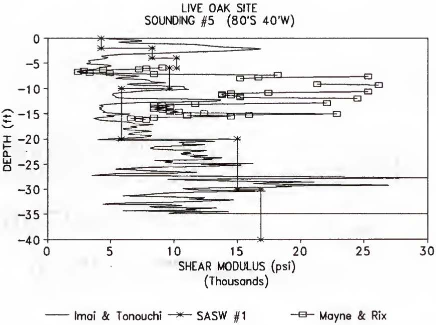

Figure 5.36 Comparison of Shear Modulus Profiles from the Live Oak Site (80'S 40'W)

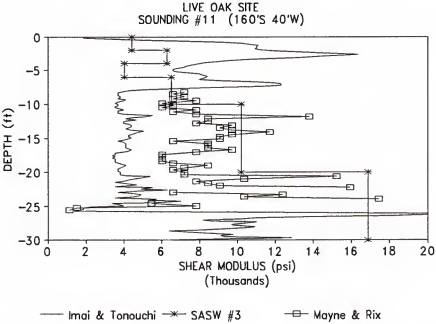

Figure 5.37 Comparison of Shear Modulus Profiles from the Live Oak Site (160'S 40'W)

locations are included in Appendix A as Figures A.58 through A.64.

Based on all the field testing performed at this site, the final decision was to construct the retention pond. It was later determined that this site was the previous location of a school building that was demolished and the land cleared for future usage. This area remained an open lot for many years. The school building had a basement which was removed and filled in when the demolition took place. This disturbance of the subsurface soils would have created varying densities which would be detected by the GPR. Based on the results of CPT soundings, these strong GPR signals appeared to have been caused by the disturbances caused by the demolition of the basement instead of any type of anomaly associated with a karst topography. This could have also been the reason why the lower velocities were recorded from the SASW dispersion curve for site 3 (at the east end of the test area).

CHAPTER 6
PAVEMENT APPLICATIONS

6.1 Introduction

This chapter contains the applications listed in Chapter 4 concerning pavement and highway usages. This primarily concerns the testing for transportation systems and the materials used during the construction of these systems. Each individual project will be covered by a separate section, including background information, the SASW testing (as well as additional field and/or lab testing), and the results obtained from the testing programs.

6.2 Test Pit Studies

This phase of testing was performed at the test pit facility located at the State Materials Office. This facility is utilized to simulate a cross-section of the roadway, and perform plate load tests, either with a static or dynamic loading, at various water table levels. Typically, these studies model a two-layer cross-section (base/subgrade or subgrade/embankment). The materials are placed under controlled conditions that are similar as they would be constructed in the field. The test pit is used to evaluate new materials prior to their acceptance for use for roadway construction by the FDOT, and the plate load results are used to establish layer coefficients that are used for pavement design. A sectional view of the test pit is shown in Figure 6.1, and a schematic of the loading system with the plate load test setup is included as Figure 6.2.

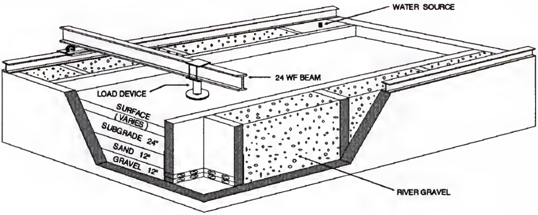

Figure 6.1 Sectional View of the Test Pit

The water level is controlled in the test pit by filling a sump to the desired elevation. The water moves through the sump along the sides of the pit and up through the concrete blocks at the bottom of the test pit walls. It then rises up through the bottom layer of gravel and overlying soils to the level in the sump. A layer of geotextile fabric is located between the sand and gravel layers to act as a separator between the two materials and permit the passage of water.

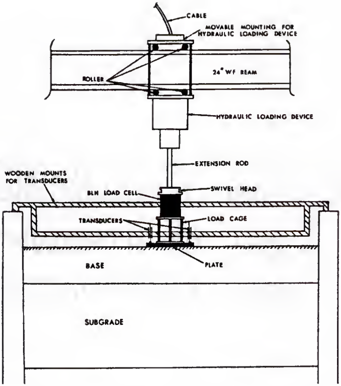

Figure 6.2 Schematic Diagram of the Test Pit Loading System (Cox, 1971)

The purpose of this phase of testing was to correlate the SASW moduli with the plate load moduli, which are the standard stiffness criteria utilized for the design of the roadway substructure. These studies also provide an opportunity to determine a range of seismic wave velocities for commonly used highway materials since conditions are controlled in the test pit.

6.2.1 Background Information

The typical testing procedures for the test pit studies included applying an initial seating load to the 12-inch diameter plate, performing a series of static plate load tests, followed by a dynamic plate load test. The seating load was 1,200 pounds for base materials and 500 pounds for subgrade materials. The load was applied until the measured deflections remained constant. This load was removed prior to the static plate load test.

The static load tests used an initial load of 1,000 pounds and the deflections of the rigid plate were measured until a maximum deformation was reached. The deflections were measured by linear variable displacement transducers (LVDT's) which were mounted on opposite sides of the plate (180° apart) in order to get an average value which compensates for tilting of the bearing plate during the loading. For base materials, the load was increased in 1,000 pound increments until a maximum load of 5,000 pounds (corresponding to a applied pressure of 44.3 psi) was achieved. For subgrade materials, a maximum load of 2,000 pounds (applied pressure of 17.6 psi), in 500 pound increments, was used. After the final loading, the load was released and the material was allowed to rebound. This process was repeated a total of three times.

The dynamic plate load test was performed after the third static load was released and the material was allowed to rebound. The hydraulic load system was set to apply a load for a specified duration of time and release it. These loadings were continued for a total of 10,000 cycles, but additional repetitions could be used to study long-term deformations. The typical load rate was a 0.5 second loading with a 2.0 second release. Currently, testing has utilized a load rate similar to the laboratory resilient modulus test (0.1 second loading and 0.9 second unload) in order to compare the two sets of results. The load was applied automatically in order to obtain an applied plate pressure of 50 psi for base materials and 20 psi for subgrade materials.

Bag samples of the materials placed in the test pit were obtained to determine a laboratory Proctor density (maximum density and optimum moisture). This design density was used to compact the material in-place (using a vibratory plate compactor) to the specification limits. For base and subgrade materials, a density of 98 percent of the maximum density as determined by a modified Proctor compaction test is specified. For embankment materials, a density of 100 percent of the maximum density as determined by a standard Proctor compaction test is specified. The as-placed densities in the test pit were obtained by use of a surface nuclear gauge, and the moisture contents were typically obtained by a Calcium Carbide gas pressure moisture tester (Speedy moisture).

The first series of tests was performed at optimum moisture content since this was the condition that the material was placed in the pit. The drained-dried tests were performed by pumping water out of the sump and allowing the water level to drop below the subgrade (at least 36 inches below the bottom of the base). The soaked series of tests was performed by filling the sump with water and allowing the water level to rise to one inch below the top of the surface layer, which becomes soaked through capillary action.

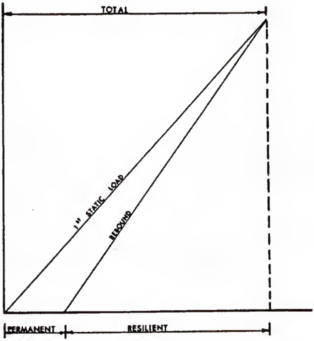

Figure 6.3 Idealized Load Cycle (Cox, 1971)

The determination of the modulus is dependent upon the deformation used for the calculation. For a dynamic loading, three types of deformations are encountered. Figure 6.3 displays these components in an idealized load/unload cycle. The total deformation occurs at the maximum displacement when the peak loading is applied. When this load is removed, the soil rebounds but not to the original condition before the load was applied. The amount of displacement after the removal of the load is the permanent deformation. The difference between the total and permanent deformations is the resilient deformation, which is the amount of displacement that the material rebounded upon removal of the load.

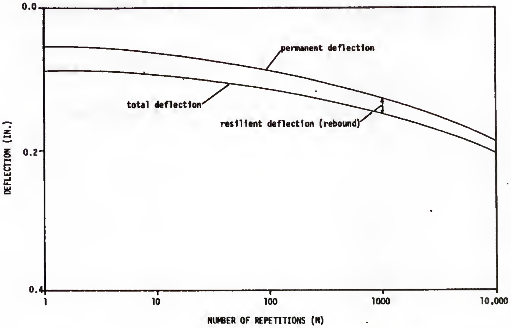

Figure 6.4 Idealized Dynamic Plate Load Test Deflection Plot (Cox, 1971)

Figure 6.4 shows how these deformations appear on results from a typical dynamic plate load test. This plot displays the two measured displacement curves for the entire 10,000 loading cycles, and how the resulting resilient deflection is determined by the difference between the two curves. This resilient deflection is used in Eqn. 2.36 to calculate the resilient modulus for an individual load cycle.

6.2.2 SASW Testing

The SASW testing was performed in between the locations used for the plate load tests, typically within a day of when the series of plate load tests for a particular moisture condition were initiated or completed. The tests were performed using the guidelines in Section 3.3.5 concerning the effects of reflected waves since there was limited space for testing (an individual compartment of the pit was 8 feet by 8 feet). The SASW testing was performed at spacings of 0.5, 1, and 2 feet. The receiver configurations were reversed to take into account any lateral variations of the test site. The results from the 2-foot spacings were not used for thin layers of surface materials (less than one foot), but were used for the subgrade materials which had a constructed thickness of 2 feet. The 2-foot spacings provided more long wavelength data which gave stiffness measurements for the underlying soils. Since more information was desired for the surface layer, the dispersion curve was created to achieve the best resolution at the shorter wavelengths.

An initial stage of testing was performed using both the geophones and accelerometers at the same location, and the results from either receiver produced similar dispersion curves. The difference between the two types of receivers was that the dispersion curves from the accelerometer data were extended to lower wavelengths than the equivalent curves from the geophone data. Therefore, subsequent SASW testing utilized only the accelerometers to be able to capture high frequency data in order to sample the material as near to the surface as possible with the sources available.

The sources were typically a wrench or small 4-oz. hammer, which limited the generation of high frequency waves and usually resulted in minimum measured wavelengths on the order of 0.25 foot. The accelerometers were attached to the surface by several means. To ensure proper coupling of the accelerometers to the ground surface, threaded spikes were driven into the ground and the accelerometers were attached to the ends of the spikes until their bottoms were in contact with the ground surface. The spikes were left in place so that the same location could be tested and because it was difficult to drive the spikes into the ground when the material was at soaked condition. Magnetic bases were purchased for the accelerometers which simplified the method of attaching the accelerometers. Roofing nails were driven into the ground, and the accelerometers were threaded onto magnetic bases which were mounted onto the heads of the nails (flush with the ground surface). As with the spikes, the nails were usually left in the ground to be used for retesting during the soaked phase. This method proved successful and provided a quicker means to switch the positions of the accelerometers, with less disturbance to the nail and the ground.

Since the testing involved a simple two-layer system and the profile was constructed in a controlled manner, the simplified method (outlined in Section 3.3.4) to determine the thickness and modulus of the surface layer was used during the analyses of the SASW results. This method provided a quick means to analyze the data. Even though there were some variations in an individual material placed in the pit, the material was placed under controlled conditions which are as close as one can get to a homogeneous layer for soils. The closer the surface layer in the test pit was to an ideal homogeneous material, the more accurate the results from this analysis proved to be. This phase of testing evaluated this method of analysis for a variety of roadway materials.

Table 6.1 contains a list of the materials used during this phase of testing. The classifications in this table are based on the AASHTO Soil Classification System and the Unified Soil Classification System (in parenthesis). The fines represent the percentage of the material which was finer than the No. 200 sieve (0.075 mm). The flexbase material could not be classified under the traditional classification systems since it was a designed mixture and no gradation information was provided. Two general categories of materials were tested: base and subgrade materials. This was dependent upon how the material was to be used for roadway construction.

Table 6.1 List of Materials Tested in the Test Pit

Material	Class.	Fines (%)	Description
Subgrades:			
SR-200	A-2-4 (SM)	13	Silty sand with traces of limerock
I-75	A-2-4 (SM)	22	Silty sand with traces of limerock
SR-30A	A-2-4 (SM)	21	Red silty sand
SR-50	A-3 (SP-SM)	10	Poorly graded sand with silt
SR-369	A-3 (SP-SM)	10	Poorly graded sand with silt
Bases:			
Flexbase	-	-	lime-stabilized coal combustion by-product
Dolomite	A-1-b (SM)	17	granular base from pit #53 -271 (Marianna)
RAP	A-1-a (GW)	2	milled or crushed existing asphalt pavement

6.2.2.1 Subgrade materials

These series of SASW tests were performed in conjunction with a Florida State University (FSU) research project which correlated the test pit plate load moduli with the laboratory resilient moduli. Since the test pit moduli had been correlated in the past with the soil support values and material layer coefficients that have been used in pavement design, a method is needed to relate these standard correlations with the laboratory resilient modulus test. The resilient modulus is the standard method that is utilized by current pavement design methodology to take into account the support value of the underlying soils for pavement systems.

Table 6.2 Laboratory Test Results of the Test Pit Subgrade Soils

Material Location	Max. Density (lb/ft^3)	Opt. Moisture (%)	LBR (%)
SR-200 Ocala	120.3	8.9	49
I-75 Alachua	124.1	9.9	108
SR-30A Panama City	125.5	8.9	88
SR-50 Brooksville	113.4	10.6	38
SR-369 Crawfordville	114.7	9.9	43

A total of five subgrades were tested in the test pit and representative samples were obtained to perform laboratory resilient modulus tests. The materials were obtained from stockpiles along the respective projects using them as a subgrade. Table 6.2 identifies the locations that the materials were obtained, and the results from the laboratory modified Proctor tests and the Limerock Bearing Ratio (LBR) tests. The LBR test is a laboratory strength test which is a modified version of the California Bearing Ratio (CBR) test that is used on the softer Florida materials for roadway construction. The LBR test is used to obtain a bearing stiffness of the material, and the results are used for pavement design purposes. Referring to Table 6.1 for a description and classification of the soils tested, the subgrade soils used for this study fell within two classifications: an A-2-4 (SR-200, SR-30A, and I-75), which is categorized by a higher percentage of fines, and an A-3 (SR-369 and SR-50). The A-3 subgrades had lower densities than the A-2-4 subgrades since they were poorly graded materials.

Each material was placed in four 6-inch thick lifts (total layer thickness of two feet). This large layer thickness was used so that the plate moduli would represent the stiffness of the surface layer alone, and not be influenced by the stiffness of the underlying soil.

SR-200 (Ocala) subgrade. This material consisted of a grey-brown silty sand with traces of rock (refer to Table 6.1). The material was placed in the test pit at 100% of the Proctor density (refer to Table 6.2) for all four lifts. Nuclear densities and Speedy moistures were performed adjacent to the plate load test sites upon their completion, and these results are presented in Table 6.3. This phase of testing was performed from July through November, 1994.

SASW tests were performed at different locations on the surface of the SR-200 subgrade at each of the three moisture conditions (optimum, drained, and soaked). A total of three plate load tests (consisting of both a static and dynamic test) were performed for each moisture condition in order to reflect any site variations. Representative dispersion curves obtained from the SASW tests for each of the moisture conditions are shown in Figure 6.5 These dispersion curves are the composite curves from the individual spacings (0.5, 1, and 2 feet) for both the normal and reverse configurations. The vertical line represents the critical wavelength which corresponds to the thickness of the surface layer.

Table 6.3 In-situ Densities and Moisture Contents for the SR-200 (Ocala) Subgrade

Test Type/#	Dry Density (lb/ft^3) & Moisture Content (%) 1	2	3
Optimum	118.5 @ 8.5%	120.9 @ 8.3%	121.8 @ 7.5%
Drained	121.6 @ 6.4%	120.4 @ 5.9%	122.7 @ 5.9%
Soaked	118.6 @ 11.4%	118.8 @ 10.4%	119.6 @ 9.8%

Figure 6.5 reveals the varying stiffness of the entire cross-section (SR-200 subgrade and underlying sand) due to the different moisture conditions. Since a transition occurred at the critical wavelength (2 feet), the dispersion curves for the drained and optimum moisture conditions reveal the interface between the SR-200 subgrade and the underlying sand. This is fairly distinct in this case because the SR-200 subgrade is a much denser, stiffer soil (maximum dry density of 120.3 lb/ft^3 and LBR of 49%) than the underlying soil (maximum dry density of 110.5 lb/ft^3 and LBR of 31%). This transition occurs close to the critical wavelength which

corresponds to the depth of the interface between the two layers. For the soaked case, the SR-200 subgrade is much less stiff than at the drier conditions, and so it is more similar to the underlying soil and no distinct transition appears.

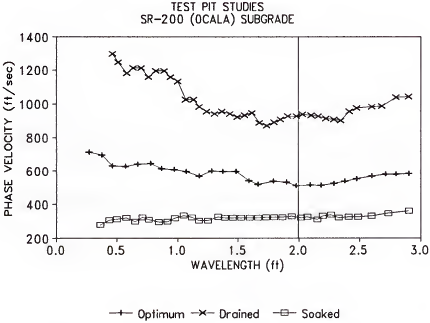

Figure 6.5 Dispersion Curves for the SR-200 (Ocala) Subgrade in the Test Pit

The dispersion curves shown in Figure 6.5 are representative curves from a series of at least two test sites performed in the test pit. Figure 6.6 shows the dispersion curves from the two test sites performed on the SR-200 material at optimum moisture. With the expanded Y-axis scale, this figure reveals the interface between the two layers more distinctly than Figure 6.5, and shows how well it corresponds to the critical wavelength. The portions of the curves less than a wavelength of two feet show some variation in the stiffness of the surface layer material. This is normal since variations in material properties and compactive energies will result in some degree of nonhomogeneity of the material during construction. The portions of the curves greater than two feet reflect the stiffness of the underlying sand subgrade. Both curves are identical at this point indicating the underlying soil is uniform between the two locations.

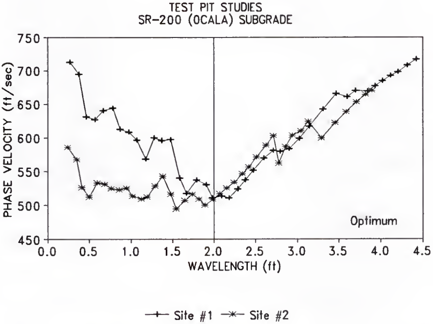

Figure 6.6 Dispersion Curves for the SR-200 (Ocala) Subgrade at Optimum Condition in the Test Pit

The analysis outlined in Section 3.3.4 was used to estimate the modulus of the surface layer. The surface wave velocities were averaged for the range of wavelengths up to the critical wavelength. The shear wave velocity was calculated by assuming a Poisson's ratio of 0.33, and the shear modulus (G_{max}) and Young's modulus (E_{max}) were determined from the appropriate elastic equations. The wet densities obtained from the in-situ nuclear tests were used to determine the total mass density for the given moisture condition (by dividing it with the gravitational constant). The results from this analysis are presented in Table 6.4. The range of surface wave velocities (V_R) from the individual test's dispersion curve is provided to show the variation of the stiffness encountered by the SASW testing. This is an indication of the consistency of the surface layer throughout its entire thickness. The two tests for the optimum (labelled Opt.) and drained-dried (labelled D-D) conditions represent the results from two different test sites, which were both tested on the same day. The results from only one of the soaked test sites (labelled Soak) were useable because the accelerometers could not be mounted firmly to the nail heads due to the extremely soft surface conditions at the other test site. Without proper coupling of accelerometer to ground surface, the SASW raw data is very noisy and results are very erratic.

The moduli in Table 6.4 show the variation of the material stiffness due to moisture condition, which is reflected in Figure 6.5. Based on the results presented in Table 6.3, the average moisture content during the optimum tests was 8.1%, 6.1% during the drained tests, and 10.5%

during the soaked tests. This variation in moisture content accounted for the differences in the moduli. This same trend applied to the plate load test results which will be presented in the following paragraphs. The SASW results indicate that this same trend exists for the elastic stiffness of this soil as well as for the stiffness obtained at higher strain levels, which is important if the two properties are to be compared.

Table 6.4 SASW Results for the SR-200 (Ocala) Subgrade

Test No.	Avg. V_R (ft/sec)	Range V_R (ft/sec)	V_S (ft/sec)	G_{max} (psi)	E_{max} (psi)
Opt.					
1	598	511-713	642	11,579	30,799
2	523	508-586	562	8,853	23,548
Avg.	560		602	10,170	27,052
D-D					
1	889	805-1025	955	25,375	67,498
2	1,089	856-1241	1,170	38,074	101,276
Avg.	989		1,063	31,403	83,533
Soak					
1	314	279-334	337	3,230	8,593

The two optimum tests produced results which were very consistent. However, the drained tests yielded a wider range of results. This variation in the SASW test results could be due to surface cracks in the material during testing. These cracks most often appeared while the material was allowed to drain. Even though the SASW test locations were chosen at sites where visible cracking was minimal, significant variations could still be encountered during testing (especially at the shorter spacings) due to the surface cracking and be reflected in a wider stiffness range. The material at the drained condition typically will have more variations in the moisture content throughout its entire thickness, and therefore, it is reasonable that there is a wider range of stiffness for the drained tests. Regardless of moisture condition, some variations in the SASW test results will occur reflecting the variability of the material and its stiffness due to the differences in densities of the material as it is constructed (refer to Table 6.3).

The results from the series of static plate load tests are included in Table 6.5. The values in this table represent averaged Young's moduli from three test sites, and are calculated from Boussinesq's equation for deflections at the center of a circular plate (Eqn. 2.36) based on the averaged deflection from the three tests. Since a static test involves loading (from 500 to 2,000 pounds in 500 pound increments) and unloading (from 2,000 to 0 pounds) the plate for three separate cycles, the three moduli for a given load in Table 6.5 represent the individual modulus for each of these cycles. The values recorded under the rebound section represent a resilient modulus for the final load (2,000 pounds) for each load cycle.

Table 6.5 Static Plate Load Test Results for the SR-200 (Ocala) Subgrade

Applied Load (lb)	Applied Stress (psi)	Averaged Young's Modulus (psi)			
			Optimum	Drained	Soaked
500	4.42	(1)	4,429	8,943	3,996
		(2)	4,471	7,958	3,318
		(3)	4,626	8,384	3,517
1,000	8.84	(1)	3,661	6,097	3,205
		(2)	5,103	8,986	3,937
		(3)	5,366	9,161	4,155
1,500	13.26	(1)	3,440	5,459	3,099
		(2)	5,459	9,236	4,262
		(3)	5,808	9,815	4,641
2,000	17.68	(1)	3,295	5,202	3,102
		(2)	5,195	8,879	4,312
		(3)	5,778	9,731	4,683
0	Rebound	(1)	6,595	10,500	5,214
		(2)	6,713	10,771	5,250
		(3)	6,948	10,959	5,339

Referring to Table 6.5, the differences in the stiffness properties for the SR-200 subgrade due to various loadings and moisture conditions are evident. The differences in the moduli resulting from the different loadings are due to the small linear elastic range of soil and the dependence of the measured moduli of soil on the applied stress (or resulting strain) level (refer to Section 2.3.4). To account for this effect, the axial strain was calculated (using Eqn. 2.31) and the moduli was plotted versus the axial strain. The resulting plot for the static plate test results (using the data contained in Table 6.5) is presented in Figure 6.7.

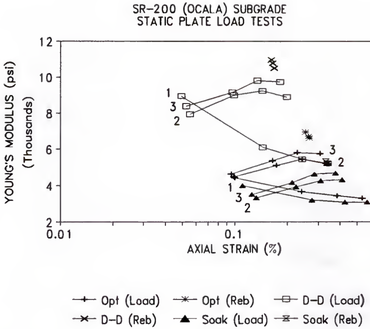

Figure 6.7 Static Plate Load Test Results for the SR-200 (Ocala) Subgrade

The numbers (1, 2, or 3) to the left of the drained and soaked curves and to the right of the optimum curves in Figure 6.7 represent the loading cycle that the data on the individual curve was obtained. Each curve is developed from the moduli obtained from the four increments of applied load. Since each test had the same increments of load, it is apparent from this figure that a series of curves can be developed for each of the applied loads. For the highest applied load (2,000 pounds), the moduli calculated from the rebound deformations (resilient moduli) can be seen to lie on the same curve as the Young's moduli obtained from the total deformations (during loading). These are represented by the three individual data points that are obtained from each of the rebound deformations for the three separate loading cycles. Both moduli (loading and rebound) are obtained at the same loading. The difference is that one is obtained during application of that load and the other is obtained during the removal of it. This implies that a comparison of Young's modulus and resilient modulus is possible as long as the strain level is considered. Since both moduli define the axial stiffness of the material, they are both related.

The variation of the moduli at the various moisture conditions of the soil can also be seen from Figure 6.7. For a given applied load, the moduli for the drained condition will be higher than the moduli at optimum moisture, which will be higher than the soaked results. This indicates that the moisture condition of the soil can be related to the strain level at which the corresponding modulus is determined. This is apparent since for a given load, the soil under the plate will deform more when it is totally saturated compared to when it is drier.

The dynamic plate load test results are presented in Table 6.6. The moduli for each individual test at the various moisture conditions is shown for the 4th and 10,000th load cycle (which represent the beginning and ending data for a typical dynamic plate load test), along with an averaged value (which was determined by using the averaged deformations from the three tests). Each individual test represents a different location on the surface of the SR-200 subgrade. Moduli were calculated from the three deformations obtained during a test: permanent, total, and resilient deformations (refer to Figures 6.3 and 6.4).

Table 6.6 Dynamic Plate Load Test Results for the SR-200 (Ocala) Subgrade

Test No.	Plate E_p (Perm.) n=4	n=10,000	Plate E_p (Total) n=4	n=10,000	Plate E_p (Resil.) n=4	n=10,000
Opt.						
1	4,538	1,427	3,000	1,277	8,850	12,103
2	5,619	2,149	3,540	1,804	9,568	11,238
3	3,412	1,439	2,506	1,288	9,440	12,313
Avg.	4,339	1,612	2,956	1,419	9,275	11,866
D-D						
1	7,453	3,248	4,768	2,642	13,234	14,160
2	7,010	3,668	4,495	2,975	12,531	15,733
3	10,489	5,405	6,157	4,011	14,905	15,560
Avg.	8,061	3,919	5,045	3,112	13,486	15,117
Soak						
1	6,648	1,491	3,612	1,271	7,911	8,634
2	4,627	1,396	2,821	1,195	7,224	8,281
3	3,479	1,161	2,340	1,019	7,152	8,379
Avg.	4,587	1,334	2,834	1,152	7,414	8,429

The applied cyclic stress used during the dynamic plate load test was 20 psi, and was used in the determination of all the moduli in Table 6.6. Since a two-foot layer thickness was used, the influence zone by the one-foot diameter plate should have been primarily restricted to the surface layer. Therefore, the plate moduli in this table, E_p, is assumed to be a stiffness parameter of the surface layer alone. No corrections were made in order to relate these plate moduli with the SASW or laboratory test results.

It can be seen from Table 6.6 that a range of moduli exists (1,019 to 15,733 psi) depending upon the number of load cycles, moisture condition, or type of deformation used for the stiffness calculation. Therefore, a means to relate the various moduli is needed. The same method to relate the moduli with respect to strain level used for the static plate load test data was used for the dynamic plate load test data. Figure 6.8 represents the results of this analysis (using only the averaged data contained in Table 6.6). Each of the averaged moduli in Figure 6.8 is labelled based on the deformation used for its calculation (P=Permanent Deformation, T=Total Deformation, R=Resilient Deformation) and the load cycle (4th or 10,000th representing the beginning or ending of the dynamic plate load test). This is done for each of the moisture conditions, which are represented by the different symbols.

Since each moduli was obtained at the same applied stress (20 psi), Figure 6.8 reveals how all the moduli fall on a single curve. The position of an individual modulus value on this curve depends upon its moisture condition, type of deformation, and loading cycle. Where the individual modulus falls on this curve and its relation to the other moduli on this curve indicates much about the soil's response to a cyclic loading and its use as a acceptable roadway material. The primary use of the curve in Figure 6.8 for this analysis is to relate the various moduli in order to compare the numerous moduli obtained from laboratory and field tests.

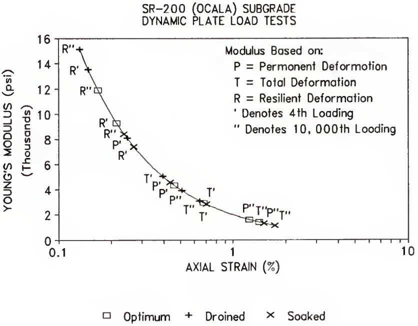

Figure 6.8 Dynamic Plate Load Test Results for the SR-200 (Ocala) Subgrade

As part of the FSU research study, laboratory resilient modulus tests were performed on representative samples for each subgrade material. Tests were performed at the FDOT State Materials Office. Two samples (4-inch diameter by 8-inch height) were prepared as close to optimum moisture and density as possible. The standard procedure was to obtain deformations of the entire 8 inch high sample (external measurements), and deformations across the middle 4 inches of the sample by a supporting cage attached to the sample (internal measurements). Friction caused by the end caps can occur during testing which will create disturbances at the top and bottom of the sample. The internal measurements record deformations outside of this disturbance zone, and are more representative of the actual stiffness properties of the test sample. The Materials Office utilizes two different internal cages to record the internal deformations. One cage has two LDVT's 180° apart, and the second has 3 LVDT's 120° apart in order to average any tilting of the cage in any direction that might occur during testing. Each cage was used for one of the two duplicate samples of each subgrade material.

The load sequence for the resilient modulus testing was performed according to SHRP (Strategic Highway Research Program) Protocol P46, which is partially based on AASHTO (American Association of State Highway and Transportation Officials) T274-82. The test involves performing a cyclic triaxial test on the prepared sample at varying stress states (obtained by varying the confining pressure and the deviator, or applied, stress) in order to determine the resilient properties of the material. The purpose of the test is not to fail the sample, but to provide stiffness information about the material over a wide range of stress states which will reflect how that material will behave under various traffic loadings.

Table 6.7 Resilient Modulus Test Results for SR-200 (Ocala) Subgrade

Confining Stress (psi)	Deviator Stress (psi)	3 Internal LVDT's Strain (%)	3 Internal LVDT's M_R (psi)	1 External LVDT Strain (%)	1 External LVDT M_R (psi)
4	2.02	0.0041	49,877	0.0056	35,911
4	3.99	0.0111	35,865	0.0160	24,977
6	5.92	0.0178	33,212	0.0254	23,307
6	8.04	0.0246	32,749	0.0344	23,347
6	10.02	0.0303	33,042	0.0427	23,480
4	1.97	0.0056	35,179	0.0080	24,625
4	3.99	0.0144	27,596	0.0202	19,592
4	8.04	0.0221	26,847	0.0307	19,380
4	8.04	0.0290	27,724	0.0401	20,075
4	10.10	0.0344	29,403	0.0474	21,308
2	1.97	0.0070	28,244	0.0101	19,578
2	4.00	0.0183	21,828	0.0262	15,296
2	6.03	0.0274	21,987	0.0402	15,014
2	8.08	0.0356	22,729	0.0510	15,855
2	10.06	0.0438	22,994	0.0623	16,161

Typical results from the resilient modulus test are presented in Table 6.7, indicating the combination of confining pressures and deviator stresses for each load sequence. This is the typical sequence for granular subgrades and embankment soils (Type 2 materials). Base materials (Type 1 materials) have a different load sequence to reflect the higher stresses that will be encountered due to the traffic loadings. One hundred repetitions of the deviator stress were applied for each load sequence, and the resilient deformation was determined from the average of the last ten repetitions. The strains in Table 6.7 were calculated by dividing the resilient deformations by the height which the measurement was recorded (4 inches for the internal measurements and 8 inches for the external measurements). The resilient modulus, M_R, was determined by dividing the deviator stress by the resilient deformation. The data in Table 6.7 represents the results from the sample using the three internal LVDT's and single external LVDT. The results from the sample using the two internal and two external LVDT's are not shown. The results from both samples were used in the analysis to combine the moduli from the various test methods, which is outlined in the following pages.

A wide range of moduli exists in Table 6.7 for this one test. The differences in these moduli occur due to the varying stress states encountered during testing. The varying stresses are related to the resulting strain on the sample by the resilient modulus. Therefore, to relate the resilient modulus to the various stresses encountered during testing, the resilient modulus was plotted versus the resulting resilient (or axial) strain. The results of this analysis for the data presented in Table 6.7 are shown in Figure 6.9.

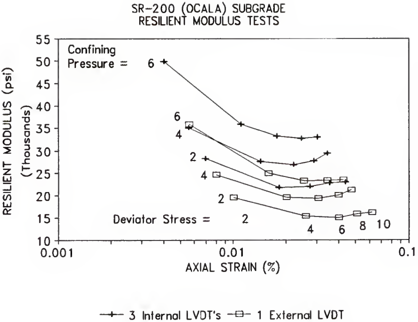

Figure 6.9 Resilient Modulus Test Results for the SR-200 (Ocala) Subgrade

Several trends appear from the results shown in Figure 6.9. The modulus results from the internal LVDT's are typically higher than the external LVDT's, indicating the entire length of the sample is being strained more than the middle portion of the sample (or that there are additional seating deflections occurring due to joints or gaps in the equipment set-up). This is reflected in the resilient strains, and both sets of moduli can be related if the strain effect is taken into account. The effects of both the confining pressure and deviator stress can be seen in Figure 6.9. For one confining pressure, a series of five deviator stresses are applied to the sample, and the process is repeated for two other confining pressures. This appears as a series of three curves in Figure 6.9 for one set of deformation results (three for the internal readings, three for the external readings, and six curves for one complete test). For increasing confining pressures, the curves are shifted up and to the left (higher modulus with lower stains) indicating a stiffer sample. For each confining pressure, the same deviator stresses are applied to the sample (refer to Table 6.7) which results in a series of five curves (one for each of the deviator stresses). For increasing deviator stress, the curves are shifted to the right and slightly down (increasing strain with a lowering of the modulus). This is an indication of more deformation occurring in the sample, resulting in a lower modulus.

A correlation of the SASW moduli with moduli from other test methods (plate load and laboratory resilient modulus tests) is impractical without taking into account the strain effect. Therefore, the approach of this research was to develop the entire curve showing the variation of Young's modulus with respect to axial strain, in which the SASW modulus represents a maximum value (i.e. elastic limit). Previous research has revealed that for granular soils the elastic threshold (the strain at which the modulus is constant) occurs at approximately 0.001 percent strain (refer to Figure 2.13). This value was used as the strain level at which the SASW moduli were obtained. Combining the Young's modulus versus axial strain results from each of the tests (Figures 6.7, 6.8, and 6.9), the plot presented in Figure 6.10 was obtained. The lines connecting the data points in Figure 6.10 represent lines of equal deviator stress (for the resilient modulus results) or applied stress (for the plate test results).

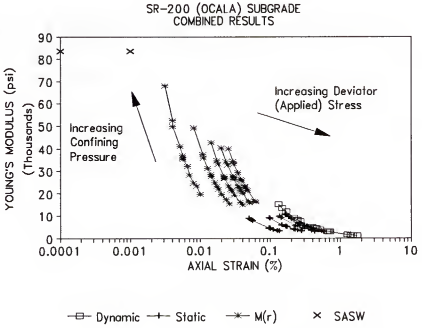

Figure 6.10 Variation of Young's Modulus and Strain for the SR-200 (Ocala) Subgrade

The legend in Figure 6.10 indicates the test that the resulting modulus was obtained. Dynamic and static refer to the respective plate load tests, M(r) refers to the laboratory resilient modulus test, and SASW refers to the surface wave seismic test. The results in Figure 6.10 are displayed as a series of curves based on the applied stress used during the test. The resilient modulus results form five curves at 2, 4, 6, 8, and 10 psi loadings. The static plate load test results form four curves at 4.42, 8.84, 13.26, and 17.68 psi. The dynamic plate load test results form a single curve at 20 psi. For increasing applied stresses, the curves shift toward the right (toward higher axial strains). The results obtained from the dynamic plate load test (at an applied stress of 20 psi) compare well with the curves for the static plate load tests since they fall to the right of the results from the static tests performed at 17.68 psi. The results from the static load tests performed at the lower applied stresses (4.42, 8.84, and 13.26 psi) compare well with the resilient modulus data obtained at applied stresses of 2, 4, 6, 8, and 10 psi.

The difference in moduli between the various test methods presented in Figure 6.10 is due to strain effect. The plate load tests are performed at higher strains and therefore, yield lower moduli than the resilient modulus test. The resilient modulus test is performed at lower strains, and therefore, yield moduli which are closer to the elastic limit. The SASW test yields a maximum limit which represents the elastic stiffness of the soil. The SASW results from the drained condition were used to obtain the maximum Young's modulus, E_{max} (refer to Table 6.4), since it represented a more reasonable value than the optimum moisture results. It is uncertain why the optimum tests were too low to represent a reasonable upper limit. For the remaining subgrades tested, the SASW results from the optimum tests were used as an elastic modulus because the resilient modulus tests were performed on samples compacted near optimum moisture. The SASW results at optimum moisture from these other materials proved to be a reasonable upper limit for the moduli comparisons.

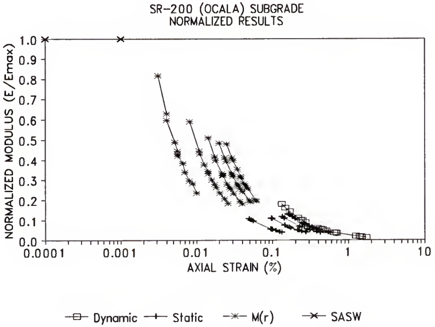

Figure 6.11 Variation of Normalized Modulus and Strain for the SR-200 (Ocala) Subgrade

In order to develop design curves for various groups of materials used for highway construction, it is necessary to compare the results such as those presented in Figure 6.10. This is accomplished by normalizing the modulus (as seen in Figures 2.11 through 2.13). Therefore, each modulus in Figure

6.10 is divided by the maximum modulus (i.e. the SASW modulus) and the normalized moduli (E/E_{max}) are plotted versus the corresponding axial strain. The results from this analysis are presented in Figure 6.11. The Y-axis ranges from 0 to 1, and these results can be compared to the results from the other subgrades tested during this phase of the research.

I-75 (Alachua) subgrade. This material consisted of a brown fine sand with traces of rock (refer to Table 6.1). The material was placed in the test pit at 98% to 100% of the Proctor density (refer to Table 6.2) for all four lifts. Nuclear densities and Speedy moistures were performed adjacent to the plate load test sites upon their completion, and these results are presented in Table 6.8. This phase of testing was performed from February through June, 1995.

Table 6.8 In-situ Densities and Moisture Contents for the I-75 (Alachua) Subgrade

Test Type/#	Dry Density (lb/ft^3) & Moisture Content (%) 1	2	3
Optimum	122.7 @ 8.0%	124.4 @ 8.2%	124.2 @ 7.5%
Drained	123.7 @ 7.3%	123.8 @ 7.3%	123.7 @ 6.9%
Soaked	121.1 @ 12.1%	122.0 @ 11.0%	121.9 @ 11.2%

The same method used to analyze the SR-200 subgrade outlined in the preceding section was used for this material, as well as for the remaining subgrades. Only the SASW results are included in this section. The results from the plate load tests (static and dynamic) and the laboratory resilient modulus tests are included as Tables B.1 through B.3 and Figures B.1 through B.3 in Appendix B. Representative dispersion curves from the SASW testing for each moisture condition are presented in Figure 6.12. The vertical line represents the critical wavelength corresponding to the layer thickness of the I-75 subgrade.

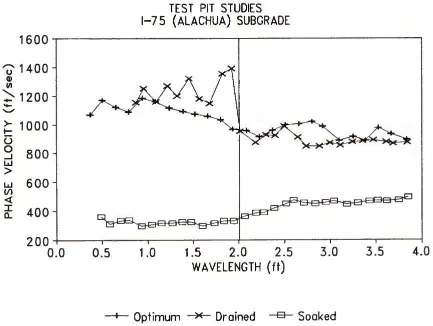

Figure 6.12 Dispersion Curves for the I-75 (Alachua) Subgrade in the Test Pit

The dispersion curves in Figure 6.12 show the same trend as the SR-200 subgrade. The optimum and drained curves show a distinct transition between the surface layer and the underlying soil near the critical wavelength. Both curves meet at this point and are similar beyond this wavelength, which reflects a material with a consistent stiffness (i.e. the underlying sand). The soaked curve does not show a distinct transition since the stiffness of the surface layer is similar to the underlying sand due to the higher moisture content. The variation of the I-75 subgrade stiffness due to moisture condition is apparent from the difference in velocities of the various dispersion curves, even though the variation between the optimum and drained curves is slight. This small difference between the optimum and drained test results can be accounted for due to the similarity of the moisture contents for the two series of tests. Referring to Table 6.8, the average moisture content for the optimum tests was 7.9%, while it was 7.2% for the drained tests. The surface of the I-75 subgrade also exhibited many small cracks during the drained tests. Since the data from the 1/2-foot spacings at the drained condition was erratic, there was very little useable data for wavelengths less than one foot.

The stiffness properties of the I-75 subgrade using the SASW dispersion curves are presented in Table 6.9. The moduli in this table were calculated using a Poisson's ratio of 0.33 and the average densities in Table 6.8 to obtain the mass densities. The SASW results from the optimum series of tests were used to establish a maximum modulus occurring at axial strains less than 0.001% (i.e. the elastic threshold). The moduli from the plate load tests and laboratory resilient modulus tests were divided by the SASW modulus in order to normalize the moduli. The resulting plot showing the variation of this normalized moduli versus axial strain is presented in Figure B.4 in Appendix B.

Table 6.9 SASW Results for the I-75 (Alachua) Subgrade

Test No.	Avg. V_R (ft/sec)	Range V_R (ft/sec)	V_S (ft/sec)	G_{max} (psi)	E_{max} (psi)
Opt.					
1	1,262	1043-1352	1,355	52,905	140,726
2	1,090	967-1214	1,171	39,491	105,047
Avg.	1,176		1,263	45,953	122,236
D-D					
1	1,164	1041-1248	1,251	44,710	118,930
2	1,240	1115-1571	1,332	50,739	134,965
Avg.	1,202		1,291	47,677	126,820
Soak					
1	324	297-362	349	3,551	9,446
2	494	429-556	531	8,248	21,940
Avg.	409		440	5,656	15,044

SR-30A (Panama City) subgrade. This material consisted of a red silty sand (refer to Table 6.1). The material was placed in the test pit at 96% to 99% of the Proctor density (refer to Table 6.2) for all four lifts. Nuclear densities and Speedy moistures were performed adjacent to the plate load test sites upon their completion, and these results are presented in

Table 6.10. This phase of testing was performed from June through November, 1994.

The SASW results are included in this section, and the results from the plate load tests (static and dynamic) and the laboratory resilient modulus test are included as Tables B.4 through B.6 and Figures B.5 through B.7 in Appendix B. Representative dispersion curves from the SASW testing for each moisture condition are presented in Figure 6.13. The vertical line represents the critical wavelength corresponding to the layer thickness of the SR-30A subgrade.

Table 6.10 In-situ Densities and Moisture Contents for the SR-30A (Panama City) Subgrade

Test Type/#	Dry Density (lb/ft^3) & Moisture Content (%)		
	1	2	3
Optimum	123.5 @ 7.3%	122.8 @ 8.1%	123.6 @ 7.5%
Drained	125.5 @ 6.2%	124.6 @ 5.0%	125.2 @ 5.5%
Soaked	119.1 @ 11.5%	120.5 @ 10.6%	119.7 @ 11.6%

The variation in the stiffness of the SR-30A subgrade can be seen in the velocity differences of the SASW dispersion curves. The transition between the surface layer and the underlying soil is clearly shown in the dispersion curve at optimum moisture, and corresponds very well with the critical wavelength. This transition is not clearly defined on the dispersion curve at drained moisture, and not enough long wavelength data was obtained during the soaked series of testing to adequately define the dispersion curve beyond the critical wavelength. The reason for this was that the nails used during the testing for the 2-foot spacing were disturbed, making proper coupling between accelerometer and ground surface impossible.

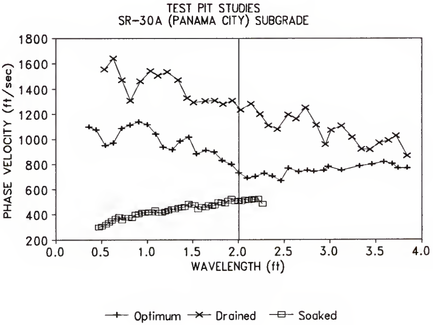

Figure 6.13 Dispersion Curves for the SR-30A (Panama City) Subgrade in the Test Pit

The stiffness properties of the SR-30A subgrade using the SASW dispersion curves are presented in Table 6.11. The moduli in this table were calculated using a Poisson's ratio of 0.33 and the average densities in Table 6.10 to obtain the mass densities. The SASW moduli from the optimum series of tests were used to establish a maximum modulus. As with the other subgrade materials, the remaining moduli were divided by this modulus to normalize each value. The normalized moduli were plotted versus the corresponding axial strains, and the resulting plot is presented as Figure B.8 in Appendix B.

Table 6.11 SASW Results for the SR-30A (Panama City) Subgrade

Test No.	Avg. V_R (ft/sec)	Range V_R (ft/sec)	V_S (ft/sec)	G_{max} (psi)	E_{max} (psi)
Opt.					
1	909	804-1138	976	27,275	72,552
2	987	801-1140	1,060	32,166	85,561
Avg.	948		1,018	29,670	78,923
D-D					
1	1,654	1335-1944	1,777	90,033	239,489
2	1,421	1280-1642	1,526	66,403	176,632
Avg.	1,538		1,652	77,770	206,867
Soak					
1	430	300-525	462	6,124	16,290
2	516	383-599	554	8,839	23,511
Avg.	473		508	7,419	19,735

SR-50 (Brooksville) subgrade. This material consisted of a brown sand with traces of rock (refer to Table 6.1). The material was placed in the test pit at 100% of the Proctor density (refer to Table 6.2) for all four lifts. Nuclear densities and Speedy moistures were performed adjacent to the plate load test sites upon their completion, and these results are presented in Table 6.12. This phase of testing was performed from February through June, 1995.

The SASW results are included in this section, and the results from the plate load tests (static and dynamic) and the laboratory resilient modulus tests are included as Tables B.7 through B.9 and Figures B.9 through B.11 in Appendix B. Representative dispersion curves from the SASW testing for each moisture condition are presented in Figure 6.14. The vertical line represents the critical wavelength corresponding to the layer thickness of the SR-50 subgrade.

Table 6.12 In-situ Densities and Moisture Contents for the SR-50 (Brooksville) Subgrade

Test Type/#	Dry Density (lb/ft^3) & Moisture Content (%) 1	2	3
Optimum	113.9 @ 8.0%	115.2 @ 7.8%	112.4 @ 7.5%
Drained	114.3 @ 6.4%	115.0 @ 6.4%	115.0 @ 6.0%
Soaked	110.5 @ 17.4%	108.8 @ 19.9%	108.2 @ 18.5%

Based on the dispersion curves in Figure 6.14, there is no sharp transition on any of the curves to indicate the interface between the surface layer and the underlying sand. The dispersion curves from this series of testing resemble typical curves obtained from a site consisting of a natural soil deposit (i.e. stiffness increasing with depth). The Proctor density of the SR-50 subgrade was 113.4 lb/ft^3, which is more similar to the underlying sand (110.5 lb/ft^3) than the subgrades from SR-200, I-75, or SR-30A (densities approximately 10 to 15 lb/ft^3 higher than the underlying sand; refer to Table 6.2). Therefore, the transition between the stiffness of the two layers was much more gradual than the first three subgrade materials.

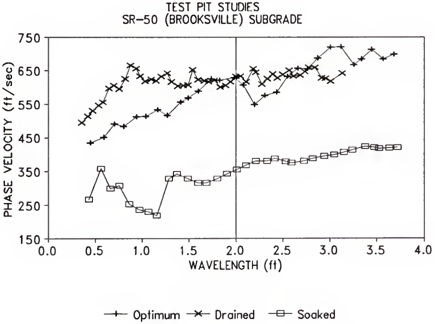

Figure 6.14 Dispersion Curves for the SR-50 (Brooksville) Subgrade in the Test Pit

Since there was no significant contrast between the two layers, the simplified method to determine the stiffness and depth of the surface layer could not be used effectively. This method only works well when the surface layer is fairly uniform and homogeneous. The depth to the interface can only be determined if the stiffness of the two layers are dissimilar, and the greater this difference, the better the transition will appear and easier to recognize. Even though the dispersion curves could not be used to identify the surface layer thickness, the variation in the stiffness of the SR-50 subgrade due to the various moisture conditions is still clearly evident in the different velocities of the SASW dispersion curves.

The surface velocities on the dispersion curves represent apparent velocities (not layer velocities) since they are dependent upon the velocities of the layers above and below the individual layer. There was no distinct surface layer of material that could be considered uniform and homogeneous. As a result, the dispersion curves violated the conditions needed to perform the simplified method of analysis, and an inversion analysis had to be performed to accurately define the stiffness profile of the SR-50 subgrade. In order to compare the stiffness of the surface layer resulting from the simplified method with the stiffness profile from an inversion analysis, both methods were performed. The stiffness properties of the SR-50 subgrade using the SASW dispersion curves (based on the velocities less than a wavelength of two feet) are presented in Table 6.13. The results from the inversion analysis are presented in Table 6.14. The inversion analysis was performed using the data from the dispersion curve at optimum moisture shown in Figure 6.14. The moduli in both tables were calculated using a Poisson's ratio of 0.33 and the average densities in Table 6.12 to obtain the mass densities.

Table 6.13 SASW Results for the SR-50 (Brooksville) Subgrade

Test No.	Avg. V_R (ft/sec)	Range V_R (ft/sec)	V_S (ft/sec)	G_{max} (psi)	E_{max} (psi)
Opt.					
1	530	485-593	569	8,566	22,787
2	533	435-630	573	8,683	23,098
Avg.	531		571	8,625	22,942
D-D					
1	605	496-666	650	11,103	29,533
2	561	463-667	602	9,539	25,375
Avg.	583		626	10,306	27,415
Soak					
1	282	258-305	303	2,551	6,785
2	298	218-358	320	2,839	7,551
Avg.	290		312	2,693	7,163

The results from the two analyses reveal that both yield similar modulus values within the first foot of the surface. The moduli from the inversion analysis were much higher for the second foot of the SR-50 subgrade. This wide range of moduli in the SR-50 subgrade layer confirms that this material was not very uniform and therefore, the results from the simplified method could not be used as the material properties for the entire layer. The inversion analysis yields a stiffness profile which increased with depth, which is similar to a natural soil deposit. As a general rule, the simplified method did not work well when the velocity of the surface layer was lower than the velocity of the underlying layer. If the velocity of the surface was higher than the underlying soil, the simplified method worked well, as with the preceding subgrades.

Table 6.14 Inversion Results for the SR-50 (Brooksville) Subgrade

Layer No.	Layer Thickness (ft)	Total Depth (ft)	V_S (ft/sec)	G_{max} (psi)	E_{max} (psi)
1	0.5	1.5	600	7,986	21,319
2	0.5	1.0	600	9,514	25,278
3	0.5	1.5	1,000	26,458	70,139
4	0.5	2.0	1,100	32,014	85,417
5	2.0	4.0	1,200	32,014	85,417
H-S	-	H-S	1,400	43,542	115,972

Comparing the SASW moduli obtained from the inversion analysis with the moduli from the plate load and resilient modulus tests, the moduli within the top foot of the SR-50 subgrade layer seemed unreasonably low. Therefore, the moduli from the bottom half of the surface layer was used to establish a maximum modulus. The remaining moduli were divided by this modulus to normalize each value. The normalized moduli were plotted versus the corresponding axial strains, and the resulting plot is presented as Figure B.12 in Appendix B.

SR-369 (Crawfordville) subgrade. This material consisted of a dark brown sand (refer to Table 6.1). The material was placed in the test pit at 98% to 100% of the Proctor density (refer to Table 6.2) for all four lifts. Nuclear densities and Speedy moistures were performed adjacent to the plate load test sites upon their completion, and these results are presented in Table 6.15. There is no data listed under the third test for the soaked condition because only two soaked plate load tests were performed on this material. This phase of testing was performed from February through May, 1994.

Table 6.15 In-situ Densities and Moisture Contents for the SR-369 (Crawfordville) Subgrade

Test Type/#	Dry Density (lb/ft^3) & Moisture Content (%) 1	2	3
Optimum	113.6 @ 8.0%	115.6 @ 7.3%	114.5 @ 7.3%
Drained	115.5 @ 6.8%	114.7 @ 5.3%	115.2 @ 5.4%
Soaked	113.1 @ 15.0%	111.8 @ 16.3%	

The SASW results are included in this section, and the results from the plate load tests (static and dynamic) and the laboratory resilient modulus tests are included as Tables B.10 through B.12 and Figures B.13 through B.15 in Appendix B. Representative dispersion curves from the SASW testing for each moisture condition are presented in Figure 6.15. The vertical line represents the critical wavelength corresponding to the layer thickness of the SR-369 subgrade.

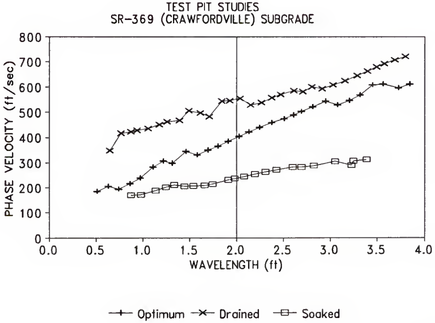

Figure 6.15 Dispersion Curves for the SR-369 (Crawfordville) Subgrade in the Test Pit

As with the SR-50 subgrade, the dispersion curves shown in Figure 6.15 have no sharp transition to indicate the interface between the surface layer and the underlying soil. Referring to Table 6.6, the Proctor density of the SR-369 subgrade was 114.7 lb/ft^3, which was similar to the underlying sand (110.5 lb/ft^3). The SR-50 and SR-369 subgrades were classified as A-3 materials, and the SR-200, I-75, and SR-30A subgrades were A-2-4 materials. Based on the gradations of the materials, the SR-50 and SR-369 subgrades were poorly graded. The densities of these two materials reflect this and were lower than the other three subgrades. The range of densities of the other three subgrades were 120.3 to 125.5 lb/ft^3, which was much higher than the underlying sand.

Comparison of LBR's is also helpful to distinguish between the two groups of subgrades. Since the underlying sand had a LBR of 31%, it was nearly as stiff as the SR-50 and SR-369 subgrades (with LBR's of 38% and 43% respectively). The LBR's of the remaining three subgrades ranged from 49% to 108%, which indicate that these were stiffer materials. All these factors account for the similarity between these two materials (SR-50 and SR-369 subgrades) and the underlying sand, and because of this the SASW dispersion curves could not be used to identify the layer thickness for either of these subgrades. Even though the dispersion curves could not be used to identify the surface layer thickness, the variation of the stiffness due to the various moisture conditions is clearly evident by comparing the three SASW dispersion curves. In this way, the SASW dispersion curves can be used as a relative indicator of stiffness. If individual material properties are desired, an inversion analysis is required which will involve additional time. This may not be needed in each case study, and it is the engineer's choice whether this step of the analysis is needed.

An inversion analysis was performed to define the stiffness profile of the SR-369 subgrade. As with the SR-50 subgrade, the stiffness of the surface layer was obtained using the simplified method to compare its results with the inversion analysis results. The stiffness properties of the SR-369 subgrade using the SASW dispersion curves are presented in Table 6.16. The results from the inversion analysis are presented in Table 6.17. The inversion analysis was performed on the dispersion curve at optimum moisture shown in Figure 6.15. The moduli in both tables were calculated using a Poisson's ratio of 0.33 and the average densities in Table 6.15 to obtain the mass densities.

Table 6.16 SASW Results for the SR-369 (Crawfordville) Subgrade

Test No.	Avg. V_R (ft/sec)	Range V_R (ft/sec)	V_S (ft/sec)	G_{max} (psi)	E_{max} (psi)
Opt.					
1	315	170-477	338	3,035	8,074
2	327	127-508	351	3,281	8,728
Avg.	321		345	3,157	8,398
D-D					
1	425	258-564	456	5,477	14,569
2	502	416-573	539	7,648	20,344
Avg.	464		498	6,517	17,337
Soak					
1	211	171-283	227	1,445	3,845
2	221	189-303	237	1,581	4,206
Avg.	216		232	1,513	4,023

Table 6.17 Inversion Results for the SR-369 (Crawfordville) Subgrade

Layer No.	Layer Thickness (ft)	Total Depth (ft)	V_S (ft/sec)	G_{max} (psi)	E_{max} (psi)
1	0.5	0.5	250	1,646	4,375
2	0.5	1.5	900	9,375	25,000
3	0.5	1.5	900	21,319	56,667
1	0.5	2.0	1,000	26,319	70,139
5	2.0	4.0	1,000	22,153	59,028
H-S	-	H-S	1,100	26,875	71,528

Comparing the results from the two analyses, the simplified method produced a lower stiffness which was similar to the inversion results for the top foot of the surface layer. The stiffness profile from the inversion analysis yielded a very low velocity layer at the surface possibly caused by the surface material drying out and becoming desiccated. This low velocity surface layer affected the SASW dispersion curves, resulting in the apparent velocities being much lower than the individual layer velocities. Similar to the SR-50 analysis, the moduli from the inversion analysis were much higher below the top foot of the surface layer. The inversion results also showed a transition at a depth of two feet, indicating the interface between the two layers which could not be detected by the dispersion curves. Since the SR-369 subgrade layer was not very uniform, as reflected by the results from the inversion analysis, the simplified method could not be used to establish material properties for the entire layer.

The moduli from the bottom half of the surface layer were used to establish a maximum modulus, since they seemed more reasonable when compared to the plate load and resilient modulus tests results. The moduli within the top foot of the SR-369 subgrade layer seemed unreasonably low. The remaining moduli were divided by this modulus to normalize each value. The normalized moduli were plotted versus the corresponding axial strains, and the resulting plot is presented as Figure B.16 in Appendix B.

Summary of subgrade results. In order to develop design curves for typical subgrade materials, the normalized modulus versus axial strain plots developed for each of the previous subgrades were combined. The individual normalized plots for each of the subgrade materials are contained in Appendix B. Due to the large amount of data from the various applied stresses, it was decided to view the data from the applied stresses of 2, 8, and 20 psi. The values of 2 and 20 psi were chosen since they represent the minimum (from the resilient modulus tests) and maximum (from the dynamic plate load tests) limits of the applied stresses used during the various tests. The 8 psi data was used since it represented an intermediate value, and contained moduli which were obtained from both the resilient modulus tests and the static plate load tests. Therefore, moduli values from all the tests were contained in these three stress levels. The resulting plot is presented as Figure 6.16. The legend of this figure indicates the subgrade, and each subgrade is represented by a different symbol. The SASW symbol represents the maximum normalized modulus, which defines the range of the elastic threshold and was assumed to occur at a strain level of 0.001%. This value has been verified by previous researchers.

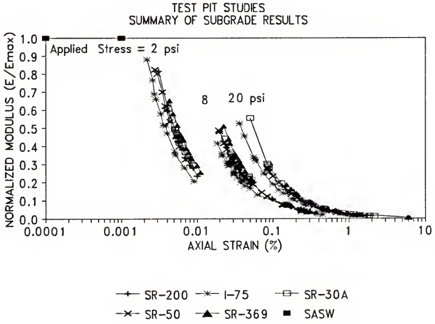

Figure 6.16 Variation of Normalized Modulus and Strain for the Subgrade Soils

The results obtained from the five different subgrade materials seem to compare well based on the evidence presented in Figure 6.16. The variations between the different materials seem reasonable, and should not present a problem in using a single equation to model this data. The most scatter occurs in the lower strain ranges for the 20 psi curve, but there was little data in this range. Most of the data on this curve falls in the higher strain levels, and the results from the different materials compare well. There seems to be little difference between the A-3 and A-2-4 materials. Therefore, one set of design curves can be developed for this group of materials.

These results compare favorable with the results from other researchers on similar materials (refer to Figures 2.12 and 2.13). The curves for the applied stresses of 8 and 20 psi yield a range of normalized moduli which are similar to the published curves. The values on the 2 psi curve are much lower than the published curves, and it is not known the reason for this. This could be due to variations in the materials tested, but the published curves did not include any specific properties of the soil.

To develop a single equation to model the results presented in Figure 6.16, three parameters had to be taken into account: the normalized Young's modulus (E/E_{max}), the axial strain (ϵ_a), and the applied stress (σ_d). A linear regression analysis was performed on the normalized modulus and strain individually for each of the three sets of data shown in Figure 6.16. This data was fitted to the basic form of a power curve equation. This relationship is represented by the following form of equation:

$$\frac{E}{E_{max}} = c_1 (\epsilon_a)^m \tag{6.1}$$

The terms c_1 and m are constants which were determined by performing a linear regression on the data for each individual deviator stress using Eqn. 6.1 expressed in logarithmic form as follows:

$$\log(\frac{E}{E_{max}}) = \log(c_1) + m \log(\epsilon_a) \tag{6.2}$$

The slopes and coefficients from this analysis were averaged to develop a basic form of the equation. A normalized form of the applied stress was input into this equation, and a trial and error process was used to determine the exponent of this term. Since the modulus is indirectly proportional to the strain and directly proportional to the stress, the exponent of the stress proved to the same as the strain, except the opposite sign. The following equation is the result of this analysis:

$$\frac{E}{E_{max}} = 0.00224 (\frac{\sigma_d}{\epsilon_a})^{0.899} \tag{6.3}$$

where: E/E_{max} = normalized Young's modulus

σ_d = deviator, or applied, stress (in psi)

ϵ_a = axial strain (%).

A power curve was used since not enough data was available at each stress level to define the entire S-shaped curve. This equation should be satisfactory for most practical applications since it was developed from data within the working range of stresses that will be normally used for the design of roadways. The equation should be used within the limits of the data that was used to develop it. For instance, the results for applied stresses of 8 to 20 psi need to be less than 0.5. Due to the S-shape of the curve, at this point the curve will be the mirror image of the portion at higher strains. Since no data was available at these lower strains, a form of the equation to be used at these lower strains was not developed. Equation 6.3 should prove adequate to incorporate modulus values obtained from either the resilient modulus or plate load tests. To evaluate the accuracy of Eqn. 6.3, it was used to calculate values of the normalized Young's modulus for the range of strains that the three curves in Figure 6.16 encompassed. The results of this analysis are presented in Figure 6.17. The lines in this figure represent the calculated values using Eqn. 6.3.

Based on the results presented in Figure 6.17, the values obtained by using Eqn. 6.3 closely fit the actual range of values, and should prove accurate for typical subgrade materials. Once the design curves such as this one are developed, they can be used to relate field test moduli and laboratory test results with design values. A series of these curves can also be used for pavement design to develop stiffness values for the individual layers of the roadway substructure which take into account the varying stress distribution of a surface load. This method can also subdivide individual layers to assign moduli to each sublayer based on the assumed stress distribution. This approach is a more rational method to develop a stiffness profile for the underlying pavement foundation which takes into account the strain level effects on the stiffness of the soil.

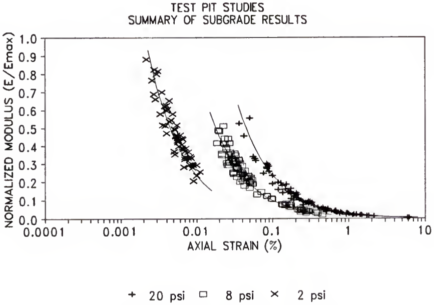

Figure 6.17 Normalized Modulus-Strain Relationships for the Test Pit Subgrade Soils

6.2.2.2 Base materials

The base materials used in the test pit during the period of time covered by this research consisted of non-standard, experimental materials to be evaluated for FDOT applications. The exception to this was a dolomite base material which was obtained from a FDOT-approved mine, but no laboratory resilient modulus tests were performed on this material which reduced the amount of stiffness data at the lower strain levels. Due to this limited testing of standard base materials, additional testing is needed to establish any design curves for FDOT-approved base materials. In spite of this, this section will outline the findings from the SASW testing.

Flexbase. This study was performed to evaluate this material for use in roadway base applications. This material was a lime-stabilized coal combustion by-product consisting of lime-fly ash bottom ash, and fixated flue gas desulferization (FGD) products. The lime generates a pozzolanic reaction with the flyash to create a material that gains strength over time. The ash was obtained from a coal burning power plant located in Palatka.

The flexbase was placed in the test pit in one lift of six inches and compacted to 100% of the design density (85.0 lb/ft^3 at 28.5%), which was provided by the producer of the flexbase. The plate load test data is not included in this report because the various batches of flexbase received by the producer were nonuniform, lacking both production moisture control and similar curing times prior to placement. Therefore, the testing yielded a large range of results and a reliable evaluation of the material was not possible.

This phase of testing was performed from October, 1992 through January, 1993. It was the first series of SASW tests in the test pit, and therefore, involved some experimentation of the testing procedures. Several methods were used to attach the accelerometers to the ground surface. Placing the accelerometers directly on the surface proved to give poor quality data. The best results came from attaching the accelerometers to threaded bolts driven into the ground surface.

The flexbase provided a case study of a very stiff material over a soft material (i.e. a typical pavement cross-section). It also provided a surface layer consisting of a fairly uniform, homogeneous material. These conditions made it a good prospect to apply the procedures outlined in Section 3.3.4 in order to estimate the thickness and stiffness of the pavement surface layer. Figure 6.18 presents typical raw data from the signal analyzer for an individual spacing (1/2-foot), and Figure 6.19 is the corresponding individual dispersion curve from this raw data. A logarithmic scale was used for the wavelength in Figure 6.19 because it aids in expanding the curve for the lower wavelengths, and makes the transition between layers more evident. This is helpful for typical pavement profiles since they have a relatively thin surface layer (less than one foot). The dispersion curve reveals a relatively constant velocity up to a wavelength of 0.5 foot, at which point the velocity drops dramatically. The vertical

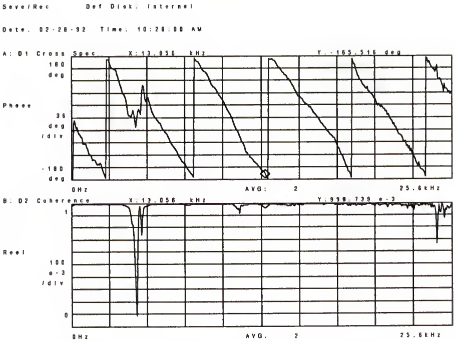

Figure 6.18 Signal Analyzer Plots for the Flexbase at Drained Condition

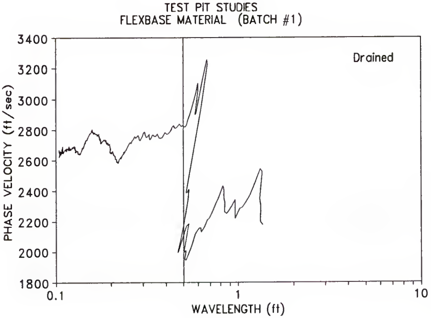

Figure 6.19 Dispersion Curve for the Flexbase at Drained Condition (1/2-Foot Spacing) in the Test Pit

line at a wavelength of 0.5 foot represents the critical wavelength. Thickness measurements of the flexbase made at the time of its removal averaged a total of six inches, which compares very well to the critical wavelength shown in Figure 6.19. This wavelength appears as an irregularity on the cross power spectrum trace (top plot in Figure 6.18), and the coherence (bottom plot in Figure 6.18) drops well below 0.9. This indicates that the raw SASW traces can be used to identify transition layers directly in the field with a high degree of accuracy. This accuracy is directly related to the differences in stiffness between the two layers and the attenuation properties of the surface layer. It is also dependent upon the thickness of the surface layer and the source being used. For this testing, a wrench impacting the ground surface was adequate to sample the flexbase layer, but this surface layer was relatively thick compared to many asphalt pavement sites. If a thin surface layer is being tested (1 to 3 inches), higher frequencies need to be generated to adequately sample this layer. This might require the use of a high frequency generator as the source.

Referring to Figure 6.18, the slope of the cross power spectrum trace before the transition is greater than the slope after the transition. This indicates that a higher velocity material is present at shallower depths (higher frequencies) than at depths below the transition (lower frequencies). The slope of the cross power spectrum trace after the transition is very consistent, indicating that the velocity of the surface material is uniform.

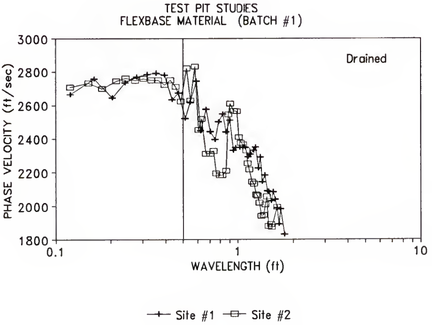

Figure 6.20 Dispersion Curves for the Flexbase at Drained Condition in the Test Pit

The composite dispersion curve is shown in Figure 6.20, which consists of the results from the individual dispersion curves at spacings of 1/2- and 1-foot for both a normal and reverse configuration. This figure shows the consistency of the flexbase between the two test sites, especially for the flexbase layer. The interface between the two layers is quite obvious due to the large difference in stiffness between the two materials. The logarithmic scale used for the wavelength highlights the lower wavelength data which is typically of more interest and accentuates the transition between the two layers.

Table 6.18 SASW Results for the Flexbase Study

Test No.	Avg. V_R (ft/sec)	Range V_R (ft/sec)	V_S (ft/sec)	G_{max} (psi)	E_{max} (psi)
D-D	Batch #1				
1	2,711	2526-2793	2,913	208,652	555,015
2	2,727	2624-2760	2,930	211,122	561,586
Avg.	2,719		2,921	209,887	558,300

Table 6.18 contains the stiffness properties for the first batch of flexbase. The surface wave velocities were obtained from the composite dispersion curves by averaging the velocities less than wavelengths of 0.5 foot. The shear wave velocity, shear modulus, and Young's modulus were calculated by assuming a Poisson's ratio of 0.3 and using a mass density calculated from the in-situ nuclear densities obtained near the plate load test locations. A series of SASW tests were only performed on the flexbase at the drained-dried condition. No testing was performed on either the optimum or soaked moistures.

The calculated moduli presented in Table 6.18 are very high since they reflect the maximum, initial tangent (i.e. elastic) conditions for this material. This material possessed excellent attenuation properties for the generated surface waves resulting in very high measured velocities in which good quality data was readily obtained. The raw data traces revealed consistent, clean data with high coherence values (except for the transition zones). Because of the high frequencies generated during the testing, the frequency effect would have to be addressed in order to compare these seismic moduli with results from conventional methods. This is similar to the variation in moduli for asphaltic concrete (AC) materials (refer to Figure 2.14). The highest recorded frequencies during the SASW testing were on the order of 25,000 Hz. In the case of an AC material, this can result in the difference of approximately one order of magnitude between the shear modulus obtained from the SASW test and one obtained at zero frequency (i.e. a static test).

Dolomite. The dolomite used for this study was obtained from Marianna, Florida (FDOT Pit No. 53-271). This material was a granular, cohesionless aggregate utilized for base applications. Based on laboratory testing of samples taken from the material as-delivered to the test pit, the modified Proctor maximum dry density was 114.7 lb/ft^3 at an optimum moisture content of 13.3%, and the LBR was 162%. The dolomite was placed in two-5.25 inch thick lifts (total layer thickness of 10.5 inches) at 100% of the Proctor density for both lifts. Nuclear densities and Speedy moistures were obtained adjacent to plate load test sites upon their completion, and these results are presented in Table 6.19. This phase of the testing was performed from November, 1994 through January, 1995.

Table 6.19 In-situ Densities and Moisture Contents for the Dolomite Study

Test Type/#	Dry Density (lb/ft^3) & Moisture Content (%) 1	2	3
Optimum	115.1 @ 13.6%	115.0 @ 14.8%	116.5 @ 13.4%
Drained	115.6 @ 12.4%	116.3 @ 11.4%	114.6 @ 14.0%
Soaked	109.8 @ 21.5%	114.9 @ 17.4%	112.9 @ 18.2%

SASW tests were performed at different locations on the surface of the dolomite layer at the three moisture conditions (optimum, drained, and soaked). The results from the soaked tests are not included because the surface of the material was very wet causing problems in attaching the accelerometers to the ground surface. The SASW tests were performed within a couple of days of the plate load tests for a particular moisture condition.

The results from the remaining SASW testing (optimum and drained conditions) are shown in Figure 6.21 and Table 6.20. Figure 6.21 contains representative dispersion curves from the series of tests performed on the dolomite. Its purpose is to compare the SASW results for the two moisture conditions and show the transition between the dolomite and underlying sand subgrade layers. The vertical line in Figure 6.21 represents the critical wavelength, which ideally equals the thickness of the surface layer. This thickness, 0.875 foot (10.5 inches), is based on the proposed design thickness of the dolomite layer. The actual thickness of the layer was determined while the material was excavated from the test pit, and ranged from 10.5 to 11.5 inches, with an average thickness of 10.9 inches (0.91 foot). The dispersion curves show a transition within the range of wavelengths from 0.8 to 1.0 foot, which is within the range of thickness of the dolomite layer.

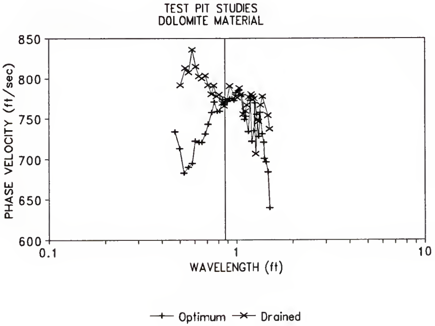

Figure 6.21 Dispersion Curves for the Dolomite in the Test Pit

The stiffness properties of the dolomite are presented in Table 6.20. The range of V_R and averaged V_R were obtained from the data on the dispersion curves less than the critical wavelength. The same procedures were used to convert these surface wave velocities to the elastic moduli. The Poisson's ratio was assumed to be 0.3 for this analysis. An inversion analysis of the SASW dispersion results was not possible since a problem was encountered in the inversion program for test sites with a stiff surface layer over a softer layer. This problem will be discussed in more detail in a later section.

Table 6.20 SASW Results for the Dolomite Study

Test No.	Avg. V_R (ft/sec)	Range V_R (ft/sec)	V_S (ft/sec)	G_{max} (psi)	E_{max} (psi)
Opt.					
1	719	660-772	777	17,112	44,492
2	680	604-736	735	15,328	39,853
3	724	667-804	782	17,366	45,150
Avg.	708		765	16,602	43,165
D-D					
1	774	713-836	836	19,579	50,905
2	770	693-837	832	19,382	50,393
Avg.	772		834	19,481	50,649

Referring to results presented in Figure 6.21 and Table 6.20, the stiffness of the dolomite at the drained condition is slightly higher than it is at optimum moisture. This difference was not as great as might be expected (less than 150 ft/sec), which was probably due to the moisture contents of the drained and optimum conditions being similar. The average moisture content for the tests at optimum was 13.9%, while it was 12.6% during the drained tests (refer to Table 6.19). The dispersion curves in Figure 6.21 can be seen to converge near the critical wavelength. Beyond this point, the two curves are quite similar since these portions of the curves represent the underlying sand subgrade. The various moisture conditions affect the surface layer most significantly and therefore, the stiffness of the underlying soil remains fairly consistent. The variations in the portion of the curves beyond the critical wavelength are due to the small spacings used during the tests which limited the amount of long wavelength data.

A similar means to relate the SASW moduli with the plate load test results based upon axial strain was used for the dolomite. One difference between these tests and those for the subgrade materials was that higher loadings were used during the static and dynamic plate load tests. The static tests used loads of 1,000 to 5,000 pounds in increments of 1,000 pounds, and the cyclic stress used during the dynamic plate load test was 50 psi. The results from the plate load tests are presented as Tables B.13 and B.14 in Appendix B.

The modulus obtained from these series of plate tests is referred to as an equivalent single layer modulus, E_e, and represents the plate modulus of a single material which would give the same deflection as the two-layer system under the same applied loading. It is a stiffness that is dependent upon both the individual stiffness of the dolomite layer as well as the underlying subgrade layer. This is due to the stress zone of the loaded plate reaching into the subgrade. The approximate depth of this stress zone is two times the plate diameter (24 inches), which is greater than the layer thickness of the dolomite. Therefore, a correction needs to be made to the moduli obtained from the plate load tests in order to reflect true layer moduli for the dolomite material. Using the Burmister two-layer design charts for vertical surface defection (Yoder and Witczak, 1975), the modulus ratio of the first to second layer moduli (E_1/E_2) is in the range of 5 to 10. Comparing plate load tests on the dolomite and underlying subgrade at similar applied loadings, the actual E_1/E_2 ratio is approximately three. Therefore, the plate moduli for the dolomite are too low and need to be corrected to reflect the true stiffness for this material. Based on previous test results for other Florida limerock and since these charts are very conservative, a value of 1.67 seems reasonable. The plate moduli (in Figures B.13 and B.14) were adjusted by this factor and the axial strains were recalculated. The results from both the static and dynamic tests were combined, and the resulting plot is shown as Figure 6.22. This is only an approximate method to determine the material stiffness properties from the plate load tests. A more sophisticated method was not used since no resilient modulus data was available and no design curves could be developed.

The legend in Figure 6.22 indicates the applied stress that each moduli was derived. Similar to the subgrade results, a series of curves can be developed based on the applied stress, with the curves shifting toward a higher axial strain for increasing applied stress. The results obtained from the dynamic plate load tests compare well with the curves for the static plate load tests since it falls just to the right of the static tests performed at 44.2 lb/in^2.

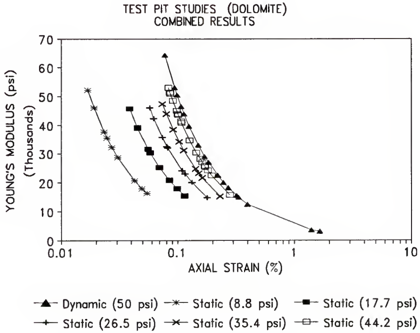

Figure 6.22 Variation of Young's Modulus and Strain for the Dolomite

The SASW moduli were in the range of 43,000 to 50,600 psi, which is lower than the moduli in Figure 6.22. This is inconsistent with the fact that the seismic moduli should be an elastic moduli, representing a maximum limit. Part of the problem might have been that the SASW shear wave velocities were obtained from measured wavelengths in the range of 0.5 to 0.9 foot. This range of wavelengths represent a small portion of the entire dolomite layer, approximately one-third of the bottom of this layer. During the SASW testing, the quality of the high frequency data was not adequate to define the top portion of the surface layer. Since the dispersion curve is obtained by averaging the data from each individual spacing, it might not reflect some of the local variations in the dispersion curve if insufficient information is available for a portion of the curve, primarily the shorter wavelengths (or shallower sampling depths). Looking at the individual dispersion curves for the 1/2-foot spacings, a higher range of surface wave velocities occurs at wavelengths less than 0.9 foot compared to the averaged composite dispersion curve. Based on the individual dispersion curves, the range of V_R for the dolomite layer is from 900 to 1,300 ft/sec, with a resulting range of E_{max} from 71,500 to 149,100 psi (average of 110,300 psi). This value seems more reasonable as an upper limit. Although, this is still an approximate value for E_{max} due to lack of high frequency SASW data. This is a case when a higher frequency source was needed to better define the stiffness properties of the surface layer. Without an accurate value of E_{max}, it would be uncertain whether the resulting normalized plot of Young's modulus truly represents the stiffness properties of the dolomite. Therefore, this plot was not produced for this analysis.

RAP (reclaimed asphalt pavement). This study was performed to evaluate the use of milled asphalt as an aggregate substitute. Due to the results of this evaluation study, the RAP material was only to be used as a base for non-traffic applications (i.e. roadway shoulders). This was the result of the large amount of permanent and total deformations during the plate load tests, and the susceptibility of this material to creep under long-term repetitive loads.

Based on laboratory testing of samples taken from the material as-delivered to the test pit, the modified Proctor maximum dry density was 120.5 lb/ft^3 at an optimum moisture content of 7.8%, and the LBR was 34%. The RAP material was placed in two-5.25 inch thick lifts (total layer thickness of 10.5 inches) at 95 to 97% of the Proctor density for both lifts. Nuclear densities and Speedy moistures were obtained adjacent to plate load test sites upon their completion, and these results are presented in Table 6.21. As opposed to the other materials tested, only two plate tests were performed for each moisture condition. This phase of testing was performed from May through August, 1993.

The plate load test data for the RAP material has not been included in this section, and only the SASW results shall be presented. Since the RAP proved to be unacceptable for typical FDOT roadway usage, a relationship between the various moduli was not developed. Representative dispersion curves from the SASW tests performed at each moisture condition are shown in Figure 6.23.

Table 6.21 In-situ Densities and Moisture Contents for the RAP Study

Test Type/#	Dry Density (lb/ft^3) & Moisture Content (%) 1	2
Optimum	120.7 @ 3.6%	121.3 @ 3.2%
Drained	118.1 @ 2.8%	124.8 @ 2.7%
Soaked	113.5 @ 14.1%	115.4 @ 9.5%

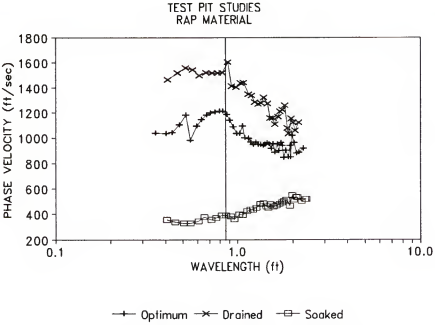

Figure 6.23 Dispersion Curves for the RAP in the Test Pit

The results presented in Figure 6.23 show very clearly the stiffness variation of this material due to the varying moisture. It also reveals the transition between the RAP layer and the underlying sand subgrade on all three dispersion curves. This transition occurs at the same wavelength for all three curves, and is very close to the critical wavelength of 0.875 foot (represented by the vertical line). The position of the critical wavelength in this figure is based on the design thickness of the RAP layer. The actual thickness of the RAP layer ranged from 10.4 to 11.25 inches, with an average thickness of 10.7 inches (0.89 foot), which was measured while the material was being excavated from the pit.

The dispersion curves in Figure 6.23 show that the minimum measured wavelengths were on the order of 0.3 to 0.4 foot. This was similar to the results obtained from the dolomite material. Since higher frequencies could not be generated to sample these lower wavelengths, the stiffness properties of approximately the top half of the RAP layer were not measured. If the surface material is not uniform and homogeneous, this incomplete stiffness profile can cause errors in evaluating the stiffness properties of the surface layer, especially if it is a thin layer. As with the dolomite tests, the source for the 1/2-foot spacings was a wrench impacting the ground surface. This proved to be insufficient to generate high frequencies needed to sample the top several inches of the surface layer. Additional testing needs to be performed on typical aggregate bases to determine if a high frequency generator needs to be obtained to adequately test these materials in the future.

Referring to the optimum and drained dispersion curves in Figure 6.23, a bump occurs on both curves at an approximate wavelength of 0.5 foot. Figure 6.24 shows an individual dispersion curve for one of the 1/2-foot spacings at drained condition, which highlights this irregularity appearing on the dispersion curves in Figure 6.23.

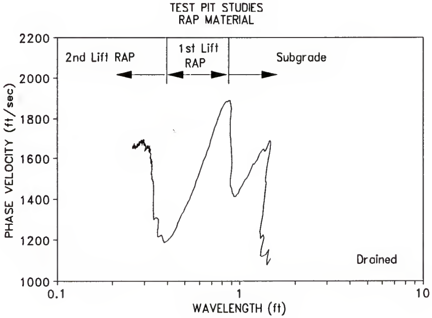

Figure 6.24 Dispersion Curve for the RAP at Optimum Condition (1/2-Foot Spacing) in the Test Pit

The wavelength at which the first and second peaks of the dispersion curve in Figure 6.24 occurs at approximately 0.4 foot, which corresponds to the interface between the first and second lifts of the RAP material (0.44 foot). The second peak drops off at a wavelength of approximately 0.9 foot, which corresponds to the interface between the RAP and underlying sand subgrade (0.88 foot). This trend appeared on the majority of the 1/2-foot spacing dispersion curves, and was not an isolated incident. This indicates that the interface between the two RAP lifts provided a boundary that was detected by the SASW test. This boundary was not a stiffness transition, but was probably due to the interface acting as a reflection surface. This behavior was unique to the RAP material since it was composed of processed pavement containing asphalt and aggregate, which provided an excellent medium for surface wave propagation.

The stiffness properties of the RAP material, based on an analysis of the surface wave velocities obtained from the dispersion curves, are presented in Table 6.22. For this analysis, a Poisson's ratio of 0.3 was assumed, and the in-situ nuclear densities in Table 6.21 were used to calculate the mass densities. The SASW results yielded a high range of Young's modulus for both the optimum and drained conditions. These results were much higher than those from the dolomite tests. Since the dolomite proved to be an acceptable base material and the RAP was not, this indicates that some caution must be used when applying the SASW results. As stated previously, the SASW results represent the elastic properties of the material. Comparisons of the elastic stiffness properties might not necessarily reflect the same trend as those at higher strain levels, which are the levels of strain for actual working conditions and those that need to be addressed during the design phase. An example of this is the LBR test results for the RAP and dolomite materials, which show that the RAP possesses a much lower stiffness (LBR = 34%) at very high strain levels (greater than 2%) than the dolomite (LBR = 162%). This is the reason why design curves need to be produced for various materials that show the relationship of the moduli for a wide range of strain levels, which incorporate strains encountered during field testing as well as those at actual working loads.

Table 6.22 SASW Results for the RAP Study

Test No.	Avg. V_R (ft/sec)	Range V_R (ft/sec)	V_S (ft/sec)	G_{max} (psi)	E_{max} (psi)
Opt.					
1	1,275	1042-1373	1,378	51,252	133,256
2	1,216	1040-1267	1,314	46,597	121,153
Avg.	1,246		1,346	48,897	127,132
D-D					
1	1,513	1423-1572	1,635	71,933	187,025
2	1,598	1495-1670	1,727	80,251	208,654
Avg.	1,556		1,681	76,035	197,691
Soak					
1	576	453-663	623	10,730	27,898
2	361	329-389	389	4,200	10,920
Avg.	468		506	7,089	18,432

6.3 Field Trench Sites

This phase of testing was performed in conjunction with a research project by Florida State University (FSU) and FDOT State Materials Office personnel in order to correlate laboratory test results (resilient modulus and LBR) with moduli obtained from field plate load tests and falling weight deflectometer (FWD). Ten locations around the state, with two test sites at each location, were chosen for this project. Each location was an existing roadway with asphalt pavement.

6.3.1 Background Information

At a typical test site, FWD tests were performed over the plate load test location. The FWD testing was performed along the outside wheel path (approximately 3 feet from the edge of pavement). Trenching operations at each site began by cutting the asphalt pavement with a saw across an entire lane approximately four feet wide, and stripping it away to reveal the underlying base layer. If the test location was a four-lane roadway, the outside lane was typically used as the test site. Care was taken during the removal of the overlying layers not to disturb the soil in the test area. When the test elevation was reached, the area was cleaned of any loose material and leveled. A 12-inch diameter steel plate was placed over the test site, which was within the wheel path of the roadway. A thin layer of plaster of paris was used to level the plate in order to transfer the load uniformly across the area of the plate. Prior to performing the plate load test, the in-situ density of the material was obtained from a surface nuclear density gauge. The in-situ moisture was determined by the Speedy moisture test method, and a sample was obtained and placed in a air-tight container in order to obtain an oven-dried moisture content of the soil.

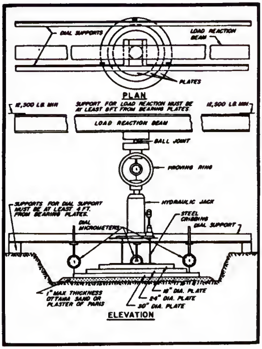

Figure 6.25 Diagram of a Typical Field Plate-Bearing Test (AASHTO, 1993)

A tanker truck filled with water (with a total load of approximately 60,000 pounds) was used to provide a reaction mass to jack against during the plate load tests. Once the plate was set into position, a hydraulic jack was placed on the plate and shims were added until contact with the truck was achieved. The jack was calibrated so that the magnitude of the applied load could be recorded. A swivel head was used in order to apply the load uniformly to the bearing plate. Two reference beams were used to attach two dial gauges used to measure the deflections of the plate. The supports of the beams were located at least 4 feet from the circumference of the bearing plate. The two dial gauges were placed 180° apart so that any tilting of the plate could be averaged. A typical layout of a plate load test, based on AASHTO procedures, is shown in Figure 6.25.

A series of three seating load cycles were performed. For each of these cycles, the plate was loaded in a minimum of five uniform increments until an average deflection of 0.030 inch was achieved. When the average deflection of 0.030 inch was reached, the load was released and a rebound deflection was recorded. The dial gauges were reset to zero, and the sequence was repeated for the second and third seating load cycles. After the series of seating loads was completed, the loading cycle was performed. The load was applied uniformly so that a minimum of five increments of load were used in order to accurately define the load-deflection curve. The load and deflections were recorded for each increment of load. The loading was continued until the average total deflection was 0.050 inch plus the average rebound deflection from the third seating load cycle, or until the capacity of the equipment was reached. After the final deflections and load were recorded, the load was released and a rebound deflection was obtained. The procedures outlined above were in accordance with the Florida Method of Testing for Nonrepetitive Static Plate Load Test of Soils and Flexible Pavement Components (FM 5-527), which is a modified version of AASHTO T-222-78.

After the completion of the plate load test on the base layer, the base material was completely excavated to reveal the underlying subgrade layer. The same procedures outlined above were used to perform a plate load test on the surface of the subgrade. The plate location was alternated to the inside wheel path to minimize the effect from the preceding plate test on the base layer. When this test was completed, the subgrade material was excavated to reveal the embankment layer. A plate test was performed on the surface of the embankment layer along the outside wheel path. As each layer was being excavated, bag samples were obtained to perform laboratory tests on the materials. The total thickness of each layer was recorded based on visual observation of the layering along the sides on the trench.

6.3.2 SASW Testing

SASW tests were performed at only six of the ten test locations throughout the state due to scheduling and availability of personnel at the time of these tests. For each location, tests were performed on the pavement surface, as well as on the surface of the base, subgrade, and embankment layers. The SASW tests were located adjacent to the bearing plate, usually within one or two feet of the plate's edge. Due to the limited space in the trench, the typical SASW spacings were restricted to 0.5 and 1 foot. Longer spacings were used for the tests on the pavement surface, typically 2, 4, and 8 feet. For each individual spacing, the configuration was reversed to average out any variation at the test site. The accelerometers were used as receivers exclusively on the pavement surface and the base layer tests. For the subgrade and embankment tests, either the accelerometers or 4.5 Hz geophones were used depending upon the type and hardness of the surface soils. The accelerometers were attached to the pavement surface with wax. For the soil layers, the accelerometers were mounted on threaded spikes which were driven into the ground surface. If the 4.5 Hz geophones were used, they were manufactured with spikes which could be pushed into the ground at the proper spacings.

The following locations were the trench sites at which SASW testing was performed (cross-sectional profiles of each test site are included in Appendix B as Figures B.17 through B.22):

(1) US-17, northbound, outside lane, Green Cove Springs, Clay County (tested June 22-23 and 29-30, 1993)

(2) SR-414, westbound, inside lane, Maitland Boulevard, Seminole County (tested August 24-25, 1993)

(3) US-441, southbound lane, Yeehaw Junction, Osceola County (tested August 30 - September 1, 1993)

(4) US-41, eastbound, outside lane, Tamiami Trail, Dade County (tested October 19-20, 1993)

(5) US-1, northbound, outside lane, Jupiter, Martin County (tested October 26-27, 1993)

(6) US-17/92, eastbound, outside lane, Haines City, Polk County (tested December 7-8, 1993).

6.3.2.1 Layer thickness measurements

For each SASW test performed on the pavement, base, and subgrade layers, a thickness of the surface layer was estimated using the resulting dispersion curves and the analysis outlined in Section 3.3.4. These values were compared to the actual thickness of each layer, and the results are presented in Table 6.23. There is a range of thickness measurements for the SASW results because a separate thickness was obtained for each of the individual spacings used during the field test (1/2- and 1-foot), as well as the normal and reversed configurations for each spacing. The average SASW thickness was determined from the minimum and maximum values within this range. A typical example showing how the layer thickness was determined from the dispersion curves is shown in Figure 6.26. These curves were obtained from the US-1 (Tamiami Trail, Dade

Table 6.23 Thickness of the Trench Site Layers

Location / Layer	Actual Thickness (in.)	Range of SASW Thickness (in.)	Average SASW Thickness (in.)
Clay Co. (Site #5)			
Pavement	5.5	4.9 - 5.5	5.7
Base	8	7.2 - 9.0	8.1
Subgrade	12	9.0 - 10.8	9.9
Clay Co. (Site #6)			
Pavement	-	5.4 - 5.9	5.7
Base	7	4.9 - 9.6	7.3
Subgrade	12 - 14	10.4 - 11.9	11.4
Seminole Co. (Site #1)			
Pavement	6	6.8 - 7.3	7.1
Base	12	9.2 - 11.9	10.8
Subgrade	12	11.4 - 13.2	12.3
Seminole Co. (Site #2)			
Pavement	6	5.0 - 6.5	5.8
Base	12	10.4 - 11.9	11.2
Subgrade	12	10.7 - 10.9	10.8
Osceola Co. (Site #3)			
Pavement	3.1	-	-
Base	8	7.8 - 9.2	8.5
Subgrade	12 - 18	14.5 - 18.7	16.6
Osceola Co. (Site #4)			
Pavement	5.5	5.4 - 5.8	5.6
Base	11	7.9 - 10.4	9.2
Subgrade	18	15.6 - 17.9	16.8

Table 6.23 (cont.)

Location / Layer	Actual Thickness (in.)	Range of SASW Thickness (in.)	Average SASW Thickness (in.)
Dade Co. (Site #1)			
Pavement	3.2	-	-
Base	13	9.6 - 12.0	10.8
Subgrade	13	11.3 - 13.2	12.3
Dade Co. (Site #2)			
Pavement	3	3	-
Base	9.5	9.6 - 10.3	10.0
Subgrade	12.5	12.7 - 14.4	13.6
Polk Co. (Site #1)			
Pavement	-	-	-
Base	9	9.4 - 10.1	9.8
Subgrade	13	12.4 - 14.4	13.4
Polk Co. (Site #2)			
Pavement	3	-	-
Base	9	8.2 - 8.5	8.4
Subgrade	13	11.4 - 14.3	12.9
Martin (Site #3)			
Pavement	-	-	-
Base	13	12.2 - 15.7	14.0
Subgrade	12 - 16	14.2 - 16.7	15.5
Martin Co. (Site #4)			
Pavement	3	-	-
Base	9	9.6 - 10.8	10.2
Subgrade	12	11.9 - 13.2	12.6

County) site #1 subgrade test. The two curves were obtained from the normal and reversed configurations for the 1/2-foot spacings. In many cases the 1/2-foot spacings yielded very low velocities and erratic data, possibly indicating disturbance of the surface soils due to the excavation process. When this occurred, the dispersion curves from the 1-foot spacings were used exclusively to determine the layer thickness.

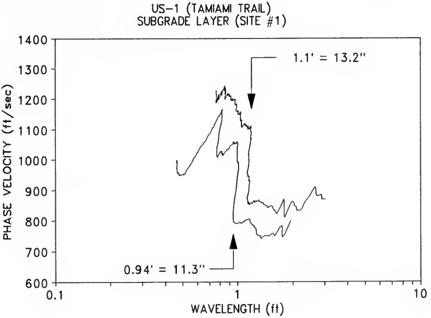

Figure 6.26 Dispersion Curves for US-1 (Tamiami Trail, Dade Co.) Site #1, Subgrade Layer

There were only five sites that the SASW test was able to detect the interface between the pavement and base layers. Referring to Table 6.23, this occurred at the sites which had a pavement thickness of at least 5.5 inches. The thickness of the pavement layer at the remaining sites varied from 3 to 4 inches. This points out a limitation of the SASW test to sample very shallow depths when an impact source is used (in this case, a wrench impacting the ground surface). In order to sample the top 3 to 4 inches of a test site, a special source is needed to generate very high frequency surface waves. In the cases where the thickness of the pavement layer could be determined from the dispersion curves, an accurate determination of the pavement stiffness was not possible because the dispersion curves did not extend to low enough wavelengths to sample the pavement layer thoroughly.

To determine how well the SASW measurements agreed with the actual ones, the two values were plotted versus each other and the resulting plot is shown in Figure 6.27. The results presented in this figure reveal that the SASW measurements agreed well with the actual measurements. A line with a slope of 1:1 has been included on this plot to indicate a perfect match between the two values. A linear regression was performed on this data, and the results (the equation of the regression line and r^2, which is the coefficient of determination) are shown on this plot. It can be seen that the regression and 1:1 lines are similar, indicating a good comparison between the SASW and actual measurements. The coefficient of correlation (r) can be determined by taking the square root of the coefficient of determination. Performing this calculation, the correlation of the regression line was high (0.92) revealing a good quality match between the two sets of data.

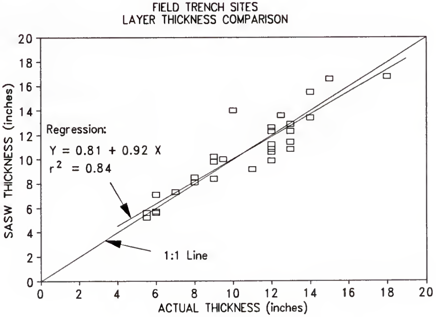

Figure 6.27 Comparison of Layer Thickness Measurements for the Trench Sites

To evaluate the accuracy of the SASW test at estimating the layer thickness, the difference between each of the SASW measurements and the actual thickness was calculated, as well as the percent difference (the difference between the SASW and actual thickness divided by the actual difference). Overall averages of the differences and the percent differences were determined for all the data, as well as for the pavement, base, and subgrade layers separately. These results are presented in Table 6.24. Two values are listed for the base and overall averages because the first value reflects the average for all the data and the second excludes the results from the US-1 (Jupiter, Martin County) site #3 base layer. The difference between the SASW and actual thickness at this test site was unusually high (4 inches), which might be due to variations across the width of the trench at this location. Based on the other results, it is believed that this one result is an exception to the effectiveness of the SASW test. Without this one result, the averages of the percent difference for the pavement, base, and subgrade layers were similar, which seem to justify the exclusion of it.

Table 6.24 Summary of Thickness Comparisons for the Field Trench Sites

Layer	Average of Difference (in)	Average of Percent Difference (%)
Pavement	0.4	7.5
Base	1.2 (0.9)	11.5 (8.9)
Subgrade	1.1	7.9
All Data	1.0 (0.9)	9.3 (8.2)

Based on the results presented in Table 6.24, the SASW test seems to be able to estimate the layer thickness to within about one inch of the actual thickness, with a percent difference of less than 10 percent. This is a reasonable accuracy for most engineering applications. It can be seen that the average difference was the least for the pavement layers, second for the base layers (without the one result), and the most for the subgrade layers. This is due to the contrast between the stiffness of the surface and underlying layers. This difference in stiffness is greater for the tests performed on the pavement surface than for those on the base or subgrade surfaces. The greater this contrast, the more distinctly the interface will appear on the dispersion curve, which will make the identification of the critical wavelength (and therefore, the surface layer thickness) more apparent. To analyze this effect, the ratio of the stiffness between the surface layer and the underlying layer was determined for various strength parameters determined during this research: plate Young's modulus, LBR, and density. These ratios were plotted versus the corresponding percent difference of the SASW thickness. The general trend revealed that the percent difference did decrease as the stiffness ratio increased (i.e. the stiffness of the two layers were more dissimilar). The results comparing the LBR data with the percent difference of the SASW measurements are presented in Figure 6.28, along with trend lines showing the approximate limits of the range of field data.

The overall summation of the differences between the SASW and actual layer thickness (maintaining the sign of the difference) was -1.60 inch, and without the US-1 (Jupiter, Martin County) site #3 base result was -5.60 inches. This indicates that the SASW results generally underpredicted the overall layer thickness. This is probably the result of the excavation of the overlying soils having removed a small portion of the layer to be tested at some of the sites, especially the subgrade layers. The actual measurements were based on visual observation of the layering from the side of the trench. The SASW tests were performed on the surface of the layer, and measured the actual thickness of the layer that remained after excavation.

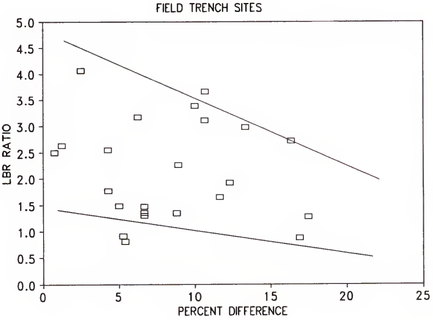

Figure 6.28 Comparison of LBR Ratio and Percent Difference of the SASW Thickness Measurements

6.3.2.2 Layer stiffness measurements

A problem was encountered with the inversion software used for this research. It was hoped that the SASW tests on the pavement surface could be analyzed, and the results could be compared with the stiffness profiles obtained from the tests performed on each of the sublayers. The inversion software was not specifically written for pavement sites, and primarily was used on soil sites, in which it proved to work well. For pavement sites, or sites with a very stiff layer(s) over softer layers, this inversion program did not yield a final solution. The final results could not be used to produce a theoretically-derived dispersion curve. Therefore, the input conditions could not be altered to produce a theoretical curve that would match the curve obtained from the field. Without this data, a comparison between the theoretical and actual field data could not be performed. Since this software was never used for pavement applications in the past, conversations with Dr. Glenn Rix, professor at the Georgia Institute of Technology, confirmed that this could happen with this program, and that there were no easy solutions which could accurately model a pavement site without any major changes in the software algorithm. As a result of this problem, a comparison of the SASW moduli with any back-calculated moduli from the FWD tests was not possible.

The various locations of the trench sites consisted of different materials which are commonly used in this state for roadway construction. For the five locations at which SASW tests were performed, limerock was used for the base material except at the US-441 (Yeehaw Junction, Osceola County) sites, which utilized a coquina base. The subgrade and embankment materials consisted of either A-3 or A-2-4 cohesionless, non-plastic materials. The exceptions were the subgrade at US-1 (Jupiter, Martin County), site #4 which was a non-plastic A-4 material and the subgrade and embankment soils at both US-41 (Tamiami Trail, Dade County) sites which were sandy limerock. A summary of the material properties for the base, subgrade, and embankment soils is presented in Table 6.25.

Each of the SASW dispersion curves from the base and subgrade layer tests was used to estimate the stiffness of the surface layer based on the analysis outlined in Section 3.3.4. For the tests on the base and subgrade layers, the results from the two sites were averaged to get a representative stiffness of that material. A number of the tests yielded very low velocities in the low wavelength ranges (i.e. shallower sampling depths), probably due to disturbance of the surface layer because of the excavation of the overlying layer. The low velocities resulted in moduli which were lower than the corresponding plate load test moduli and the results from the laboratory resilient modulus tests. Therefore, the results of these tests were not used in determining the stiffness of that particular layer. All of the SASW tests on the embankment layers revealed the presence of low velocity soils near the surface. This was expected since the embankment materials consisted of sandy soils which became quite disturbed as the overlying subgrade layer was excavated. As a result, the only means to estimate a representative stiffness for these soils was to perform an inversion analysis.

Table 6.25 Material Properties for the Trench Site Soils

Test Site / Layer	AASHTO Class.	Lab Density / Field Density (lb/ft^3)	LBR (%)
US-17 (Site #5) Green Cove Springs			
Base (Limerock)	-	119.2 @ 10.8 112.1 @ 11.2	108
Subgrade (Grey Sand)	A-2-4	98.2 @ 13.6 99.4 @ 8.6	48
Embankment (Grey Brown Sand)	A-3	102.8 @ 15.0 100.8 @ 9.7	88
US-17 (Site #6)			
Base (Limerock)	-	116.6 @ 12.2 119.9 @ 11.1	25
Subgrade (Grey Sand)	A-3	100.3 @ 15.1 101.5 @ 12.2	48
Embankment (Yellow Grey Sand)	A-3	98.5 @ 17.5 100.0 @ 11.7	25
SR-414 (Site #1) Maitland Blvd.			
Base (Limerock)	-	123.6 @ 9.8 124.1 @ 8.5	107
Subgrade (Red Brown Sand)	A-2-4	117.7 @ 6.4 111.7 @ 7.5	65
Embankment (Brown Sand)	A-2-4	108.5 @ 12.3 112.6 @ 7.0	16
SR-414 (Site #2)			
Base (Limerock)	-	120.8 @ 11.9 115.1 @ 10.2	114
Subgrade (Red Brown Sand)	A-2-4	118.0 @ 8.2 112.9 @ 11.3	88
Embankment (Yellow Sand)	A-3	104.5 @ 14.0 103.5 @ 12.7	26

Table 6.25 (cont.)

Test Site / Layer	AASHTO Class.	Lab Density / Field Density (lb/ft^3)	LBR (%)
US-441 (Site #3) Yeehaw Junction			
Base (Coquina)	-	132.0 @ 7.3 127.6 @ 5.1	168
Subgrade (Grey Sand)	A-3	117.7 @ 9.2 119.0 @ 3.8	53
Embankment (Yellow Fine Sand)	A-3	103.3 @ 14.0 104.0 @ 3.4	17
US-441 (Site #4)			
Base (Coquina)	-	132.8 @ 5.9 132.1 @ 4.6	228
Subgrade (Grey Sand w/Rock)	A-3	121.1 @ 8.8 121.9 @ 7.0	84
Embankment (Grey Fine Sand)	A-3	101.9 @ 15.0 115.4 @ 3.3	57
US-41 (Site #1) Tamiami Trail			
Base (Limerock)	-	131.0 @ 7.0 130.9 @ 7.3	133
Subgrade (Sandy Limerock)	-	128.0 @ 8.0 117.4 @ 7.3	151
Embankment (Sandy Limerock)	-	123.0 @ 10.1 122.2 @ 8.8	186
US-41 (Site #2)			
Base (Limerock)	-	132.0 @ 8.0 134.5 @ 6.8	117
Subgrade (Sandy Limerock)	-	132.0 @ 7.6 129.1 @ 8.2	186
Embankment (Sandy Limerock)	-	122.1 @ 10.6 120.2 @ 7.9	96

Table 6.25 (cont.)

Test Site / Layer	AASHTO Class.	Lab Density / Field Density (lb/ft^3)	LBR (%)
US-17/92 (Site #1) Haines City			
Base (Limerock)	-	120.9 @ 11.1 124.9 @ 10.1	104
Subgrade (Brown Silty Sand)	A-2-4	116.8 @ 10.1 111.1 @ 10.1	46
Embankment (Brown Tan Sand)	A-3	107.9 @ 11.6 107.4 @ 10.7	46
SR-414 (Site #2)			
Base (Limerock)	-	121.4 @ 10.2 119.1 @ 10.6	88
Subgrade (Brown Silty Sand)	A-2-4	119.2 @ 10.6 111.7 @ 8.6	65
Embankment (Brown Tan Sand)	A-3	107.7 @ 11.2 111.7 @ 10.2	26
US-1 (Site #3) Jupiter			
Base (Limerock)	-	132.4 @ 7.4 123.7 @ 7.3	188
Subgrade (Grey Sand w/Rock)	A-4	118.8 @ 8.8 115.9 @ 4.8	40
Embankment (Brown Sand)	A-4	105.0 @ 11.0 110.1 @ 3.4	40
US-1 (Site #4)			
Base (Limerock)	-	130.0 @ 7.3 128.3 @ 6.0	119
Subgrade (Grey Sand w/Rock)	A-4	116.5 @ 9.7 115.0 @ 3.5	40
Embankment (Dark Grey Sand)	A-3	108.7 @ 11.5 109.6 @ 2.0	27

The inversion program worked well with these test results since the embankment sites consisted of natural soil deposits, with a stiffness profile that increased with depth. The stiffness of the embankment soils was obtained from the stiffness profiles produced from the inversion analyses. The layers that were 0.5 to 1 foot below the ground surface were used in order to get an undisturbed stiffness which represented the in-place conditions of these soils. Since the inversion analysis yielded actual layer velocities, the lower velocity layers near the surface reflected the disturbance due to the excavation, and the deeper layers reflected the actual conditions of the embankment soils.

Because testing was performed on the base, subgrade, and embankment layers, the stiffness results were divided into these three categories. Since the subgrade and embankment soils were similar types of materials (primarily A-3 and A-2-4), they were grouped together. The main difference between these materials was the compactive effort used during construction. The results from the base layer and subgrade/ embankment layer tests will be discussed separately in the following sections.

Base layer tests. As previously indicated, the results from the two test sites were averaged to obtain a representative stiffness of the base material for each test location, except for the sites that produced results which indicated very low velocities near the surface. The reason for these low velocities was probably due to the disturbance of the surface soils by the excavation procedures. If the inversion program was able to work on the data from these sites, it could have been used to estimate a stiffness of the base layer below the disturbance zone. At the majority of the test sites, the data from the 1/2-foot spacings produced lower velocities for the surface layer than the corresponding data from the 1-foot spacings. Since the 1/2-foot spacings sampled soils closer to the ground surface, this was evidence that the excavation did produce significant disturbance of the surface soils.

The plate load tests on the base layer were performed at the same time as the SASW tests, and the two tests were performed within one or two feet of each other. The final result of the plate load tests consisted of a load-deflection curve, revealing the deflection of the rigid plate due to each of the applied loadings to the plate. Figure 6.29 shows a typical stress-deflection curve for the US-441 (Yeehaw Junction, Osceola County) site #3 test data. The stress was calculated from the applied loads divided by the plate area (113.1 in^2). This figure shows the three seating load cycles, each applied in uniform loadings to an average total deflection of 0.03 inch. Upon reaching this deflection, the load was released and a rebound deflection was obtained, which represents the permanent deformation of the soil. After the third seating load, the loading cycle was performed in a similar fashion except the load was increased until a deflection of at least 0.50 inch was obtained (including any offset of the curve). Only the load cycle is used to obtain stiffness properties of the material for typical FDOT applications. The modulus used for the standard pavement design criteria is the plate modulus obtained from the Burmister equation (Eqn. 2.36) using a reference deflection of 0.05 inch. This value is a secant modulus which represents the slope of the line intersecting the zero offset deflection and the point on the stress-deflection curve at a deflection of 0.05 inch plus the offset. Figure 6.30 shows what this modulus (labelled secant modulus @ 0.05") represents on the load cycle curve shown in Figure 6.29. Figure 6.30 also shows the other moduli that were obtained from the stress-deflection curve and used for this analysis to be compared to the SASW moduli. The initial tangent modulus is represented by the slope of the line along the initial linear portion of the stress-deflection curve. The resilient modulus is represented by the slope of the line between the maximum (total) deflection and the rebound (permanent) deflection.

The curve in Figure 6.30 is a typical stress-deflection curve for soils because it contains a small linear portion. Except for very small strain levels, soils are nonlinear materials since they typically experience a permanent deformation upon removal of a load. In this nonlinear range, the modulus decreases with increasing deflection (or strain). This can be seen by the difference in slopes between the

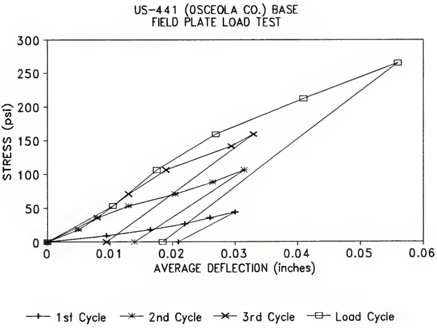

Figure 6.29 Field Plate Load Test Results for the US-441 (Osceola Co.) Base Layer

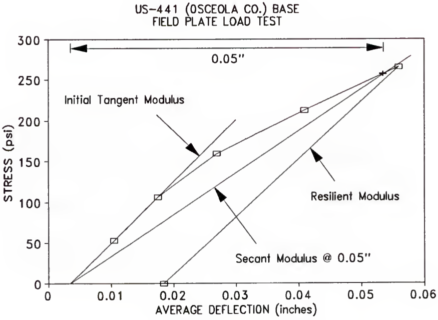

Figure 6.30 Load Cycle Curve for the US-441 (Osceola Co.) Base Layer

initial tangent and secant moduli. The resilient modulus and the initial tangent modulus are nearly parallel, indicating similar values. When the soil is loaded within its linear elastic range, the initial tangent and resilient moduli will be equal. Since the material tested consisted of a crushed rock, there was little permanent deformation compared to a softer material (i.e. a sandy soil) and the resilient modulus was similar to the initial tangent modulus.

The various types of moduli shown in Figure 6.30 were calculated from each of the stress-deflection curves obtained at each of the test sites. These results are presented in Table 6.26, along with the SASW results. The values in this table include the initial tangent modulus (labelled as E_i @ int.), the secant modulus taken at a deflection of 0.05 inch (labelled as E_p @ 0.05"), and the resilient modulus (labelled as E_r @ reb.). As with the SASW moduli, the plate moduli in Table 6.26 are the averaged values from the two test sites from each location. The difference between the two values was small (less than 5,000 psi) for each of the locations except for one (US-17/92, Polk County). In this case, only one of the SASW tests produced a reasonable dispersion curve (site #1), and the plate modulus listed in this table is the result from this site. No secant modulus for the US-41 (Tamiami Trail, Dade County) location is shown in Table 6.26 because the maximum possible load was reached without obtaining a total deflection of 0.05 inch at both test sites. The values in parenthesis represent corrected moduli for the stiffness of the individual base layers. Since the field plate load tests were performed on a layered system, the influence zone of the loaded plate reached into the underlying soil layers which consisted of different materials than the base layers. As with the test pit studies, the Burmister design graphs for vertical surface deflections of a two-layer system was used to obtain the correction factors. Based on this analysis, these correction factors varied from 1.10 to 1.30.

Table 6.26 Stiffness Results of the Base Layer Tests from the Trench Sites

Test Site	SASW E_{max} (psi)	E_i @ int. (psi)	E_p @ 0.05" (psi)	E_r @ reb. (psi)
US-17 Clay	110,145	46,070 (57,588)	39,940 (47,928)	43,953
SR-414 Seminole	110,145	39,538 (51,399)	31,301 (37,561)	38,256
US-441 Osceola	124,897	45,917 (59,692)	35,433 (42,520)	49,728
US-41 Dade	213,077	103,703 (114,073)	--	101,411
US-17/92 Polk	89,647	37,094 (45,626)	31,613 (36,355)	40,188
US-1 Martin	129,844	54,638 (68,298)	39,940 (49,925)	54,728

The values in Table 6.26 reveal the strain dependence of the moduli for the base materials. The SASW moduli represents a seismic stiffness measured at strains in the elastic threshold of soils, producing a maximum limit for the stiffness. As shown in Figure 6.30, the secant modulus (at 0.05 inch deflection) was lower than the initial tangent modulus since the plate load test produced deflections well into the nonlinear range of the base materials. The similarity between the resilient moduli and the initial tangent moduli was due to the stiffness of the base materials tested, and the small amount of resilient deformation encountered during testing. The SASW values represent the actual range of truly elastic behavior of the soil, which is at strain levels beyond the detection of the plate load test for all but very stiff materials.

A study was performed to compare the various moduli listed in Table 6.26. Any analysis similar to the test pit subgrade study to develop a modulus versus strain curve for the field plate moduli was not possible. This was due to the high applied stresses used during the field plate load tests, which could not be compared to lower applied stresses used for the laboratory resilient modulus tests. Since the plate load tests usually define a small portion of the moduli-strain curve, the resilient modulus data was needed to define the intermediate strain levels in which the modulus changes the most. Therefore, the comparison of the moduli in Table 6.26 was accomplished by plotting each value versus the SASW moduli and performing a linear regression by forcing the equation through zero. This comparison was thought to be the best possible alternative since each plate moduli was obtained at similar strain levels, especially the secant moduli which were obtained at similar deflections. Also, the plate moduli typically fall within the higher strain level portion of the moduli-strain curve. For this portion of the moduli-strain curve, the variation in modulus is relatively small compared to the intermediate strains. Therefore, this small variation in modulus allows for a direct correlation between plate and SASW moduli, independent of the strain level, with a relatively small amount of error. The results from the statistical analyses for each of the individual moduli, as well as the laboratory LBR values, are presented in Table 6.27. The values of E_p, E_i, and E_r are the secant, initial tangent, and resilient moduli respectively. The values of the corrected moduli (labelled as Corr. E_p and E_i) are included to reflect the stiffness of the base layer alone. The coefficient of correlation (r), which is the square root of the coefficient of determination (r^2), is included to give an indication of the quality of the regression equation.

Based on the results from Table 6.27, a linear relationship between the SASW and plate moduli seems to be reasonable, especially once a correction is made to reflect the true material stiffness of the base layer. The relationship between the SASW moduli and the initial tangent moduli (as well as the resilient moduli) provided a better comparison than the secant moduli. This is probably due to the secant moduli being obtained at a higher strain level than the corresponding initial tangent moduli or resilient moduli. The SASW moduli seem to compare more favorably with moduli obtained at smaller strains which are nearer to the elastic range of the materials tested. A plot showing the relationships between the SASW and corrected plate moduli (E_p and E_i), as well as the lines resulting from the linear regression analyses is presented as Figure 6.31. Similar plots showing the relationships between the SASW moduli and uncorrected plate moduli and the laboratory LBR are included in Appendix B as Figures B.23 and B.24.

Table 6.27 Linear Regression Results for the Base Moduli Comparisons from the Trench Sites

Parameter	Slope	Correlation
E_p	0.318	0.48
Corr. E_p	0.389	0.99
E_i	0.437	0.99
Corr. E_i	0.519	0.99
E_r	0.436	0.97
LBR	0.00094	0.85

Based on these analyses, comparisons of moduli are more successful for the initial tangent moduli which are corrected for any layering effects. It is reasonable that the comparisons of uncorrected moduli yielded a higher degree of scatter since these moduli represent a composite stiffness, whereas the SASW moduli reflect a layer stiffness. Any comparisons with the laboratory LBR are only approximate at best, since there was a large amount of scatter among this data. The results from the test pit base studies (dolomite versus RAP materials) revealed that the LBR stiffness related very poorly to the SASW modulus. This is due to the difference in the strain levels that the two tests were performed, and because the LBR test was performed at a soaked moisture condition which represents a worse-case situation and not at the conditions that existed in the field during the time of the SASW tests.

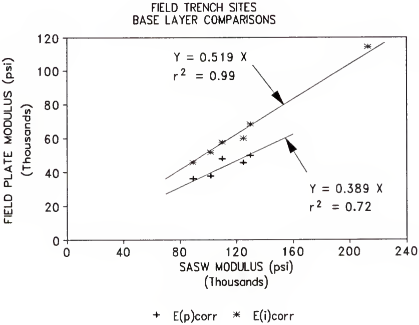

Figure 6.31 Comparison of Corrected Plate and SASW Base Layer Moduli for the Trench Sites

In order to evaluate the effectiveness between any correlation between SASW and plate moduli, the accuracy of the results must be related to the final results (i.e. the design layer thickness). The steps to determine the design layer thickness need to be outlined in order to understand the methodology used for this evaluation. The structural number of pavement (SN) is computed by multiplying the individual layer coefficients (a_i) by the thickness of the layer, and adding the individual components for the surface, base, and subgrade layers. During the pavement design phase, a required SN is obtained from established AASHTO procedures based on traffic loading, environmental conditions, and the underlying soil stiffness. Layer coefficients are chosen based on the materials used during construction, and a thickness for each layer is selected so that the provided SN will be greater than the required SN. If the required SN is constant, then an individual layer coefficient is inversely (and linearly) proportional to the desired thickness of that layer. Based on a relationship between granular base layer coefficients versus plate load test moduli (Smith and Lofroos, 1981), a difference in plate moduli of 10,000 psi (corresponding to a range of SASW moduli of 20,000 to 25,000 psi) would result in a change of layer coefficient of 0.04. For Florida bases, an upper value of layer coefficient has been established at 0.18, which corresponds to a plate modulus of 40,000 psi. If the anticipated error is 10,000 psi, the resulting coefficient is reduced to 0.14, resulting in a decrease of 28.6 percent. Therefore, if a 10 inch base layer is used for a value of 40,000 psi, a modulus of 30,000 psi would result in an actual layer thickness of 12.9 inches.

Laboratory resilient modulus tests were performed on the bag samples obtained at each layer from all of the test sites. Two duplicate samples were recompacted in the laboratory to the field densities and moisture contents. Since the field moisture content varied from the optimum moisture content in some cases, the in-situ density was difficult to obtain and a large difference between laboratory and field densities existed. A difference between the resilient modulus testing of base and subgrade/embankment materials is the magnitude of load and the loading sequence. Base materials, typically classified by SHRP procedures as Type 1, are tested using higher stress states since they will experience a larger amount of the traffic loading than the underlying soils. An example of typical results from a resilient modulus test for Type 1 materials is presented in Table 6.28. These results were obtained from the US-441 (Yeehaw Junction, Osceola County) site #3 base layer bag samples.

As with the test pit subgrade study's resilient modulus data, the results from Table 6.28 were plotted to reveal the variation of the resilient modulus versus the axial strain, which are presented in Figure 6.32. The two different symbols in this figure represent the moduli calculated from either the deformations obtained from the average of the three internal LVDT's (sampled over the middle four inches of the sample) or the deformation from the one external LVDT (sampled over the entire sample length of eight inches).

Table 6.28 Resilient Modulus Test Results for the US-441 (Osceola County) Base

Confining Stress (psi)	Deviator Stress (psi)	3 Internal LVDT's Strain (%)	3 Internal LVDT's M_R (psi)	1 External LVDT Strain (%)	1 External LVDT M_R (psi)
3	3.09	0.0085	36,287	0.0112	27,567
3	5.93	0.0191	31,092	0.0244	24,321
3	9.99	0.0294	30,396	0.0376	23,779
5	5.01	0.0115	43,592	0.0148	33,872
5	10.07	0.0251	40,149	0.0320	31,481
5	15.72	0.0383	41,036	0.0493	31,918
10	9.99	0.0165	60,402	0.0217	45,915
10	20.12	0.0318	63,317	0.0414	48,609
10	29.98	0.0501	59,861	0.0647	46,312
15	10.11	0.0126	80,162	0.0188	53,797
15	14.98	0.0195	76,807	0.0293	51,204
15	29.90	0.0392	76,220	0.0609	49,103
20	15.15	0.0153	99,025	0.0200	75,801
20	19.96	0.0206	96,722	0.0265	75,482
20	40.08	0.0429	93,429	0.0553	72,529

The results from Figure 6.32 show that higher values are generally obtained from base materials than from subgrade materials (refer to the typical subgrade results shown in

Figure 6.9). Since base materials consist of crushed rock, it is expected that they would be stiffer than a granular, sandy soil (i.e. typical subgrade material). As with the subgrade results, the internal readings revealed less deformation (and therefore, higher modulus) than the corresponding external readings. Both sets of data reveal that the modulus increases as the confining stress increases. Also, a series of curves can be developed for each of the individual deviator stresses. This series of curves reveal a trend of increasing stiffness with increasing confining stress and a slight decrease with increasing deviator stress, since the curves shift upward and to the right.

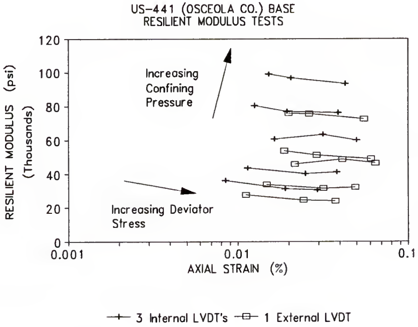

Figure 6.32 Resilient Modulus Test Results for the US-441 (Osceola Co.) Base

The same approach used for the test pit subgrade study to compare the SASW moduli with the resilient modulus results was used for this study. Each resilient modulus value was divided by the SASW modulus (the values presented in Table 6.26) in order to normalize the moduli so that the results from each location could be compared. Due to the many deviator stress levels used for a typical resilient modulus test on Type 1 materials, only the data from the deviator stresses of 3, 9, 10, 20, and 40 psi were analyzed. The data from the 9 and 10 psi stress levels were combined for this analysis. The results from this analysis are presented in Figure 6.33.

The results in Figure 6.33 reveal a series of curves which can be developed for the varying deviator stresses. Each symbol represents the test location by county, and shows the amount of scatter that occurs for an individual stress level. The results from the US-41 (Tamiami Trail, Dade County) sites were not used for this analysis because these resilient moduli were very low in comparison to the field plate moduli. This seemed to be due to the difference in the densities between the laboratory samples (128.7 lb/ft^3) and the in-situ nuclear gauge measurements (134.5 lb/ft^3). This could also be due to some natural cementation occurring in the limerock over a long period of time, making the material in the field much stiffer than a reconstituted sample. Some of the data presented in Figure 6.33 were obtained from plate load tests at applied stresses of 8.8, 17.7, and 35.4 psi (the data at the lower limits of each curve). There were not many plate load test results at such low stress levels, and these few results were included to determine how the two sets of moduli compared.

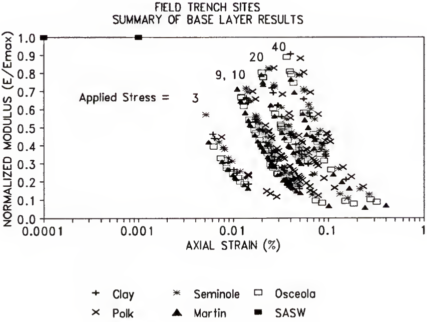

Figure 6.33 Variation of Normalized Modulus and Strain for the Base Layer Trench Sites

As indicated by the resilient modulus test results, the series of curves in Figure 6.33 reveal a trend upward and to the right for increasing mean effective stresses (which is equal to $\{\sigma_d + 3\sigma_c\}/3$ for a resilient modulus test, where σ_d is the deviator stress and σ_c is the confining pressure). This is consistent with the fact that granular base materials will become denser (more stiff) as the amount of confinement increases. It can be seen that at higher deviator stresses, the curves would intersect the point at which the normalized modulus was one (i.e. the elastic threshold) at a higher strain level. This is consistent with field studies which show that for stiff, thick layers the field and SASW moduli become more similar. This suggests that a stiffer material (i.e. crushed rock) can exhibit a larger elastic range than a corresponding softer material (i.e. sandy soil). Therefore, an elastic modulus can be obtained from these stiffer materials at higher deformations (higher strain levels). The moduli resulting from standard field methods are obtained at higher strain levels than the SASW test method, but since the elastic threshold of these stiff materials is higher, the two results are more similar.

A regression analysis using the form of a power curve equation (Eqns. 6.1 and 6.2) was performed on just the resilient modulus data presented in Figure 6.33. The following equation is the result of this analysis for the base layer materials:

$$\frac{E}{E_{\max}} = 0.00262\left(\frac{\sigma_d}{\epsilon_a}\right)^{0.830} \qquad (6.4)$$

where: E/E_{max} = normalized Young's modulus

σ_d = deviator, or applied, stress (in psi)

ϵ_a = axial strain (%).

Equation 6.4 was used to produce a series of curves for the resilient modulus data presented in Figure 6.33, and the results are shown in Figure 6.34. This figure contains only the data used to produce Eqn. 6.4 (the resilient modulus data), and includes no plate load test results. Figure 6.35 presents all the data with a series of curves derived from Eqn. 6.4 included on the plot. A comparison between Figures 6.34 and 6.35 will reveal the location of the plate test results and their relation to the resilient modulus results. The plate load test results can be seen to fall slightly below the derived curves. These curves were produced for deviator stresses of 9.5, 20, and 40 psi, and the plate load test results were obtained from applied loads of 8.8, 17.7, and 35.4 psi. Therefore, the plate load test data compares well with the resilient modulus data and the results from Eqn. 6.4. It can also be seen that the plate load test results fall within the higher strain levels (greater than 0.1%) compared to the laboratory resilient modulus test results (0.005% to 0.1%). This indicates the need for graphs like Figure 6.35 (and Equation 6.4) to show the relationship between modulus and strain. Any comparisons of moduli between different test methods need to be performed by taking the strain effect into account. Otherwise, the moduli would represent different conditions, and a comparison between them could prove meaningless.

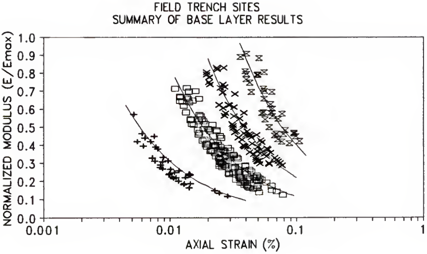

+ 3 psi □ 9, 10 psi × 20 psi ⌧ 40 psi

Figure 6.34 Variation of Normalized Modulus and Strain for the Base Layer Resilient Modulus

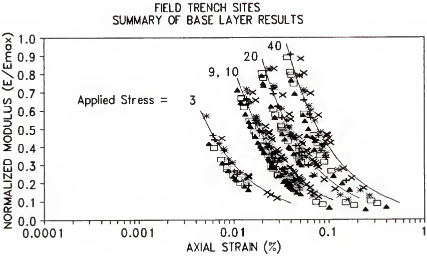

+ Clay * Seminole □ Osceola
× Polk ▲ Martin

Figure 6.35 Normalized Modulus-Strain Relationships for the Base Layer Trench Sites

The form of equation used in Eqn. 6.4 is not exactly the correct form of equation needed to model the S-shaped curve that is normally encountered for the modulus-strain relationship of soils (refer to Figures 2.11 or 2.13). Due to the limited amount of data in range of higher normalized modulus (0.5 to 1.0), any attempts at fitting an equation through this data would be very approximate. Since most of the laboratory and field data falls below a normalized modulus in the range of 0.5 to 0.6, a form of equation used for this analysis should prove adequate to model this data. Although, larger errors might be encountered at higher normalized modulus (greater than 0.5), since a true form of the equation was not used in this analysis. It is believed that this error should be within tolerable limits since the results in Figures 6.34 and 6.35 show that the derived curves fit the data within the whole range of measured strains rather well.

As with the plate modulus results, the variation in the actual design thickness resulting from a difference in the resilient modulus is needed to be known in order to evaluate the effectiveness of any comparison between SASW and resilient moduli. Based on equations relating resilient modulus to the structural layer coefficient for untreated base materials (Huang, 1993), a resilient modulus of 44,300 psi corresponds to a coefficient of 0.18 (the upper limit for Florida base materials). The range of scatter in the comparison plots is approximately 10,000 psi. Applying this range of error to the maximum modulus of 44,300 psi, the corresponding layer coefficient for a modulus of 34,300 psi is 0.15, resulting in a 20 percent error. This means if a 10 inch layer is designed for a layer coefficient of 0.18, a 12 inch layer is needed for a coefficient of 0.15. Based upon a standard price range of a limerock base material of $3.00 to $5.00 per ton, this difference in layer thickness for the base would account for an overall cost difference of approximately $2,000 to $3,300 per lane per mile of constructed roadway.

Subgrade/Embankment layer tests. A similar analysis used on the base layer test results was performed on the results from the tests conducted on the subgrade and embankment layers. The plate load test data and the resilient modulus results were correlated with the SASW moduli separately because very little data was obtained from the plate load tests at similar applied stresses as the resilient modulus tests. The inversion program had problems on the subgrade layer results and could not be used to eliminate the effect of the disturbance. Therefore, the maximum modulus of the subgrade layers was determined from the SASW dispersion curves using the simplified method to estimate the stiffness of the surface layer. Since the embankments consisted of natural soil deposits, this method could not be used to determine an accurate stiffness to represent the embankment soils. The inversion program worked well under these site conditions and was used to develop a stiffness profile for the embankment test sites. The modulus for the embankment was determined by using the shear wave velocities for the layers of the resulting stiffness profile at a depth of 0.5 to 1 foot below the test surface. This stiffness should reflect the existing conditions of the embankment materials, and eliminate most of the disturbance zone due to excavation.

Table 6.29 Stiffness Results of the Subgrade/Embankment Layer Tests from the Trench Sites

Test Site	SASW E_{max} (psi)	E_i @ int. (psi)	E_p @ 0.05" (psi)	E_r @ reb. (psi)
Clay Co. Subgrade	48,353	33,791 (35,481)	28,750 (30,188)	32,290
Clay Co. Embankment	43,958	25,780	19,657	21,246
Seminole Co. Subgrade	39,382	22,404 (22,404)	15,400 (15,400)	19,580
Seminole Co. Embankment	44,653	23,902	18,343	24,737
Osceola Co. Subgrade	50,560	27,309 (28,674)	21,472 (22,546)	26,302
Osceola Co. Embankment	36,875	16,685	13,397	16,843
Polk Co. Subgrade	56,579	35,176 (38,694)	29,798 (32,778)	36,511
Polk Co. Embankment	48,383	25,320	22,442	25,980
Martin Co. Subgrade	60,533	41,733 (50,080)	32,552 (39,062)	45,681
Martin Co. Embankment	33,924	16,996	10,392	18,146

The results from the field tests (SASW and plate load tests) for the subgrade and embankment layers are included in Table 6.29. The same three types of moduli used in the previous section were obtained from the stress-deflection curves. As with the base layer results, the SASW moduli in this table were averaged from the results of two test sites, but several of the SASW moduli were the result from a single test because of low velocities near the ground surface. These lower velocities near the ground surface were more common for the subgrade and embankment layers since these materials were less stiff and more easily disturbed. All of the plate load test results were within 10,000 psi between the two sites, and were averaged together. The only exception was the US-1 (Jupiter, Martin County) subgrade tests which showed a wide variation. In this case, the plate load test results were obtained from only site #3 (the same site as the SASW results).

The results in parenthesis in Table 6.29 represent the corrected moduli for the subgrade layer results. Since the stress zone of the plate reached into the embankment layer, the resulting plate moduli represented a stiffness of the two-layer system. The Burmister design curves were used to establish correction factors to convert the plate moduli to a layer stiffness. These correction factors ranged from 1.0 to 1.20. The moduli from the Seminole County sites did not need a correction because the stiffness of the subgrade and embankment layers were similar. In fact, the correction factors for the subgrade layers were less than the base layers because typically the stiffness of the subgrade and embankment layers were more similar than the stiffness of the base and subgrade layers. The embankment results did not need a correction since they consisted of existing soil deposits, which were assumed to extent below the zone of influence of the plate load test.

The subgrades and embankments for all of these sites consisted of similar materials, primarily soils classified as A-2-4 and A-3 materials (sands to silty sands). The results from the US-41 (Tamiami Trail, Dade County) have been omitted because these materials consisted of sandy limerock. The primary difference between the materials from the two layers was the density requirements needed during construction of the roadway. The design densities for the embankment layers utilize less compactive effort than the subgrade layers. This can be seen in the difference between the densities of the subgrade and embankment layers in Table 6.25, especially in the laboratory densities where the compactive energy is more controlled. These resulting higher densities would produce a stiffer soil which would generate higher wave velocities. This difference is evident in Figure 6.36, which presents the comparison of the SASW and initial tangent (E_i) moduli. Except for one subgrade result (Maitland Boulevard, Seminole County), the subgrade tests resulted in higher moduli than the embankment tests. A linear regression forcing the equation of the line through zero was performed on both the subgrade and embankment results separately. The results (the equation of the regression line and the correlation) of both analyses are presented in Figure 6.36. As with the base materials, the regression lines show that the SASW moduli increased as the plate moduli increased. The results from the subgrade materials increased more rapidly (steeper slope) than the embankment results. The subgrade results were more scattered than the embankment results, indicating a higher degree of possible error in the regression results (as reflected by the lower r^2 value). The plots comparing the secant modulus at a 0.5-inch deflection and the resilient modulus are presented as Figures B.25 and B.26 in Appendix B. These figures also include the results of the regression analyses. Each of these results indicate similar trends as Figure 6.36. A comparison of laboratory LBR versus SASW modulus is presented in Appendix B as Figure B.27. It displays a wide amount of scatter among the subgrade results, with limited practical use to correlate the two parameters. However, this figure does indicate a positive trend of increasing moduli with LBR.

A summary of the results obtained from the statistical analyses for each of modulus and LBR values is presented in Table 6.30. This table includes the slope of the regression line and the coefficient of correlation (r) of the subgrade and embankment results for each of the stiffness parameters analyzed. These results are displayed on the moduli comparison plots for the subgrade and embankment layers presented in Figures 6.36, and B.25 through B.27. Table 6.27 presents similar statistical results for the base layer tests for comparison.

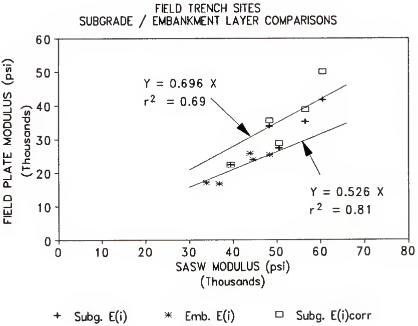

Figure 6.36 Comparison of E_i and SASW Subgrade/Embankment Moduli for the Trench Sites

An analysis to determine how a variation in the correlation between SASW and plate moduli can affect the actual design thickness of the subgrade layer was performed. Based on correlations between field plate modulus and structural layer coefficients (Van Til et al., 1972), the layer coefficient increases by approximately 0.02 for every increase in plate modulus of 5,000 psi for the typical range of Florida subgrade materials (15,000 to 30,000 psi). A difference in plate modulus of 5,000 psi corresponds to a range of SASW modulus of 10,000 to 15,000 psi. This amount of variation in the layer coefficient (0.02), based on a reference plate modulus of 25,000 psi, would result in an error of 16.7 percent. Therefore, if a 12 inch subgrade layer is used for a value of 25,000 psi, a modulus of 20,000 psi would result in an actual layer thickness of 14 inches (with all other conditions remaining the same).

Table 6.30 Linear Regression Results for the Subgrade/Embankment Moduli Comparisons from the Trench Sites

Stiffness	Subgrade		Embankment	
Parameter	Slope	Correlation	Slope	Correlation
E_p	0.469	0.85	0.412	0.86
Corr. E_p	0.558	0.81	0.412	0.86
E_i	0.558	0.81	0.526	0.90
Corr. E_i	0.696	0.83	0.526	0.90
E_r	0.638	0.84	0.516	0.91
LBR	0.00113	0.75	0.00052	0.93

The resilient modulus tests for both the subgrade and embankment samples were performed as Type 2 materials, with the exception of the US-41 (Tamiami Trail, Dade County) samples which were limerock and were performed as Type 1 materials. Because of this, the subgrade and embankment results from the Dade County sites were not used for the following analysis. The load sequence for Type 2 materials is shown in Table 6.7, which was the same loadings used for the test pit subgrade samples. The resilient modulus data was normalized by dividing each value by the corresponding SASW modulus (shown in Table 6.29). The data from each location was combined for the applied stresses of 2 and 8 psi. A regression analysis using the form of a power curve was performed on this data. The following equation is the result of this analysis for the subgrade layer materials:

$$\frac{E}{E_{max}} = 0.00345\left(\frac{\sigma_d}{\epsilon_a}\right)^{0.899} \qquad (6.5)$$

where: E/E_{max} = normalized Young's modulus

σ_d = deviator, or applied, stress (in psi)

ϵ_a = axial strain (%).

A series of curves was obtained from this equation at applied stresses of 2 and 8 psi. These results are presented in Figure 6.37. This figure contains only the resilient modulus data which was used in the regression analysis to obtain Eqn. 6.5. The plate load test data was not used in the regression analysis since few results were collected in the low stress range. The plate load test results that were obtained at stresses of 8.8, 17.7, and 35.4 psi are included, along with the resilient modulus data, in Figure 6.38. A series of curves using Eqn. 6.5 at 2, 8, 17.7, and 35.4 psi have been included in this figure as a comparison between laboratory and field results. Based on the results presented in Figure 6.38, Eqn. 6.5 can be used to model higher stress levels accurately. Even though there was a wide amount of scatter in the plate load test results, the generated curves fit within the middle of this data range.

As with the plate modulus, an analysis to determine how the variation between SASW and laboratory resilient modulus could effect the actual design thickness of the subgrade layer was performed. Based on equations relating resilient modulus to structural layer coefficients for granular subbase materials (Huang, 1993), the range of resilient moduli corresponding to the typical range of Florida field plate moduli for subgrades, 15,000 to 30,000 psi (representing a range of layer coefficients of 0.07 to 0.14), is 10,000 to 20,500 psi. If the mid-range is used as a reference value (15,000 psi) and a maximum range of error is 5,000 psi, the corresponding difference in the layer coefficient is 0.03. Based on the layer coefficient of the reference modulus (0.11), the resulting error due to this variation is 27.3 percent. This means if a 12 inch layer is designed for a layer coefficient of 0.11, a 15 inch layer is needed for a coefficient of 0.08. Based upon a standard price range of a stabilized subgrade material (typically a sand stabilized with limerock) of $2.00 to $3.00 per ton, this difference in layer thickness for the subgrade would account for an overall cost difference of

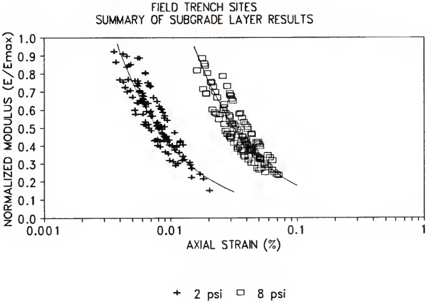

Figure 6.37 Variation of Normalized Modulus and Strain for the Subgrade Layer Resilient Modulus

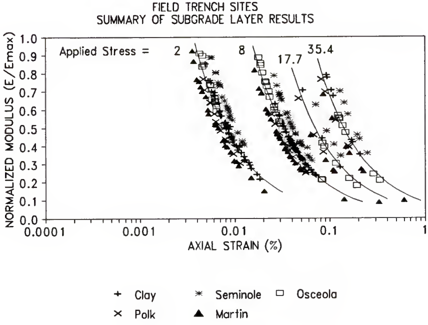

Figure 6.38 Normalized Modulus-Strain Relationships for the Subgrade Layer Trench Sites

approximately $1,800 to $2,700 per lane per mile of constructed roadway.

The same procedures used on the subgrade tests were performed on the embankment results. The following equation is the result of this analysis for the embankment layer materials:

$$\frac{E}{E_{max}} = 0.00370\left(\frac{\sigma_d}{\epsilon_a}\right)^{0.930} \qquad (6.6)$$

where: E/E_{max} = normalized Young's modulus

σ_d = deviator, or applied, stress (in psi)

ϵ_a = axial strain (%).

Figure 6.39 presents the resilient modulus data at applied stresses of 2 and 8 psi, which were used in the regression analysis to obtain Eqn. 6.6. The curves in Figure 6.39 represent the results obtained from Eqn. 6.6 for applied stresses of 2 and 8 psi. Figure 6.40 includes the field plate load tests results at applied stresses of 17.7 and 35.4 psi, along with the resilient modulus data. The curves in this figure were generated by use of Eqn. 6.6 for applied stresses of 2, 8, 17.7, and 35.4 psi. Based on these results, this equation can be used to model embankment soils at higher stress levels with a reasonable degree of accuracy.

Summary of stiffness results. The results from the two previous sections for the base, subgrade, and embankment tests

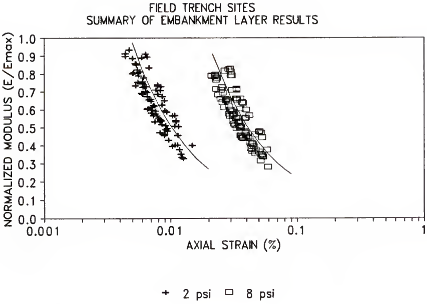

Figure 6.39 Variation of Normalized Modulus and Strain for the Embankment Layer Resilient Modulus

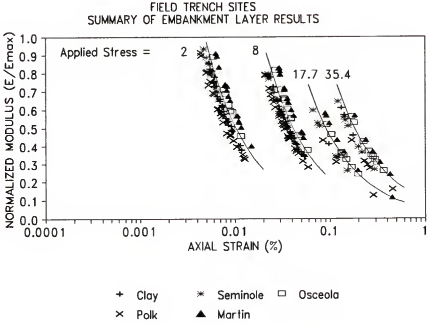

Figure 6.40 Normalized Modulus-Strain Relationships for the Embankment Layer Trench Sites

were combined to determine if a relationship between the SASW modulus and field plate modulus could be developed. Since three different moduli were evaluated (the initial tangent, secant at 0.5-inch deformation, and resilient moduli), each was compared with the corresponding SASW modulus. The plate modulus values which were uncorrected for any layering effects were compared to the SASW moduli. These results are presented in Appendix B as Figure B.28. Two regression lines are included in this figure. The top line is the regression for the initial tangent (E_i) and resilient (E_r) moduli, which produced the same regression. The bottom line is the regression for the secant modulus at a 0.5-inch deformation (E_p). These results reveal that a better match occurs by using the initial tangent or resilient modulus than the secant modulus.

The modulus values which were corrected for layering effects in order to reflect the stiffness of the individual layer tested were compared to the SASW moduli. The results using the values of E_i are presented in Figure 6.41. By correcting the modulus, the comparison between the two values improved. This was expected since the SASW results represent a surface layer stiffness, which also applies to the corrected plate moduli. Figure 6.41 reveals a good comparison between the corrected values of E_i for all three soil types over a wide range of results. It can be seen that the stiffness increased from the embankment to the subgrade to the base, with some overlap between the embankment and subgrade materials. A linear relationship provided an adequate means of relating the two parameters for at least an initial estimate. The same method was used to compare the corrected values of E_p and SASW moduli, and these results are presented in Appendix B as Figure B.29. This comparison was better than using the uncorrected values of E_p or E_i, but was not as good as using the corrected E_i values.

A comparison of the laboratory LBR and SASW modulus was performed using all the data from the base, subgrade, and embankment tests, as well as the results from the test pit subgrade study. The results are shown in Figure 6.42. The two lines in this figure were obtained from the linear regression analyses from the subgrade tests (top line) and the embankment tests (bottom line). The equations resulting from these two regressions are presented in Figure B.27 in Appendix B. Even with the large amount of scatter in the data, most of the data falls within the limits of one of these two regression lines. Since the same energy was used to compact the LBR samples in the laboratory (using the modified Proctor procedures), it is uncertain which one of these lines an individual material would follow. The LBR test is performed using a sample which has been soaked for two days and the value of LBR represents a high strain stiffness, making any correlations between an elastic modulus and the LBR very approximate. Since the two values of stiffness represent two different sets of conditions, any comparison using Figure 6.42 needs to be

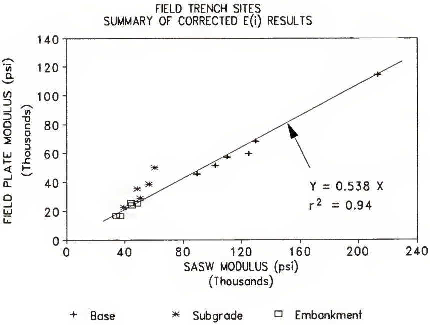

Figure 6.41 Comparison of Corrected E_i and SASW Moduli for the Trench Sites

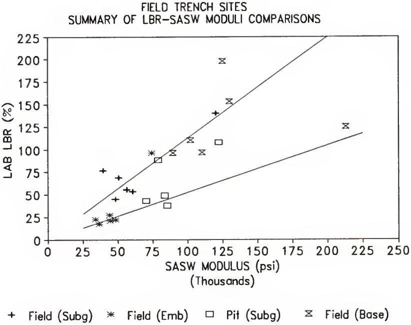

Figure 6.42 Comparison of LBR and SASW Moduli for the Trench Sites

approached as only an initial estimate with further testing required. The purpose of Figure 6.42 is to show that a general trend of increasing modulus with increasing LBR does exist for a wide variety of materials.

The normalized modulus-strain relationships developed for the field base, subgrade, and embankment test results as well as those from the test pit subgrade study were compared. Table 6.31 contains each of the relationships developed from these series of tests. Each of these equations was developed by performing a regression analysis using the form of a power curve, which is presented in Equations 6.1 and 6.2. This approach to express the field and laboratory data with a numerical relationship was only an approximation, since the actual form of the normalized modulus-strain relationship for soils is a S-shaped curve. For most practical applications, the results using the form of Equations 6.1 and 6.2 should prove adequate. Since the design traffic loadings and the data collected from most field tests occur at relatively high strain levels, the portion of the curve defined by the bottom half of the normalized modulus-strain relationship is primarily used. For the situations that the normalized modulus is in the range of 0.6 to 0.9, care must be taken using these results. In this range, the developed equations might not be representing the actual soil behavior accurately, resulting in a higher degree of error.

Table 6.31 Summary of Moduli-Strain Relationships

Materials Tested	Moduli-Strain Relationship
Test Pit Subgrades	$E/E_{max} = 0.00224(\sigma_d/\epsilon_a)^{0.90}$
Field Bases	$E/E_{max} = 0.00262(\sigma_d/\epsilon_a)^{0.83}$
Field Subgrades	$E/E_{max} = 0.00345(\sigma_d/\epsilon_a)^{0.90}$
Field Embankments	$E/E_{max} = 0.00370(\sigma_d/\epsilon_a)^{0.93}$

Based on the equations in Table 6.31, the values of the constants were similar. The value of c_1 ranged from 0.00224 to 0.00370, and the value of m ranged from 0.83 to 0.93. The two studies on the subgrades produced similar equations, with the same value of m. The value of m increased from the base to the subgrade materials, and from the subgrade to embankment materials. If the value of c_1 remains constant, an increasing value of m would shift the normalized modulus-strain curve to the right, which would represent a less stiff material (more strain for the same value of modulus). To compare the equations in Table 6.31, a series of curves was developed using each relationship at a reference deviator stress of 10 psi. The results of this analysis are presented in Figure 6.43.

The results from Figure 6.43 show that the field base tests provided the stiffest results, since it is the left-most curve. The field embankment results were the right-most curve, indicating these were the least stiff materials. The results from the two subgrade studies (field and test pit) were in the middle of the base and embankment results. These results were reasonable since base materials consist of crushed rock and should provide the stiffest layer of the roadway substructure. The subgrade materials should provide a stiffer material than the underlying embankment soils since subgrades are typically stabilized with materials to increase their stiffness, and they are compacted to a higher density.

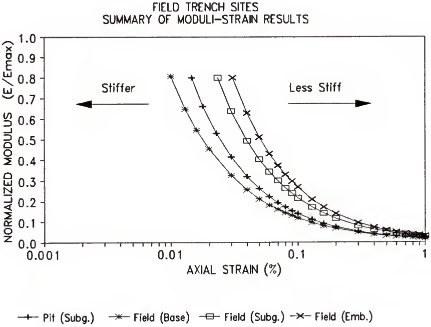

Figure 6.43 Comparison of Normalized Modulus-Strain Relationships for a 10 psi Deviator Stress

There seemed to be more variation between the two subgrade results in Figure 6.43 than would be anticipated. If there was a difference between the two curves, it was believed that the field curve should produce stiffer results than the test pit curve because of the existing traffic loadings making the field sites considerable more dense than a newly constructed section (i.e. the test pit). This was not the case, and it is believed that the field subgrade curve was shifted further right than it should be because of disturbance of the surface soils during the excavation process. This would cause the SASW test results to be lower than they should have been. Based on the information presented in Figure 6.41, three of the subgrade results fell above the regression line, indicating that the SASW moduli were low compared to the plate moduli. The plate modulus was less affected by any disturbances since the test procedures require three seating load cycles prior to the load cycle, which aid in compacting the site. To evaluate the effect of this disturbance, the normalized modulus-strain curves were reproduced using the SASW moduli from the regression line in Figure 6.41 rather than the actual field test results. The equation for the test pit subgrade study (Eqn. 6.3) compared well with these results, indicating that disturbance due to the excavation seemed to have influenced the field subgrade test results. Therefore, it is believed that the test pit subgrade curve is more representative of the typical soil responses of subgrade materials.

The problems of disturbance during excavation seemed to have only affected the subgrade results. Since the base materials consisted of crushed rock and were much stiffer, they could withstand more disturbance without significantly affecting their stiffness. To reveal the base layer, the asphalt pavement layer was cut by saw and stripped away in sections which involved much less disturbance than the underlying layers which involved a backhoe to remove the overlying soils. The embankment soils were disturbed as much as, if not more, than the subgrade soils, but inversion analyses were performed for these tests. Due to problems with the software, inversion analyses could not be performed for the subgrade tests because these test results produced a typical pavement profile (i.e. stiff over soft soils). The embankment tests produced typical soil site results (i.e. stiffness profile which increased with depth). Using the stiffness profiles obtained from the inversion analyses, the velocities of the surface layers were ignored and the layers below 0.5 to 1 foot were used to establish representative SASW moduli for the embankment soils. Therefore, using the inversion results the effects of any disturbance during excavation of the surface soils were eliminated, which seemed to have worked well based on the final results of this analysis.

6.4 Florida Institute of Technology Test Sites

This testing was performed on the campus of the Florida Institute of Technology (FIT) in Melbourne. Two sites were tested: an existing field at the Campus Ministries parking lot consisting of natural embankment sands and a constructed test strip consisting of a cemented coquina. As of this writing, only the results of the first site (the Campus Ministries site with the embankment sands) have been finalized. A layout of the test site at the Campus Ministries showing all the tests that were performed is shown in Figure 6.44.

6.4.1 Background Information

This testing was performed in conjunction with the research being performed by Dr. Paul Cosentino, professor at FIT, to measure low strain level resilient moduli with a modified pavement pressuremeter (PPMT). Typical pavement subgrade strains are on the order of magnitude of 10^{-4}, and for the PPMT to approximate this strain level, cycles (volume of water pumped into and out of the membrane) need to be conducted at volumes of 0.2 to 0.5 cm^3. The smallest volume increment that could be accurately controlled with the PPMT is 0.5 cm^3. Therefore, the initial research (Erbland, 1993) modified the PPMT L/D (length to diameter) ratio from 7.2 to 9.6 to allow smaller strains to be accurately measured and to ensure cylindrical expansion. With this modification, measurements can be made at strain levels as low as $3.6x10^{-4}$ (using a 0.2 cm^3 volume increment).

This research also proposed a modified method to perform pressuremeter tests to effectively measure resilient moduli in the field. After the pressuremeter has been inserted at the appropriate test depth (usually in a preformed borehole), it

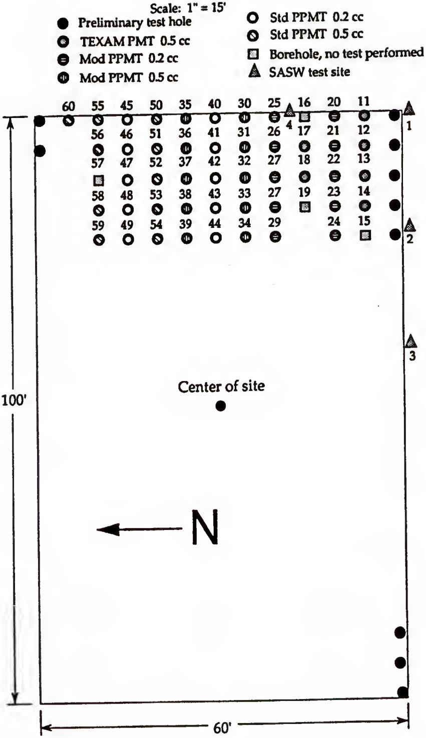

Figure 6.44 Plan View of the FIT Campus Ministries Site (Erbland, 1993)

is inflated in 5 cm^3 increments until the soil response indicates the test is in the elastic range, and then the load/unload cycles are performed. There are three 10 cycle stages which consist of removing and adding 0.5 cm^3 (or 0.2 cm^2) of water from the probe and recording the pressure after waiting 15 seconds. After the load/unload cycles have been performed, the pressuremeter test is continued (in 5 cm^3 increments) until the maximum volume of the probe is reached. This proposed resilient modulus PPMT test is shown graphically in Figure 6.45.

Conversion of volume changes into hoop strain (or relative radial increase, $\Delta R/R_o$), $\epsilon_{\theta\theta}$, is accomplished using the following equation:

$$\Delta R = \sqrt{\frac{V_o + V_{cor}}{\pi l}} - R_o \tag{6.7}$$

where: ΔR = increase in probe radius

V_o = initial probe volume

V_{cor} = corrected volume increase

l = inflatable length of probe

R_o = initial probe radius.

Young's moduli are determined from selected points on the plot of pressure versus percent strain. The program, PRESRED, used for the FIT research outputs moduli for each cycle, resilient (unload) moduli, and cyclic (reload) moduli as well as secant moduli.

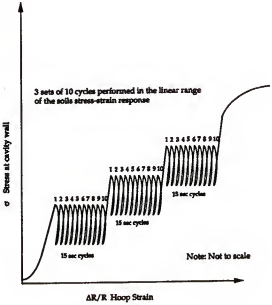

Figure 6.45 Proposed Resilient Modulus PPMT Test (Erbland, 1993)

The strain level (or relative radial increase, $\Delta R/R_0$) is determined from an associated volumetric strain ($\Delta V/V_0$) where ΔR is the increase in PPMT probe radius, ΔV is the change in volume of the probe, R_0 and V_0 are the initial PPMT probe radius and volume respectively. Therefore, the strain level is dependent on the volume of water used pumped into and out of the probe during resilient moduli testing, as well as the initial volume of the probe (i.e. $\Delta R/R_0 = \Delta V/V_0 = 0.2/258 = 3.6x10^{-4}$). The final determination of low strain level measurements seems to be the accuracy of the PPMT control unit to read small volume increments.

6.4.2 SASW Testing

A total of 15 SASW tests were performed at the Campus Ministries test site. Three spacings were used (2, 4, and 8 feet) during testing since the pressuremeter tests were performed near the ground surface (depths of 3 feet). Since the pressuremeter tests were performed on the east end of this site, only the four SASW performed near the southeast corner of the site were analyzed for moduli determination.

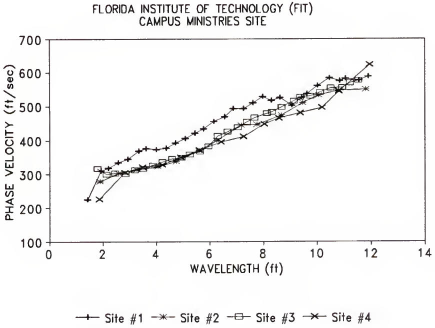

Figure 6.46 Dispersion Curves for the FIT Campus Ministries Site

The dispersion curves for the four test sites shown in Figure 6.44 are included as Figure 6.46. All four sites were very uniform, as indicated by the SASW results. The results of the inversion analyses from these four dispersion curves are presented in Table 6.32. The inversion was based upon assumed values of the Poisson's Ratio of 0.30 and a mass density of 3.20 lb/ft^3. The H-S in Table 6.32 represents the half-space used in the inversion analysis for the particular site.

From the moduli profile presented in Table 6.32, it can be seen that the test site consisted of two layers. The surface layer seemed to be approximately 2 feet thick with a Young's modulus of about 5,600 psi. The underlying layer consisted of soils with a Young's modulus of approximately 32,000 psi. This distinction could be the difference between fill and native soils. Based on the preliminary boreholes, a stratum change did occur within 2 feet of the surface and was the reason the pressuremeter tests were performed at a depth of 3 feet (so that testing was performed in a uniform soil stratum).

Using an E_{max} equal to 32,500 psi and assuming an elastic threshold at a strain level of 0.001% (1x10^{-5} cm/cm), the upper limits of the modulus versus strain level curve can be determined. Combining the results from the PPMT and SASW tests, the plot which is presented in Figure 6.47 can be developed. The higher strain levels were determined from

Table 6.32 SASW Results for the FIT Campus Ministries Site

Layer No.	Layer Thickness (ft)	Total Depth (ft)	Young's Modulus (psi)
Site No. 1			
1	1.0	1.0	6,670
2	1.0	2.0	7,500
3	1.0	3.0	30,760
4	2.0	5.0	32,500
H-S	H-S	H-S	36,940
Site No. 2			
1	2.0	2.0	5,200
2	1.0	3.0	30,760
3	1.0	4.0	32,500
H-S	H-S	H-S	36,300
Site No. 3			
1	2.0	2.0	5,550
2	1.0	3.0	26,740
3	1.0	4.0	32,500
H-S	H-S	H-S	37,000
Site No. 4			
1	0.5	0.5	2,080
2	0.5	1.0	7,080
3	1.0	2.0	5,200
4	1.0	3.0	33,400
H-S	H-S	H-S	36,940

three different pressuremeters (with three different initial volumes) and by altering the volume changes used during the cyclic loadings (0.2, 0.5, and 2.0 cm^3).

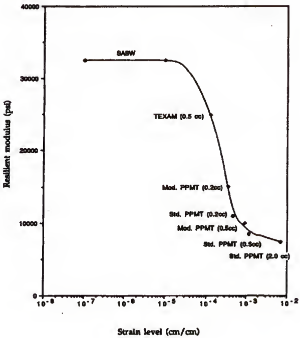

Figure 6.47 Variation of Moduli and Measured Strain with the PPMT (Erbland, 1993)

6.5 US-98 (Panama City) Test Site

This testing was performed along US-98 in Panama City. The SASW testing was initiated at the request of the District III Geotechnical Engineer because of a subsidence problem along US-98 which was believed to be the result of a leaking cross-drain. This leaking cross-drain was thought to have caused some of the soil to wash out from around the pipe directly underneath the roadway. The pipe was two feet in diameter and crossed under the roadway at a depth of approximately 10 feet. Over the years, this section of US-98 has experienced settlement problems, and FDOT Maintenance Office has been forced to repair the roadway by patching the area with asphalt. An emergency situation arose when a truck parked along the side of the road, and the paved section of the shoulder collapsed due to the weight of the truck. A means to evaluate the subsurface conditions of this site was needed to determine if the roadway had to be closed immediately. If a collapse in one of the travel lanes was possible, the road needed to be closed to ensure the safety of the public and allow repairs to be performed. These repairs would be time consuming, and since this incident occurred during the busy season for the beaches, it would be very costly for the businesses and inconvenient for the public. This section of US-98, known locally as Front Beach Road, is a two-lane highway which is located adjacent to motels and businesses directly on the beach. Therefore, it was hoped that the site conditions could be evaluated quickly, and determine if there was any immediate danger to the public. If not, the preferred option was to keep the roadway open to traffic during the summer season, and perform repairs during the off-season when there would be less traffic.

6.5.1 SASW Testing

This case study provided a practical application of the SASW test, and one in which no other test method could be utilized effectively. With the problem occurring underneath a paved section of the roadway, no penetration tests could be used without coring through the asphalt. This would involve closing one lane of the roadway and be very time consuming. This option was unfavorable because traffic at this time was very heavy. Since the cause of the problem was thought to have been generated ten feet underneath the pavement, this was too deep for other test methods such as the FWD, dynaflect, or GPR to be used.

At the time of this request, there was concern about the SASW test being able to provide sufficient results to make a decision, since it was known that problems with the inversion program would prevent a stiffness profile from being generated for pavement sites. Therefore, two methods of analyses were utilized to ensure that the SASW tests would provide meaningful results. The first was to perform SASW tests along the unpaved sites adjacent to the roadway (along the shoulder areas) directly over the pipe section and at a control site. The control site was located 100 feet away from the pipe section, and was a section of the highway in good condition. Since unpaved sections were tested, the inversion program could be used to produce stiffness profiles, and the profiles from the centerline of pipe and control sections could be compared. The second method of analysis was to perform a series of tests on the pavement surface over the centerline of the pipe, and at a control section. Even though the inversion program could not be used in these cases, the dispersion curves from the sites over the centerline of pipe and the control section could be compared. If the velocities near the surface were similar, then the differences between the dispersion curves for the longer wavelengths (greater sampling depths) would provide a relative difference in the stiffness of the underlying embankment soils between the two sites. Since the control site was a section of the roadway in good condition, comparing its results with the results of the tests over the pipe section provided a means to evaluate how much damage had occurred near the pipe. Based on the relative stiffness decrease at the cross-drain sites, an evaluation of what to do with the roadway was possible.

SASW testing was performed on July 7 and 8, 1993. A series of three sites were tested on the eastbound lane's pavement surface. Two of these sites were over the centerline of the cross-drain, with one being along the inside wheel path (approximately 3 feet from the edge of pavement) and the other being along the outside wheel path (approximately 9 inches from the edge of pavement). The third test was located approximately 100 feet east of the cross-drain, which was used as a control section of the highway. Another series of two SASW tests were performed adjacent to the edge of the westbound roadway, along a 3-foot paved apron. One site was over the cross-drain, and the second site was located approximately 100 feet east of the cross-drain. A third series of two SASW tests was performed adjacent to the westbound roadway and apron, along the unpaved shoulder area of the highway. The test over the cross-drain was located at the site where the collapsed occurred. This site was repaired by filling in the hole with sandy shell material. The second SASW test site was located approximately 100 feet west of the cross-drain. The shoulder of the highway consisted of many paved areas used for driveways and parking areas, but the SASW tests were performed at sites which were unpaved and had a sandy shell material at the surface. A plan view of this section of US-98, showing the locations of the SASW tests (indicated by an X), is presented in Figure 6.48.

The spacings used for the SASW tests on the pavement surface were 1, 4, 8, and 16 feet. Since longer wavelength data was more important (due to the cross-drain being located approximately 10 feet below the surface), longer spacings than are normally needed for pavement sites were used, and several of the shorter spacings were omitted. These field tests were performed in July, and the heat melted the wax used to attach the accelerometers to the pavement surface. As a result, this was the first test site which utilized the magnetic bases. Nails were hammered into the pavement at the appropriate spacings, and the accelerometers mounted onto the magnetic bases were attached to the head of the nails. This method proved to be successful for the roadway and apron pavement sites. For the shoulder sites, the test spacings were 2, 6, 12, and 20 feet. Longer spacings were utilized in order to capture longer wavelength data, which sampled deeper soil deposits. The 1 Hz geophones were placed directly on the ground surface at the appropriate spacings after the loose soil was brushed away and the site was leveled.

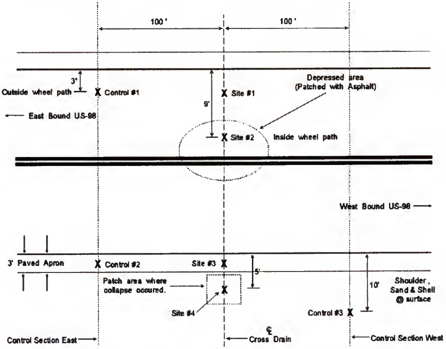

Figure 6.48 Plan View of the US-98 (Panama City) Site

6.5.2 SASW Results

The dispersion curves from the series of SASW tests on the eastbound lane's pavement surface were compared together.

Since the surface layers had similar velocities, the velocities at longer wavelengths on the dispersion curves were compared to evaluate the relative difference in stiffness of the underlying soils in the vicinity of the cross-drain. If the depth to the pipe was 10 feet, wavelengths at approximately 20 feet should represent the approximate location of the cross-drain on the dispersion curves (based on Eqn. 2.3, which provides the approximate depth below ground surface for the steady state R-wave test method). The three dispersion curves for the test sites shown in Figure 6.48 as sites #1 and #2, and control #1 are presented in Figure 6.49.

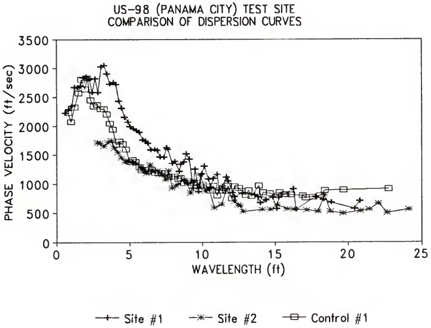

Figure 6.49 Dispersion Curves for the US-98 (Panama City) Pavement Test Sites

The results in Figure 6.49 reveal that the three sites had similar stiffness profiles. The control section represents a section of the roadway which was in good condition, with no signs of deterioration or undue distress. Therefore, the dispersion curve from the control section (labelled control #1) represents the desired stiffness profile for this section of the roadway. The two curves from the sites along the centerline of the cross-drain were similar to the control site. This indicates that there were no major differences at sites #1 or #2 which might result in a catastrophic failure (i.e. a void under the road).

The portion of the dispersion curves in the range of wavelengths from 15 to 25 feet show that the underlying embankment soils at the control site were slightly stiffer than the soils in the vicinity of the cross-drain. This could be the result of the leaking pipe washing out the soils from around this area, or it could be due to the soils around the pipe being saturated, or it could be due a difference in the soil types between the two test sections. Since there have been subsidence problems with the roadway over the cross-drain, it is believed that the soils around the pipe were being washed out slowly. Based upon the averaged values of the velocities from the dispersion curves in the range of wavelengths from 15 to 25 feet, there was a relative decrease in the surface wave velocities of 13% for site #1 (697 ft/sec) and 29% for site #2 (568 ft/sec) compared to the control site

(802 ft/sec). This would result in a relative decrease in the modulus of 24% for site #1 and 50% for site #2 compared to the control site. Therefore, this decrease in stiffness of the underlying embankment soils was noticeable and significant enough to affect the long-term condition of the roadway.

The series of SASW tests performed on the apron strip adjacent to the highway (the locations shown in Figure 6.48 as site #3 and control #2) could not be used to compare the stiffness profiles between the two sites. The dispersion curves from the two sites revealed a large difference between the velocities of the surface layers. Therefore, the dispersion curves could not be used to compare the stiffness of the underlying soils. The data from these sites was very erratic, especially at the longer wavelengths, and much of the data from the longer spacings could not be used. Without this long wavelength data, comparing the stiffness profiles would not be helpful because the larger sampling depths were needed to be compared at this site. This erratic data at the longer spacings was believed to be caused by reflected waves created by the interfaces between the roadway, apron, and shoulder. Since the apron was a narrow strip, the SASW tests could not be located in accordance with the guidelines established in Section 3.3.5 (Effects of Reflected Waves). If reflected waves influenced the results from the tests, previous research has shown that they would cause more disturbances in the low frequency (longer wavelength) range, which seems to have been the case in this particular situation.

Inversion analyses were performed on the series of SASW tests on the unpaved shoulder sites (the locations shown in Figure 6.48 as site #4 and control #3). Due to the need for a well defined stiffness profile, a large amount of thin layers (2.5 feet thick) were used during the inversion analyses. The inversion process was time-consuming in this case because a very good match between the field and theoretical dispersion curves was desired to ensure the accuracy of the final profiles. The results of these analyses are presented in Figure 6.50.

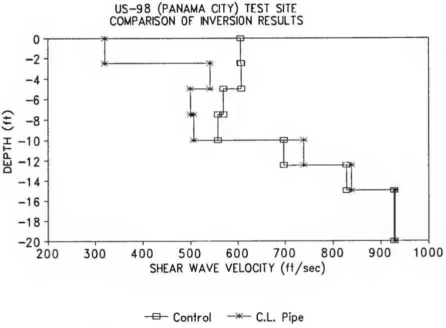

Figure 6.50 Comparison of the S-Wave Velocity Profiles from the US-98 (Panama City) Shoulder Test Sites

The results in Figure 6.50 show that the control site was stiffer within the top 10 feet of the surface than the site over the centerline of the cross-drain. The lower stiffness at the top 2.5 feet of the surface for site #4 was caused by filling in the collapsed area with loose material. In the range of depths from 2.5 to 10 feet, the shear wave velocities of the site over the cross-drain averaged about 100 ft/sec lower than the corresponding control site. These lower velocities could be due to many factors, but the overall lower stiffness profile does seem to be the cause of the subsidence of the roadway over the pipe. The stiffness profiles from the inversion analyses indicate that the subsidence of the roadway is a gradual process caused by a reduction of soil support of the underlying soils rather than a void forming under the roadway. If a void was developing under the test site, the inversion analysis at the site over the cross-drain would have produced much lower velocities. Below depths of 10 feet, the two curves in Figure 6.50 were nearly identical, indicating that the stiffness profiles below the pipe and the control section were the same. The layer in the range of depths from 10 to 12.5 feet revealed that the velocity at the site over the cross-drain was slightly higher (739 ft/sec) than at the control site (696 ft/sec). This increase in stiffness at these depths might be due to the 2-foot cast iron cross-drain at site #4, which was located at this range of depths. It is uncertain whether the inversion analysis is sensitive enough to detect a small object this deep below the surface in every case, especially if a quick inversion analysis is performed. Without knowing where the pipe was located for this study, this difference in velocities would have been attributed to a difference in soil types between the two sites.

After all the field testing and data reduction was completed, the decision was made to delay any repairs on the road which would close the highway to the public until a later date. Based on the SASW results, there did not seem to be any immediate threat to the public, but the results indicated that the subsidence of the roadway would continue because of the lower stiffness values of the embankment soils in the vicinity of the cross-drain. It was decided that if the road continued to settle during this period, the FDOT Maintenance Office would continue to patch the depressed area of the roadway with asphalt. This decision was made also because the traffic using this portion of US-98 consisted of primarily cars and light trucks. The heavier trucks used Alternate US-98 (Back Beach Road). Therefore, the lighter traffic loadings on this road would produce low stresses on the underlying soils, which would cause a lower amount of settlement in the roadway than if higher loadings were present on the surface. At the present date, no problems are known to have occurred with this section of US-98. No major repairs have been initiated to this roadway to alleviate this problem permanently.

CHAPTER 7
SUMMARY, CONCLUSIONS, AND RECOMMENDATIONS

7.1 Summary

The primary goal of this research was the development of SASW technology for geotechnical and pavement applications. The capacity to perform SASW tests on both soil and pavement sites was desired to enhance the versatility of the equipment since the State Materials Office is active in both areas of testing. Along with the purchase of the equipment and software, training was needed to perform all the steps required of a standard SASW test, including basic theory, field procedures, data reduction, and software analysis. An outside consultant, Dr. Glenn Rix from the Georgia Institute of Technology, was hired by the FDOT to provide the services to assist in this effort. His recommendations were used to purchase specific equipment, and he provided the required software and training in the use of the equipment and software.

Once the equipment and software were acquired, the next step was to gain experience in performing actual SASW field tests for various applications and under different field conditions. At the same time, knowledge of basic seismic theory needed to be expanded to understand the principles of the SASW test method. Both of these goals were accomplished. The actual SASW field procedures are quite simple and could be performed by a field technician who is comfortable with electronic equipment and computers (due to the particular signal analyzer used for this research). This analyzer was chosen because of its versatility, and can be used for other applications. The SASW field test uses a small capacity of the total functions of this signal analyzer. Because of this wide range of features, it is a complex piece of equipment and some time is needed to feel comfortable in using it. The functions on the signal analyzer are menu-driven, which allows the operator to use the analyzer with a minimal amount of memorization. As with any test method, some experience is needed so that the operator knows which changes to the signal analyzer settings are needed to obtain the optimum test results. The same person operating the signal analyzer in the field should be able to use the DISP program, which creates the field composite dispersion curve. In fact, it would be best to create the dispersion curve in the field with a portable computer so that the operator can preview the quality of the data and determine if retesting was necessary. The inversion analysis needs to be performed by an individual who has a concept of some basic seismic theory, since a theoretical dispersion curve is developed from a given profile. The user will need to know how to alter this profile to change the theoretical dispersion curve in order to match it with the field dispersion curve. The user also needs to know if the results from the inversion analysis are reasonable.

After the initial goals were accomplished, the primary goal of this research was addressed, which was to use this test on various FDOT applications (on both geotechnical and pavement sites). The SASW results could then be evaluated to determine if it is a practical test method which can be utilized in further FDOT applications, and if its use could be expanded in any one of the applications covered by this research. This test method was evaluated whether it was a viable production-oriented field test method or whether it was a research tool.

7.2 Conclusions

The conclusions from this research are outlined in the following two sections with the results from the geotechnical and pavement sites referenced in separate sections.

7.2.1 Geotechnical Applications

Based on the results of the testing performed on the geotechnical applications, the following conclusions can be made:

(1) This research expanded on previous work to prove that the SASW test is effective in monitoring the improvement of subsurface soils (contained in a construction debris landfill site) by dynamic compaction. By comparing the before-compac-

tion and after-compaction stiffness profiles, the percent improvement and depth of improvement was obtained. By using empirical relationships, a relative degree of density could be evaluated.

(2) For ground modification projects (but not restricted to dynamic compaction projects) at sites where penetration testing is not possible, the SASW test is an attractive alternative to the typical acceptance method (i.e. conical test loads). The SASW test can be performed the same day that the dynamic compaction is completed, which could save approximately two weeks of the overall project time. This case study was the first time that SASW test results and CTL data were obtained from a dynamic compaction site.

(3) The site using the 20-ton dynamic compaction weight as a source proved that results can be obtained in sampling very deep soil deposits. This application has some use to the FDOT in the area of deep foundations, but can never be production-oriented compared to penetration testing due to the need of dropping such a massive weight.

(4) The SASW test proved to be a field test which can be performed under very difficult situations and at sites which had limited access. The tests at the Polk County Parkway revealed that equipment could be carried to the site, and testing could be performed with water at the ground surface. However, SASW testing would not be possible at sites with standing water above 1 or 2 inches, and this test method is

limited by the size of the source which can be carried to the test site.

(5) The simplified method to determine the surface layer thickness and stiffness for pavement layers worked well for some specific soil sites. For instance, the dispersion curves from the SASW tests at the proposed Polk County Parkway proved that the phosphatic clays near the surface could be delineated from the underlying layer. This could be useful since the SASW test samples a larger volume of soil than a penetration test. Therefore, an area could be mapped out by the use of SASW test and a program of penetration testing and sampling could be planned that will concentrate on the critical areas (ones showing the deepest deposits of low stiffness soils).

(6) The Polk County Parkway case study was the first time that SASW and DMT results were compared, and the first known application of SASW tests on such a soft surficial soil (as the phosphatic clay). Based on these results, the comparison between the SASW and DMT elastic shear moduli was very poor for clays. The DMT shear moduli was 2 to 4 times higher than the SASW moduli. A comparison of Young's modulus and constrained modulus proved to be just as poor.

(7) As with the softer soils near the surface, the SASW test proved to be effective in mapping out areas of stiff underlying layers relatively near the surface. This can be useful to delineate areas which have competent limerock near the surface. The effectiveness of this application is based

on the size of source used during testing, which will determine the survey's effective sampling depth. This is the first known effort to map out the top of a natural limerock formation using the SASW test method.

(8) The comparisons between several relationships (Imai & Tonouchi, Jamiolkowski, Olsen, and Mayne & Rix) to estimate the elastic shear and Young's modulus from CPT data and the SASW modulus yielded similar results (typically within 20 percent agreement) for depths of soils less than 0.5D (where D is the maximum receiver spacing used during the SASW field test). For deeper soil deposits, the comparisons were typically less favorable because the SASW stiffness profile was not as well-defined due to the limited maximum spacing. These results expand on previous studies by increasing the database of sampled soils, and the first comprehensive study of Florida soils.

(9) Based on conversations with Dr. Glenn Rix, it was uncertain how effective the SASW test would be at detecting cavities. The results of this research proved that the SASW test was successful at detecting a known void under a given test site. However, the void appeared as a low velocity layer in the stiffness profile. Therefore, it's unknown whether this layer was a void or a low velocity soil without the use of a penetration test. The success of the SASW test at detecting a void will be dependent on the size of the void,

the depth to the void, and the size of the spacings used during the SASW field test.

(10) The Kanapaha case study proved to be the first time that SASW and DCP results were compared. Based on these findings, the comparisons between the DCP and the SASW elastic Young's modulus revealed that the SASW results were consistently 1.2 to 3.0 times higher than the corresponding DCP values. A relationship between the SASW Young's modulus and the CBR from the DCP test was developed, which revealed a typical range of shear wave velocities for limerock at this test site between 750 to 850 ft/sec. This range of results seem reasonable based on previous work, but is the first instance that seismic velocities from SASW testing have been obtained for Florida limerock.

(11) The SASW test produced similar results at the same site over a long period of time. Based on a comparison of these results, a maximum relative difference of 10 to 15 percent can be expected from the SASW test results, which verified similar results from previous research.

(12) Comparisons between the CPT elastic shear modulus results derived for clays and the SASW moduli revealed that the values obtained from the Mayne and Rix relationship (developed from seismic CPT data) agreed better with the SASW moduli than the relationships derived strictly from standard CPT correlations. These results expand on previous work by

increasing the number of soil sites tested using this equation, and including Florida soils in the overall database.

(13) Comparisons between the SASW and ground penetrating radar (GPR) test methods were not possible because anomalies detected by the GPR at the Live Oak site proved to be the result of soil disturbances caused by the demolition of a basement at the test site, and not from any sinkhole activity.

(14) Based on the findings of this research, the primary limitation of the SASW test for soil sites is a source to provide adequate seismic waves for large spacings (greater than 80 feet). A source for these larger spacings is difficult to use and cumbersome to transport. For practical considerations, without special equipment (for instance, a bulldozer) and using a readily available source (for instance, a drop weight), the maximum spacing is currently limited to 40 to 80 feet. This corresponds to approximate sampling depths of 20 to 40 feet. Therefore, if deeper soil deposits need to be ascertained than additional testing needs to be performed (either with SPT, CPT, or some other penetration test method). This is a common limitation identified by others using this test method.

7.2.2 Pavement Applications

Based on the results of the testing performed on the pavement applications, the following conclusions can be made:

(1) The inversion software used for this research (developed by Dr. Glenn Rix) did not work properly on the majority of results from typical pavement sites (i.e. stiff over soft profile). Inversion software developed by other researchers, specifically written for pavement analyses, have proved to be effective at obtaining stiffness profiles for pavement sites. As a result, the simplified method (outlined in Chapter 3, Section 3.3.4) to determine the stiffness and thickness of the surface layer for a uniform material was used to analyze the results from the majority of the pavement sites. This method worked well in most cases, but was limited to producing results for only the surface layer. The results from this analysis were dependent upon how closely the surface layer was to a uniform and homogeneous material. Since the materials used for the roadway substructure are constructed with required material and density specifications, this assumption did not seem to be unreasonable.

(2) The SASW test was successful in showing the difference in the stiffness of various materials used in the test pit due to varying moisture conditions (at optimum, drained, and soaked moistures). As with the corresponding plate modulus, the SASW modulus increased as the moisture content of the in-place materials decreased. This research was the first case study in which the moisture content of the tested soils could be controlled completely (due to testing in the FDOT's test pit).

(3) This research was the first time that plate load, resilient modulus, and SASW tests were performed in conjunction with each other for an extensive number of test sites. Based on these results, the SASW modulus compared well to the plate modulus, for both the test pit and field plate tests, as well as the laboratory resilient modulus results. The SASW modulus provided an elastic stiffness of the material which could be used as a maximum value. The results from both the static and dynamic plate load tests from the test pit studies compared well with the SASW modulus.

(4) To compare the moduli from the various test methods utilized for this research, each modulus was related to the strain level and the applied stress at which it was determined. The plate, SASW, and resilient moduli were combined to show the variation of the Young's modulus and axial strain for a group of materials. Using this approach, these relationships were developed for the base, subgrade, and embankment materials from the field trench sites and for the subgrade materials from the test pit study. This was the first time this approach was utilized for Florida materials, and provided design curves which apply specifically to a wide range of Florida materials.

(5) Individual relationships were developed to compare the SASW modulus with the field plate load test modulus and the laboratory LBR. Based on these results, the best comparison occurred when the initial tangent modulus from a field

plate load test, which was corrected for layering effects, was used. A single relationship to compare field plate and SASW moduli was applicable to the base, subgrade, or embankment materials. This study provided new results specifically related to Florida materials.

(6) The SASW test results were successful in measuring the surface layer thickness to within one inch of the actual layer thickness in most cases, with a maximum percent error of 10 percent. These results were typical of similar efforts by other researchers, but this was the first such study for Florida systems. The SASW results will be dependent upon the difference between the stiffness of the surface layer and the underlying layer. If this difference is great, the thickness measurements will be more accurate.

(7) The thickness and stiffness of the pavement layers of the field sites could not be detected if the actual pavement thickness was less than 4 inches. The source used for these tests was a wrench impacting the pavement surface, which proved to be insufficient to generate high frequency waves to adequately define the pavement layer. Similar results were obtained by previous studies, which generally recommended the use of a high frequency generator as a source to sample the top inch or two of the pavement layer.

(8) The SASW test results were successfully incorporated with modulus results from a pavement pressuremeter test (PPMT) to develop a relationship of modulus versus strain directly in

the field. This case study was the first application to combine the PPMT and SASW test results. This has the advantage of developing the modulus-strain curve at the conditions which exist in the field. The only other method to develop this curve is to incorporate the results from laboratory tests which have the disadvantage of needing to recreate the field conditions.

(9) Even without the use of the inversion procedure, the SASW test has proved to be successful at evaluating the stiffness profile for a roadway. This was accomplished by comparing dispersion curves from two sites, one at the site of interest and the second at a control site (one in good condition). The relative difference in stiffness can be determined from the dispersion curves. This approach has been used in previous studies, but this case study applied this technique to a new application that sampled deeper embankment soils (approximately 10 feet below the pavement surface). This method is only a quick, simplified approach, and is limited because it needs to be performed on two sites which have similar surface velocities. Based on the results of this study, the simplified analysis works well for a two-layer system. It should not be used for an in-depth analysis of a complete roadway cross-section, and does not fully utilize the potential of the SASW test results.

(10) Several limitations of the SASW test for pavement sites have been noted during the course of this research. The

primary limitation is the inversion software to develop a stiffness profile for the pavement system. Other inversion programs which were developed for pavement testing have been shown to perform properly at pavement sites. In addition, a special high frequency source is needed to sample the top 4 inches of the pavement layer. Without this capability, the only other nondestructive test method capable of detecting a relatively thin pavement layer would be the ground penetrating radar (GPR). Finally, testing performed on severely cracked pavements or near joints on concrete pavements probably will not produce reliable data because of the contamination of the signal due to reflected waves. Layers consisting of severely cracked pavements or bases consisting of large aggregates might also violate the profile used for the inversion analysis (uniform, homogeneous, isotropic layers), and therefore, the inversion results would be suspect. Nondestructive testing on cracked pavements presents a problem with any test method currently available, and no existing test can accurately develop a stiffness profile at these sites.

7.3 Recommendations

The primary goal was to evaluate the SASW technology for both geotechnical and pavement applications. Based on the findings of this research, the SASW test method is a very versatile test with a wide assortment of applications well suited to the transportation field. Therefore, it is recommended that SASW testing continue at the FDOT State Materials Office in order to support the conclusions of this research, to improve the testing procedures, to use the equipment for new applications, and to train other personnel on the use of the equipment and proper testing procedures. In addition, it is recommended that additional studies be performed to expand on the work initiated by this research. For instance, SASW testing is being performed regularly by the State Materials Office on several equivalency studies (evaluating new materials for use on state projects), which would involve FDOT personnel performing these tests. The following studies are also recommended:

(1) A comparison study of the SASW, GPR, and electrical resistivity test methods will be performed at a site (possibly the Kanapaha site) to evaluate the results of each method, and how effective these results are at assessing the site's subsurface conditions, including the top of limerock and the existence of any voids.

(2) SASW, plate, and resilient modulus test results are needed on additional roadway materials (base, subgrade, and embankment soils), especially typical base materials utilized in the test pit, to confirm that the developed relationships of normalized modulus versus strain are adequate to define typical materials in use by this state. If not, additional relationships need to be developed and transitions between groups (or classifications) of materials need to be addressed.

(3) The comparisons between the SASW and the PPMT were only performed at a site consisting of natural soil deposits, which would be representative materials used as embankment sands. The PPMT results from a site consisting of a base material (cemented coquina) were not completed at the present time. Once the pressuremeter results are obtained, the SASW and PPMT results will be combined to determine if a modulus-strain relationship can be developed for this base material. If so, additional studies need to be performed to determine if this type of testing can be used on an existing roadway to develop the modulus-strain relationships of the base, subgrade, and embankment layers directly in the field.

(4) A field testing program will be initiated to perform integrity testing of drilled shafts. Even though this testing involves compression waves rather than surface waves, the SASW equipment can be used to perform non-destructive integrity testing which can assess the depth, diameter, existence of defects, and low-strain stiffness of deep foundations.

(5) A study will be performed to develop a procedure which incorporates the modulus versus strain relationships into the pavement design process. It is believed that these relationships can be used to define a modulus profile for each pavement sublayer which takes into account the varying stress (and strain) levels encountered by the roadway substructure. This method would be more accurate than assigning a single

modulus to each layer, and result in a more economic design of the roadway.

(6) Testing will be performed to relate the falling weight deflectometer (FWD) and Dynaflect results with the SASW modulus. Since the FWD and Dynaflect are the primary methods used to determine soil support values (SSV) used for pavement design, the SASW results need to be compared to these standard tests if it is to be used in the pavement design process at the present time. The reason why this analysis was not performed for this research was because the inversion process could not be performed on the pavement sites in order to develop a modulus profile. Also, the standard FDOT method to obtain the SSV from the FWD and Dynaflect tests is to analyze the deflection data from these test methods. The modulus profile at a test site is typically not developed, and would have to be developed if these results are to be compared to the SASW results.

(7) A study will be initiated to develop specifications for deep dynamic compaction projects to incorporate the SASW test results for a field quality control and acceptance method. This will be accomplished by using the data collected by the SASW and CTL tests from the Veteran's Expressway site, and developing a rational method based on an elastic settlement analysis to predict the anticipated stiffness increase needed for adequate compaction of the subsurface soils.

(8) A research project will be performed in conjunction with the State Materials Office that will investigate the implementation of the Seismic Pavement Analyzer (SPA) which was described in Chapter 3, Section 3.3.2.1 for applications by the FDOT. The SPA is a trailer unit (similar to the FWD and Dynaflect) which utilizes the SASW technology. The inversion software used for the SPA will be used to process previously obtained SASW dispersion data. The data obtained from the tests performed on the pavement surface (at the field trench sites) will be reanalyzed. The effectiveness of the SASW test method to develop an accurate stiffness profile from the pavement surface will be studied by comparing the SASW results at the pavement surface to those from the individual layers (base, subgrade, and embankment).

(9) Since the existing inversion software obtained by Dr. Glenn Rix did not work on the pavement sites, additional studies will be performed to utilize different inversion software that is available to process the SASW field data. As stated in Chapter 3, Section 3.2.2 there are many efforts underway in order to develop improvements in this process. This work is focusing on modeling the actual field conditions more effectively and to make this process less operator dependent. Automated operations will make this process more efficient. With more powerful computers, more complex (and therefore, more realistic) algorithms can be used to improve the accuracy of this process, such as modeling 3-D solutions

or using neural networks. Little of the actual SASW field procedures has changed over the past 10 to 15 years. The primary changes are in the form of the software used to analyze the field data. This software is also what makes this test method so powerful, compared to conventional seismic test methods.

(10) Studies will be implemented to improve on the sources for both pavement and soil sites. A high frequency source is needed for pavement sites, and a source discussed in Chapter 3, Section 3.1.3 (such as a V-meter or piezoelectric shaker) will be purchased in order to sample the pavement layer more completely. For soil sites, a source is needed to deliver a large amount of energy into the ground, but be compact enough to be transported around the state and operated by a two man crew.

(11) In further field studies, the geology of the site needs to be considered to evaluate the test results, as well as being used to plan and design the overall field testing program. A typical source to obtain a general idea of the geology for the state of Florida is available from Brooks (1981).

APPENDIX A
GEOTECHNICAL APPLICATIONS' DATA

A.1 Introduction

This appendix includes additional field data for all of the geotechnical applications listed in Chapter 5. It is organized by the same sections numbers and titles that are used in Chapter 5.

A.2 Dynamic Compaction Site

The following figures (A.1 through A.15) are all the SASW field data not included in Chapter 5. Figures A.1 through A.10 are the plots containing the SASW dispersion curves and shear wave velocity profiles from the initial (before dynamic compaction) and final (after dynamic compaction) tests. Figures A.11 through A.15 are the plots showing the comparisons of the field shear wave velocity profiles with those derived from empirical relationships.

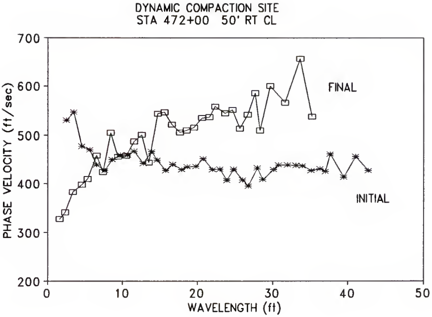

Figure A.1 Dispersion Curves from the Dynamic Compaction Site (Sta 472+00, 50' Rt)

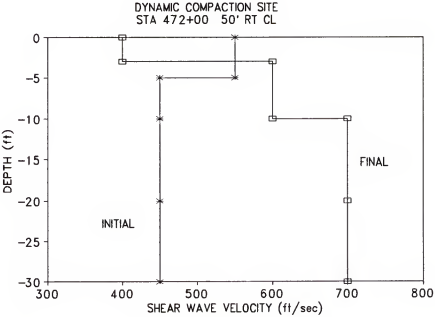

Figure A.2 S-Wave Velocity Profiles from the Dynamic Compaction Site (Sta 472+00, 50' Rt)

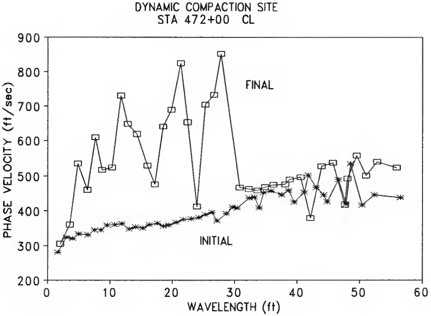

Figure A.3 Dispersion Curves from the Dynamic Compaction Site (Sta 472+00, C.L.)

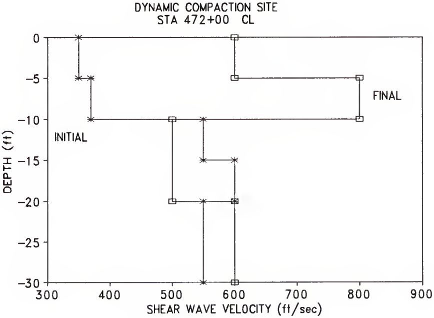

Figure A.4 S-Wave Velocity Profiles from the Dynamic Compaction Site (Sta 472+00, C.L.)

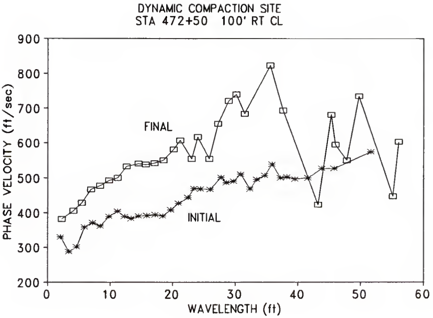

Figure A.5 Dispersion Curves from the Dynamic Compaction Site (Sta 472+50, 100′ Rt)

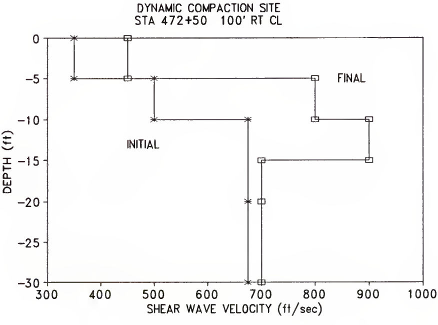

Figure A.6 S-Wave Velocity Profiles from the Dynamic Compaction Site (Sta 472+50, 100′ Rt)

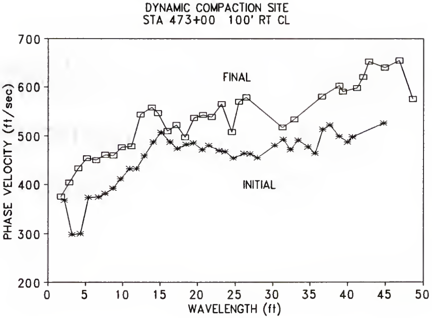

Figure A.7 Dispersion Curves from the Dynamic Compaction Site (Sta 473+00, 100′ Rt)

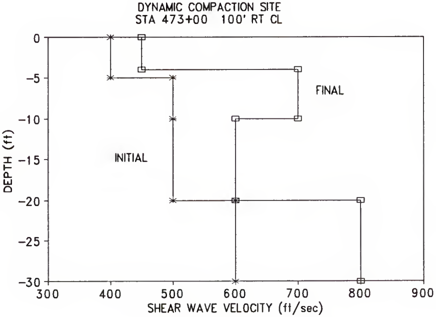

Figure A.8 S-Wave Velocity Profiles from the Dynamic Compaction Site (Sta 473+00, 100′ Rt)

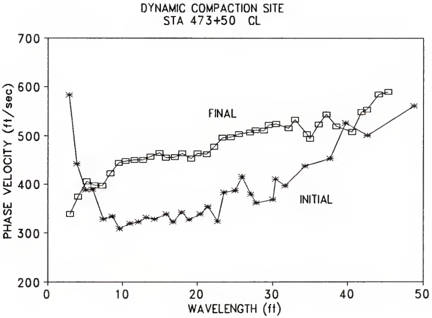

Figure A.9 Dispersion Curves from the Dynamic Compaction Site (Sta 473+50, C.L.)

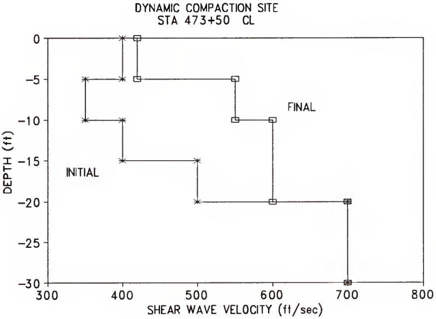

Figure A.10 S-Wave Velocity Profiles from the Dynamic Compaction Site (Sta 473+50, C.L.)

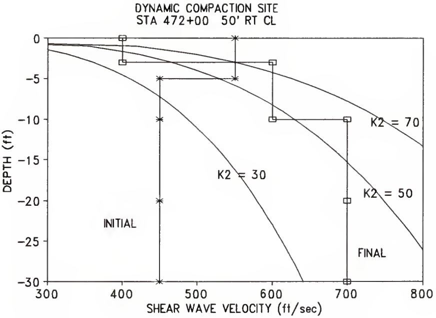

Figure A.11 Comparison of S-Wave Velocity Profiles from the Dynamic Compaction Site (Sta 472+00, 50′ Rt)

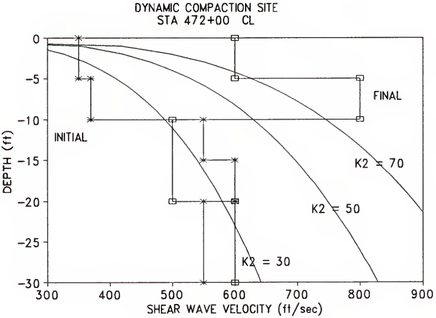

Figure A.12 Comparison of S-Wave Velocity Profiles from the Dynamic Compaction Site (Sta 472+00, C.L.)

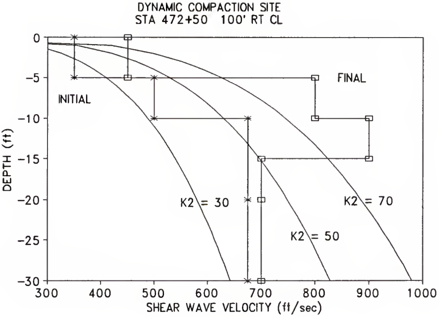

Figure A.13 Comparison of S-Wave Velocity Profiles from the Dynamic Compaction Site (Sta 472+50, 100' Rt)

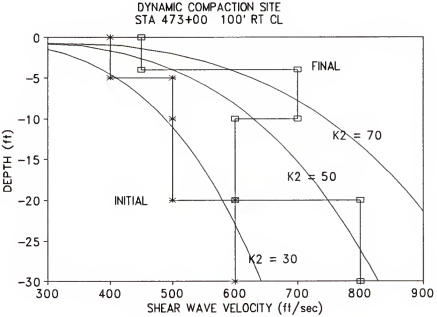

Figure A.14 Comparison of S-Wave Velocity Profiles from the Dynamic Compaction Site (Sta 473+00, 100' Rt)

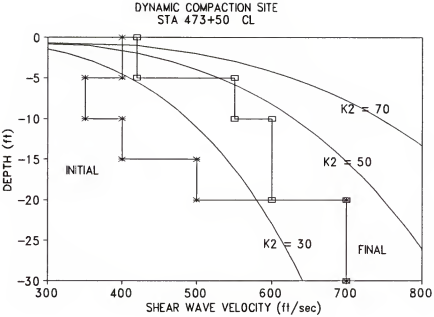

Figure A.15 Comparison of S-Wave Velocity Profiles from the Dynamic Compaction Site (Sta 473+50, C.L.)

A.3 Polk County Parkway

The following figures (A.16 through A.25) are all the SASW field data not included in Chapter 5. Figures A.16 through A.19 are the plots containing the SASW dispersion curves. Figures A.20 through A.25 are the plots showing the comparisons of the SASW shear wave velocity profiles with those derived from empirical relationships using the dilatometer (DMT) field data.

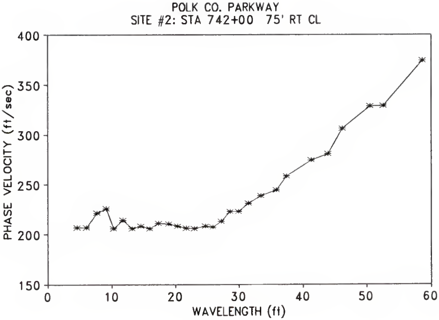

Figure A.16 Dispersion Curve from the Polk Co. Parkway (Sta 742+00, 75′ Rt)

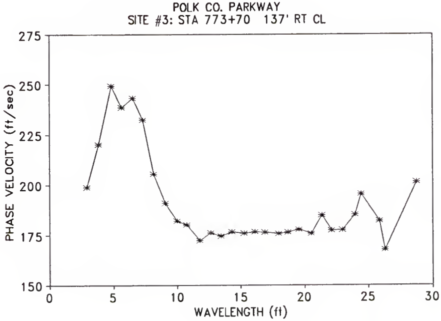

Figure A.17 Dispersion Curve from the Polk Co. Parkway (Sta 773+70, 137′ Rt)

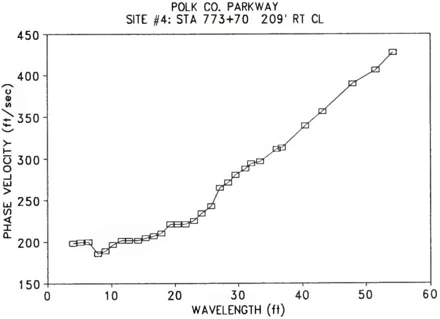

Figure A.18 Dispersion Curve from the Polk Co. Parkway (Station 773+70, 209' Rt)

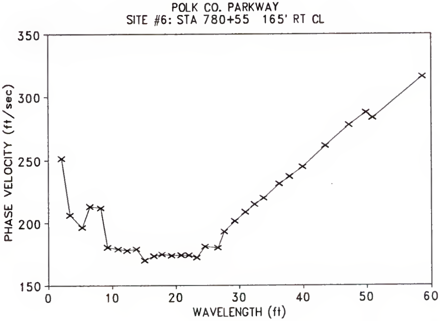

Figure A.19 Dispersion Curve from the Polk Co. Parkway (Sta 780+55, 165' Rt)

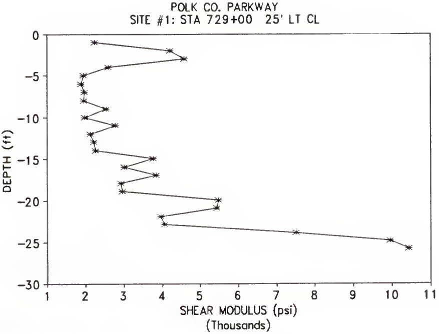

Figure A.20 DMT Shear Modulus Profile from the Polk Co. Parkway (Sta 729+00, 25' Lt)

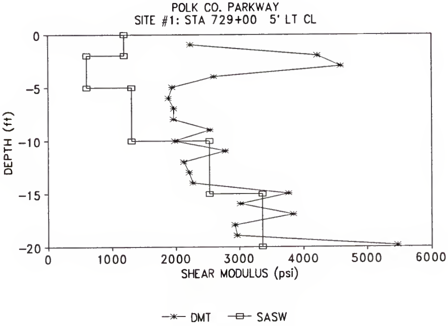

Figure A.21 Comparison of Shear Modulus Profiles from the Polk Co. Parkway (Sta 729+00, 5' Lt)

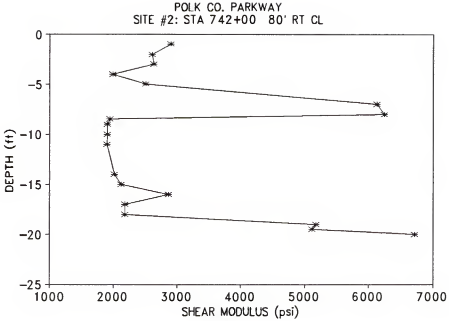

Figure A.22 DMT Shear Modulus Profile from the Polk Co. Parkway (Sta 742+00, 80′ Rt)

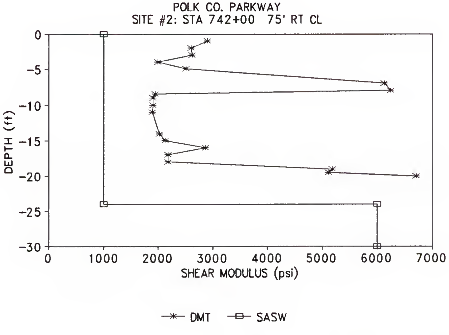

Figure A.23 Comparison of Shear Modulus Profiles from the Polk Co. Parkway (Sta 742+00, 75′ Rt)

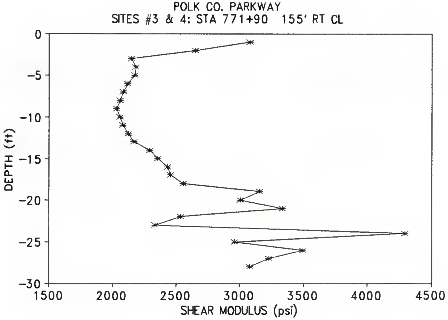

Figure A.24 DMT Shear Modulus Profile from the Polk Co. Parkway (Sta 771+90, 155' Rt)

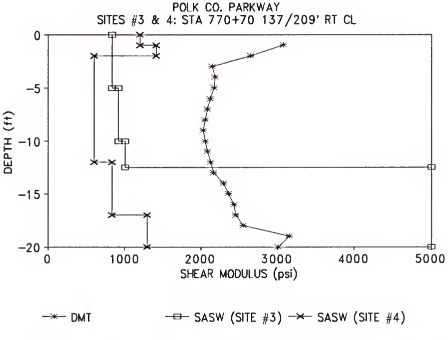

Figure A.25 Comparison of Shear Modulus Profiles from the Polk Co. Parkway (Sta 770+70, 137/209' Rt)

A.4 Kanapaha Site

The following table (A.1) and figures (A.26 through A.48) are all the SASW field data not included in Chapter 5. Table A.1 contains the results from the SASW inversion analyses for each of the sites not in Chapter 5 (those which did not appear to detect a stiff limerock layer within the SASW sampling depth). These results include the layer thickness and shear wave velocities, as well as the shear moduli and Young's moduli determined from elastic equations (by assuming a Poisson's ratio and mass density). Figures A.26 through A.37 are the plots containing the tip resistance (q_c) versus depth plots from the CPT soundings. Figures A.38 through A.48 are the plots showing the comparisons of the SASW shear modulus profiles with those derived from empirical relationships using the CPT field data (the Imai and Tonouchi relationship, Eqn. 2.20).

Table A.1 Additional SASW Results for the Kanapaha Site

Layer Thickness (ft)	Total Depth (ft)	Shear Wave Velocity (ft/sec)	Shear Modulus (psi)	Young's Modulus (psi)
Site No.2				
5.0	5.0	680	9,630	24,080
5.0	10.0	700	10,210	25,520
5.0	15.0	720	10,800	27,000
H-S	H-S	850	15,050	37,630
Site No.3				
11.5	11.5	550	6,300	15,760
5.0	16.5	850	15,050	37,630
H-S	H-S	850	15,050	37,630
Site No.4				
5.0	5.0	600	7,500	18,750
5.0	15.0	750	11,720	29,300
5.0	20.0	850	15,050	37,630
H-S	H-S	850	15,050	37,630
Site No.7				
1.5	1.5	470	4,600	11,510
2.5	4.0	760	12,030	30,080
10.0	14.0	700	10,210	25,520
H-S	H-S	900	16,875	42,200

Table A.1 (Continued)

Layer Thickness (ft)	Total Depth (ft)	Shear Wave Velocity (ft/sec)	Shear Modulus (psi)	Young's Modulus (psi)
Site No.9				
5.0	5.0	450	4,220	10,550
5.0	10.0	700	10,210	25,520
5.0	15.0	900	16,875	42,200
H-S	H-S	900	16,875	42,200
Site No.10				
5.0	5.0	500	5,210	13,020
6.0	11.0	750	11,720	29,300
4.0	15.0	900	16,875	42,200
H-S	H-S	900	16,875	42,200
Site No.13				
2.0	2.0	550	6,300	15,760
3.0	5.0	500	5,210	13,020
5.0	10.0	750	11,720	29,300
5.0	15.0	1,000	20,830	52,080
H-S	H-S	1,000	20,830	52,080
Site No.14				
5.0	5.0	450	4,220	10,550
5.0	10.0	700	10,210	25,520
3.0	13.0	950	18,800	47,010
H-S	H-S	950	18,800	47,010

Table A.1 (Continued)

Layer Thickness (ft)	Total Depth (ft)	Shear Wave Velocity (ft/sec)	Shear Modulus (psi)	Young's Modulus (psi)
Site No.15				
7.0	7.0	450	4,220	10,550
6.0	13.0	1,000	20,830	52,080
H-S	H-S	1,000	20,830	52,080
Site No.16				
3.0	3.0	400	3,330	8,330
3.0	6.0	750	11,720	29,300
5.0	11.0	900	16,875	42,200
H-S	H-S	900	16,875	42,200

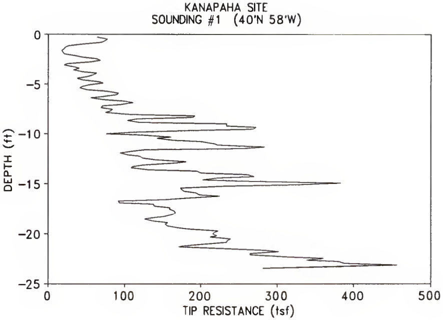

Figure A.26 CPT Tip Resistance Profile from the Kanapaha Site (40'N 58'W)

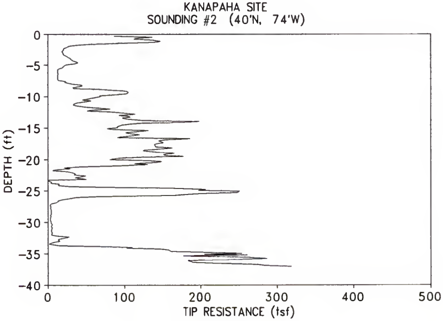

Figure A.27 Cone Resistance Profile from the Kanapaha Site (40'N 74'W)

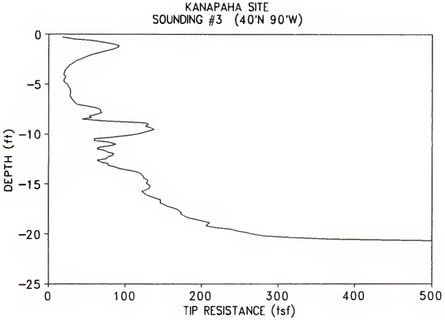

Figure A.28 CPT Tip Resistance Profile from the Kanapaha Site (40'N 90'W)

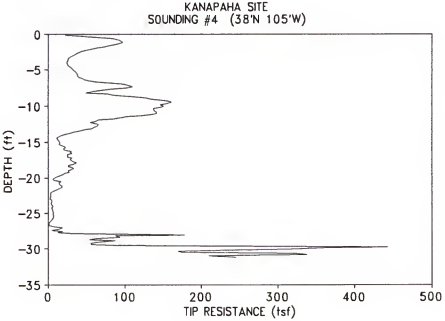

Figure A.29 CPT Tip Resistance Profile from the Kanapaha Site (38'N 105'W)

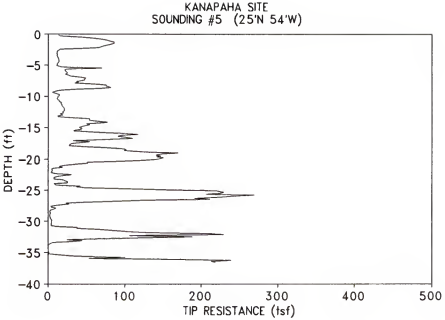

Figure A.30 CPT Tip Resistance Profile from the Kanapaha Site (25'N 54'W)

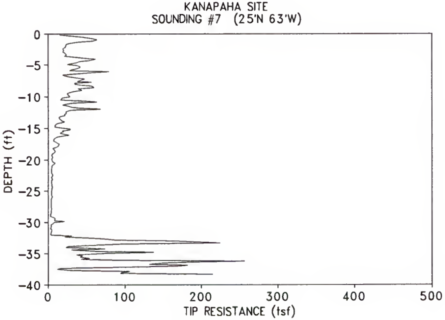

Figure A.31 CPT Tip Resistance Profile from the Kanapaha Site (25'N 63'W)

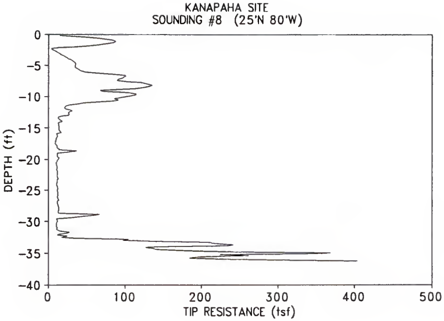

Figure A.32 CPT Tip Resistance Profile from the Kanapaha Site (25'N 80'W)

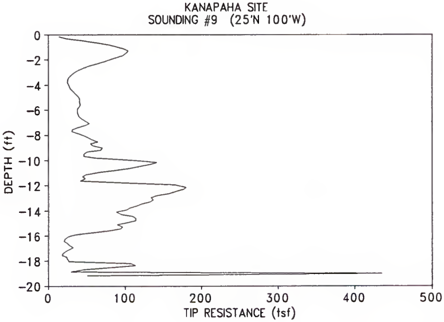

Figure A.33 CPT Tip Resistance Profile from the Kanapaha Site (25'N 100'W)

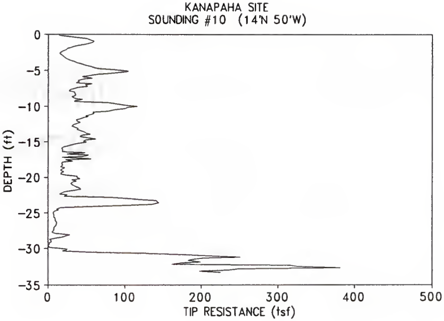

Figure A.34 CPT Tip Resistance Profile from the Kanapaha Site (14'N 50'W)

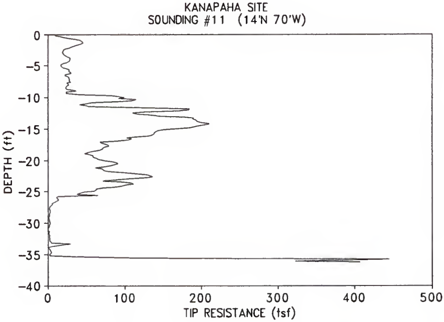

Figure A.35 CPT Tip Resistance Profile from the Kanapaha Site (14'N 70'W)

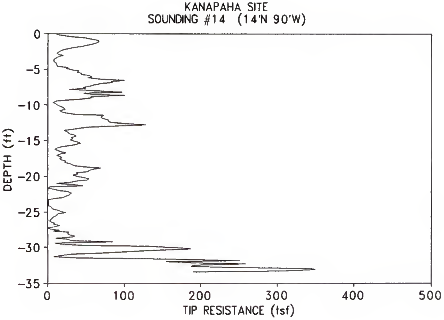

Figure A.36 CPT Tip Resistance Profile from the Kanapaha Site (14'N 90'W)

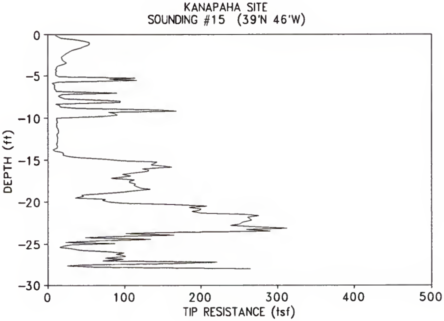

Figure A.37 CPT Tip Resistance Profile from the Kanapaha Site (39'N 46'W)

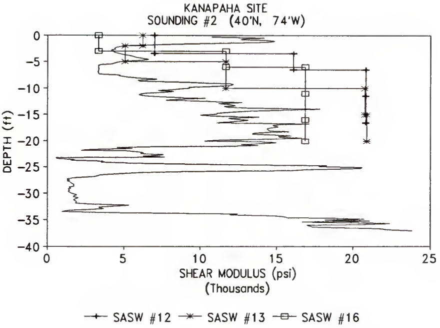

Figure A.38 Comparison of Shear Modulus Profiles from the Kanapaha Site (40'N 74'W)

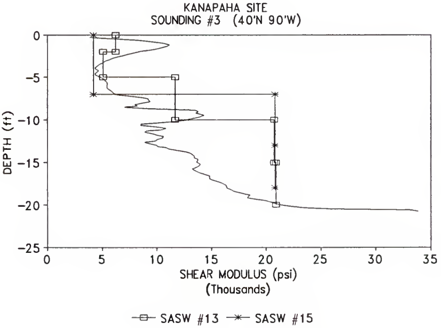

Figure A.39 Comparison of Shear Modulus Profiles from the Kanapaha Site (40'N 90'W)

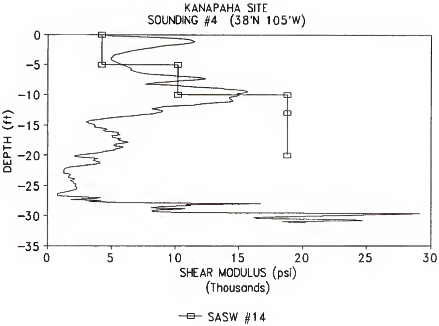

Figure A.40 Comparison of Shear Modulus Profiles from the Kanapaha Site (38'N 105'W)

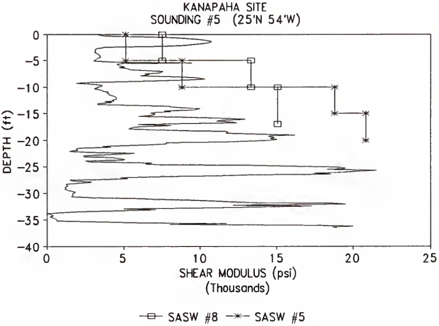

Figure A.41 Comparison of Shear Modulus Profiles from the Kanapaha Site (25'N 54'W)

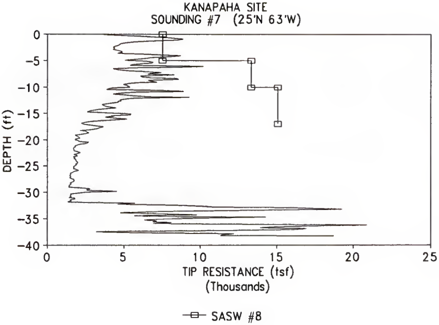

Figure A.42 Comparison of Shear Modulus Profiles from the Kanapaha Site (25'N 63'W)

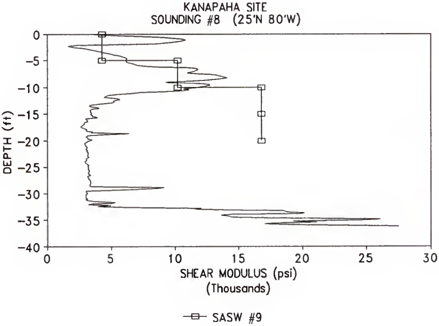

Figure A.43 Comparison of Shear Modulus Profiles from the Kanapaha Site (25'N 80'W)

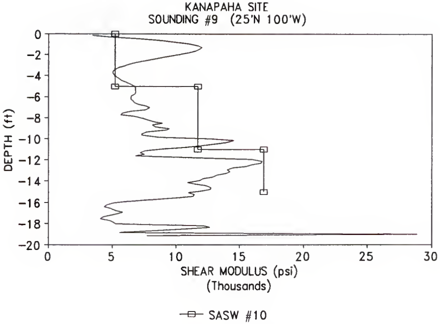

Figure A.44 Comparison of Shear Modulus Profiles from the Kanapaha Site (25'N 100'W)

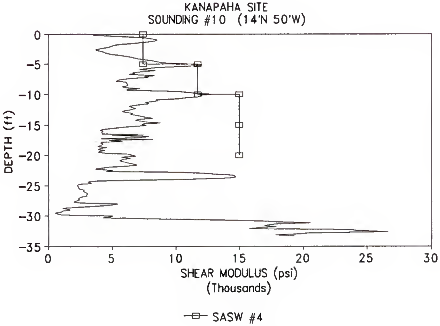

Figure A.45 Comparison of Shear Modulus Profiles from the Kanapaha Site (14'N 50'W)

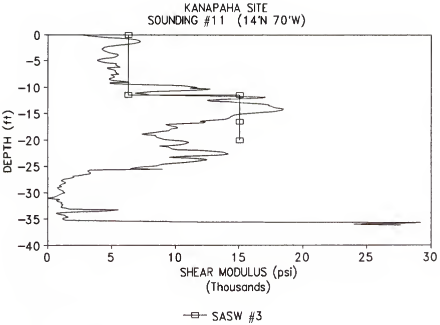

Figure A.46 Comparison of Shear Modulus Profiles from the Kanapaha Site (14'N 70'W)

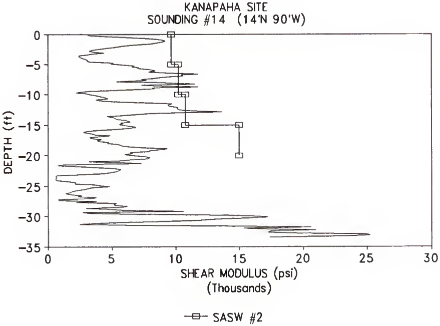

Figure A.47 Comparison of Shear Modulus Profiles from the Kanapaha Site (14'N 90'W)

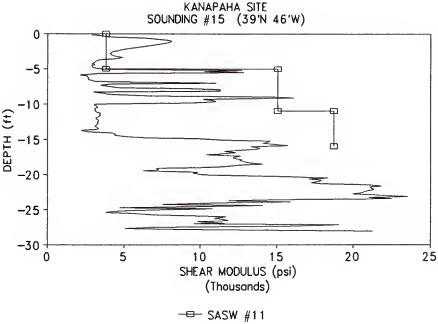

Figure A.48 Comparison of Shear Modulus Profiles from the Kanapaha Site (39'N 46'W)

A.5 Live Oak Site

The following figures (A.49 through A.64) are the CPT and SASW field data not included in Chapter 5. Figures A.49 through A.57 contain the tip resistance (q_c) versus depth plots from the CPT soundings. Figures A.58 through A.64 are the plots comparing the shear modulus profiles derived from empirical relationships using either the Imai and Tonouchi relationship (Eqn. 2.20) or the Mayne and Rix relationship (Eqn. 2.28) for the cohesive soils, and the SASW shear modulus profiles (if the SASW test was located near the CPT sounding). The clay layer was identified from the CPT data (using the Robertson and Campanella criteria).

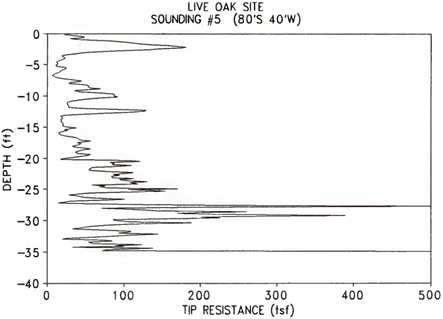

Figure A.49 CPT Tip Resistance Profile from the Live Oak Site (80'S 40'W)

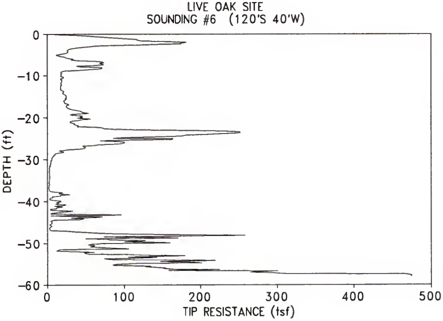

Figure A.50 CPT Tip Resistance Profiles from the Live Oak Site (120'S 40'W)

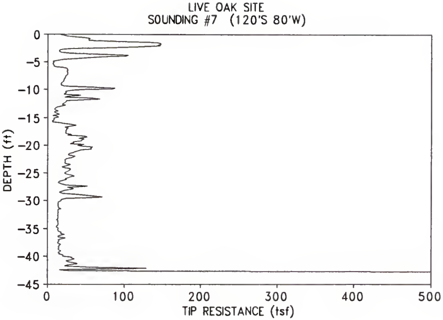

Figure A.51 CPT Tip Resistance Profile from the Live Oak Site (120'S 80'W)

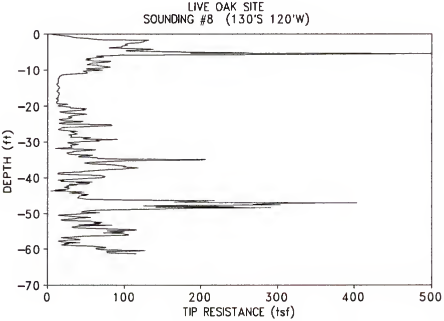

Figure A.52 CPT Tip Resistance Profile from the Live Oak Site (130'S 120'W)

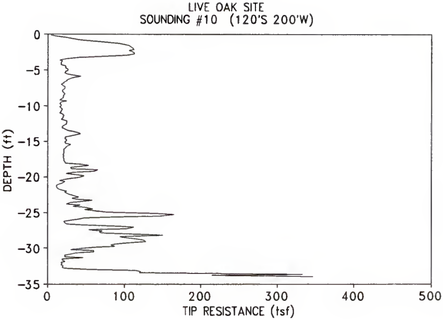

Figure A.53 CPT Tip Resistance Profile from the Live Oak Site (120'S 200'W)

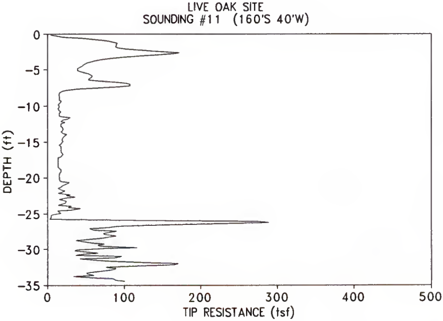

Figure A.54 CPT Tip Resistance Profile from the Live Oak Site (160'S 40'W)

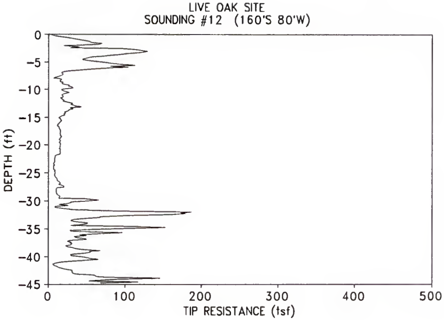

Figure A.55 CPT Tip Resistance Profiles from the Live Oak Site (160'S 80'W)

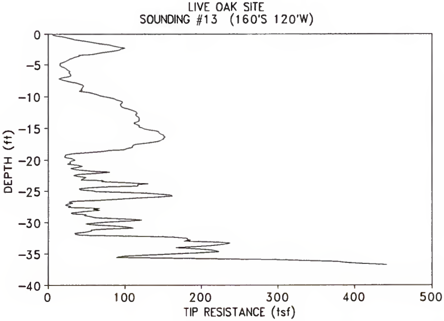

Figure A.56 CPT Tip Resistance Profile from the Live Oak Site (160'S 120'W)

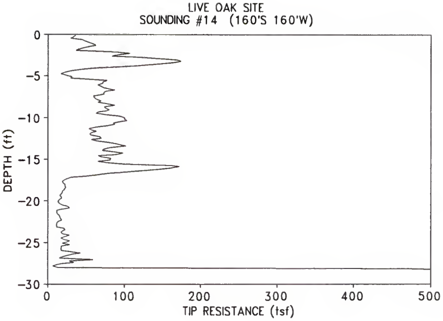

Figure A.57 CPT Tip Resistance Profiles from the Live Oak Site (160'S 160'S)

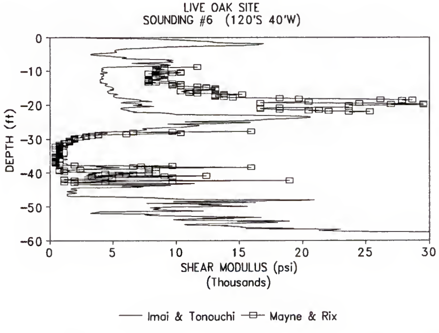

Figure A.58 Comparison of Shear Modulus Profiles from the Live Oak Site (120'S 40'W)

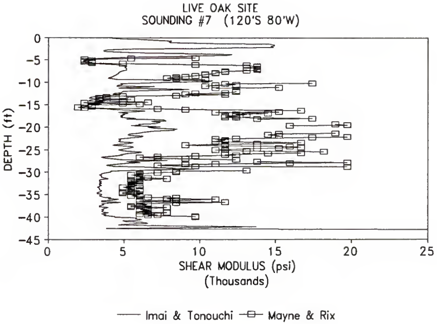

Figure A.59 Comparison of Shear Modulus Profiles from the Live Oak Site (120'S 80'W)

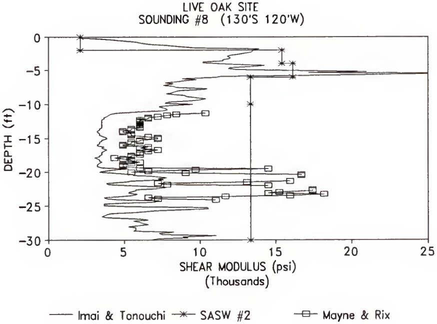

Figure A.60 Comparison of Shear Modulus Profiles from the Live Oak Site (130'S 120'W)

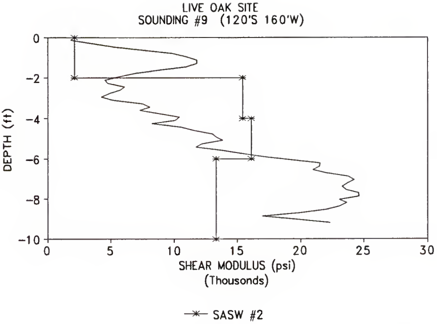

Figure A.61 Comparison of Shear Modulus Profiles from the Live Oak Site (120'S 160'W)

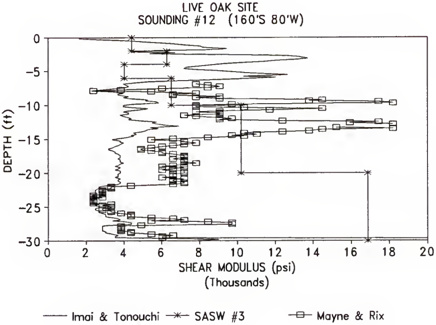

Figure A.62 Comparison of Shear Modulus Profiles from the Live Oak Site (160'S 80'W)

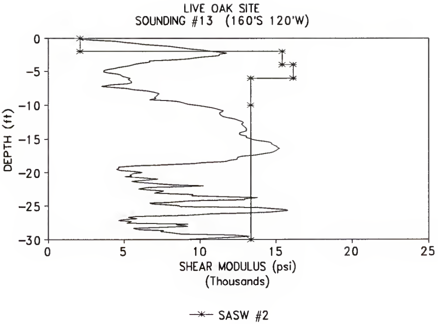

Figure A.63 Comparison of Shear Modulus Profiles from the Live Oak Site (160'S 120'W)

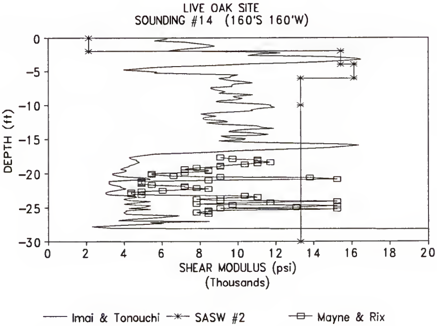

Figure A.64 Comparison of Shear Modulus Profiles from the Live Oak Site (160'S 160'W)

APPENDIX B
PAVEMENT APPLICATIONS' DATA

B.1 Introduction

This appendix includes additional field data for all of the pavement applications listed in Chapter 6. It is organized by the same sections numbers and titles that are used in Chapter 6.

B.2 Test Pit Studies

The following tables (B.1 through B.14) and figures (B.1 through B.16) are all the plate load test data and laboratory resilient test results not included in Chapter 6. Tables B.1, B.4, B.7, and B.10 and Figures B.1, B.5, B.9, and B.13 present the static plate load test results for the I-75 (Alachua), SR-30A (Panama City), SR-50 (Brooksville), and SR-369 (Crwafordville) subgrade respectively. Tables B.2, B.5, B.8, and B.11 and Figures B.2, B.6, B.10, and B.14 present the dynamic plate load test results. Tables B.3, B.6, B.9, and B.12 and Figures B.3, B.7, B.11, and B.15 present the laboratory resilient modulus test results. Figures B.4, B.8, B.12, and B.16 present the combined plots of the normalized Young's modulus versus axial strain. Table B.13 presents the static plate load test results from the dolomite study, and Table B.14

contains the dynamic plate load test results. The modulus values in Tables B.13 and B.14 are uncorrected values. A correction factor was applied in order to convert them to moduli which reflect the layer stiffness of the dolomite.

Table B.1 Static Plate Load Test Results for the I-75 (Alachua) Subgrade

Applied Load (lb)	Applied Stress (psi)	Averaged Young's Modulus (psi)			
			Optimum	Drained	Soaked
500	4.42	(1)	17,073	30,290	1,867
		(2)	18,412	34,778	2,439
		(3)	24,711	30,290	2,934
1,000	8.84	(1)	14,015	21,586	1,950
		(2)	17,551	33,536	3,216
		(3)	22,627	32,379	3,786
1,500	13.26	(1)	13,809	19,838	2,179
		(2)	21,341	32,756	3,807
		(3)	24,711	34,354	4,457
2,000	17.68	(1)	13,225	19,563	2,408
		(2)	20,751	29,575	4,183
		(3)	23,623	33,536	4,923
0	Rebound	(1)	23,061	37,218	4,675
		(2)	24,409	32,974	5,046
		(3)	24,569	36,853	5,528

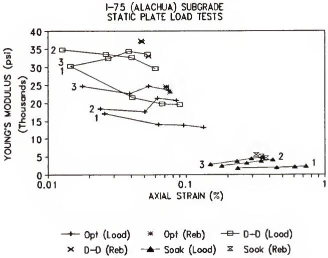

Figure B.1 Static Plate Load Test Results for the I-75 (Alachua) Subgrade

Table B.2 Dynamic Plate Load Test Results for the I-75 (Alachua) Subgrade

Test No.	Plate E_p (Perm.) n=4	n=10,000	Plate E_p (Total) n=4	n=10,000	Plate E_p (Resil.) n=4	n=10,000
Opt.						
1	24,842	15,391	13,882	10,727	31,467	35,400
2	15,391	10,977	10,336	8,329	31,467	34,537
3	101,143	42,909	27,765	19,944	38,270	37,263
Avg.	26,061	16,724	14,648	11,389	33,449	35,697
D-D						
1	23,213	15,064	15,910	11,899	50,571	56,640
2	34,537	21,134	19,397	14,750	44,250	48,828
3	67,429	27,765	28,320	19,135	48,828	61,565
Avg.	34,537	20,038	20,038	14,699	47,730	55,169
Soak						
1	2,344	1,410	1,641	1,223	5,467	9,195
2	15,064	4,627	5,827	3,147	9,503	9,833
3	3,756	2,152	2,787	1,856	10,809	13,486
Avg.	3,952	2,159	2,632	1,792	7,881	10,541

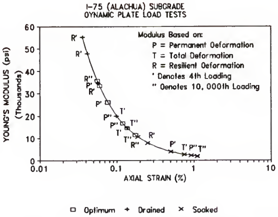

Figure B.2 Dynamic Plate Load Test Results for the I-75 (Alachua) Subgrade

Table B.3 Resilient Modulus Test Results for I-75 (Alachua) Subgrade

Confining Stress (psi)	Deviator Stress (psi)	3 Internal LVDT's Strain (%)	3 Internal LVDT's M_R (psi)	1 External LVDT Strain (%)	1 External LVDT M_R (psi)
4	1.91	0.0029	69,474	0.0091	21,669
6	3.95	0.0082	48,318	0.0278	14,209
6	6.03	0.0150	40,267	0.0289	20,847
4	8.01	0.0214	37,474	0.0307	26,070
4	5.95	0.0274	36,314	0.0366	27,177
4	1.99	0.0028	72,364	0.0040	49,441
4	3.99	0.0100	40,000	0.0141	28,248
4	5.95	0.0178	33,380	0.0244	24,435
4	8.05	0.0250	32,200	0.0339	23,764
4	10.03	0.0302	33,212	0.0402	24,981
2	1.91	0.0036	53,803	0.0052	37,087
2	3.99	0.0144	27,757	0.0202	19,740
2	6.02	0.0233	25,865	0.0325	18,523
2	8.01	0.0303	26,479	0.0424	18,903
2	10.05	0.0360	27,955	0.0498	20,196

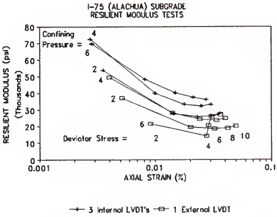

Figure B.3 Resilient Modulus Test Results for the I-75 (Alachua) Subgrade

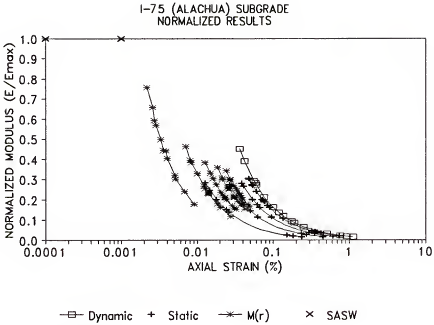

Figure B.4 Variation of Normalized Modulus and Strain for the I-75 (Alachua) Subgrade

Table B.4 Static Plate Load Test Results for the SR-30A (Panama City) Subgrade

Applied Load (lb)	Applied Stress (psi)	Averaged Young's Modulus (psi)		
		Optimum	Drained	Soaked
500	4.42	(1) 6,904	20,525	2,257
		(2) 5,188	17,634	2,497
		(3) 5,556	15,268	2,594
1,000	8.84	(1) 3,786	17,151	2,268
		(2) 5,814	18,145	3,000
		(3) 6,097	18,548	3,162
1,500	13.26	(1) 3,249	15,084	2,391
		(2) 5,869	18,594	3,358
		(3) 6,476	18,594	3,598
2,000	17.68	(1) 3,112	15,222	2,507
		(2) 5,614	18,277	3,523
		(3) 6,198	18,898	3,737
0	Rebound	(1) 6,773	18,701	3,928
		(2) 7,146	19,203	4,117
		(3) 7,160	19,502	4,247

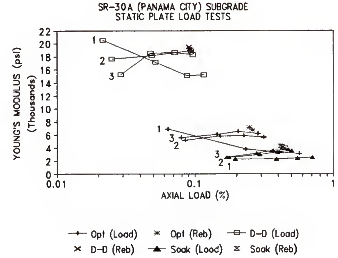

Figure B.5 Static Plate Load Test Results for the SR-30A (Panama City) Subgrade

Table B.5 Dynamic Plate Load Test Results for the SR-30A (Panama City) Subgrade

Test No.	Plate E_p (Perm.) n=4	Plate E_p (Perm.) n=10,000	Plate E_p (Total) n=4	Plate E_p (Total) n=10,000	Plate E_p (Resil.) n=4	Plate E_p (Resil.) n=10,000
Opt.						
1	5,851	2,702	3,858	2,216	11,328	12,313
2	2,981	1,412	2,185	1,253	8,185	11,150
3	5,264	2,400	3,531	1,994	10,727	11,800
Avg.	4,308	2,007	3,000	1,714	9,879	11,735
D-D						
1	50,571	19,397	13,615	9,699	18,632	19,397
2	44,250	26,222	17,700	14,020	29,500	30,128
4	38,270	23,600	15,560	11,512	26,222	22,476
Avg.	43,794	22,717	15,447	11,481	23,865	23,213
Soak						
1	2,467	806	1,755	723	6,077	6,975
2	5,710	1,445	3,013	1,221	6,378	7,867
3	6,293	1,203	3,092	1,011	6.077	6,321
Avg.	4,057	1,086	2,448	940	6,174	6,998

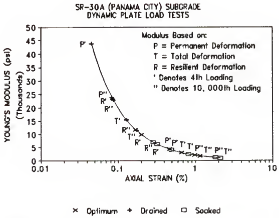

Figure B.6 Dynamic Plate Load Test Results for the SR-30A (Panama City) Subgrade

Table B.6 Resilient Modulus Test Results for SR-30A (Panama City) Subgrade

Confining Stress (psi)	Deviator Stress (psi)	3 Internal LVDT's Strain (%)		1 External LVDT Strain (%)	
		Strain (%)	M_R (psi)	Strain (%)	M_R (psi)
6	1.99	0.0046	43,027	0.0055	36,264
6	4.03	0.0122	33,101	0.0146	27,650
6	6.06	0.0205	29,525	0.0244	24,823
6	7.98	0.0276	28,913	0.0334	23,892
6	10.01	0.0349	28,723	0.0421	23,791
4	1.99	0.0052	38,641	0.0065	30,793
6	4.07	0.0149	27,361	0.0178	22,817
4	6.02	0.0236	25,508	0.0284	21,197
4	8.11	0.0323	25,147	0.0389	20,842
4	10.02	0.0393	25,480	0.0476	21,056
2	2.05	0.0070	29,181	0.0088	23,429
2	4.00	0.0197	20,279	0.0245	16,335
2	6.01	0.0311	19,309	0.0386	15,565
2	8.07	0.0402	20,062	0.0505	15,980
2	10.06	0.0463	21,728	0.0581	17,311

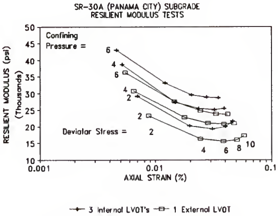

Figure B.7 Resilient Modulus Test Results for the SR-30A (Panama City) Subgrade

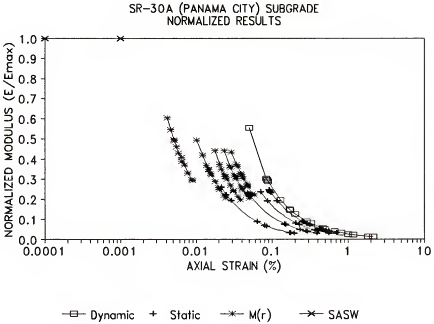

Figure B.8 Variation of Normalized Modulus and Strain for the SR-30A (Panama City) Subgrade

Table B.7 Static Plate Load Test Results for the SR-50 (Brooksville) Subgrade

Applied Load (lb)	Applied Stress (psi)	Averaged Young's Modulus (psi)		
		Optimum	Drained	Soaked
500	4.42	(1) 10,433	14,672	3,802
		(2) 9,485	15,915	5,491
		(3) 9,884	16,190	5,691
1,000	8.84	(1) 6,660	12,520	3,734
		(2) 10,610	16,330	6,589
		(3) 10,492	16,190	6,476
1,500	13.26	(1) 6,345	11,640	3,968
		(2) 10,919	17,073	7,317
		(3) 11,179	16,768	7,298
2,000	17.68	(1) 6,281	11,080	4,192
		(2) 10,376	16,843	7,336
		(3) 11,112	17,151	7,557
0	Rebound	(1) 12,244	17,565	8,067
		(2) 12,447	18,795	8,316
		(3) 12,244	18,517	8,681

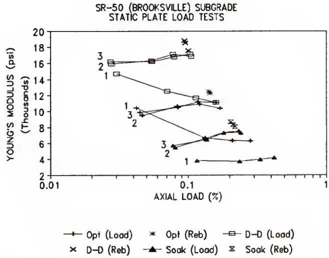

Figure B.9 Static Plate Load Test Results for the SR-50 (Brooksville) Subgrade

Table B.8 Dynamic Plate Load Test Results for the SR-50 (Brooksville) Subgrade

Test No.	Plate E_p (Perm.)		Plate E_p (Total)		Plate E_p (Resil.)	
	n=4	n=10,000	n=4	n=10,000	n=4	n=10,000
Opt.						
1	7,696	3,168	5,130	2,739	15,391	20,229
2	10,977	3,858	7,152	3,301	20,522	22,839
3	8,634	3,226	5,597	2,728	15,910	17,700
Avg.	8,906	3,390	5,843	2,900	16,992	20,038
D-D						
1	59,000	35,400	16,091	13,882	22,125	22,839
2	16,857	6,586	9,440	5,149	21,455	23,600
3	20,824	9,195	10,892	6,648	22,839	24,000
Avg.	24,136	10,386	11,543	7,200	22,125	23,470
Soak						
1	36,308	6,586	8,906	4,481	11,800	14,020
2	5,187	1,074	3,505	987	10,809	12,207
3	4,384	1,276	2,804	1,157	7,780	12,421
Avg.	6,690	1,607	3,978	1,428	9,811	12,834

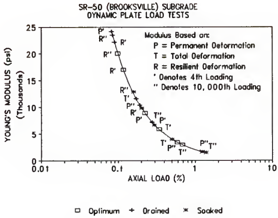

Figure B.10 Dynamic Plate Load Test Results for the SR-50 (Brooksville) Subgrade

Table B.9 Resilient Modulus Test Results for SR-50 (Brooksville) Subgrade

Confining Stress (psi)	Deviator Stress (psi)	3 Internal LVDT's Strain (%)	3 Internal LVDT's M_R (psi)	1 External LVDT Strain (%)	1 External LVDT M_R (psi)
6	1.95	0.0028	70,270	0.0070	27,907
6	3.95	0.0082	48,466	0.0164	24,067
6	6.09	0.0138	44,130	0.0211	28,897
6	8.15	0.0198	41,162	0.0299	27,258
6	3.95	0.0253	39,525	0.0381	26,255
4	2.08	0.0035	59,856	0.0053	39,061
4	4.02	0.0103	39,124	0.0157	25,666
4	6.01	0.0171	35,198	0.0257	23,362
4	2.06	0.0224	35,496	0.0339	23,489
4	10.02	0.0288	34,822	0.0431	23,275
2	2.00	0.0039	51,282	0.0059	33,970
2	3.96	0.0128	31,059	0.0193	20,531
2	5.91	0.0203	29,113	0.0305	19,353
2	8.09	0.0286	28,262	0.0417	19,383
2	10.10	0.0378	26,737	0.0544	18,553

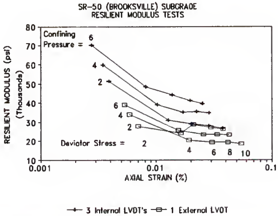

Figure B.11 Resilient Modulus Test Results for the SR-50 (Brooksville) Subgrade

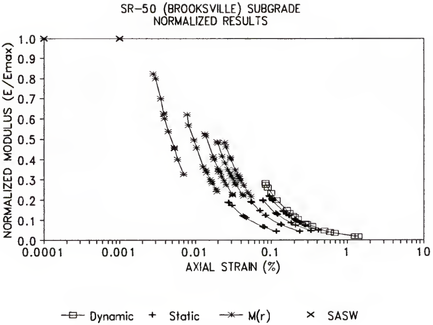

Figure B.12 Variation of Normalized Modulus and Strain for the SR-50 (Brooksville) Subgrade

Table B.10 Static Plate Load Test Results for the SR-369 (Crawfordville) Subgrade

Applied Load (lb)	Applied Stress (psi)	Averaged Young's Modulus (psi)			
			Optimum	Drained	Soaked
500	4.42	(1)	2,990	4,558	2,545
		(2)	4,388	4,626	2,474
		(3)	4,211	4,865	2,664
1,000	8.84	(1)	2,903	3,764	2,380
		(2)	5,145	5,397	3,210
		(3)	5,062	5,796	3,440
1,500	13.26	(1)	2,956	3,766	2,420
		(2)	5,470	5,968	3,591
		(3)	5,773	6,359	3,833
2,000	17.68	(1)	3,069	3,904	2,417
		(2)	5,548	6,208	3,682
		(3)	5,878	6,743	4,058
0	Rebound	(1)	6,797	7,026	4,702
		(2)	6,773	7,429	4,829
		(3)	7,000	7,533	4,866

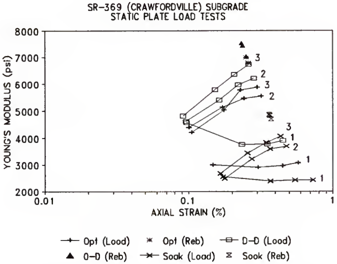

Figure B.13 Static Plate Load Test Results for the SR-369 (Crawfordville) Subgrade

Table B.11 Dynamic Plate Load Test Results for the SR-369 (Crawfordville) Subgrade

Test No.	Plate E_p (Perm.)		Plate E_p (Total)		Plate E_p (Resil.)	
	n=4	n=10,000	n=4	n=10,000	n=4	n=10,000
Opt.						
1	4,000	1,321	2,672	1,174	8,045	10,567
2	3,105	1,367	2,356	1,223	9,766	11,607
3	6,051	2,014	3,736	1,716	9,766	11,607
4	5,446	1,825	3,522	1,595	9,972	12,643
Avg.	4,344	1,579	2,962	1,389	9,316	11,559
D-D						
1	3,078	1,396	2,269	1,263	8,634	13,234
2	23,213	5,510	6,941	3,827	9,902	12,531
3	8,091	3,522	4,720	2,810	11,328	13,882
Avg.	6,103	2,539	3,766	2,219	9,833	13,193
Soak						
1	2,687	313	1,921	298	6,743	6,321
2	3,454	376	2,277	356	6,679	6,617
Avg.	3,022	342	2,084	324	6,711	6,466

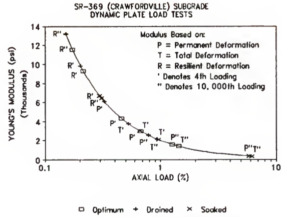

Figure B.14 Dynamic Plate Load Test Results for the SR-369 (Crawfordville) Subgrade

Table B.12 Resilient Modulus Test Results for SR-369 (Crawfordville) Subgrade

Confining Stress (psi)	Deviator Stress (psi)	3 Internal LVDT's Strain (%)	3 Internal LVDT's M_R (psi)	1 External LVDT Strain (%)	1 External LVDT M_R (psi)
6	1.97	0.0049	40,619	0.0073	27,172
6	4.02	0.0128	31,529	0.0180	22,396
6	5.95	0.0198	30,127	0.0265	22,463
6	8.00	0.0274	29,224	0.0355	22,551
6	9.99	0.0341	29,318	0.0445	22,443
4	1.97	0.0064	30,661	0.0083	23,843
4	8.00	0.0166	24,096	0.0215	18,615
4	6.01	0.0255	23,569	0.0333	18,055
4	7.98	0.0327	24,404	0.0435	18,345
4	10.04	0.0398	25,226	0.0534	18,801
2	1.99	0.0085	23,343	0.0111	17,928
2	4.04	0.0212	19,057	0.0279	14,493
2	6.09	0.0312	19,504	0.0422	14,423
2	8.04	0.0397	20,265	0.0541	14,861
2	10.08	0.0513	19,659	0.0682	14,777

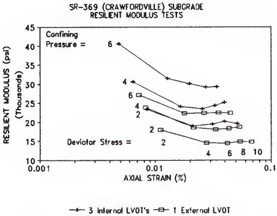

Figure B.15 Resilient Modulus Test Results for the SR-369 (Crawfordville) Subgrade

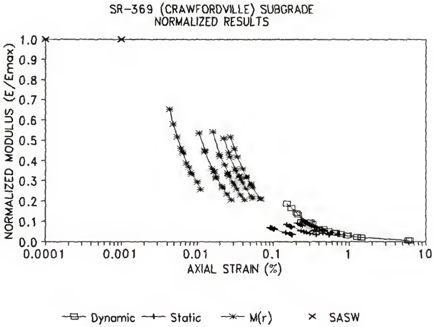

Figure B.16 Variation of Normalized Modulus and Strain for the SR-369 (Crawfordville) Subgrade

Table B.13 Static Plate Load Test Results for the Dolomite Study

Applied Load (lb)	Applied Stress (psi)	Averaged Young's Modulus (psi)		
		Optimum	Drained	Soaked
4,000	8.84	(1) 21,341	31,300	10,731
		(2) 17,229	22,627	9,781
		(3) 19,361	27,618	12,437
2,000	17.68	(1) 15,145	23,329	9,229
		(2) 18,233	23,475	10,701
		(3) 18,970	27,416	12,478
3,000	26.53	(1) 14,446	19,563	8,872
		(2) 19,229	25,378	11,987
		(3) 21,422	27,618	13,741
4,000	35.37	(1) 13,963	18,733	9,150
		(2) 20,525	26,358	13,042
		(3) 23,043	28,455	14,875
5,000	44.21	(1) 14,581	18,233	9,399
		(2) 20,820	26,376	13,491
		(3) 24,453	29,071	15,419
0	Rebound	(1) 24,776	30,787	15,293
		(2) 26,156	30,586	16,919
		(3) 26,983	31,723	16,302

Table B.14 Dynamic Plate Load Test Results for the Dolomite Study

Test No.	Plate E_c (Perm.) n=4	n=10,000	Plate E_c (Total) n=4	n=10,000	Plate E_c (Resil.) n=4	n=10,000
Opt.						
1	29,748	11,879	14,874	8,045	29,748	24,930
2	24,414	10,028	12,249	6,941	24,583	22,548
3	30,256	11,028	13,774	7,564	25,286	24,082
Avg.	27,874	10,926	13,546	7,489	26,352	23,812
D-D						
1	35,400	11,919	15,874	8,429	28,780	28,780
2	37,263	14,449	17,612	9,699	33,396	29,500
3	44,250	14,332	19,135	9,972	33,714	32,778
Avg.	38,618	13,460	17,438	9,316	31,796	30,256
Soak						
1	24,930	2,757	10,028	2,201	16,777	10,926
2	17,879	1,702	8,064	1,503	14,689	12,873
3	17,970	2,138	8,872	1,826	17,525	12,509
Avg.	19,777	2,116	8,917	1,799	16,239	12,041

B.3 Field Trench Sites

The following figures (B.17 through B.29) are the results from the testing performed at the field trench sites which were referenced but not included in Chapter 6. Figures B.17 through B.22 are the cross-sectional profiles for the trench sites at which SASW testing was performed. Figures B.23 and B.24 are the comparison results of the plate load moduli and LBR with the SASW moduli for the base layer materials. Figures B.25 through B.27 are the comparison results of the plate load moduli and LBR with the SASW moduli for the subgrade and embankment layer results. Figures B.28 and B.29 are the comparison results of the plate load moduli with the SASW moduli for all the data (from the base, subgrade, and embankment results).

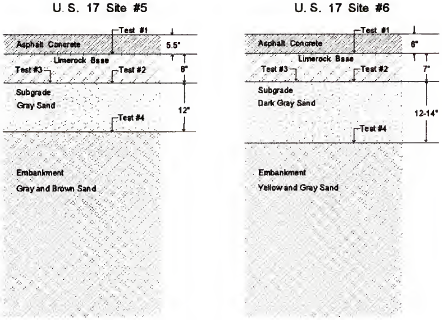
U.S. 17 Site #5

U.S. 17 Site #6

Figure B.17 Profiles of the Clay Co. Trench Sites

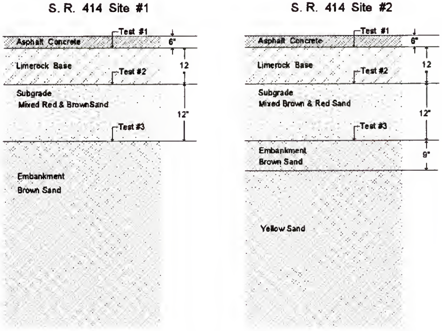
S.R. 414 Site #1

S.R. 414 Site #2

Figure B.18 Profiles of the Seminole Co. Trench Sites

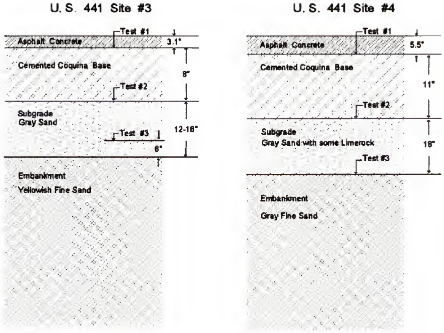

Figure B.19 Profiles of the Osceola Co. Trench Sites

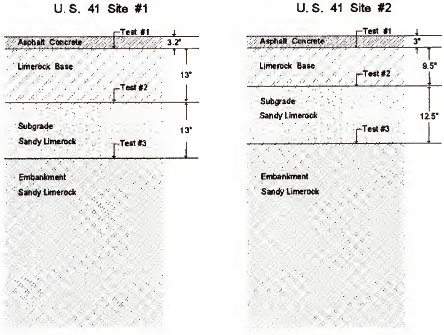

Figure B.20 Profiles of the Dade Co. Trench Sites

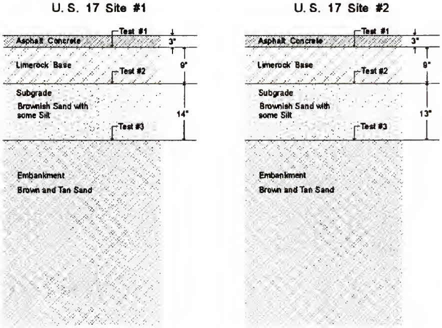

Figure B.21 Profiles of the Polk Co. Trench Sites

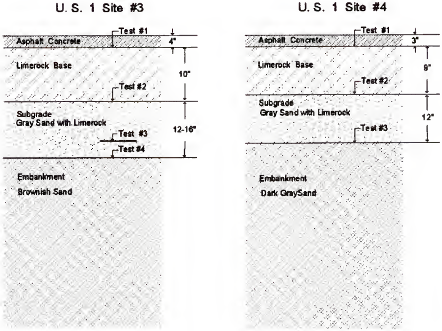

Figure B.22 Profiles of the Martin Co. Trench Sites

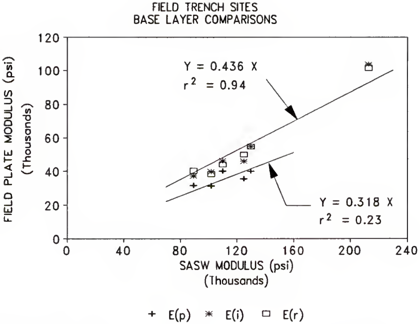

Figure B.23 Comparison of Uncorrected Plate and SASW Base Layer Moduli for the Trench Sites

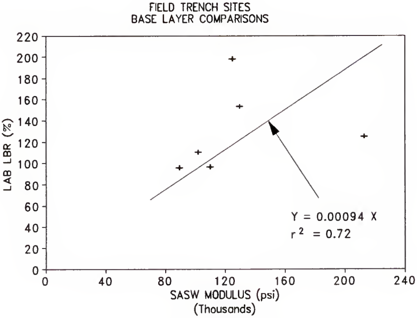

Figure B.24 Comparison of LBR and SASW Moduli for the Base Layer Trench Sites

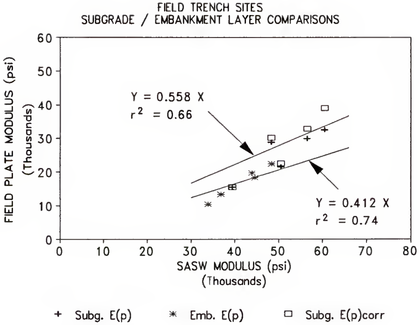

Figure B.25 Comparison of E_p and SASW Subgrade/Embankment Moduli for the Trench Sites

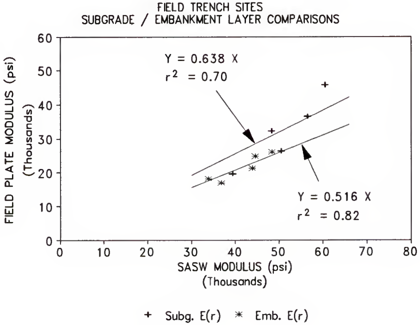

Figure B.26 Comparison of E_r and SASW Subgrade/Embankment Moduli for the Trench Sites

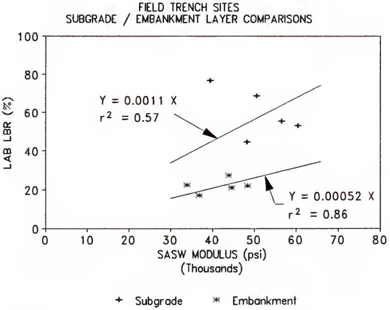

Figure B.27 Comparison of LBR and SASW Moduli for the Subgrade/Embankment Layer Trench Sites

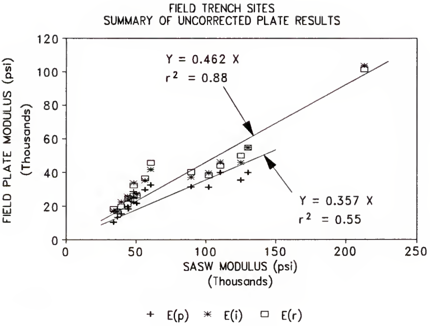

Figure B.28 Comparison of Uncorrected Plate and SASW Moduli for the Trench Sites

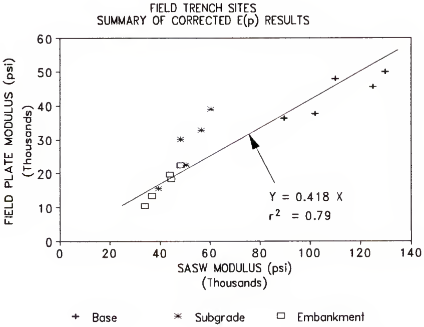

Figure B.29 Comparison of Corrected E_p and SASW Moduli for the Trench Sites

REFERENCE LIST

Anderson, D. G. and Stokoe, K. H. II, "Shear Modulus: A Time-Dependent Property", Dynamic Geotechnical Testing, ASTM STP 654, American Society for Testing and Materials, Philadelphia, 1978, pp. 66-90.

Anderson, D. G. and Woods, R. D., "Comparison of Field and Laboratory Shear Modulus", Proceedings of the Conference on In Situ Measurement of Soil Properties, American Society of Civil Engineers, New York, 1975, pp. 69-91.

American Association of State Highway and Transportation Officials, Standard Specifications for Transportation Materials and Methods of Sampling and Testing, Sixteenth Edition, AASHTO, Washington, D.C., 1993.

American Society of Testing and Materials, Annual Book of ASTM Standards, Section 4, Volume 4.08, ASTM, Philadelphia, 1995.

Bay, J. A. and Stokoe, K. H. II, "Field and Laboratory Determination of Elastic Properties of PCC Using Seismic Techniques", Transportation Research Board, 71st Annual Meeting, Washington, D. C., January 1992.

Bowen, B. R., Stokoe, K. H. II, Roesset, J. M., and Jirsa, J. O., "Evaluation of Cracked and Repaired Beams and Columns Using Surface Stress Waves", Proceedings of the 1992 NSF Structures, Geomechanics and Building Systems Grantees' Conference, National Science Foundation, San Juan, Puerto Rico, 1992.

Briaud, J. L., "The Pressuremeter Test for Highway Applications", Publication No. FHWA-IP-89-008, Federal Highway Administration, Washington, D.C., July 1989.

Brooks, H. K., Geological Map of Florida, University of Florida Institute of Food and Agricultural Science, Center for Environmental and Natural Resources, Gainesville, 1981.

Burnham, T. and Johnson, D., "In Situ Foundation Characterization Using the Dynamic Cone Penetrometer", Report No.

MN/RD-93/05, Minnesota Department of Transportation, May 1993.

Cox, E. A., "A Review of the Florida DOT Test-Pit Program", Research Project S-1-63, Engineering and Industrial Experiment Station, University of Florida, December 1971.

Drnevich, V. P., Hossain, M. M., Wang, J., and Graves, R. C., "Determination of Layer Moduli in Pavement Systems by Nondestructive Testing", Transportation Research Record 1278, Transportation Research Board, Washington, D. C., 1990, pp. 18-26.

Erbland, P. J., "Modifying the Pavement Pressuremeter to Enable Low Strain Level Resilient Moduli Determination", M.S. thesis, Division of Engineering Sciences, Florida Institute of Technology, 1993.

Gucunski, N. and Woods, R. D., "Instrumentation for SASW Testing", Recent Advances in Instrumentation, Data Acquisition and Testing in Soil Dynamics, Geotechnical Special Publication No. 29, American Society of Civil Engineers, New York, 1991, pp. 1-16.

Hardin, B. O. and Black, W. L., "Vibration Modulus of Normally Consolidated Clay", Journal of the Soil Mechanics and Foundations Division, Proceedings of the American Society of Civil Engineers, Vol. 94, No. SM 2, March 1968, pp. 353-369; Closure in Vol. 95, No. SM 6, November 1969, pp. 1531-1537.

Hardin, B. O. and Drnevich, V. P., "Shear Modulus and Damping in Soils: Measurement and Parameter Effects", Journal of the Soil Mechanics and Foundations Division, Proceedings of the American Society of Civil Engineers, Vol. 98, No. SM 6, June 1972a, pp. 603-624.

Hardin, B. O. and Drnevich, V. P., "Shear Modulus and Damping in Soils: Design Equations and Curves", Journal of the Soil Mechanics and Foundations Division, Proceedings of the American Society of Civil Engineers, Vol. 98, No. SM 7, July 1972b, pp. 667-692.

Harrell, S. and Stokoe, K. H. II, "Integrity Evaluation of Drilled Piers by Stress Waves", Research Report 257-1F, Center of Transportation Research, The University of Texas at Austin, January 1984.

Heisey, J. S., Stokoe, K. H. II, and Meyer, A. H., "Moduli of Pavement Systems from Spectral Analysis of Surface Waves", Transportation Research Record 852, Transportation Research Board, Washington, D.C., 1982a, pp. 22-31.

Heisey, J. S., Stokoe, K. H. II, Hudson, W. R., and Meyer, A. H., "Determination of In Situ Shear Wave Velocities from Spectral Analysis of Surface Waves", Research Report 256-2, Center of Transportation Research, The University of Texas at Austin, December 1982b.

Heukelom, W. and Foster, C. R., "Dynamic Testing of Pavements", Journal of the Soil Mechanics and Foundations Division, Proceedings of the American Society of Civil Engineers, Vol. 86, No. SM 1, February 1960, pp. 1-27.

Hiltunen, D. R. and Woods, R. D., "SASW and Crosshole Test Results Compared", Earthquake Engineering and Soil Dynamics II - Recent Advances in Ground Motion Evaluation, Geotechnical Special Publication No. 20, American Society of Civil Engineers, New York, 1988, pp. 279-289.

Hiltunen, D. R. and Woods, R. D., "Influence of Source and Receiver Geometry on the Testing of Pavements by the Surface Waves Method", Nondestructive Testing and Backcalculation of Moduli, ASTM STP 1026, American Society for Testing and Materials, Philadelphia, 1989, pp. 138-154.

Hiltunen, D. R. and Woods, R. D., "Variables Affecting the Testing of Pavements by the Surface Waves Method", Transportation Research Record 1260, Transportation Research Board, Washington, D. C., 1990, pp. 42-52.

Hossain, M. M. and Drnevich, V. P., "Numerical and Optimization Techniques Applied to Surface Waves for Backcalculation of Layer Moduli", Nondestructive Testing and Backcalculation of Moduli, ASTM STP 1026, American Society for Testing and Materials, Philadelphia, 1989, pp. 649-669.

Hryciw, R. D., "Small-Strain-Shear Modulus of Soil by Dilatometer", Journal of Geotechnical Engineering, American Society of Civil Engineers, Vol. 116, No. 11, November 1990, pp. 1700-1716.

Huang, Y. H., Pavement Analysis and Design, Prentice-Hall, Inc., Englewood Cliffs, New Jersey, 1993.

Jones, R., "In-Situ Measurement of the Dynamic Properties of Soil by Vibration Methods", Geotechnique, Vol. 8, No. 1, March 1958, pp. 1-21.

Jones, R., "Surface Wave Technique for Measuring the Elastic Properties and Thicknesses of Roads: Theoretical Development", British Journal of Applied Physics, Vol. 13, 1962, pp. 21-29.

Jones, R., "Following Changes in the Properties of Road Bases and Sub-Bases by the Surface Wave Propagation Method", Civil Engineering and Public Works Review, Vol. 58, No. 682, May 1963, pp. 613-617.

Kausel, E. and Roesset, J. M., "Stiffness Matrices for Layered Soils", Bulletin of the Seismological Society of America, Vol. 71, No. 6, December 1981, pp. 1743-1761.

Kim, D. and Stokoe, K. H. II, "Characterization of Resilient Modulus of Compacted Subgrade Soils Using Resonant Column and Torsional Shear Tests", Transportation Research Board, 71st Annual Meeting, Washington, D. C., January 1992.

Kokusho, T., Yoshida, Y., and Esashi, Y., "Dynamic Properties of Soft Clay for Wide Strain Range", Soils and Foundations, JSSMFE, Vol. 22, No. 4, December 1982, pp. 1-18.

Krohn, C. E., "Geophone Ground Coupling", Geophysics, Vol. 49, No. 6, June 1984, pp. 722-731.

Lukas, Robert G., "Dynamic Compaction for Highway Construction, Volume 1: Design and Construction Guidelines", Report No. FHWA/RD-86/133, Federal Highway Administration, Washington, D.C., July 1986.

Mayne, P. W. and Rix, G. J., "G_{max}-q_c Relationships for Clays", Geotechnical Testing Journal, GTJODJ, Vol. 16, No. 1, March 1993, pp. 54-60.

Meier, R. W. and Rix, G. J., "An Initial Study of Surface Wave Inversion Using Artificial Neural Networks", Geotechnical Testing Journal, GTJODJ, Vol. 16, No. 4, December 1993, pp. 425-431.

Nazarian, S. and Desai, M. R., "Automated Surface Wave Method: Field Testing", Journal of Geotechnical Engineering, American Society of Civil Engineers, Vol. 119, No. 7, July 1993, pp. 1094-1111.

Nazarian, S. and Stokoe, K. H. II, "Evaluation of Moduli and Thicknesses of Pavement Systems by Spectral-Analysis-of-Surface-Waves Method", Research Report 256-4, Center of Transportation Research, The University of Texas at Austin, December 1983.

Nazarian, S. and Stokoe, K, H. II, "Nondestructive Testing of Pavements Using Surface Waves", Transportation Research Record 993, Transportation Research Board, Washington, D.C., 1984, pp. 67-79.

Nazarian, S. and Stokoe, K. H. II, "In Situ Determination of Elastic Moduli of Pavement Systems by Spectral-Analysis-of-Surface-Waves Method: Practical Aspects", Research Report 368-1F, Center of Transportation Research, The University of Texas at Austin, August 1985.

Nazarian, S. and Stokoe, K. H. II, "In Situ Determination of Elastic Moduli of Pavement Systems by Spectral-Analysis-of-Surface-Waves Method (Theoretical Aspects)", Research Report 437-2, Center of Transportation Research, The University of Texas at Austin, November 1986a.

Nazarian, S. and Stokoe, K, H. II, "Use of Surface Waves in Pavement Evaluation", Transportation Research Record 1070, Transportation Research Board, Washington, D. C., 1986b, pp. 132-144.

Nazarian, S. and Stokoe, K. H. II, "Nondestructive Evaluation of Pavements by Surface Wave Method", Nondestructive Testing and Backcalculation of Moduli, ASTM STP 1026, American Society for Testing and Materials, Philadelphia, 1989, pp. 119-137.

Nazarian, S., Stokoe, K, H. II, and Hudson, W. R., "Use of Spectral Analysis of Surface Waves Method for Determination of Moduli and Thicknesses of Pavement Systems", Transportation Research Record 930, Transportation Research Board, Washington, D. C., 1983, pp. 38-45.

Nazarian, S., Stokoe, K. H. II, and Briggs, R. C., "Nondestructively Delineating Changes in Modulus Profiles of Secondary Roads", Transportation Research Record 1136, Transportation Research Board, Washington, D.C., 1987, pp. 96-107.

Nazarian, S., Stokoe, K. H. II, Briggs, R. C., and Rogers, R., "Determination of Pavement Layer Thicknesses and Moduli by SASW Method", Transportation Research Record 1196, Transportation Research Board, Washington, D.C., 1988, pp. 133-150.

Nazarian, S., Yuan, D., and Baker, M. R., "Automation of Spectral Analysis of Surface Waves Method", Dynamic Geotechnical Testing II, ASTM STP 1213, American Society for Testing and Materials, Philadelphia, 1994, pp. 88-100.

Olsen, R. S., "Using the CPT for Dynamic Site Response Characterization", Earthquake Engineering and Soil Dynamics II - Recent Advances in Ground Motion Evaluation, Geotechnical Special Publication No. 20, American Society of Civil Engineers, New York, 1988, pp. 374-388.

Riaund, J. L. and Miran, J., "The Cone Penetrometer Test", Publication No. FHWA-SA-91-043, Federal Highway Administration, Washington, D.C., February 1992a.

Riaund, J. L. and Miran, J., "The Flat Dilatometer Test", Publication No. FHWA-SA-91-044, Federal Highway Administration, Washington, D.C., February 1992b.

Richart, F. E., Hall, J. R., and Woods, R. D., Vibrations of Soils and Foundations, Prentice-Hall, Englewood Cliffs, New Jersey, 1970.

Rix, G. J. and Leipski, E. A., "Accuracy and Resolution of Surface Wave Inversion", Recent Advances in Instrumentation, Data Acquisition and Testing in Soil Dynamics, Geotechnical Special Publication No. 29, American Society of Civil Engineers, New York, 1991, pp. 17-32.

Rix, G. J. and Stokoe, K. H. II, "Stiffness Profiling of Pavement Subgrades", Transportation Research Record 1235, Transportation Research Board, Washington, D.C., 1989, pp. 1-9.

Rix, G. J., Jacobs, L. J., and Reichert, C. D., "Evaluation of Nondestructive Test Methods for Length, Diameter, and Stiffness Measurements on Drilled Shafts", Transportation Research Board, 72nd Annual Meeting, Washington, D.C., January 1993.

Roesset, J. M., Chang, D., Stokoe, K. H. II, and Aouad, M., "Modulus and Thickness of the Pavement Surface Layer from SASW Tests", Transportation Research Record 1260, Transportation Research Board, Washington, D. C., 1990, pp. 53-63.

Sanchez-Salinero, I., Roesset, J. M., Shao, K., Stokoe, K. H. II, and Rix G. J., "Analytical Evaluation of Variables Affecting Surface Wave Testing of Pavements", Transportation Research Record 1136, Transportation Research Board, Washington, D.C., 1987, pp. 86-95.

Seed, H. B., Wong, R. T., Idriss, I. M., and Tokimatsu, K., "Moduli and Damping Factors for Dynamic Analyses of Cohesionless Soils", Journal of Geotechnical Engineering, American Society of Civil Engineers, Vol. 112, No. 11, November 1986, pp. 1016-1032.

Sheu, J., Stokoe, K. H. II, Roesset, J. M., and Hudson, W. R., "Applications and Limitations of the Spectral-Analysis-of-Surface-Waves Method", Research Report 437-3F, Center of Transportation Research, The University of Texas at Austin, November 1986.

Sheu, J. C., Stokoe, K. H. II, and Roesset, J. M., "Effect of Reflected Waves in SASW Testing of Pavements", Transportation Research Record 1196, Transportation Research Board, Washington, D.C., 1988, pp. 51-61.

Smith, L. L. and Lofroos, W. N., "Pavement Design Coefficients: A Re-evaluation of Florida Base Materials", Research Report FL/DOT/OMR-235/81, State of Florida Department of Transportation, February 1981

Stokoe, K. H. II and Woods, R. D., "In Situ Shear Wave Velocity by Cross-Hole Method", Journal of the Soil Mechanics and Foundations Division, Proceedings of the American Society of Civil Engineers, Vol. 98, No. SM 5, May 1972, pp. 443-460.

Stokoe, K. H. II, Lee, S. H., and Knox, D. P., "Shear Moduli Measurements Under True Triaxial Stresses", Proceedings of the Advances in the Art of Testing Soils Under Cyclic Conditions, Geotechnical Engineering Division, American Society of Civil Engineers, New York, 1985, pp. 166-185.

Stokoe, K. H. II, Nazarian, S., Rix, G. J., Sanchez-Salinero, I., Sheu, J., and Mok, Y., "In Situ Seismic Testing of Hard-To-Sample Soils by Surface Wave Method", Earthquake Engineering and Soil Dynamics II - Recent Advances in Ground Motion Evaluation, Geotechnical Special Publication No. 20, American Society of Civil Engineers, New York, 1988, pp. 264-278.

Stokoe, K. H. II, Rix, G. J., and Nazarian, S., "In Situ Seismic Testing with Surface Waves", Proceedings of the 12th International Conference on Soils Mechanics and Foundation Engineering, A. A. Balkema, Rotterdam, 1989, pp. 331-334.

Sykora, D. W. and Koester, J. P., "Correlations Between Dynamic Shear Resistance and Standard Penetration Resistance in Soils", Earthquake Engineering and Soil Dynamics II - Recent Advances in Ground Motion Evaluation, Geotechnical Special Publication No. 20, American Society of Civil Engineers, New York, 1988, pp. 389-404.

Szendrei, M. E. and Freeme, C. R., "Road Responses to Vibration Tests", Journal of the Soil Mechanics and Foundations Division, Proceedings of the American Society of Civil Engineers, Vol. 96, No. SM 6, November 1970, pp. 2099-2124.

Tarantola, A., Inverse Problem Theory: Methods for Data Fitting and Model Parameter Estimation, Elsevier Science Publishers, B.V., Amsterdam, 1987.

Tokimatsu, K., "Effects of Multiple Modes on Rayleigh Wave Dispersion Characteristics", Journal of Geotechnical Engineering, American Society of Civil Engineers, Vol. 118, No. 10, October 1992, pp. 1529-1543.

Townsend, F. C., Theos, J. F., and Shields, M. D., "Dynamic Load Testing of Drilled Shaft", Final Report to Association of Drilled Shaft Contractors, March 1991.

Vardoulakis, I. and Vrettos, C., "Dispersion Law of Rayleigh-Type Waves in a Compressible Gibson Half Space", International Journal for Numerical and Analytical Methods in Geomechanics, Vol. 12, 1988, pp. 639-655.

Van Til, C. J., McCullough, B. F., and Vallerga, B. A., "Evaluation of AASHTO Interim Guides for Design of Pavement Structures", National Cooperative Highway Research Program (NCHRP) Report No. 128, Highway Research Board, Washington D. C., 1972.

Vucetic, M., "Effect of Soil Plasticity on Cyclic Response", Journal of Geotechnical Engineering, American Society of Civil Engineers, Vol. 117, No. 1, January 1991, pp. 89-107.

Webster, S. L., Grau, R. H., and Williams, T. P., "Description and Application of Dual Mass Dynamic Cone Penetrometer", Instruction Report GL-92-3, Waterways Experiment Station, Mississippi, 1992.

Weintraub, D., "Development of an Automated Airfield Dynamic Cone Penetrometer (AADCP) Prototype and the Evaluation of Unsurfaced Airfield Seismic Surveying using Analysis of Surface Waves (SASW) Technology", Ph.D. dissertation, University of Florida, 1993.

Yoder, E. J. and Witczak, M. W., Principles of Pavement Design, John Wiley & Sons, Inc., New York, Second Edition, 1975.

Yuan, D. and Nazarian, S., "Rapid Determination of Layer Properties of Pavements from Surface Wave Method", Transportation Research Record 1377, Transportation Research Board, Washington, D. C., May 1993a, pp. 159-166.

Yuan, D. and Nazarian, S., "Automated Surface Wave Method: Inversion Technique", Journal of Geotechnical Engineering, American Society of Civil Engineers, Vol. 119, No. 7, July 1993b, pp. 1112-1126.

BIOGRAPHICAL SKETCH

David J. Horhota earned a Bachelor of Science in Civil Engineering degree from the University of Florida in 1986. Upon graduation, he entered into the Professional Engineer Trainee Program of the Florida Department of Transportation at the Bureau of Materials and Research in Gainesville. This two year program consisted of various phases to provide experience in the many areas of the transportation field. After completing this program, he entered into the Senior Engineer Trainee Program which consisted of specialized training in the areas of soils materials and geotechnical engineering. He began graduate studies in 1989 at the University of Florida while continuing to work for the Department. In 1990, he obtained his Professional Engineering License. During that same year, he was accepted for Educational Leave with Pay by the Department to continue his studies full-time. He obtained his Master of Engineering degree in 1991 specializing in the area of geotechnical engineering. His research for this degree was titled "Investigation of Organic Soil Usage on FDOT Projects". At the same time, he received an extension of the Educational Leave for a second year to complete the classwork in order to obtain his Doctor of Philosophy degree in civil engineering.

After returning to State Materials Office (the new designation for the Bureau of Materials and Research) for full-time duties, he assisted the Geotechnical Engineer in foundation studies, geotechnical operations and investigations, and geotechnical research. During this same period, he conducted the research needed to fulfill the Ph.D. requirement. In 1994, he was promoted to the Geotechnical Engineer position at the State Materials Office. The duties of this position consisted of supervising the Soils Research and Field Operations Sections and the Test Pit Facility. In 1995, he was given the additional duties of overseeing the Soils Foundations Laboratory of the Materials Office. In 1996, the Soil Support Section was transferred under his direct supervision. This section is responsible for the field plate load, dynaflect, and falling weight deflectometer testing for the Materials Office. He was also given the responsibilities of overseeing the Accelerated Pavement Testing Facility which will be constructed on the grounds of the State Materials Office.

I certify that I have read this study and that in my opinion it conforms to acceptable standards of scholarly presentation and is fully adequate, in scope and quality, as a dissertation for the degree of Doctor of Philosophy.

Frank C Townsend

Frank C. Townsend, Chair
Professor of Civil Engineering

I certify that I have read this study and that in my opinion it conforms to acceptable standards of scholarly presentation and is fully adequate, in scope and quality, as a dissertation for the degree of Doctor of Philosophy.

David Bloomquist, Cochair
Associate Professor of
Civil Engineering

I certify that I have read this study and that in my opinion it conforms to acceptable standards of scholarly presentation and is fully adequate, in scope and quality, as a dissertation for the degree of Doctor of Philosophy.

Paul Y. Thompson
Professor of Civil Engineering

I certify that I have read this study and that in my opinion it conforms to acceptable standards of scholarly presentation and is fully adequate, in scope and quality, as a dissertation for the degree of Doctor of Philosophy.

Jamshid M. Armaghani
Research Engineer
Florida Department of
Transportation

I certify that I have read this study and that in my opinion it conforms to acceptable standards of scholarly presentation and is fully adequate, in scope and quality, as a dissertation for the degree of Doctor of Philosophy.

Daniel P. Spangler

Daniel P. Spangler
Associate Professor of Geology

This dissertation was submitted to the Graduate Faculty of the College of Engineering and to the Graduate School and was accepted as partial fulfillment of the requirements for the degree of Doctor of Philosophy.

December 1996

Winfred M. Phillips
Dean, College of Engineering

Karen A. Holbrook
Dean, Graduate School